BL 014

FOR REFERENCE ONLY

FOR REFERENCE ONLY

40 0671104 X

ProQuest Number: 10290273

All rights reserved

INFORMATION TO ALL USERS
The quality of this reproduction is dependent upon the quality of the copy submitted.

In the unlikely event that the author did not send a complete manuscript
and there are missing pages, these will be noted. Also, if material had to be removed,
a note will indicate the deletion.

ProQuest 10290273

Published by ProQuest LLC (2017). Copyright of the Dissertation is held by the Author.

All rights reserved.
This work is protected against unauthorized copying under Title 17, United States Code
Microform Edition © ProQuest LLC.

ProQuest LLC.
789 East Eisenhower Parkway
P.O. Box 1346
Ann Arbor, MI 48106 – 1346

Computational Fluid Dynamic Investigation of Blood Flow Through Heart Valve Prostheses

Paul Wilson

A thesis submitted in partial fulfilment of the requirements of The Nottingham Trent University for the degree of Doctor of Philosophy

This research program was carried out in the Department of Mechanical and Manufacturing Engineering, Faculty of Engineering and Computing, The Nottingham Trent University, Nottingham, NG1 4BU, UK.

April 1997

PkD
qT /WIL

Computational Fluid Dynamic Investigation of Blood Flow Through Heart Valve Prostheses

By
Paul Wilson

Abstract

This thesis describes a computational fluid dynamic (CFD) analysis, and associated experimental validations, relating to a prototype conduit valve prosthesis under development at Nottingham Trent University. Current commercially available valved conduits are little more than short lengths of graft tubing into which are sewn conventional cardiac valve prostheses. These valves rely for their efficient closure, at least in part, on the vortex flow generated as the blood passes from one chamber of the heart to another (atrium to ventricle or ventricle to aortic root). They are therefore not ideally suited to controlling flow in a straight tube outside the heart and so the development programme was initiated to produce a purpose built mechanical valved conduit with the blood guided round a ball occluder, delivering not only superior flow characteristics but also the prospect of good haemodynamics.

The initial stages of the work described here concentrated on the comparison of steady non-Newtonian and Newtonian blood flow through the prosthesis at varying Reynolds numbers. The conclusion was that as differences between the two types of flow were small, neither could be shown to be more applicable to the analysis of the valve conduit. Therefore both flow situations were modelled in the final time dependent analysis to fully assess any differences between the two blood models under more realistic flow conditions.

The analysis was conducted using the CFD package PHOENICS. The model was required to simulate time varying inlet flow velocity, determine fluid forces acting on the occluder, predict occluder displacement and redefine the finite volume grid when necessary.

Experimental validation consisted of video recording the movement of the ball occluder in a model of a conduit valve under cyclic flow conditions to determine the occluder's position with respect to time. Comparison between the experimental and computational results showed that the overall performance of the CFD model was good but some detailed predictions were unreliable due to previously undetected errors in PHOENICS. Representation of field values using MPEG video bit streams proved to be a particularly efficient method of analysing the fluid properties over the entire flow cycle.

The main conclusions are:

The fact that only small differences were observed between the non-Newtonian and Newtonian blood models indicate that the use of a blood analogue is quite acceptable in experimentally determining the occluder's dynamic performance, but can not fully predict the true haemolytic and thrombogenic potentials.

The haemolytic and thrombogenic potentials of the conduit were low because of the low shear stresses and shear rates which apply for most of the flow cycle; higher values occur, but only for a small period of time, during the initial opening phase of the occluder.

CFD is the only current method available to allow access to field values at any point and time within the flow cycle and therefore it provides a powerful tool in the pre-clinical trials of new cardiac prostheses.

'I will praise thee; for I am fearfully and wonderfully made: marvellous are thy works; and that my soul knoweth right well.'

PSALM 139,14

Acknowledgements

Firstly, I wish to thank Professor C.R. Gentle, my Director of Studies, for all the help, guidance and support over the past three years. Whose knowledge and experience has been invaluable in the development and final completion of this thesis.

To Dr Martin Lacey, my Second Supervisor, for his advice and support over the past three years.

To my Mother and Brother, for their support over the years, for making my stays at home relaxing and comfortable and ensuring I at least eat properly some of the time. I could not wish for better.

My friends, who have encouraged and supported me; Dawn who had to put up with my tiredness and moods, Baf and Kiddie for listening and helping in any way they could, Bafs' wife Amanda for the lovely meals every Wednesday. I cannot imagine what things would have been like without them.

To my friends and colleagues at college, especially Mark, Steve, Jon, Bob and Rob for their good company, wit, humorous off-the-cuff comments and help in the final assembly of this thesis.

To Dr Shirley Ashforth-Frost and Dr Stuart Hartle for their help and advice in 'getting to grips' with PHOENICS.

The technical staff at the University for ensuring the computer worked when I needed it to, and to Rob Potter for the assistance in carrying out the Lab work.

To God for all his love and comfort.

Table Of Contents

Appendices

List Of Figures

List Of Tables

Nomenclature

Symbol	Meaning	Unit
a	Constant, Modified Cross[58] and Carreau-Yasuda[61]	
A_p	Occluder surface area perpendicular to flow axis	m^2
d	Conduit diameter	m
F_τ	Streamwise shear stress force	N
F_p	Streamwise pressure force	N
H	Haematocrit expressed as a percentage	
i	Phase	
j	Indices for y direction cell corner points	
K	Constant	
k	Indices for z direction cell corner points	
k	Index for current time step	
LPOR	Low face cell porosity	
m	Constant, Cross[57] and Modified Cross[58]	
m_o	Mass of occluder	kg
n	Constant used in Power Law, Carreau[60] and Carreau-Yasuda[61]	
NPOR	North face cell porosity	
NX	Number of cells in the x direction (BFC)	
NY	Number of cells in the y direction (BFC)	
NZ	Number of cells in the z direction (BFC)	
P	Pressure	Pa
P1	First phase pressure (BFC)	Pa
r	Elemental radius	m
	Volume fraction	
R^2	Quality of fit of curve	
R1	Volume fraction of first phase	
R2	Volume fraction of second phase	

Rb	Ball radius	m
S	Constant used in Cassons[54] equation	Pa $s^{1/2}$
S	Source term	
t	Time	s
V	Velocity	m/s
V1	First phase local y direction velocity (BFC)	m/s
V2	Second phase local y direction velocity (BFC)	m/s
VPOR	Cell volume porosity	
w	Time varying inlet velocity	m/s
W1	First phase local z direction velocity (BFC)	m/s
W2	Second phase local z direction velocity (BFC)	m/s
x	Distance along Cartesian ordinate X-axis	m
y	Distance along Cartesian ordinate Y-axis	m
z	Distance along Cartesian ordinate Z-axis	m
Z_o	Occluder displacement	m
α	Wormersley number	
α_o	Critical shear rate, above which non-Newtonian concentrate disperse systems act in a Newtonian manner, Quemada[55,56]	$s^{1/2}$
$\dot{\gamma}$	Shear rate	s^{-1}
Γ	Diffusion coefficient	
∂	Partial differential	
Δt	Time step size	s
η	Non-Newtonian viscosity	Pa s
η_o	Zero-shear rate viscosity	Pa s
η_∞	Infinite shear rate viscosity	Pa s
λ	Characteristic time	s
μ_a	Apparent viscosity of non-Newtonian fluid	Pa s
μ_{eff}	Effective viscosity	Pa s
μ_l	Laminar viscosity	Pa s

μ_p	Viscosity of plasma	Pa s
μ_r	Relative viscosity	Pa s
μ_t	Turbulent viscosity	Pa s
μ_∞	Intrinsic viscosity at infinite shear, Quemada[55,56]	Pa s
ν	Kinematic viscosity: $\nu = \frac{\mu}{\rho}$	m^2/s
ρ	Density	kg/m^3
τ	Shear stress	Pa
τ_y	Shear stress at flow yield of non-Newtonian fluid	Pa
φ	Field variable	
ω	Cardiac frequency	rad/s

Valve Nomenclature

The diagram below shows the terms used when describing sections of the valve prosthesis and computational model geometry.

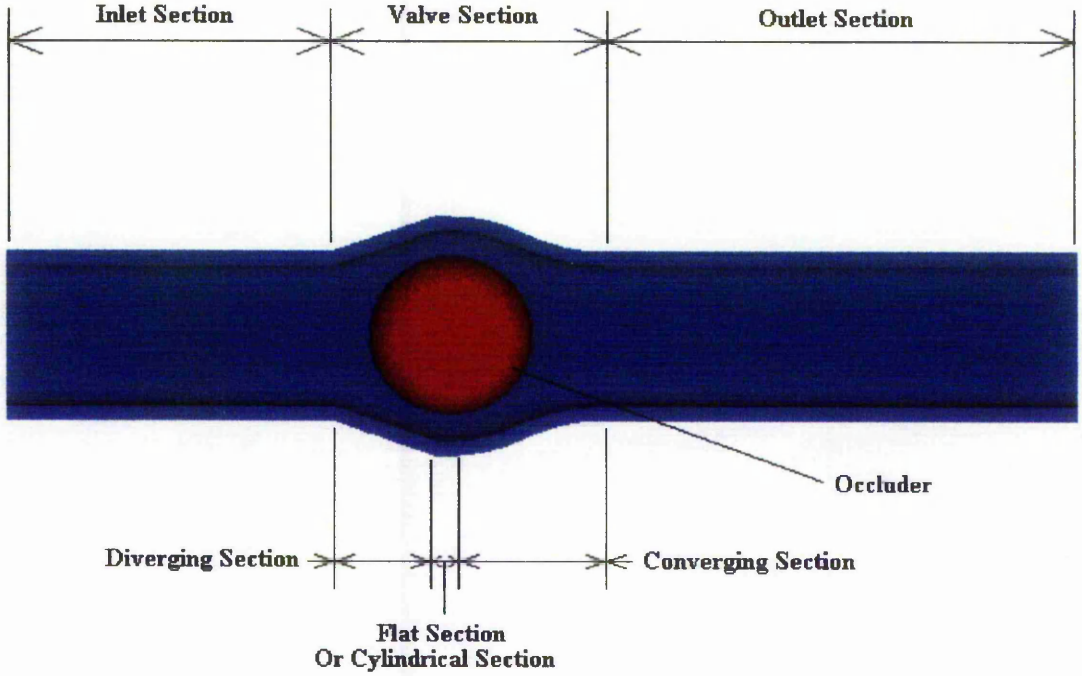

Chapter One

Introduction

1.1 Introduction

In 1952 Charles Hufnagel[1] successfully sewed an artificial valve into a patient's aorta to replace a diseased natural valve, thereby improving the flow of blood from the heart; this was the birth of prosthetic heart valves. Cardiac valve substitutes have now been in regular use for well over 30 years and the number and variations of valves available shows the size of the market and their acceptance within the medical community. Due to the consequences of valve failure, before any valve can be used it must first undergo a series of rigorous tests to ensure haemodynamic suitability and effectiveness. This has led to the valves currently in production being almost totally reliable.

The effectiveness of current valves as replacements has led in turn to their use in reconstructive surgery. For example, a prosthetic valve in a graft tube can be used to rebuild the aorta[2-9], or an additional exit from the ventricle can be constructed to provide a double outletting ventricle[10-17]. This new application has led to the development of purpose-built valve conduits.

Conduit valves are generally conventional heart valve prostheses mounted in short lengths of graft tube and are used both for replacement of a degenerating ascending aorta or aortic valve and as aortic shunts (producing a double outletting ventricle) as seen in Figure 1.1. They are mainly used in paediatrics to overcome congenital deformities and so ideally the valve should remain suited to the recipient for a normal life span. This requires not only increased longevity of acceptable mechanical and haemodynamic function but also, ideally, the obviation of anticoagulation treatment.

Commercially available conduits are usually an aortic or mitral valve mounted into a graft tube. The valves most commonly used are bioprosthetic, like Polystan's VPC porcine valved pulmonary grafts[12-21]. This valve is more sophisticated than other bioprosthetic conduits as it has a profiled body, but it is only intended for low pressure use in the pulmonary trunk and cannot provide acceptable long term performance. Therefore

mechanical valves offer the best prospect. The most common mechanical valve found in conduits is the Björk-Shiley tilting disk[22]. None of the mechanical valves found in commercial conduits were designed for this particular application but for placement in a tissue annulus, therefore they do not provide the most efficient haemodynamic performance. Recognising this limitation, work was started within the university to design a mechanical conduit valve with superior haemodynamics compared to conventional graft mounted valves so that a valve implanted into an infant would still be suitable in adult life.

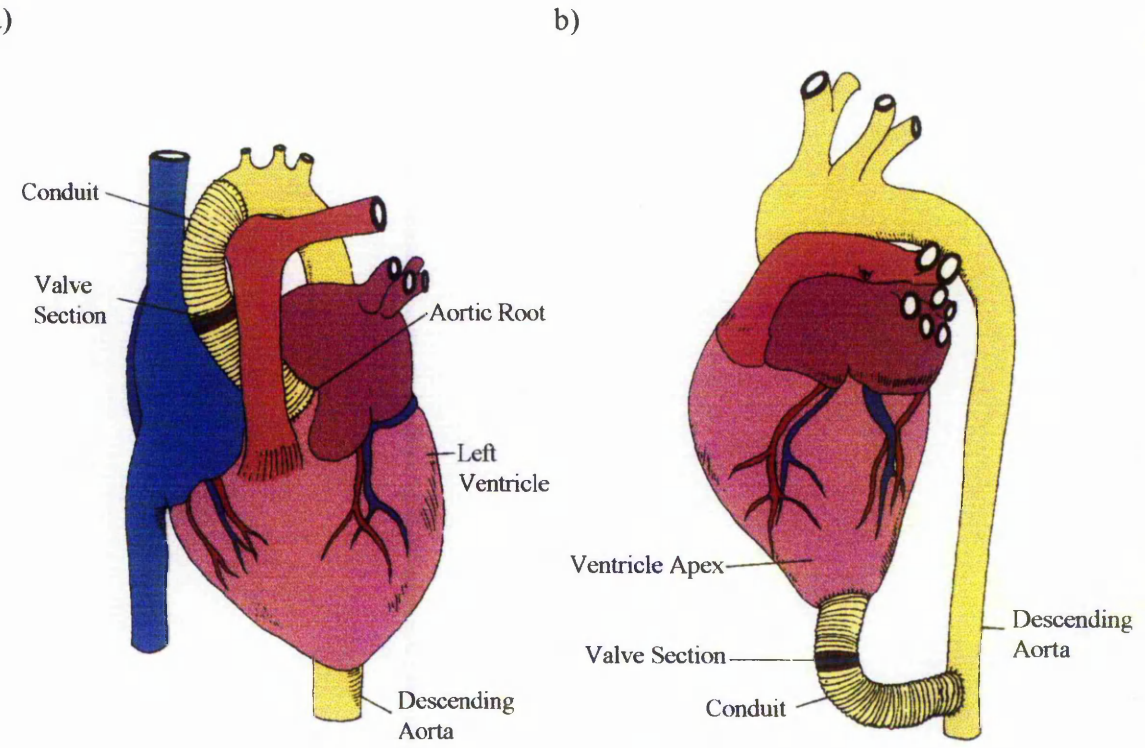

Figure 1.1: Conduit valve a) replacement of a degenerating aorta, b) aortic shunt.

The preliminary development of such a valve can be seen in Tansley[23], based on a Gentle conduit valve[24]. Computational fluid dynamics (CFD) was extensively used to determine valve design with the most efficient pressure/flow characteristics in steady flow.

The work here concerns the further development of this prototype conduit valve at The Nottingham Trent University, largely by means of CFD. The use of CFD in the analysis of

heart valve prostheses is becoming more popular as the accuracy, stability, speed and user-friendliness of commercial CFD software packages increases. Applying CFD allows valve design to be optimised to minimise not just pressure drop but also haemolytic and thrombogenic potentials, based on shear stress and shear rates induced by the valve prosthesis, before any prototype valves are produced for *in vitro* testing and clinical trials.

1.2 Heart Valve Prostheses

Heart valve prostheses can be split into two main sub groups, namely bio prostheses and mechanical prostheses. Each type of valve has its own pressure/flow characteristics, advantages and disadvantages. A brief summary of the two sub groups of valve prostheses will follow in order to explain the reasons for pursuing only a mechanical design in this work.

Bio Prostheses

There are two kinds of biological prostheses: homograft (allograft) valves which are fabricated with biological tissues transplanted from a human donor, and heterograft (xenograft) valves which are made from animal tissue, usually porcine or bovine. A typical bio prosthesis is shown in Figure 1.2. These valves consist of a fabric covered plastic stent on to which the preserved tissue valve is connected. This whole assembly is then implanted and secured by a sewing ring.

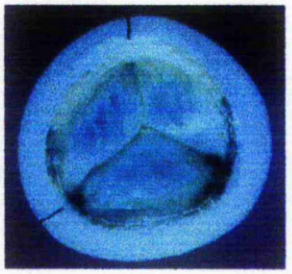

Figure 1.2: Bio prosthesis.

The intention is to reproduce the shape and function of a natural (aortic) valve as closely as possible and hence the advantages are:

- good flow characteristics,
- low incidence of thrombus,
- require little anticoagulation.

Unlike the natural valve, where all the tissue is living and therefore undergoes replacement over a seven year period, these valves are made of dead, fixed material which has low structural integrity. Hence they have the disadvantage that calcification and cyclic stressing cause the valve to progressively fail and the patient therefore often needs further replacement valves. For this reason they are often limited to elderly patients.

Mechanical Prostheses

A number of mechanical valve types exist, e.g. caged ball, bi-leaflet, tri-leaflet, disc, and tilting disc. Development is still ongoing with new valves being developed, e.g. central axis valve by Haggag[25]. A commonly used mechanical prosthesis, the Björk-Shiley monostrut is shown in Figure 1.3. It is typical of mechanical prostheses in that it consists of a rigid fabric-covered ring supporting a restraining mechanism inside which is a free-floating occluder.

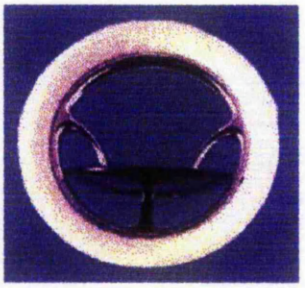

Figure 1.3: Tilting disc heart valve.

The principal advantages of mechanical prostheses are that they provide long term durability and consistency in manufacture in a range of sizes. However they are not free from disadvantages:

- require anticoagulation treatment,
- can produce unacceptable noise,
- flow characteristics can cause thrombus and haemolysis.

1.3 Dynamics Of The Cardiovascular System

In order to understand more fully some of the advantages and disadvantages of the various valves it is necessary to look further at their environment. The following sections describe the biological systems associated with heart valve prostheses. These systems include the circulatory system, the dynamics of the cardiac cycle and the properties and constituents of human blood.

1.3.1 Circulatory System

The circulatory system is the means by which every cell in the body receives a continuous supply of blood. The blood carries nutrients and oxygen to the cells, and removes waste products and carbon dioxide. The pumping action of the heart ensures a flow of blood through the blood vessels. The blood vessels form an extensive network of elastic tubes that reach all parts of the human body. The circulatory system is formed by two distinct systems, Figure 1.4 shows the basic components of the circulatory system.

Pulmonary System

Deoxygenated blood from the body flows into the right atrium and passes through the triscupid valve into the right ventricle which contracts forcing blood into the pulmonary artery. The artery is divided and carries blood to right and left lungs. Within the lungs the

artery breaks up into numerous smaller arteries, then into arterioles and finally into pulmonary capillaries which surround the alveoli in the lungs' tissue. Here the blood gives up carbon dioxide and absorbs oxygen. The pulmonary capillaries unite to form veins and the blood is then returned to the heart by the four pulmonary veins which empty into the left atrium. This blood then enters the left ventricle which contracts forcing the blood into the aorta to begin the systemic circulation cycle.

Systemic System

Oxygenated blood leaves the left ventricle via the aorta This branches into smaller arteries which carry the blood to all the organs and tissue within the body. These arteries sub divide repeatedly until the arterioles are reached. Arteries have muscular walls which, together with varying channel diameter, allow the arterial blood pressure and capillary blood flow to be maintained. The capillaries have thin walls so that exchange can take place between the plasma and the interstitial fluid. The oxygen held within the red blood cells is given up and carbon dioxide is absorbed. The capillaries unite to form larger vessels called venules which in turn become veins and carry the blood back to the heart. The veins join before the heart to form two trunks, the inferior vena cava which collects blood from the trunk and lower extremities, and the superior vena cava which collects blood from the head and upper extremities. Both these vessels enter the right atrium, from where the blood enters the right ventricle which contracts to start the pulmonary circulation cycle.

1.3.2 Blood Vessels

The vessels that carry blood vary in size and composition. Near the heart the vessels are large and elastic, and the ability of these vessels to distend and contract evens out the pressure pulses developed by the heart. Resistance vessels control the blood flow at a more intimate level. Muscular arterioles and precapillary sphincters provide the principal resistance to blood flow and it is this which governs pressure in the arterial tree.

Exchange vessels are capillaries often composed of a single wrapped cell. Across the walls of these vessels occurs an exchange between blood and tissue fluids of oxygen, carbon dioxide, nutrients, water, inorganic ions, vitamins, hormones, metabolic products, and immune substances. The shape of capillaries can vary from plain to sinusoidal in order to slow blood flow. Capacitance vessels are found after the capillaries where blood is collected in venules which are tributaries of veins. These vessels provide a low pressure blood reservoir through which blood returns to the heart.

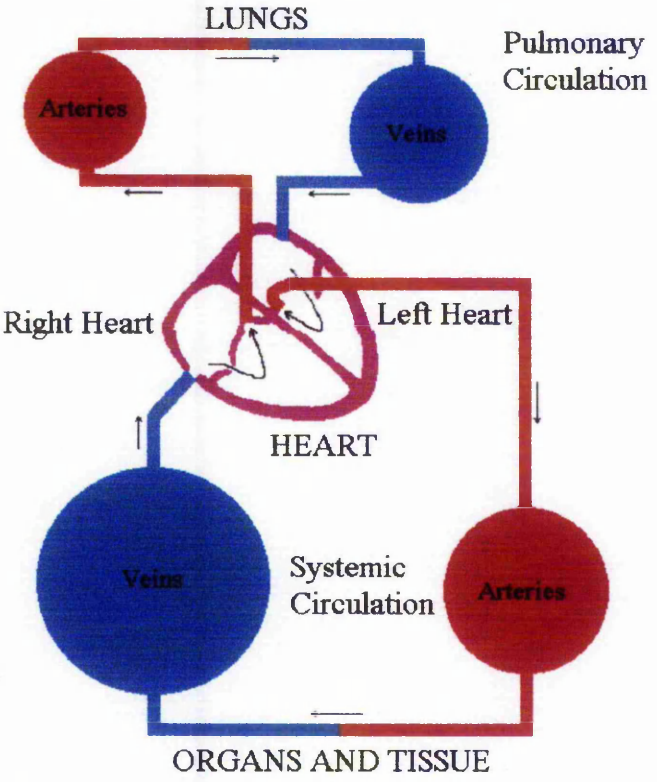

Figure 1.4: Main components of the circulatory system.

1.3.3 The Human Heart

The heart is a hollow, muscular organ, approximately the size of a man's fist, weighing about 0.5 kg and located behind the breastbone, towards the left side of the chest. The major components of the heart can be seen in Figure 1.5. The heart is divided by a septum into two sides, right and left, and no communication exists between these two sides after birth.

Each side of the heart is further subdivided into two chambers, an upper chamber or atrium, and a lower chamber or ventricle. The atria and ventricles communicate with one another by means of the atrio-ventricular openings. Unidirectional flow is maintained by the triscupid valve (right side) and the mitral valve (left side). The triscupid valve is composed of three cusps and the mitral two cusps. Within the heart papillary muscles are attached to the cusps by chordae tendineae to act as shock absorbers when the cusps snap shut. The chordae act like parachute cords to prevent the cusps everting and allowing gross leakage.

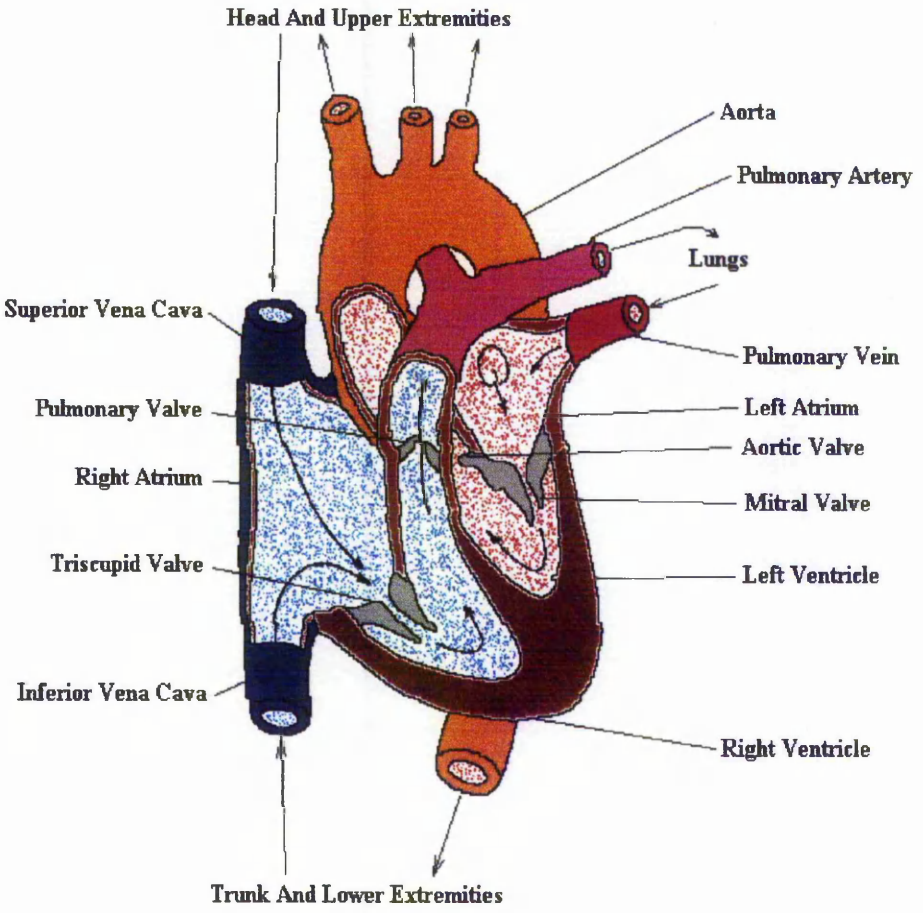

Figure 1.5: The major components of the human heart.

The heart's action originates in the sino-atrial node as an electrical impulse which causes the atria to contract. The electrical impulse then moves around the ventricles causing them to

contract; the action of contraction is known as systole. For the atria this period is short but for the ventricles it is longer (0.3 s) and more powerful as the ventricle is required to force the blood throughout the body. After contraction a relaxation or diastole occurs within the atria and ventricles, with the ventricular diastole continuing over a period of 0.5 s. At the exit of the ventricles are semilunar valves, namely the aortic valve (left side) and pulmonary valve (right side). These valves prevent backflow into the ventricles. During rest the heart beats approximately 70 times per minute pumping a total of 5 litres of blood every minute. The dynamics of each heart beat are as follows:

> During diastole the atria fill with blood, once filled they experience contraction. Contraction starts at the top and travels down to the lower parts of the ventricles. The pressure in the atria is initially higher than that in the ventricles causing the mitral and triscupid valves to open and force blood into the ventricles. The pressure in the lower chambers grows and when ventricular pressure exceeds that of the atrium the mitral and triscupid valves shut to prevent blood from flowing back into the atria. The ventricles, now filled with blood, contract and eject blood through the semilunar valves into the aorta and pulmonary artery. The atria, meanwhile, re-enter diastole and are refilled with blood. The arterial pressure grows greater than the falling pressure of the ventricles and the semilunar valves shut. The ventricles then await the next batch of blood from the atria.

1.4 Characteristics Of Blood

Blood consists of a plasma base in which a number of different cells and proteins are suspended. The effect of this disperse system is to cause blood to flow as a 'pseudo-plastic' with viscosity increasing with decreasing shear rate. The following section will describe the components which make blood.

Erythrocytes, Red Blood Cells (RBC)

These form the bulk of blood cells. Their primary function is to carry oxygen suspended in haemoglobin which forms the contents of the flexible membrane of the RBC, as shown in Figure 1.6.

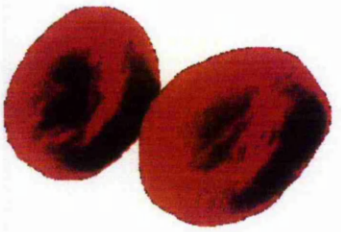

Figure 1.6: Red blood cells.

The cells are circular bi-concave discs approximately 8×2 μm, seen singly in the form of a pale buff colour but in masses appearing red. RBCs originate in the bone marrow, especially in that of the short, flat, and irregular bones, in the cancellous tissue at the ends of the long bones and in the marrow in the shafts of the ribs and in the sternum. While developing in the bone marrow the cells pass through several stages of growth. Initially the cells are large containing a nucleus but no haemoglobin; they are then charged with haemoglobin and finally lose their nucleus and then pass out for circulation in the blood. The average life of a RBC is 120 days, at the end of which they are disintegrated in the reticuloendothelial system, principally the spleen and liver. The 'globin' of the haemoglobin is broken down into amino-acids to be used as protein and the iron in the 'haemo' is removed for use in the formation of future RBCs. Figure 1.7 shows the complete life cycle of RBCs.

The concentration of RBC is approximately 5×10^{12} per litre of blood. Expressed as a percentage by volume, haematocrit (H) is typically 42-45%. This concentration can vary from 21% (anaemia) to 75% (polycythaemia). Due to the high content of erythrocytes in blood they have a greater influence on blood viscosity than any other constituent.

Leukocytes, White Blood Cells

These cells are transparent and are larger and fewer than RBCs. There are five types of leukocytes whose primary function is the destruction of infection by phagocytic action. Polymorphonuclear cells form about 75% of the total white cell count. They are formed in the red marrow of bone and contain a many-lobed nucleus with granular protoplasm.

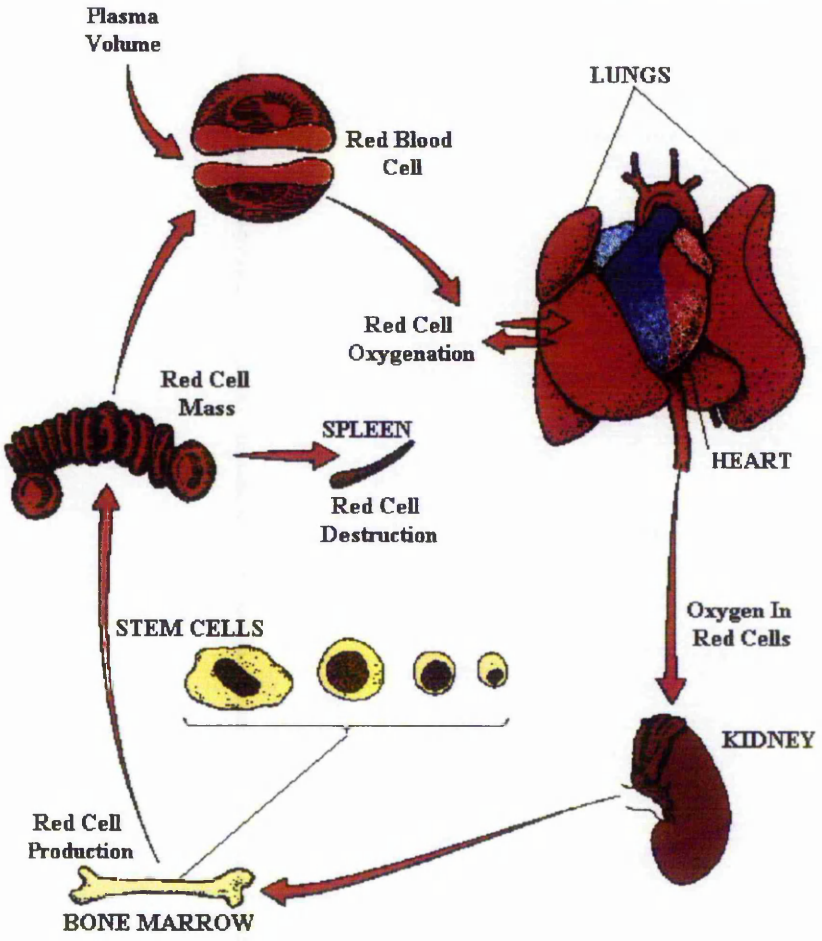

Figure 1.7: Life cycle of red blood cells.

There are three types of polymorphonuclear cells, neutrophils, eosinophils and basophils, all of which are 9.4 μm in diameter. Lymphocytes are the second largest sub group forming 25% of the total white cell count. They develop in the lymph glands, spleen, liver and lymphatic tissue as well as the bone marrow. The cells are non-granular and have no power

of amoeboid movement. They are smaller in size than polymorphonuclear cells with a diameter of 7.4 μm. Monocytes are a sub set of lymphocytes, making up about 5%. These cells are larger, with a diameter of 9.4 μm with the ability of amoeboid movement and are phagocytic in action. They constitute only a small fraction of total blood cells, 7.33×10^{9} per litre, and their removal has no significant effect on the viscosity of blood.

Platelets

Platelets stimulate the clotting of blood. It is usual to remove platelets from blood samples before *in vitro* testing. Removal of platelets cause only a slight reduction in the overall viscosity of blood. The concentration of platelets is 300×10^{9} per litre of blood.

Plasma

Plasma is an aqueous solution containing mainly organic compounds such as proteins, lipids, amino acids, glucose, etc. Plasma acts as a medium for the transport of nutrients, salts, fats, glucose and amino-acids to the tissues, and to carry away waste materials. These constituents not only affect plasma viscosity but also the viscosity of whole blood.

1.5 Haemodynamic Factors

Two main consequences exist with the implantation of valve prostheses, namely haemolysis and thrombosis.

Haemolysis

Haemolysis is the destruction of RBCs and is associated with the loss of haemoglobin into the plasma. In normal conditions most of the haemoglobin is contained within the RBC with only a small quantity being contained within the plasma. Under certain circumstances haemoglobin may escape from a RBC and enter the plasma causing a colour change to the

plasma. If the rate of destruction, possibly due to a malfunctioning valve prosthesis, exceeds the rate of RBC production by the bone marrow a condition known as haemolytic anaemia will result. This, however, is rare.

Thrombosis

Thrombosis is the aggregation of platelets, RBCs, leukocytes, and fibrin into a mass. Examination of thrombus shows blood cells entangled in fibrin threads. Four factors are necessary to induce thrombosis:-

1. Calcium salts present in blood.
2. Cell injury producing thromboplastin.
3. Thrombin which formed from prothrombin in the presence of thromboplastin.
4. Fibrin formed from fibrinogen in the presence of thrombin.

These clots may form at the blood/tissue or blood/prosthesis interface and can become detached causing interference with the body's organs, i.e. blocking vessels and hence restricting blood flow. This phenomenon is known as thrombo-embolism.

Clinical experience has shown that there are well defined consequences that must be addressed when designing or even choosing a prosthesis.

i) Bulk Shear Stress

The destruction of erythrocytes, causing haemolysis, in bulk flow is dependent upon the magnitude and duration of high in-bulk shear stress. A number of researchers, e.g. Blackshear[26], Williams[27], and Rooney[28], estimate the relationship between in-bulk shear stresses and duration of exposure. Hellmus and Brown[29] use a threshold, for haemolysis, of 500 N/m^2 applied for a duration atleast of 1×10^{-3} s. This is representative of the 'flight time'

of a blood cell through a valve prosthesis. They also concluded that the levels of shear stress to induce haemolysis could be found in normal valve prostheses.

ii) Shear Stress At The Prosthetic Wall

The value of shear stress to cause cell damage at the prosthesis surface is much lower than in the case above. Shear stress values below 150 N/m^2 can cause haemolysis. The mechanisms involved to induce this haemolysis are not fully understood. There have been a number of investigations into this phenomenon by examining the effect of surface roughness (Bacher and Williams[30]), the properties of the material that form the surface of the prosthesis (Lampert and Williams[31] and Monroe et al.[32]), and haemolysis at wall contact (Wielogorski et al.[33]). Blackshear[34] presents the argument that additional stresses are encountered as erythrocytes adhere to, and are then torn from, the prosthetic surface and also that high shear stresses near a prosthetic surface increase the cell contact and hence the risk of haemolysis.

iii) Endothelium Damage Due To Jet Impingement

This type of damage occurs when a prosthesis causes a strong jet of blood to be directed into a blunt impact with the vessel wall. As reported by Fry[35], it begins to occur at shear stresses as low as 40 N/m^2, with steady erosion of the cells occurring at a higher shear stress of 90 N/m^2. This particular flow characteristic is highly dependent on the geometry of the valve prosthesis. Dewey *et. al.*[36] and Nerem *et. al.*[37] show that changes to the endothelium cell orientation and regeneration can occur at shear stress values of as little as 0.5 N/m^2.

iv) Thrombus

Thrombus can form in areas of haemostasis or low shear rate. Evidence shows (Nunez et al.[38], Aston and Mulder[39], Narducci et al.[40], etc) that thrombus can form at critical sites

severely affecting the performance of the valve by restricting occluder movement. Dintenfass[41] brings to the attention a critical lower shear rate, 7 s^{-1}, below which clotting can be accelerated by a factor of a thousand. Thrombosis can also occur at higher shear rates as the aggregation of cells takes place in eddies, an environment where the contents are damaged erythrocytes. The ability to model the development of thrombus growth within a computational model is discussed in Section 4.3.

The consequences mentioned above can exist within the flow regime of any valve prosthesis. It is the responsibility of the valve designer to ensure that the threshold values are not present, thus reducing the risk of haemolysis and thrombus. Experimental *in vitro* methods are available to measure flow parameters, such as velocity, pressure, shear stress, and turbulence intensity. These parameters can also be found through computational analysis for both steady and time-dependent flow regimes.

Chapter Two

Blood Rheology

2.1 Introduction

The purpose of this chapter is to describe the non-Newtonian nature of blood. It has been found that in *in-vivo* blood flows, where the average shear rate exceeds 100 s^{-1}, blood can be modelled as a Newtonian analogue fluid[42]. In a cylindrical flow section shear rates will vary radially, with a zero value at the flow axis and maximum value close to the wall.

The CFD package PHOENICS[43] was used to simulate blood flow through a conduit valve using various mathematical blood models. The results of this analysis (Section 2.4) show variations in flow characteristics between the Newtonian and non-Newtonian blood models.

The CFD models in this chapter and further chapters assume blood to be a continuum and its average rheological properties are taken to be universally applicable for both Newtonian and non-Newtonian flows.

2.2 Non-Newtonian Nature Of Blood

The rheological behaviour of blood can be characterised by a shear rate dependent non-Newtonian viscosity and its viscoelasticity[44]. It is argued that erythrocytes have a greater influence on the viscosity of blood than any other constituent. Two possible ways erythrocyte cells influence blood viscosity are:

a) *Rouleaux formation*: Work in this area[45,46] has shown that the breakdown of rouleaux, normally aggregations of 6-10 erythrocytes, causes the non-Newtonian behaviour of blood. The aggregation of several rouleaux can also occur, known as secondary aggregation.

b) *Erythrocyte deformation*: The above hypothesis is not agreed on by other researchers[47]. They state the non-Newtonian behaviour of blood is caused by

absorption of energy by erythrocytes as they deform. It has been shown that shear thinning is reduced in suspensions of hardened cells.

Other research[48-50] has shown that viscosity changes occur because of both the mechanisms mentioned above, i.e. aggregation of cells at low shear rates and cell deformation at higher shear rates.

2.3 Review Of Blood Models

Blood models developed offer a means of predicting the viscosity of blood in complex flows. Two general categories exist into which the blood models can be placed, i.e. heterogeneous and homogeneous.

2.3.1 Heterogeneous Blood Models

In vessels with a diameter of less than 0.5 mm blood can no longer be considered a continuum. These models[50-53] will not contribute to numerical investigations, particularly in vessels with large diameters, and may produce additional uncertainties to those produced by homogeneous models.

2.3.2 Homogeneous Blood Models

It is a considerable simplification to think of blood as a homogeneous fluid but flow regimes exist in which this assumption is acceptable. A large number of viscosity models have been developed using the assumption of homogeneity. A few of the most common blood models are as follows:

1. ***Casson***[54]

$$\sqrt{\tau} = \sqrt{\tau_y} + S\sqrt{\dot{\gamma}}$$

where, $S=72.42\times10^{-3}$ Pa $s^{1/2}$

$\tau_y=2.89\times10^{-3}$ Pa

5. ***Modified Cross***[58]

$$\eta = \eta_\infty + (\eta_o - \eta_\infty)\frac{1}{\left(1+\left(\lambda\dot{\gamma}\right)^m\right)^a}$$

2. *Quemada*[55,56]

$$\eta_r = \frac{\eta_a}{\eta_p} = \left(1 - \frac{1}{200} KH\right)^{-2}$$

$$K = \frac{\eta_o \eta_\infty \alpha_o \sqrt{\dot{\gamma}}}{1 \times 10^{-3} + \left(\alpha_o \sqrt{\dot{\gamma}} / 1000\right)}$$

where, H=45
μ_o=4.33×10^{-3} Pa s
μ_p=1.26×10^{-3} Pa s
μ_∞=2.07×10^{-3} Pa s
α_o=0.73 s$^{1/2}$

3. *Power Law*

$$\tau = K\dot{\gamma}^{n}$$

$$\mu_a = K\dot{\gamma}^{n-1}$$

where, K=13.4×10^{-3} n-1
n=0.785

4. *Cross*[57]

$$\eta = \eta_\infty + (\eta_o - \eta_\infty)\frac{1}{1 + \left(\lambda\dot{\gamma}\right)^{m}}$$

where, η_∞=3.45×10^{-3} Pa s
η_o=5.6×10^{-2} Pa s
m=1.028
λ=1.007 s

where, η_∞=3.45×10^{-3} Pa s
η_o=5.6×10^{-2} Pa s
m=2.406
a=0.254
λ=3.736 s

6. *Simplified Cross*[59]

$$\eta = \eta_\infty + (\eta_o - \eta_\infty)\frac{1}{1 + \lambda\dot{\gamma}}$$

where, η_∞=5×10^{-3} Pa s
η_o=0.13 Pa s
λ=8.0 s

7. *Carreau*[60]

$$\eta = \eta_\infty + (\eta_o - \eta_\infty)\left[1 + \left(\lambda\dot{\gamma}\right)^2\right]^{\frac{n-1}{2}}$$

where, η_∞=3.45×10^{-3} Pa s
η_o=5.6×10^{-2} Pa s
n=0.3568
λ=3.131 s

8. *Carreau-Yasuda*[60]

$$\eta = \eta_\infty + (\eta_o - \eta_\infty)\left[1 + \left(\lambda\dot{\gamma}\right)^{a}\right]^{\frac{n-1}{a}}$$

where, η_∞=3.45×10^{-3} Pa s
η_o=5.6×10^{-2} P as
a=1.25
n=0.22
λ=1.902 s

The spread of predicted shear stress for a given value of shear rate is large when comparing these models, i.e. 0% for $\dot{\gamma}$ =0.1 s^{-1} to 25% for $\dot{\gamma}$ =1000 s^{-1}. A full comparison of various blood models can be obtained from Easthorpe and Brooks[61] and Tansley[62]. For shear rates greater than 100 s^{-1} the viscosity of blood can be seen to be constant, see Figure 2.1, with a value in the range of 3.323×10^{-3} to 3.5×10^{-3} Pa s. The use of non-Newtonian viscosity models in flows where the average shear rate exceeds 100 s^{-1} might seem

unnecessary, therefore, as the variation in predicted viscosity against shear rate is small. However, within these flows areas of low shear rate occur in which the viscosity will vary considerably producing variations in the predicted dependant variables (pressure and velocity).

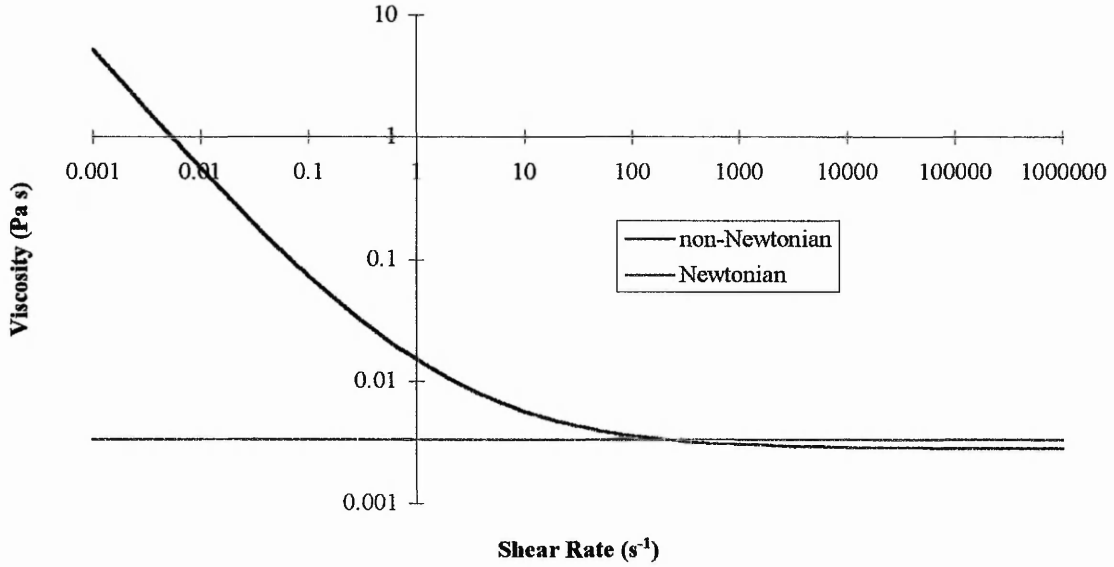

Figure 2.1: Viscosity-Shear rate relationship.

2.4 CFD Investigation On The Effects Of Using Various Blood Models On Flow Through A Gentle Conduit Valve

CFD investigation was undertaken to analyse the effects of a number of blood models, i.e. Casson[54], Quemada[55,56], Power Law, Cross[57], Modified Cross[58], Carreau[60], and Carreau-Yasuda[60] on the flow through a Gentle conduit valve prosthesis to determine if the non-Newtonian viscosity of blood should be taken into account when modelling flow through a prosthetic heart valve and, if so, which model should be used. Three flow conditions were considered: two laminar flows, based on Reynolds numbers of 1000 and 4000, and one turbulent flow, based on a Reynolds number of 8000. The density of blood was assumed to be 1056.17 kg/m^3 and the Reynolds number was calculated using a dynamic viscosity of 3.323×10^{-3} Pa s and an inlet diameter of 20 mm. A Body Fitted Co-ordinate (BFC) grid was generated to represent the valve geometry and the governing equations

solved using the CFD package PHOENICS. Convergence was satisfied when the residuals for velocity and pressure fell below 1×10^{-7}. For each model the velocity, pressure, shear stress and shear rate were recorded.

2.5 Results From Flow Analysis

The following sections summarise the results from the CFD analysis. The results presented include flow velocities, shear stress distribution, shear rate distribution, pressure drop and fluid forces acting on the occluder.

2.5.1 Flow Velocities

The following figures show velocity contours within the finite volume domain. Figures 2.2-2.9, 2.10-2.17 and 2.18-2.25 are for flows with Reynolds numbers of 1000, 4000 and 8000 respectively. The unit of velocity within the figures is m/s.

i) Reynolds Number Of 1000

In general all the models exhibit the same basic flow patterns. As the fluid flows through the diverging section of the valve it accelerates to form a jet within the converging outlet section. This jet persists into the outlet section of the models where it begins to decay due to viscous dissipation. Downstream and close to the occluder an area of either stasis or recirculation can be found. The peak velocities for the models lie within the range of 0.23 and 0.25 m/s with only the Power Law (Figure 2.5) and Carreau-Yasuda (Figure 2.9) models showing an area of stasis behind the occluder, the other models all showing recirculation

ii) Reynolds Number Of 4000

The flow patterns found within these models at this Reynolds number are similar to the

ones described above with the exception that behind the occluder only areas of recirculation can be found. The maximum velocities range from 0.83 to 0.91 m/s. The jets formed in the outlet section of the valve extends a greater distance into the outlet where it decays less rapidly. The Power Law (Figure 2.13) and Carreau-Yasuda (Figure 2.17) models now show an area of recirculating flow comparable to the other models.

ii) Reynolds Number Of 8000

The flow patterns again are very similar to the previous two models showing that there is no fundamental difference between the laminar and turbulent cases. The peak velocities vary between 1.61 and 1.69 m/s. The convergent inlet section is now almost filled entirely by accelerating flow and the width of the free stream jet in the outlet section has also increased. Recirculation exists in all models except the Quemada model (Figure 2.20) where an area of stasis is present.

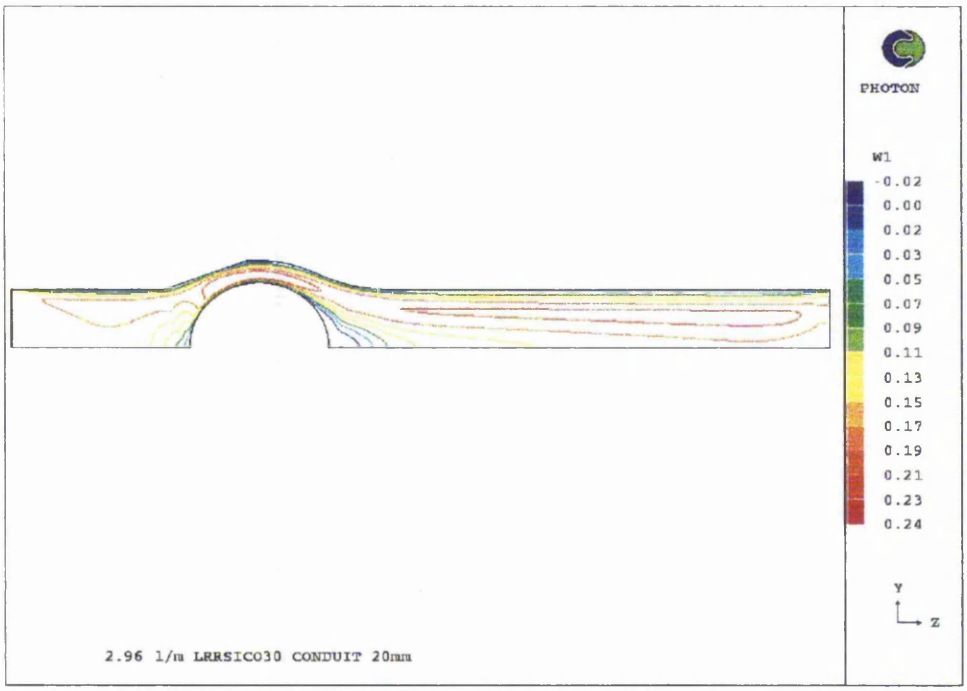

Figure 2.2: Newtonian model, Re 1000.

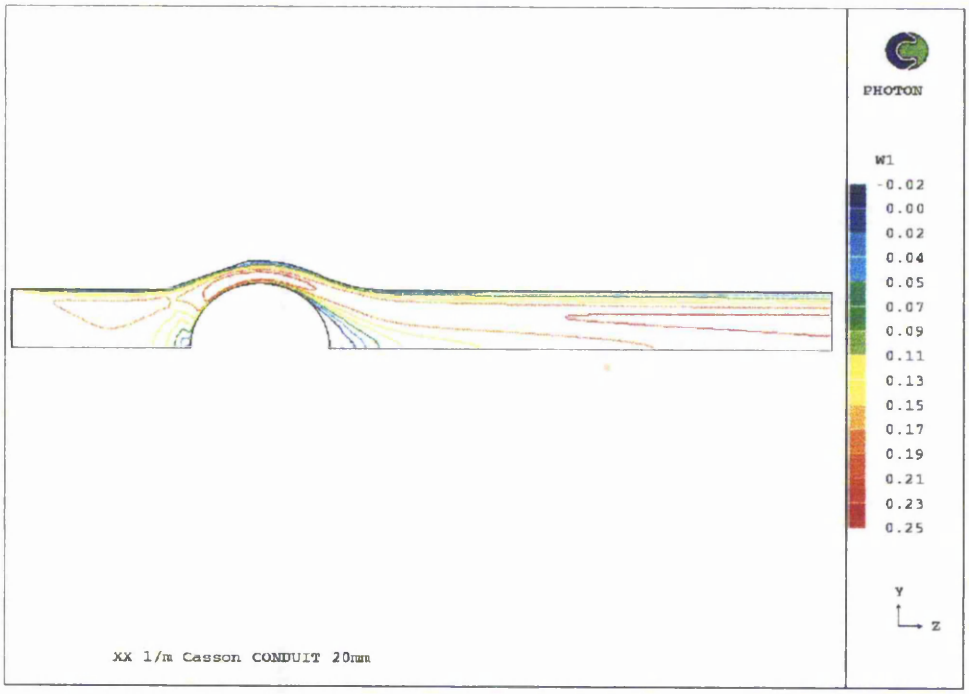

Figure 2.3: Casson model, Re 1000.

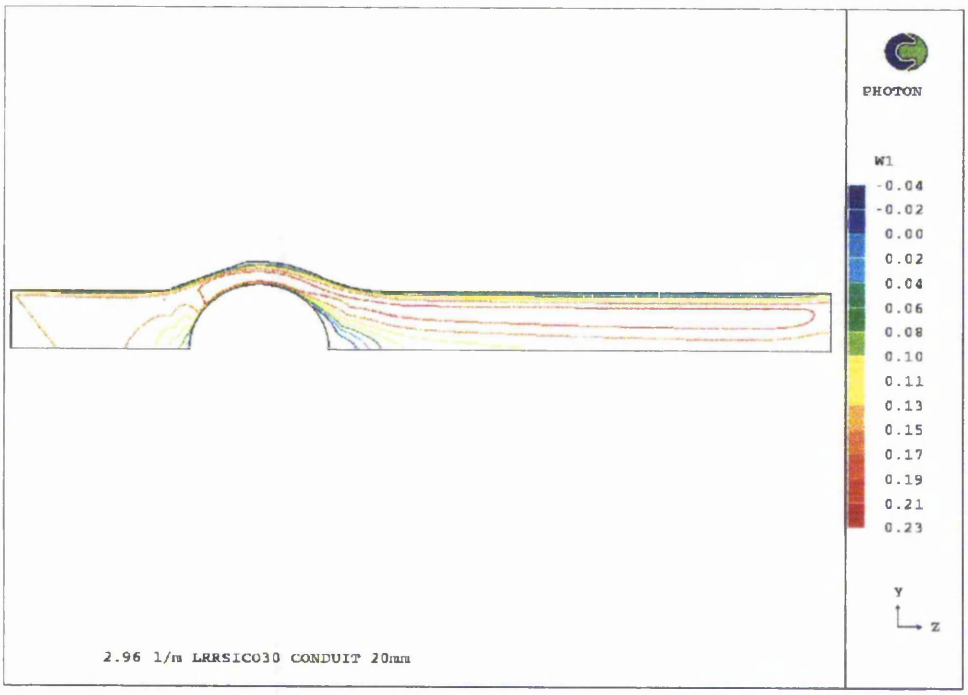

Figure 2.4: Quemada model, Re 1000.

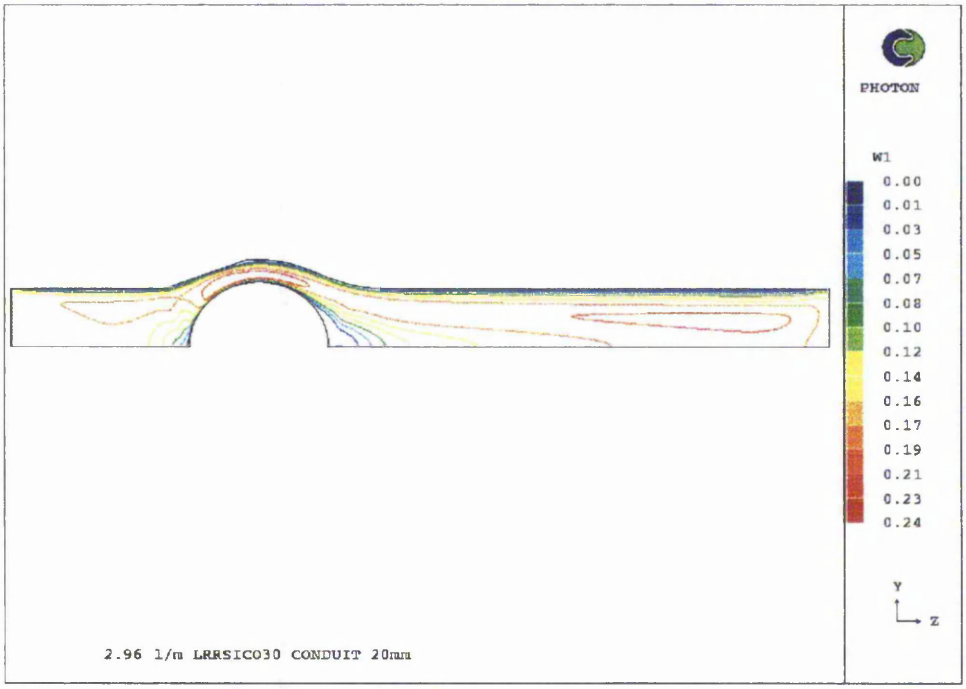

Figure 2.5: Power Law model, Re 1000.

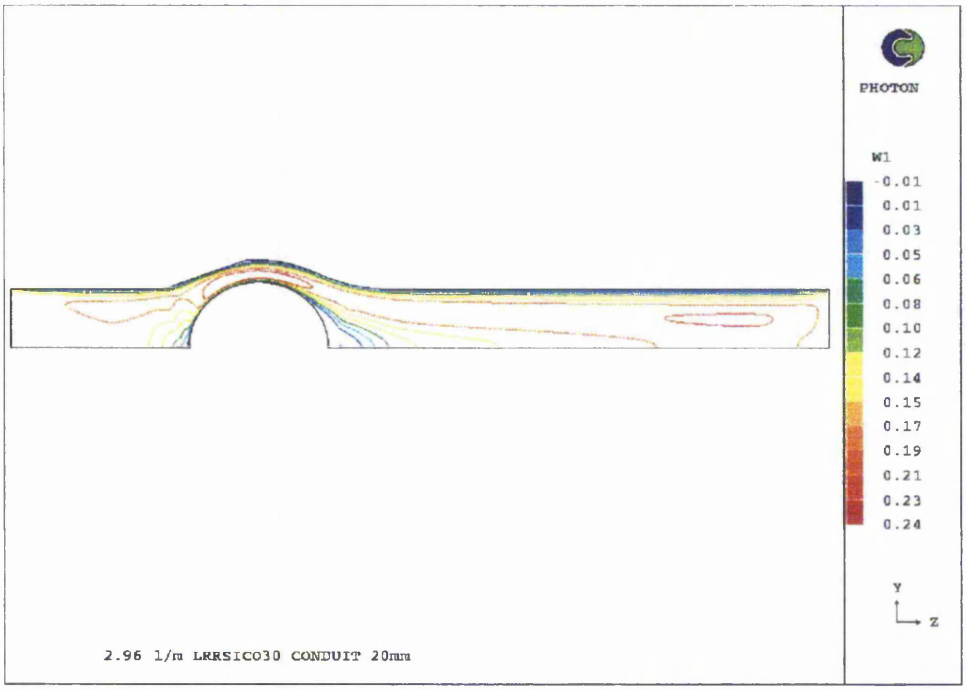

Figure 2.6: Cross model, Re 1000.

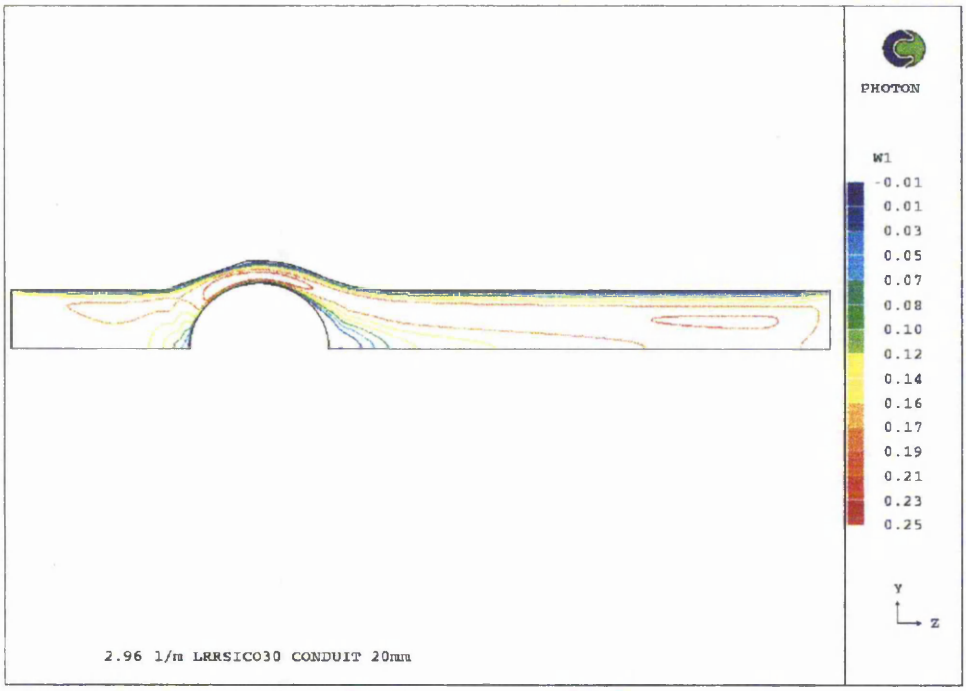

Figure 2.7: Modified Cross model, Re 1000.

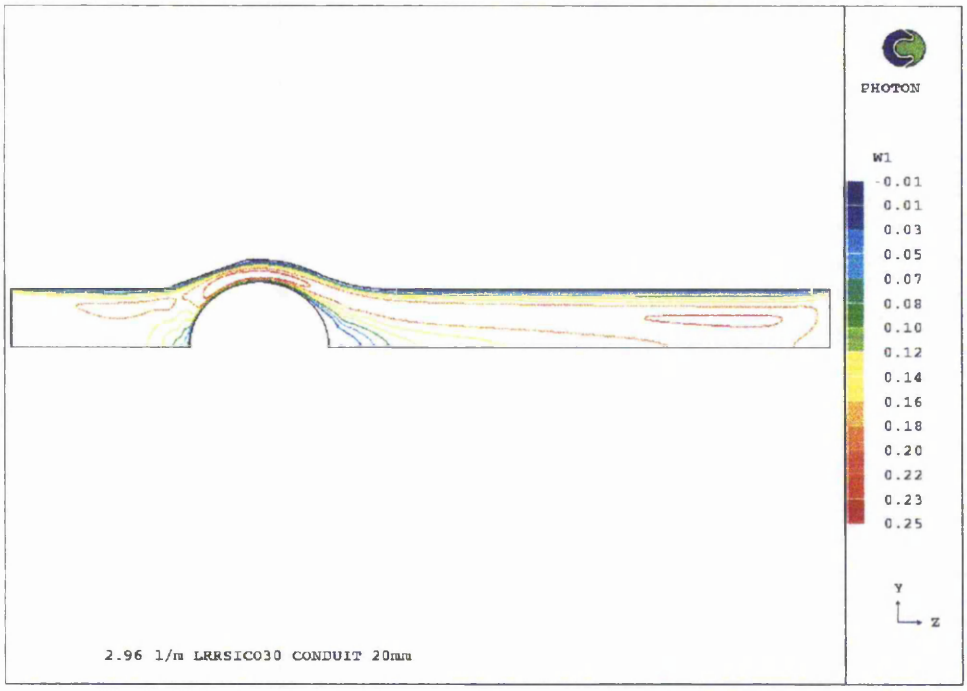

Figure 2.8: Carreau model, Re 1000.

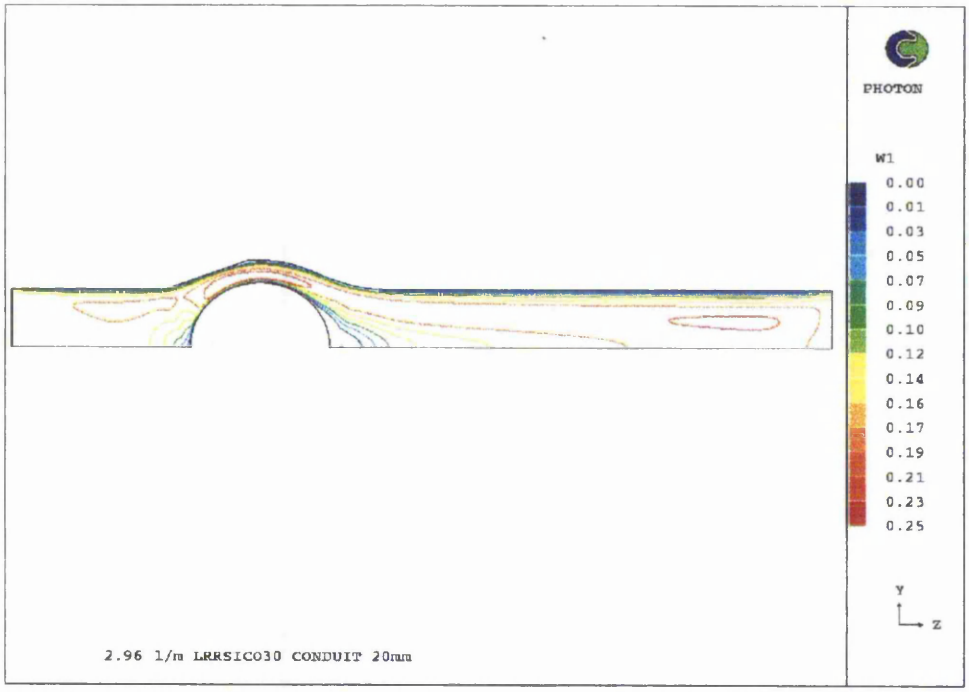

Figure 2.9: Carreau-Yasuda model, Re 1000.

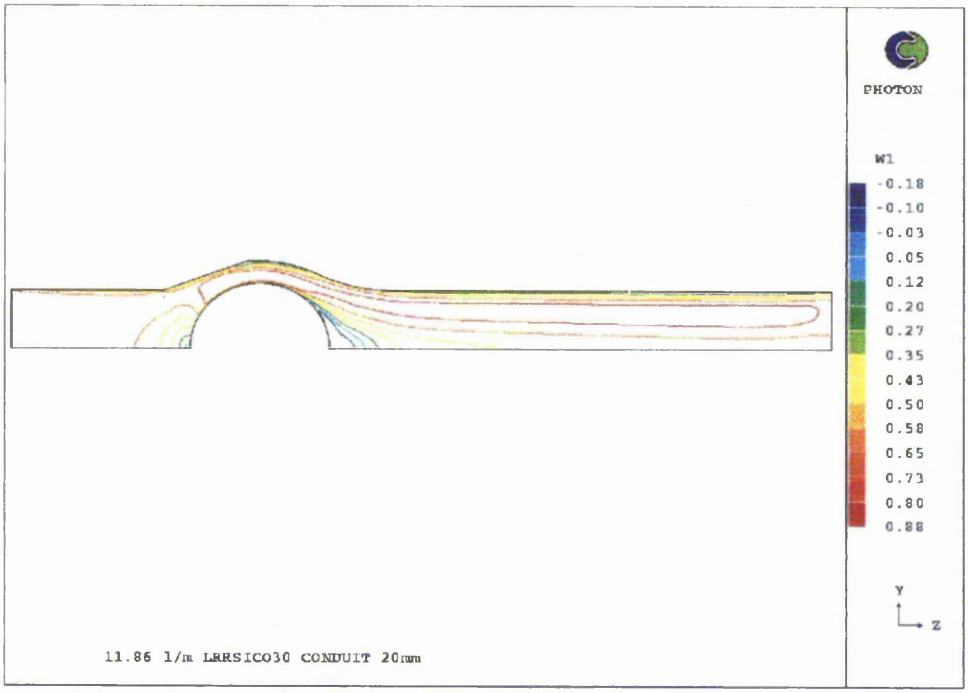

Figure 2.10: Newtonian model, Re 4000.

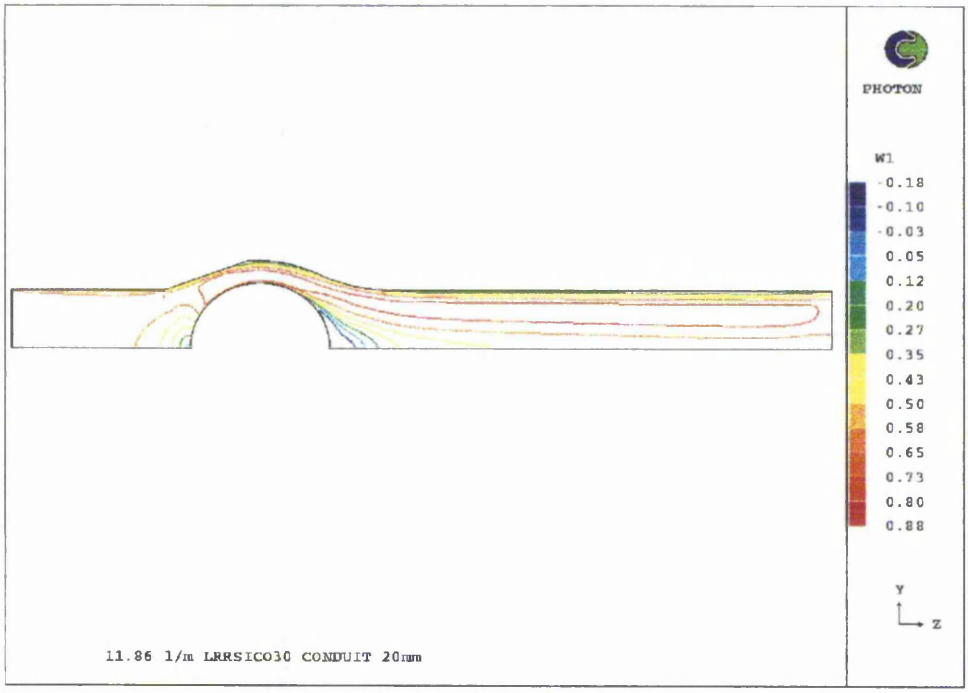

Figure 2.11: Casson model, Re 4000.

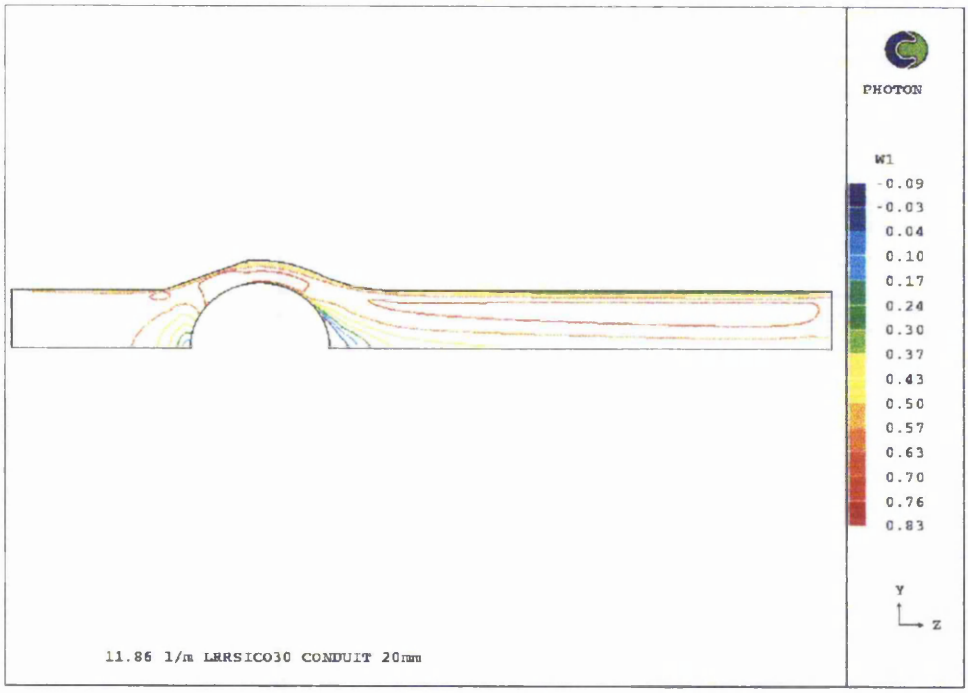

Figure 2.12: Quemada model, Re 4000.

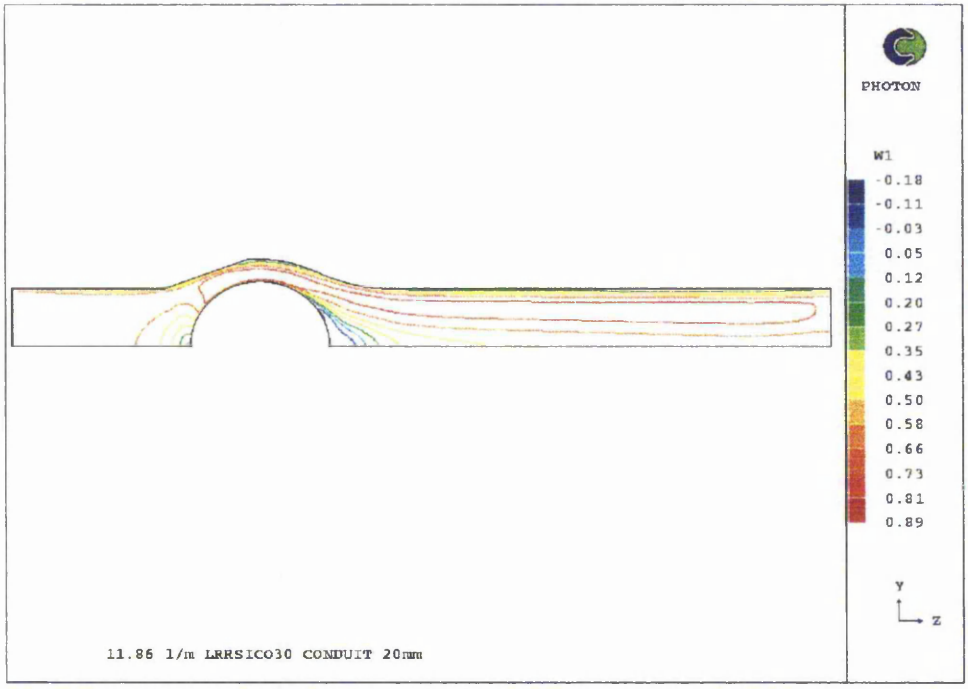

Figure 2.13: Power Law model, Re 4000.

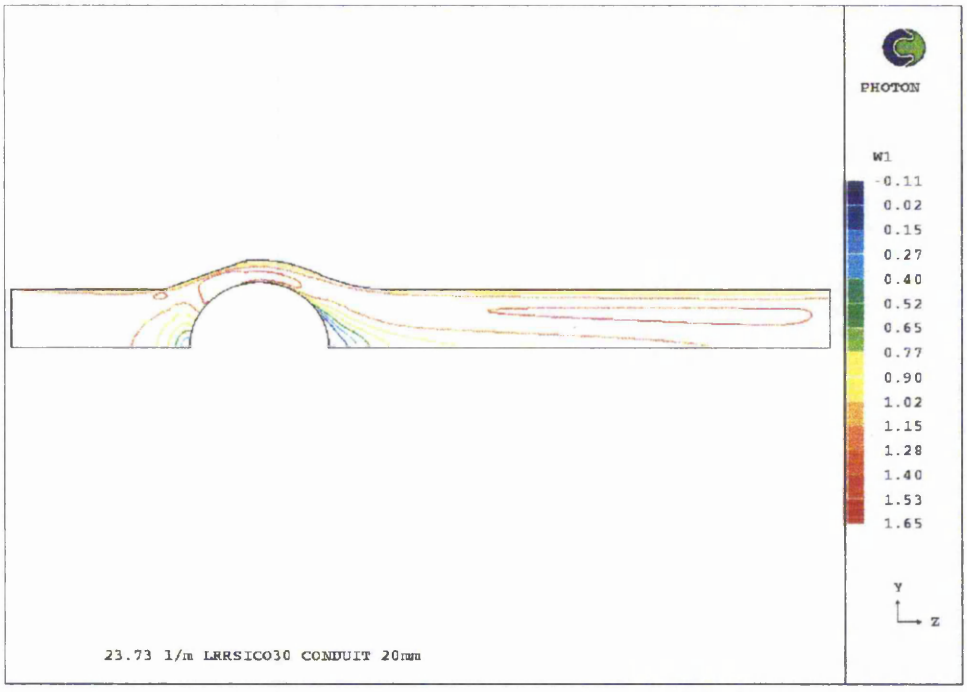

Figure 2.14: Cross model, Re 4000.

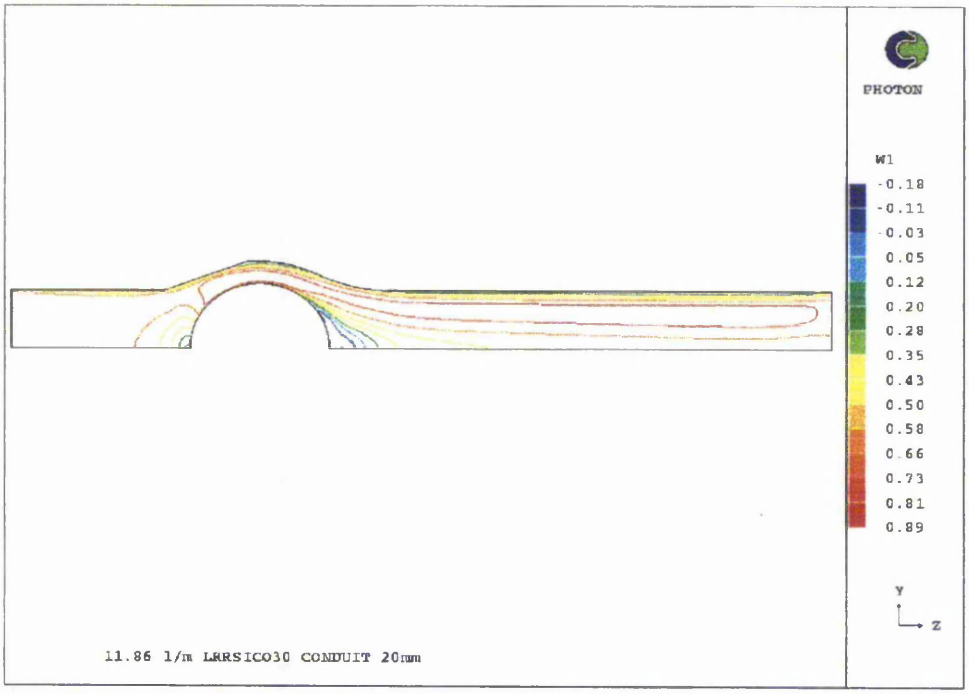

Figure 2.15: Modified Cross model, Re 4000.

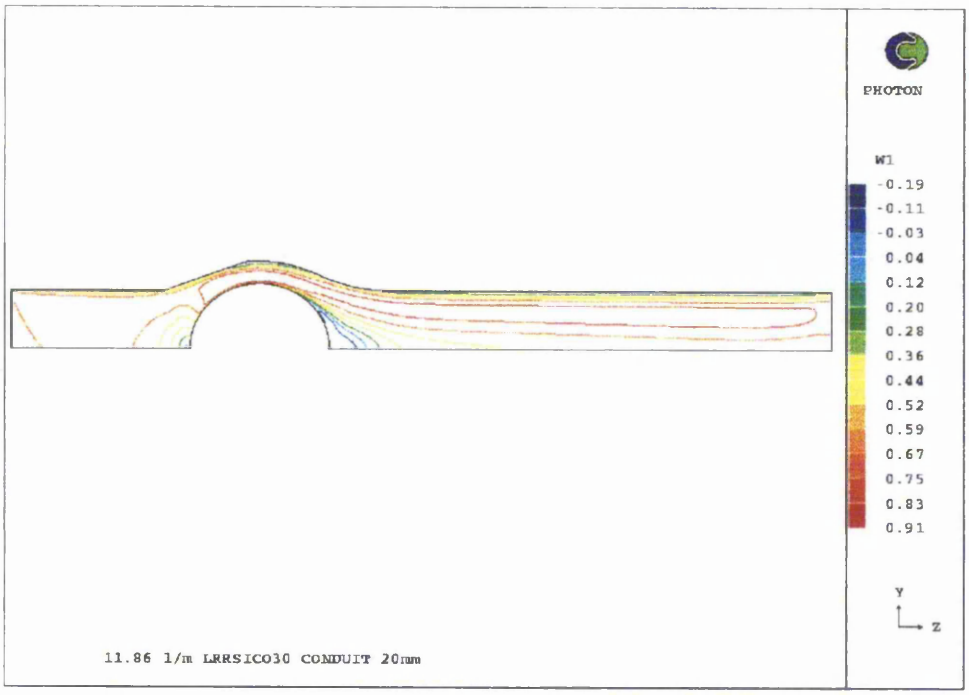

Figure 2.16: Carreau model, Re 4000.

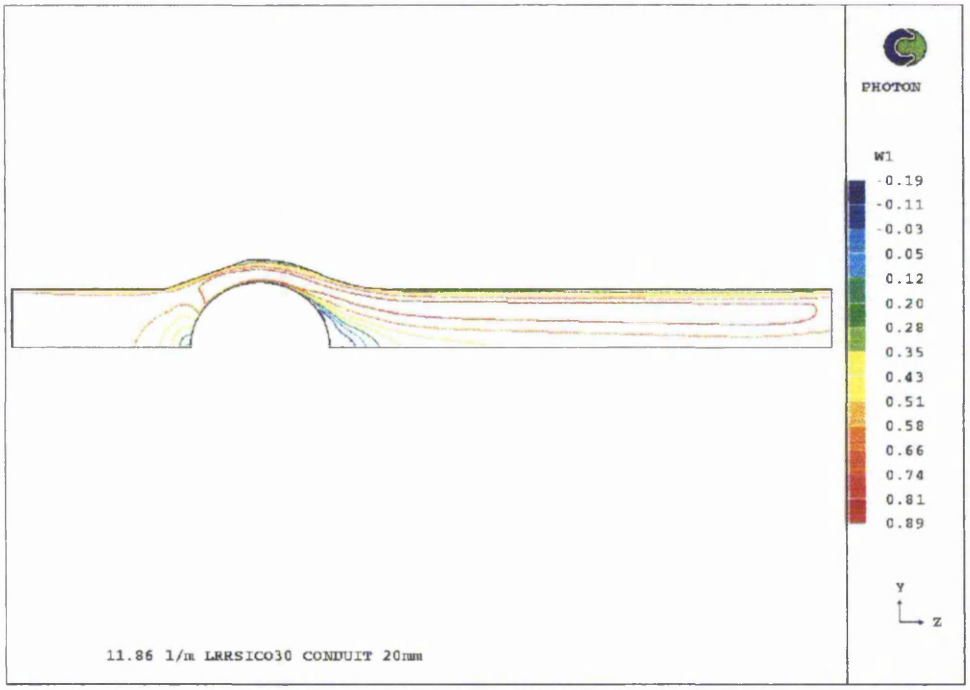

Figure 2.17: Carreau-Yasuda model, Re 4000.

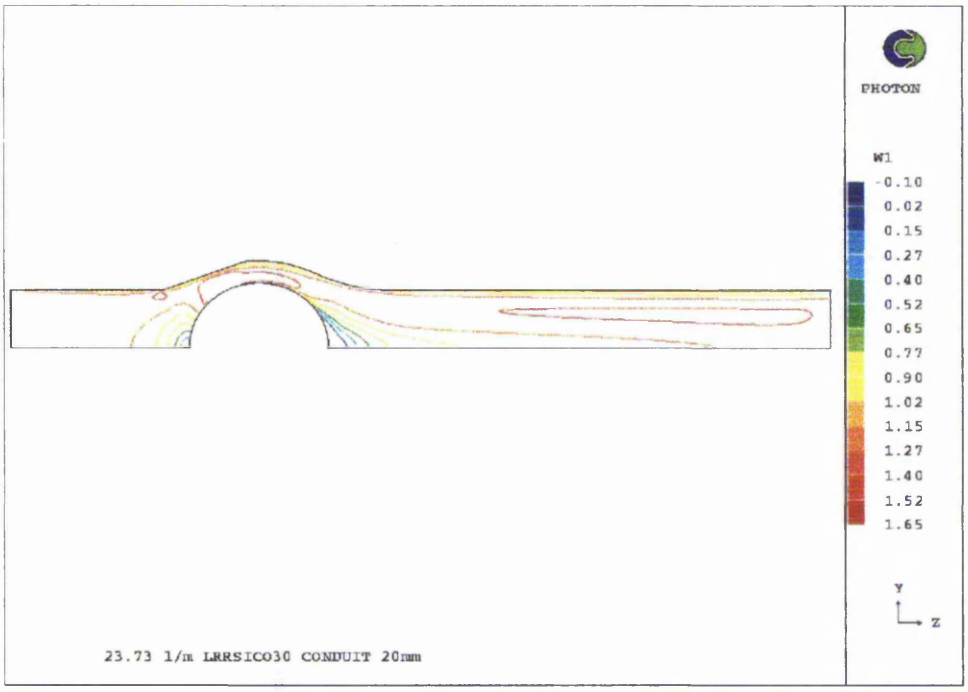

Figure 2.18: Newtonian model, Re 8000.

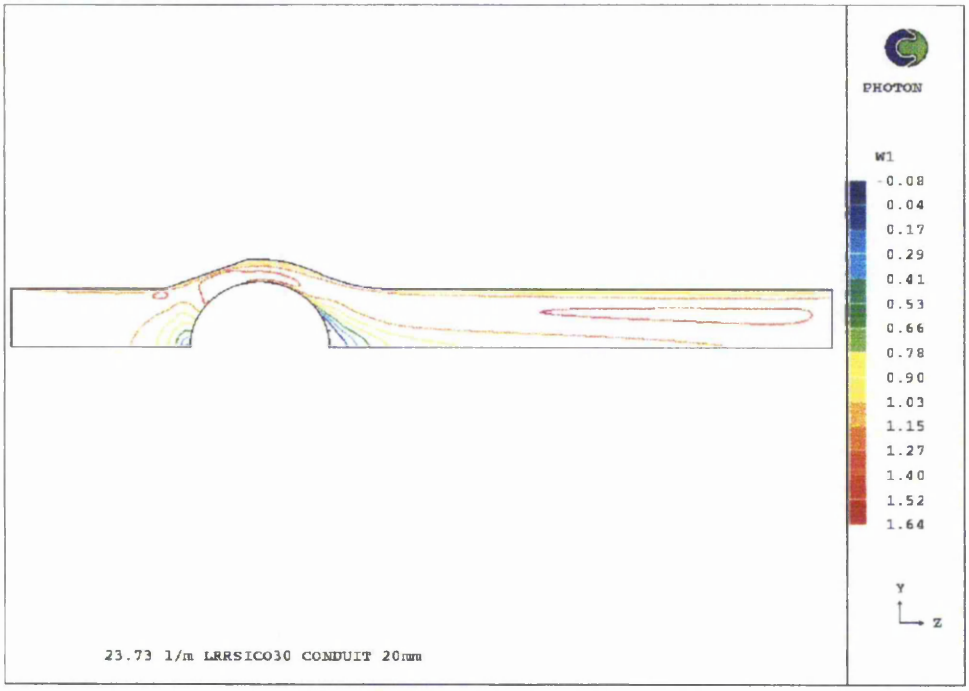

Figure 2.19: Casson model, Re 8000.

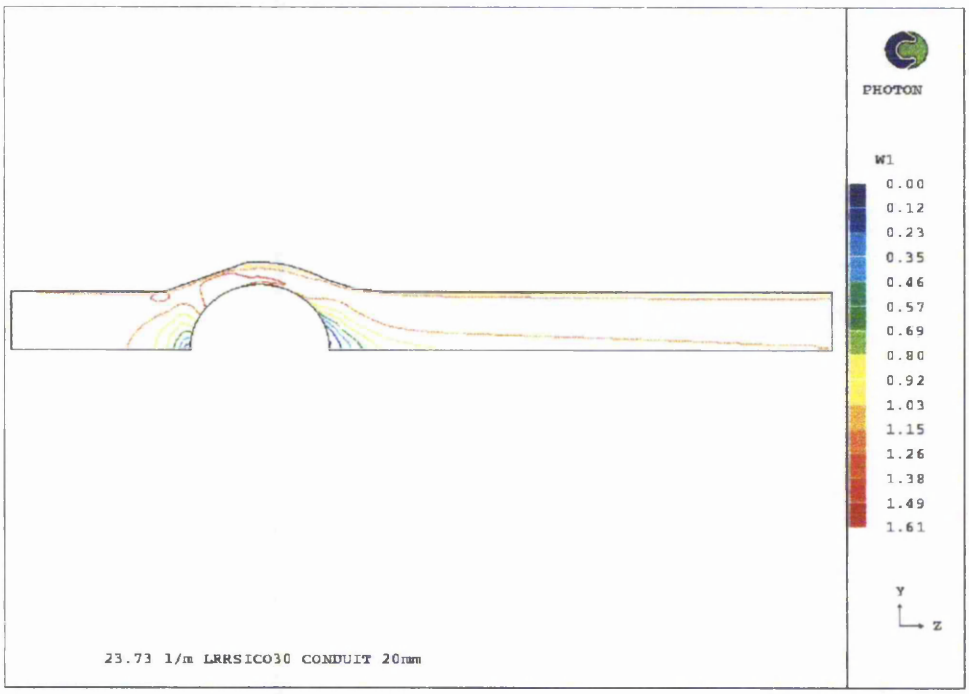

Figure 2.20: Quemada model, Re 8000.

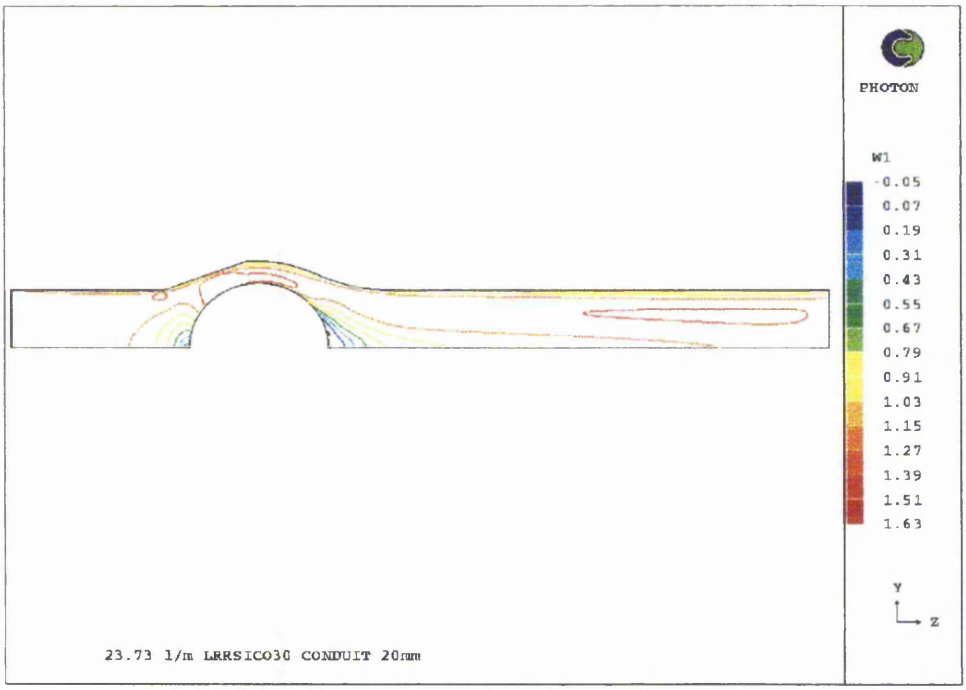

Figure 2.21: Power Law model, Re 8000.

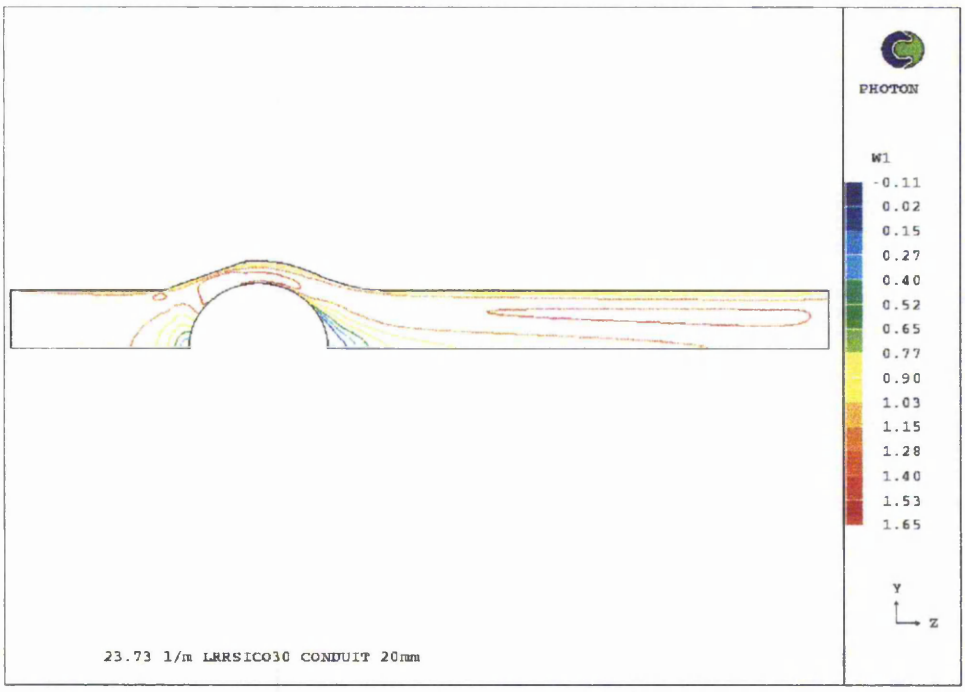

Figure 2.22: Cross model, Re 8000.

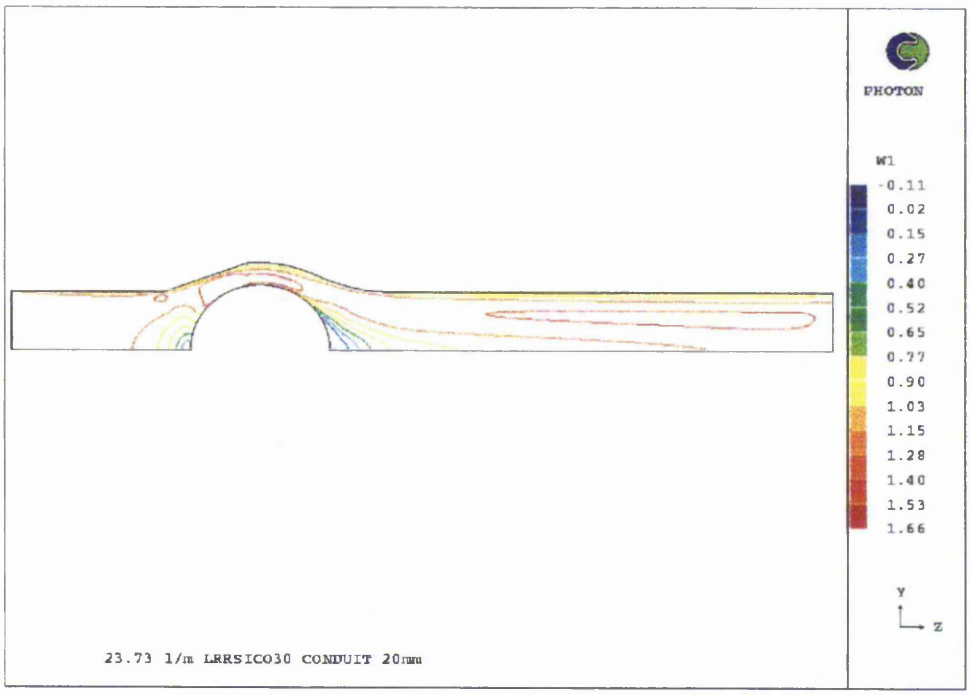

Figure 2.23: Modified Cross model, Re 8000.

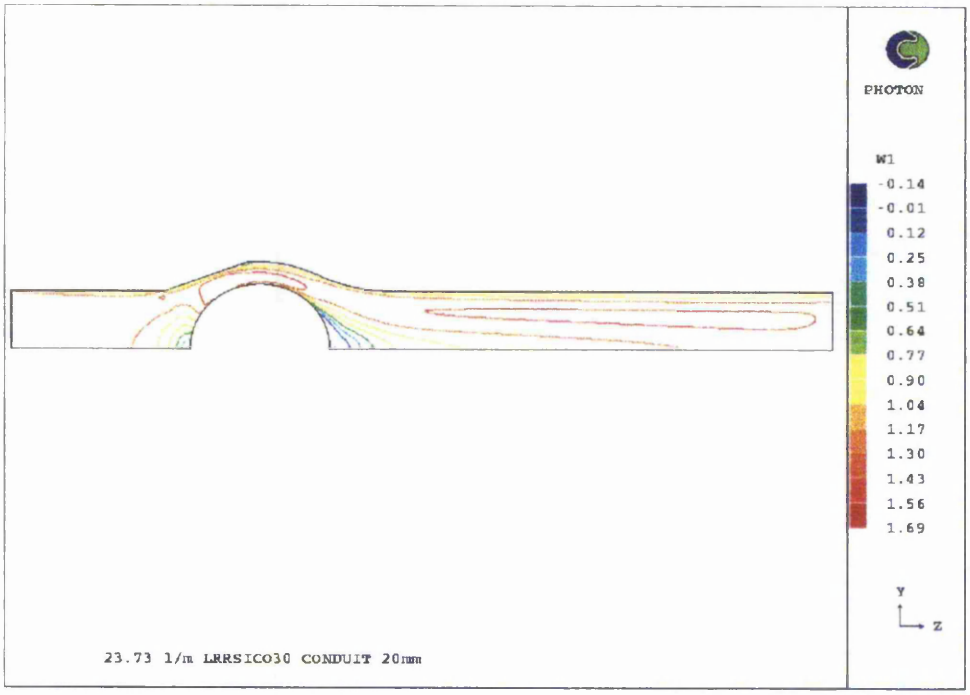

Figure 2.24: Carreau model, Re 8000.

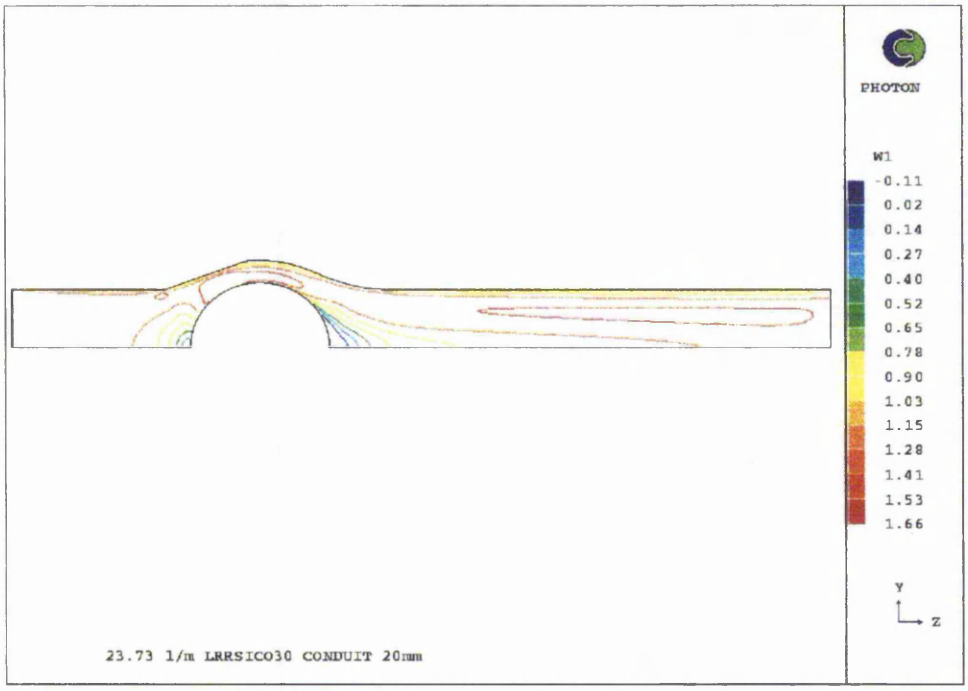

Figure 2.25: Carreau-Yasuda model, Re 8000.

2.5.2 Shear Stress Distribution

The distribution in shear stress for the Newtonian and Casson models, for Reynolds number 1000, can be seen in Figures 2.26 and 2.27, while Figures 2.28 and 2.29 show similar distributions for a Reynolds number of 8000. The unit of shear stress within the figures being Pa. The shear stress was calculated from the product of the effective viscosity and shear rate. For the laminar flow models the effective viscosity was equal to the laminar viscosity and for the turbulent models it was equal to the sum of the laminar and turbulent viscosity. For the low Reynolds number flow models (Re 1000 and Re 4000), the highest values of shear stress occurred along the occluder surface. A second area of high shear stress was also found along the diverging inlet section of the valve housing. The high Reynolds number models (Re 8000) showed an area of high shear stress in front of the occluder. Concentrated areas of high stress were also seen along the valves diverging inlet

section and within the flat section of the valve housing. Peak shear stresses were higher in the turbulent situations than the laminar ones.

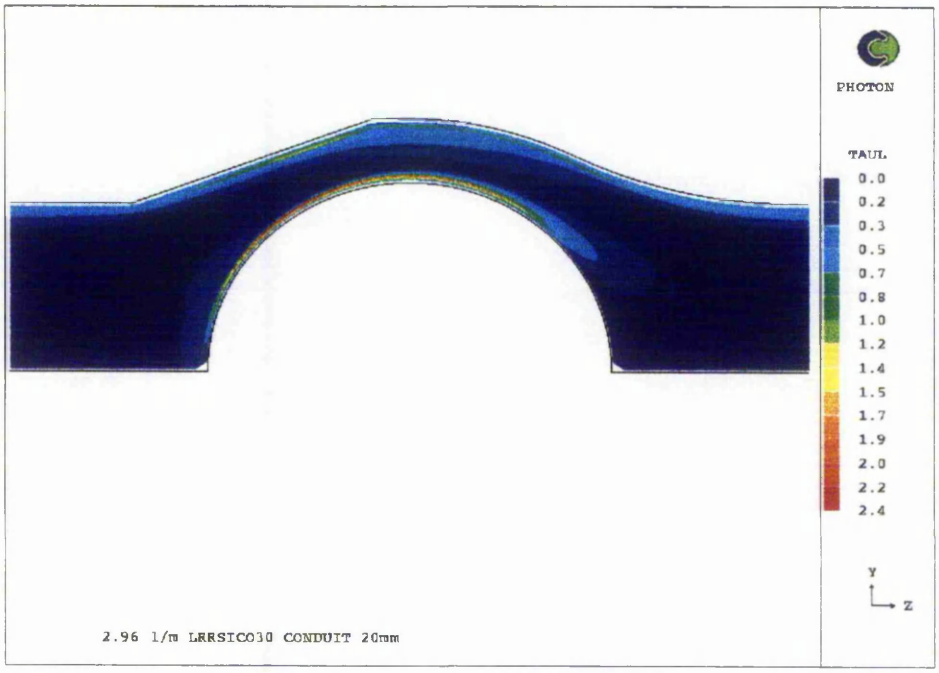

Figure 2.26: Shear stress distribution for Newtonian model, Re 1000.

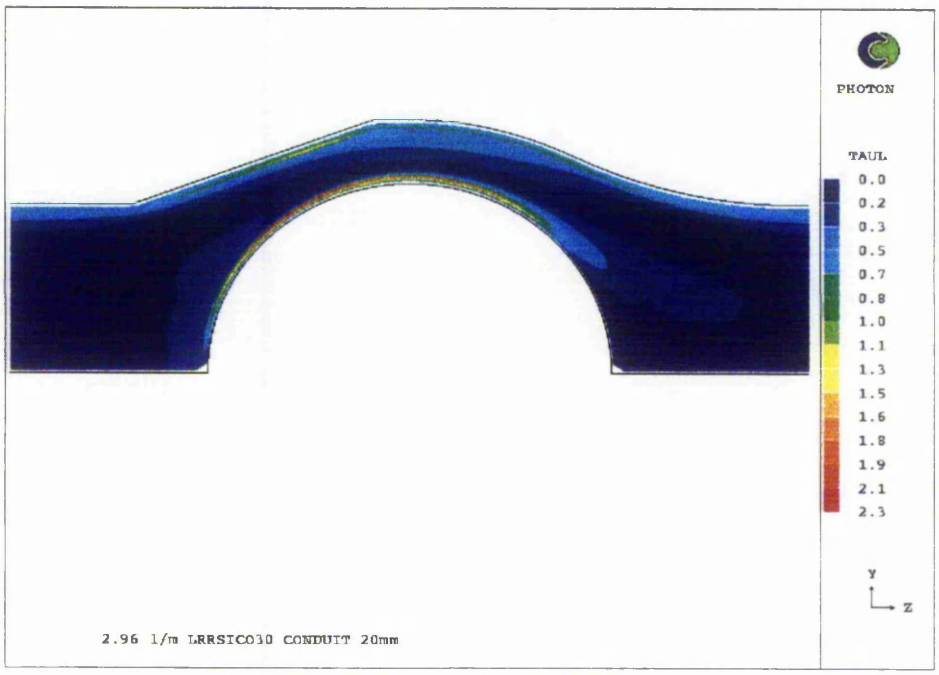

Figure 2.27: Shear stress distribution for Casson model, Re 1000.

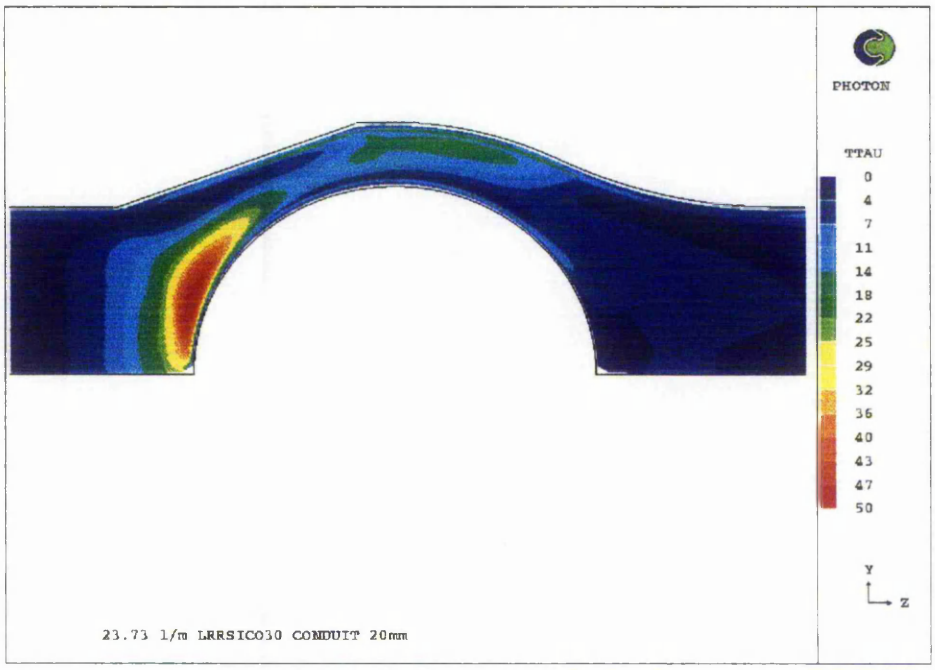

Figure 2.28: Shear stress distribution for Newtonian model, Re 8000.

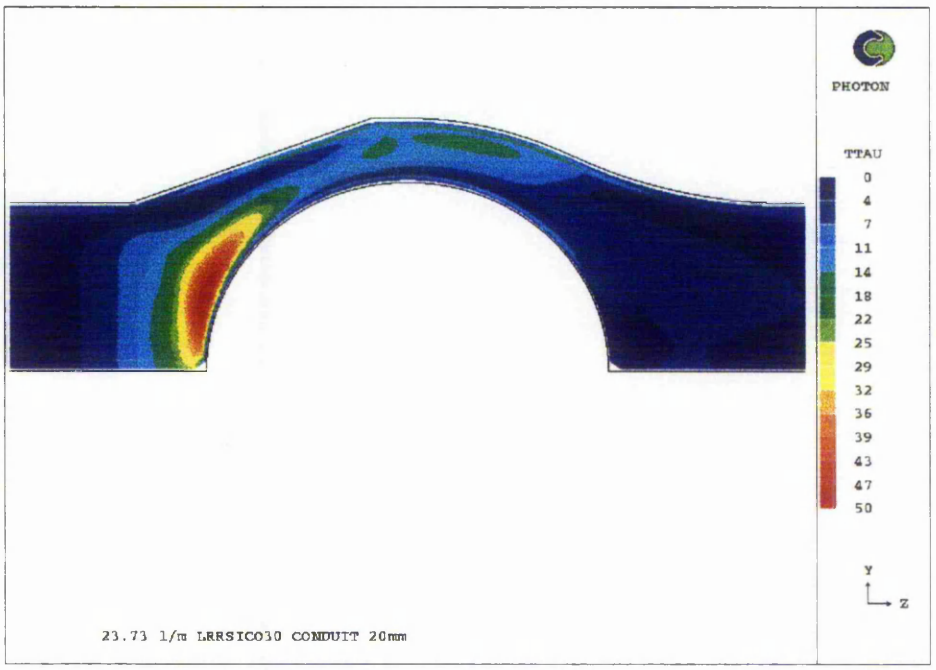

Figure 2.29: Shear stress distribution for Casson model, Re 8000.

2.5.3 Shear Rate Distribution

The distribution of shear rate is similar to the distribution of shear stress shown in Figures 2.26-2.29, due to the relationship that shear stress is equal to the product of shear rate and dynamic viscosity. For all models the highest shear rates occur within the central portion of the valve prosthesis, namely along the valve and occluder wall. The results presented in Figure 2.30 show the average shear rate per unit volume found within the geometric domain of the model. The values obtained for the chart were found from the sum of the cell shear rate value multiplied by the cell volume which was then divided by the total volume. For the lowest Reynolds number flow (Re 1000) the average shear rate varied between 45.18 s^{-1} and 51.01 s^{-1} with the Quemada model showing the lowest average value and the Carreau model the highest. As the Reynolds number was increased to 4000 the average shear rate was found to lie between 123.5 s^{-1} and 181.5 s^{-1}; again the Quemada model showed the lowest average value and the Carreau showing the highest. The results from the turbulent analysis show a greater variation in the predicted average shear rate with a range of 296.3 s^{-1} to 345.94 s^{-1}.

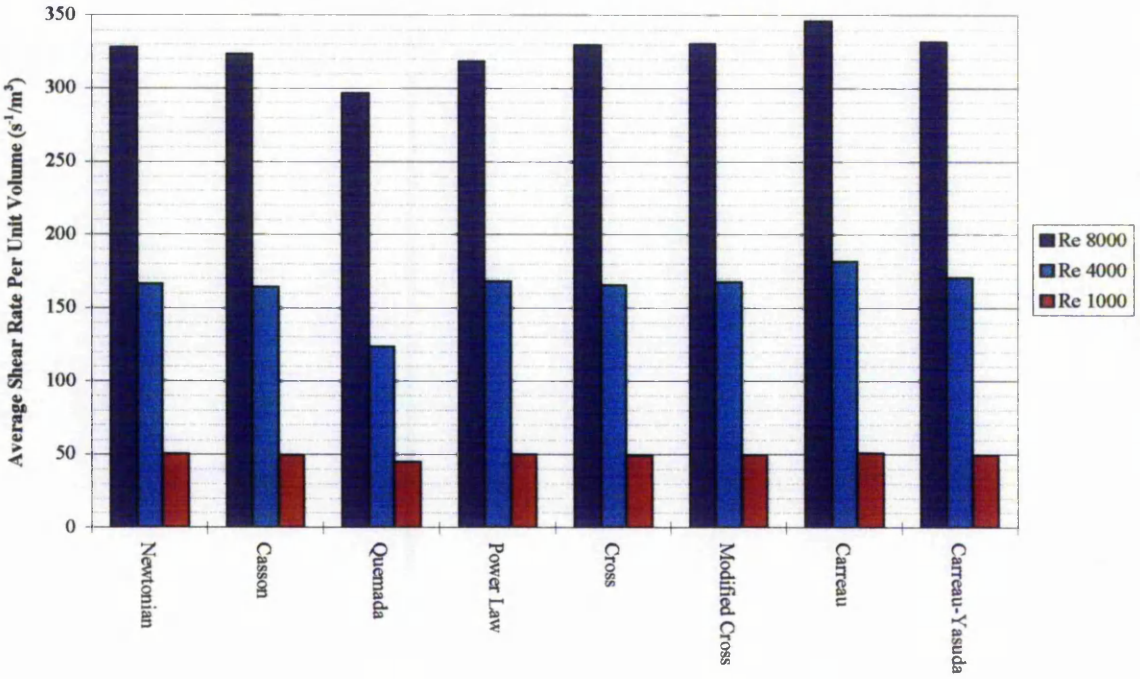

Figure 2.30: Average shear rate per unit volume.

The chart shown in Figure 2.31 represents the proportion of the flow domain where the shear rate was found to be less than 100 s^{-1}. The values were obtained from dividing the total cell volume with shear rate values less than 100 s^{-1} by the total volume cell volume. The shear rate value of 100 s^{-1} indicates a threshold where above that value blood can be represented as a analogue Newtonian fluid. At the lowest Reynolds number over half the flow domain is below the threshold of 100 s^{-1}, reducing to approximately one tenth when the Reynolds number increases to 4000. When the Reynolds number reaches 8000 only one twentieth of the flow has shear rate less than 100 s^{-1}.

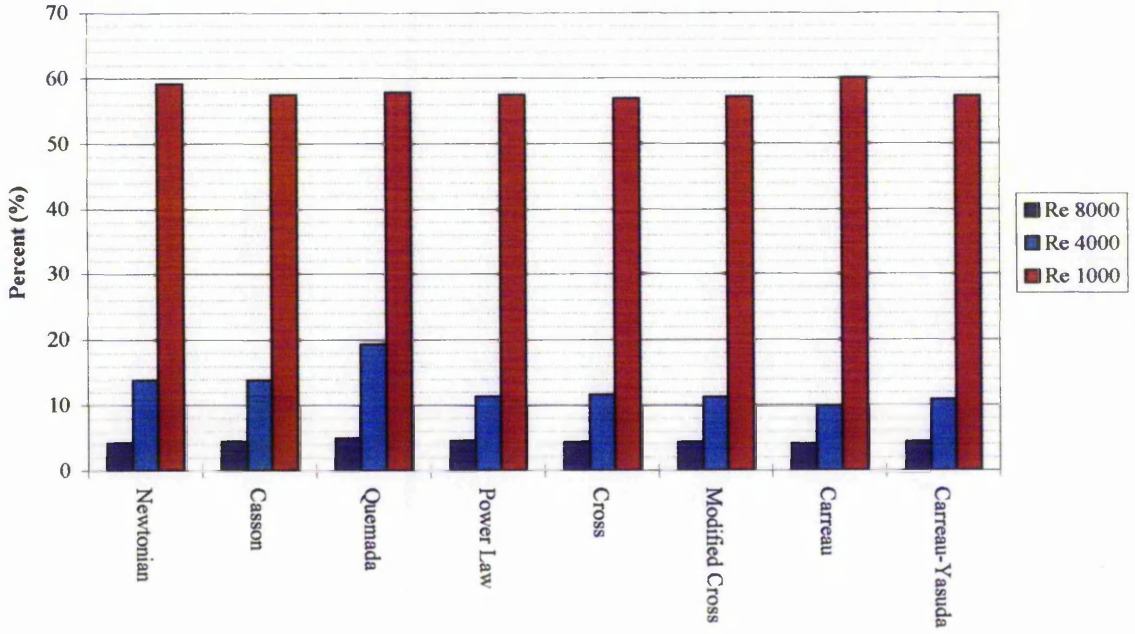

Figure 2.31: Proportion of flow with shear rate less than 100 s^{-1}.

2.5.4 Pressure Drop

Pressure readings were taken at two points, the first 28.6 mm upstream of the valve diverging section section and the second 72.8 mm downstream of the valve converging section. The pressure drop for the laminar flow models can be seen in Figure 2.32. The chart shows a considerable variation in pressure drop from one model to another, with a spread between 17.41 and 35.39 Pa for Re 1000, and 146.76 to 278.27 Pa for Re 4000. The lowest pressure drops were predicted by the Quemada model and the highest by the

Carreau model, for all flowrates. The results from the turbulent flow model can be seen in Figure 2.33. Again a wide spread in the results can be seen with pressure drops ranging from 420.9 Pa (Quemada model) to 861.75 Pa (Carreau model).

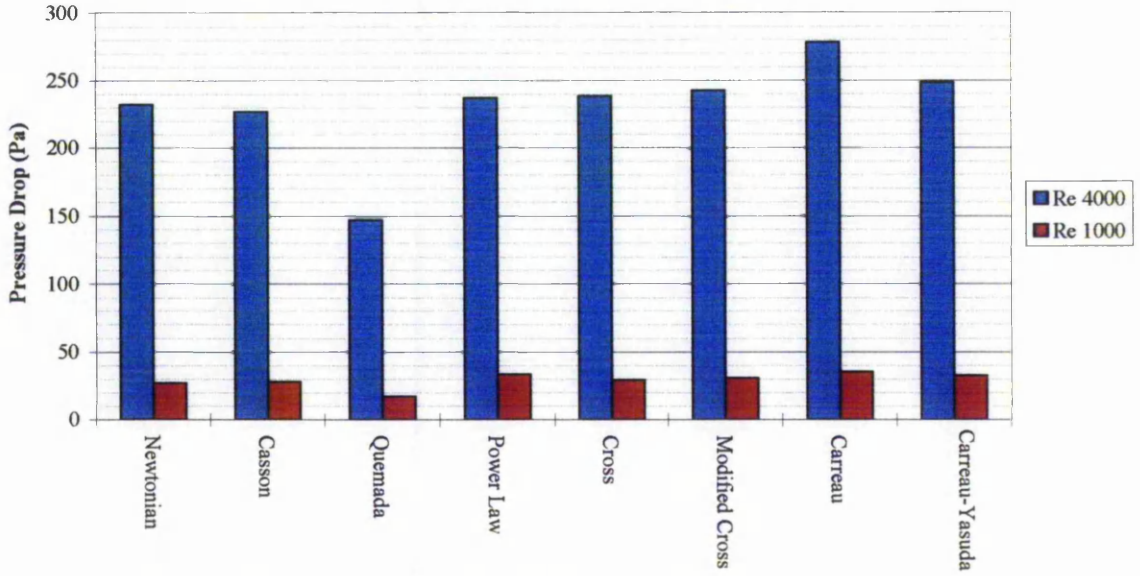

Figure 2.32: Pressure drop across the valve conduit, Re 1000 and Re 4000.

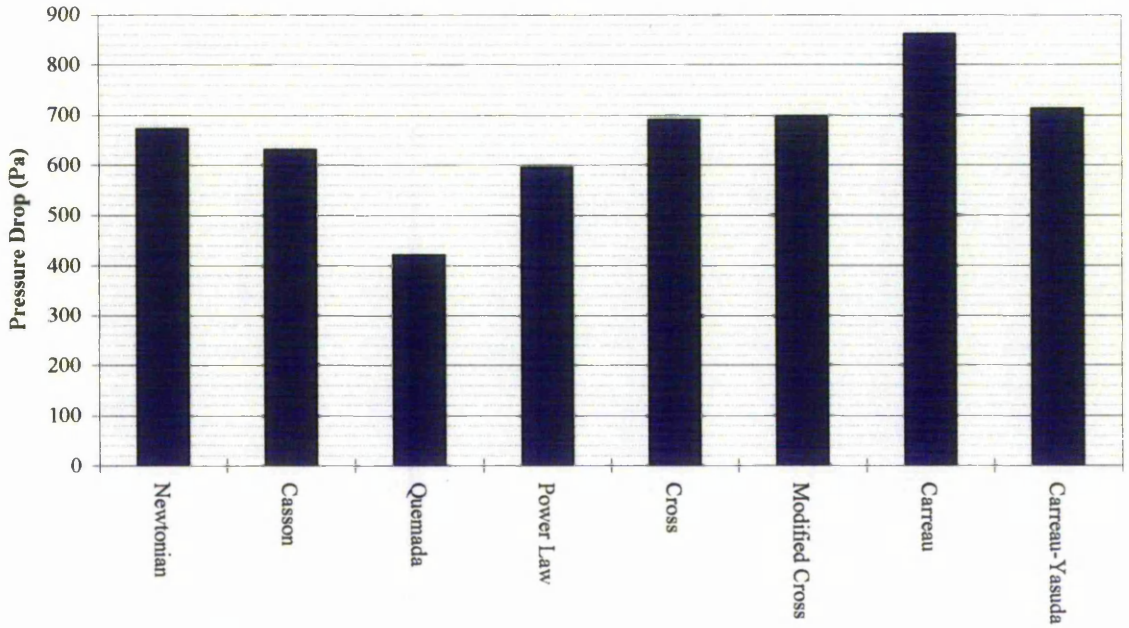

Figure 2.33: Pressure drop across the valve conduit, Re 8000.

2.5.5 Fluid Forces Acting On Occluder

The fluid force acting on the occluder is an important parameter since it governs the opening characteristics of the ball. It is considered to be the sum of the streamwise pressure and streamwise shear stress acting over the surface of the occluder. Equations (1) and (2) show the form in which these forces were calculated.

$$F_P = \sum P \partial A_P \tag{1}$$

$$F_\tau = \int_0^{2Rb} 2\pi \mu_{eff} r \frac{dw}{dy} \partial z \tag{2}$$

Where, F_P = Streamwise pressure force acting over occluder surface,
P = Pressure,
A_P = Occluder surface area perpendicular to flow axis,
F_τ = Streamwise shear stress force,
μ_{eff} = Effective viscosity,
r = Elemental radius,
Rb = Ball radius.

(N.B. For laminar flow the effective viscosity, μ_{eff}, was equal to the laminar viscosity, μ_l. For turbulent flow μ_{eff} was equal to the laminar viscosity plus the turbulent viscosity, μ_t.)

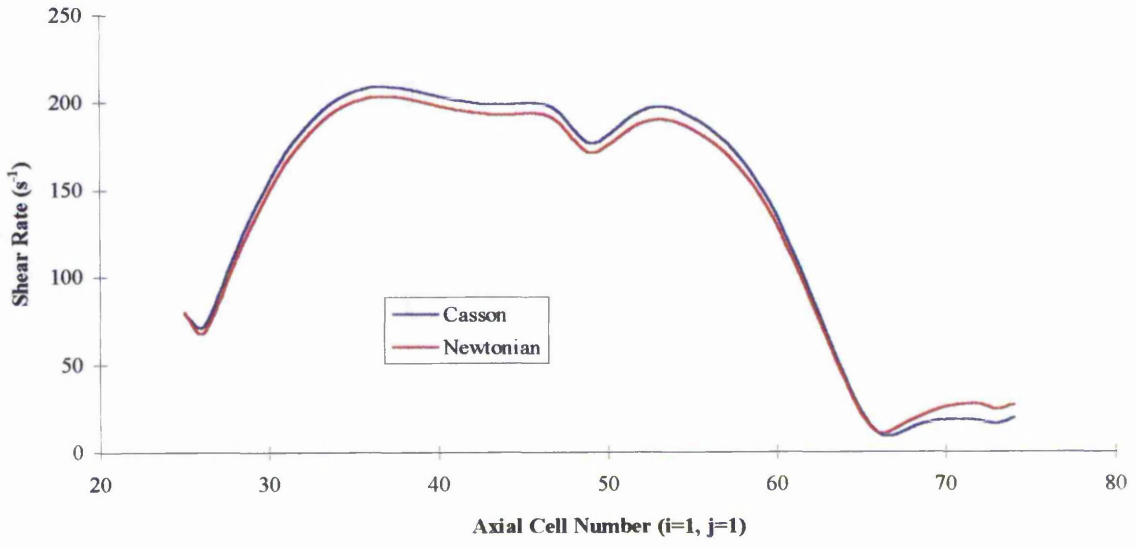

Figure 2.34: Shear rate distribution along occluder surface (Re 1000).

The occluder experiences extremes of shear rate along its surface as shown in Figure 2.34 for the Newtonian and Casson models, with low values of shear rate at the front and back of the occluder, and high shear rate values along the middle and top surface. This range of shear rate is due to areas of low velocity upstream and downstream of the occluder and an area of accelerating and decelerating flow as the fluid passes through the valve section.

In Figure 2.35 the sum of streamwise forces acting on the occluder for all models is shown. There is considerable variation in the results, as might be expected due to the varying pressure fields predicted for each model, i.e. those models predicting low pressure drop produce low occluder force and those models predicting high pressure drops produce large occluder forces.

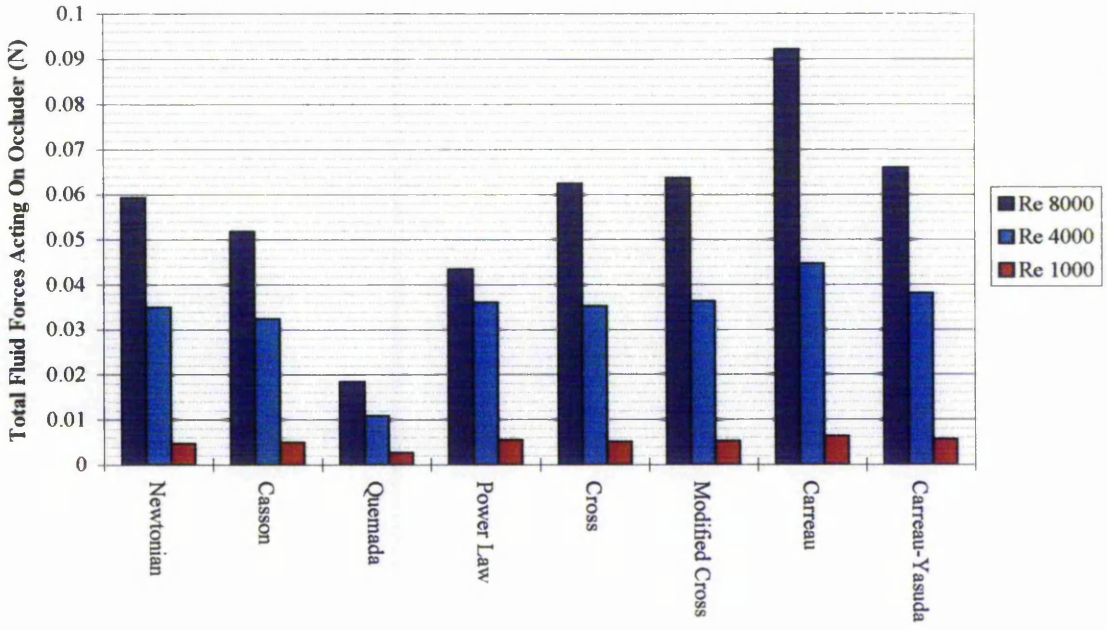

Figure 2.35: Sum of streamwise forces acting on occluder.

a)

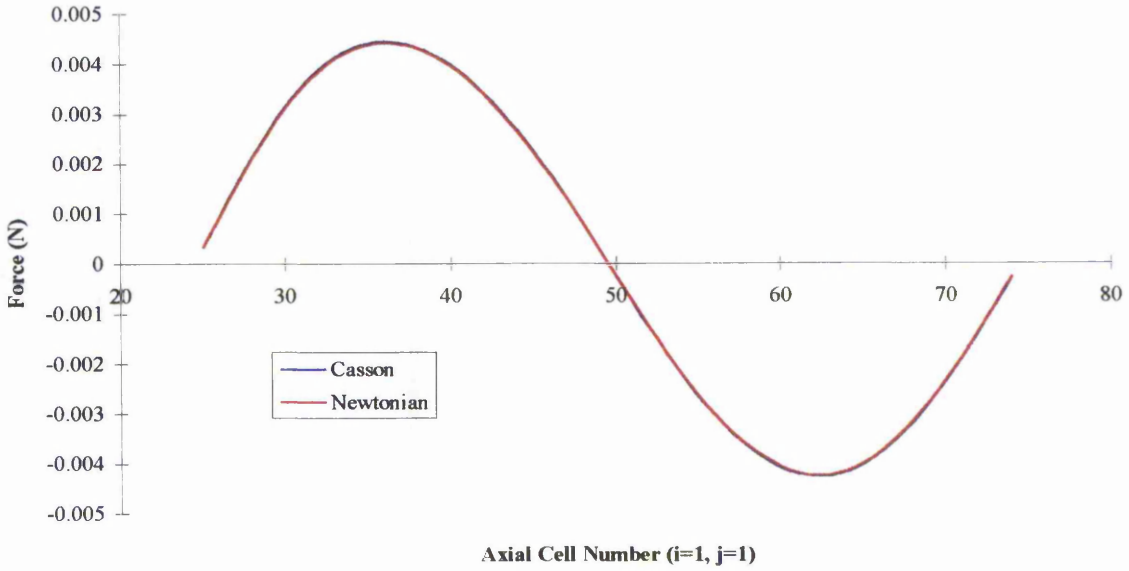

b)

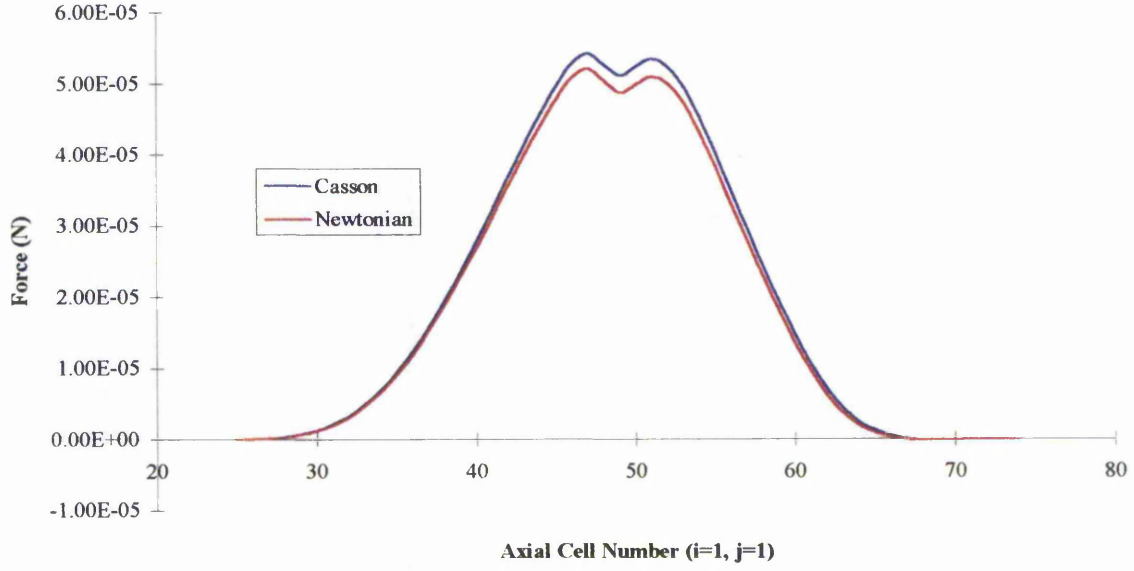

Figure 2.36: Force on occluder at Re 1000 a) streamwise pressure, b) streamwise shear stress.

The greatest contribution to the total force acting on the occluder was found to be the streamwise pressure force. In Figure 2.36 both streamwise pressure and shear stress force acting over the occluder surface are shown for the Newtonian and Casson model with a Reynolds number of 1000. The streamwise pressure profiles are almost exactly the same but an increase in streamwise shear stress force can be seen corresponding with the increase in shear rate found in Figure 2.34.

2.6 Discussion Of Blood Models

The application of non-Newtonian blood models to flow within vessels of similar size to the aorta is a contentious one. All sampled blood, used to determine the relationship between shear rate and viscosity, produces a viscosity curve that tends to a constant value as the applied shear rate exceeds 100 s^{-1}, as seen in Figure 2.37. The figure also shows that an ever increasing error is incurred if constant blood viscosity is assumed for low values of shear rate i.e. less than 100 s^{-1}.

The non-Newtonian blood models used in this analysis all produce a similar curve to that seen in Figure 2.37. Each model produces its own unique curve, due to the fact that the viscosity-shear rate relationship of blood varies from sample to sample.

As mentioned in section 2.2.2 the value of predicted viscosity can vary considerably from 0% for $\dot{\gamma} = 0.1$ s^{-1} to 25% for $\dot{\gamma} = 1000$ s^{-1}. This has been shown to have a considerable effect on the results produced by the computational analysis. The results predicted for the Quemada and Carreau models show greater deviation from the other models as the proportion of the flow field with a shear rate less than 100 s^{-1} decreases. It is interesting to note that as the Reynolds number increases the differences in the predicted pressure drop and occluder force between models also increase. This would be expected as 95% of the flow field has a shear rate value greater than 100 s^{-1} and the values of viscosity predicted for high shear flows can vary by up to 25%.

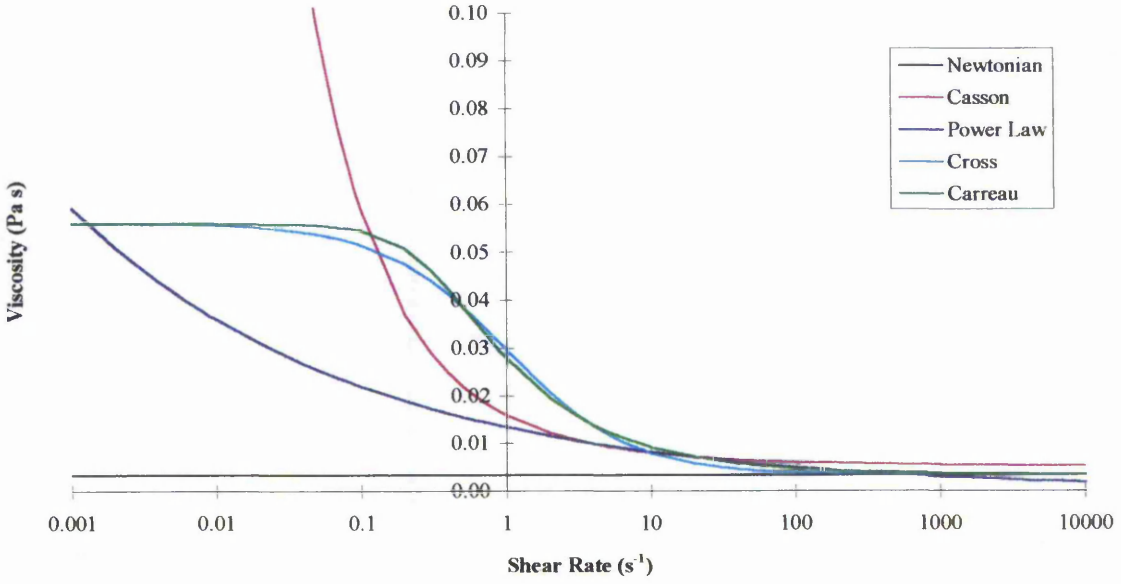

Figure 2.37: Viscosity-Shear rate relationship.

The cumulative effects of varying viscosity values on the flow field have been shown to be quite considerable with some models predicting stasis behind the occluder (Power Law and Carreau-Yasuda at Re 1000, and Quemada at Re 8000) while the other models predicted recirculation.

It can be seen that non-Newtonian blood models can influence the flow field for both high and low shear rate flows. As data from *in vitro* analysis of blood flow through a conduit valve is not available, a comparable analysis between experimental and computational results was not possible. Therefore the decision to adopt a non-Newtonian blood model for future analysis is based solely on the computational results.

From the results obtained it was decided that further analysis would consist of using both Newtonian and non-Newtonian (using Casson models) viscosity relationships. Cassons model was chosen partly due to its application to previous analysis conducted within the department but mostly because it produces values which are at the middle of the range seen in the various models.

Chapter Three

Heart Valve Design And Investigation Techniques

3.1 Heart Valve Design

The design of a prosthetic heart valve can be approached by the same methods used to design any mechanical component which is to be manufactured; each has to perform to and satisfy a particular set of design criteria. The fact that a prosthetic valve exists in an environment of living tissue does, however, present additional criteria and challenges to the designer. There are two categories into which these additional criteria can be placed:

i) Mechanical Performance Criteria

- The prosthesis must remain within its physical and geometric limits throughout its life.
- Structural integrity must not be compromised through repeated stress loading and fluctuating fluid forces.
- The valve must present negligible resistance to physiological flow.
- It must imitate natural valve performance characteristics. i.e. open and close at the appropriate points during the cardiac cycle.

ii) Biological Performance Criteria

- Haemolysis and thrombosis must not develop after valve implantation.
- Does not increase the risk of infection.
- Damage to endothelium cells must not occur.
- No adverse chemical reaction must exist that may cause damage to tissue.

A more complete definition of valve design can be found in Swales *et al.*[63] and Black[64]. The development of new analysis tools, such as CFD, has allowed a greater understanding of the dynamics of both valve and flow, providing a means to design more efficient and haemodynamically suited valves to replace malfunctioning cardiovascular valves.

3.2 Investigation Techniques

The analysis of *in vivo* situations can be conducted by experimental and computational methods. Each method having its own advantages, disadvantages, limitations, and scope for development.

The haemolytic and thrombogenic potentials, as well as efficient mechanical performance, of any valve prosthesis must be determined to a high degree of accuracy and confidence before implantation. There are several mechanisms by which haemolysis is induced. The main mechanisms, relevant to fluid dynamics, are shear stress related haemolysis and thrombosis which is related to stasis and shear rate. The optimum design can only be achieved by full access to both shear stress and shear rate within the flow regime of the valve prosthesis. Many experimental techniques cannot obtain shear rate directly but use assumptions about the nature of the turbulence, i.e. isotropy. Experimental techniques have the advantage of being able to use accurate geometric models but lack realistic blood analogue fluids. Computational models can predict blood behaviour with a higher degree of accuracy by using shear rate dependent viscosity models, e.g. Casson[54], Power Law, Quemada[55,56], Cross[57], Carreau[60], but memory and processor performance limit the size and representation of the temporal and spatial domain.

This section reviews some of the work to date conducted on heart valve prostheses using both experimental methods, e.g. Laser Doppler Anemometry, and CFD methods, e.g. commercial CFD software and user defined software. The papers referenced below are only a small selection of work conducted in this area and are only used as examples.

3.2.1 Experimental Analysis

Over the past few decades experimental techniques have increased in complexity and accuracy. A few experimental *in vitro* techniques used are listed below :

a) Laser Doppler Anemometry (LDA),
b) Ultrasound Doppler Anemometry (UDA),
c) Three Dimensional Magnetic Resonance Velocity Mapping,
d) Hot Wire/Hot Film Anemometry,
e) Flow Visualisation Studies,
f) Pitot Tube Measurements,
g) Static Pressure Measurements,
h) Flow Metering.

Each technique has advantages, disadvantages and limitations, as reviewed by Tansley *et al.*[65] . The international standard ISO 5840[66] describes the types of tests new valves are required to undergo before clinical trials are conducted.

Prosthesis analyses by Yoganathan *et al.*[67-69] , Chew *et al.*[70,71], Figliola and Mueller[72], and Haggag[73] use LDA to determine flow velocity, turbulence intensity, and shear stress/rate of a number of valve prostheses, i.e. caged ball, tilting disc, bi-leaflet, caged disc, porcine, and central axis. Most models use a simplified model of the ventricle and aorta, and steady fully developed flow at the inlet. Blood is represented by a analogue solution usually a water/glycerine mix. The data obtained from these studies allow valve efficiency, and the thrombogenic and haemolytic potentials to be predicted. This type of study provides an effective comparative analysis between existing and new heart valve prostheses.

Further studies by Schoephoerster and Chandran[74], Hanle *et al.*[75], Walker and Yoganathan[76], Woo and Yoganathan[77], and Nygaard *et al.*[78] examine valve function over the systole/diastole cycle. LDA is used to evaluate flow velocity, turbulence intensity, and shear stress/rate at predetermined intervals during the cardiac cycle. The types of valves used are as those mentioned above. The geometry and blood representation are the same as above with the exception of Schoephoerster and Chandran[79] who use a model of the left ventricle to analyse the flow dynamics of mitral valve prostheses. A more advanced model has a distensible ventricle rather than a rigid one. Walker *et al.*[80] investigated the effect of

tilting disc heart valve orientation on flow through a curved aortic model. Gentle and Leefe[81] compare the performance of a ball type conduit valve and a Björk-Shiley conduit disc valve with an aortic stenosis, under pulsatile flow, in terms of pressure drop and power loss.

3.2.2 Computational Fluid Analysis

The use of CFD in the analysis of prosthetic heart valves is small compared to experimental *in vitro* techniques.

The valve prostheses are analysed using either user defined solution codes or commercially available codes. CFD codes provide an approximate solution to the Navier-Stokes equation and with that determine shear rate, shear stress, and turbulent intensity. Constitutive equations can be used to calculate viscosity producing non-Newtonian blood flow models. The spatial domain can be represented by either finite volumes or finite elements, the density of which should produce grid independent results. Unlike *in vitro* techniques, all variables, i.e. flow velocity, pressure, turbulent intensity, shear stress, and shear rate, are available at any location within the boundaries of the geometric model.

Early work in this field used user defined numerical discretization algorithms to solve the non-linear, second order, partial-differential equations (PDEs) that describe the fluid motion within a discretized spatial and temporal domain. Today the user has access to commercial codes, some of which permit alterations to the source coding by the user.

Tansley *et al.*[65] describe the application of CFD to prosthesis analysis and conclude,

> '*CFM has a major role to play in the analysis of prosthetic heart valve flow and design because of the improved availability of data afforded and the increased correlation between CFM and clinical flow regimes, due to the ability to consider realistic blood models.*'

Work by Thalassoudis *et al.*[82], Tansley *et al.*[83], Jones *et al.*[84], King *et al.*[85], Underwood and Mueller[86,87], Merchant and Mazumdar[88], Stevenson and Yoganathan[89], Stevenson *et al.*[90] and Gentle and Wilson[91] has shown CFD to be a valuable analysis tool. The valve geometry can be represented as either a two dimensional or axisymetric model of the ventricle, sewing ring, sinus, aortic wall, and valve prosthesis, as shown in Figure 3.1. This diagram is also representative of many *in vitro* test sections. This similarity allows results obtained from CFD analysis to be compared against those obtained from *in vitro* techniques, providing a means to validate CFD models.

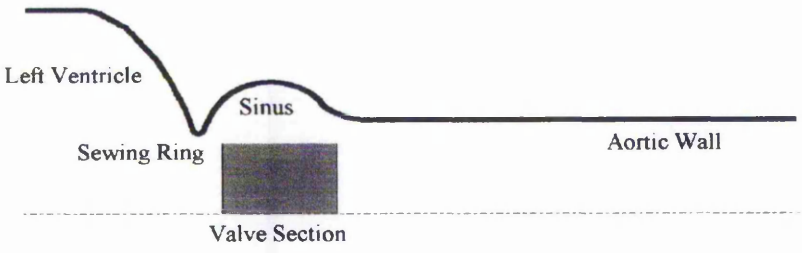

Figure 3.1: Model representation.

3.2.3 Discussion Of Experimental And CFD Techniques

Experimental techniques have been in use for many years, the most popular being LDA and UDA. The information obtained from these systems allows the haemolytic and thrombogenic potentials of valve prostheses to be predicted. Standard analysis protocols (ISO 5840) allow prostheses of different designs to be compared against each other.

To determine flow related data using LDA requires a solution, usually a water/glycerine mix, seeded with light scattering particles. Therefore the fluids used are Newtonian blood analogues and lack the ability to represent the non-Newtonian property of blood, which reduces correlation with *in vivo* results.

The data retrieved from experimental work is limited to areas where intrusion of the beams by valve components does not occur. This limits readings to being taken at planes proximal

and distal to the valve prosthesis. Some open valve geometry allows data to be recorded within the valve domain but this is only possible under steady flow conditions. Measuring data within the valve section under pulsatile flow conditions is extremely difficult, if not impossible, therefore limiting the prediction of haemolysis and thrombosis.

The results from experimental analysis provide an insight into the flow dynamics of valve prostheses through either axisymetric or three dimensional models under steady or transient flow conditions. The information retrieved allows the haemodynamic performance of valve prostheses to be quantified providing an effective means of comparison.

The application of CFD to valve prostheses is still relatively new when compared to existing experimental techniques. Many limitations of experimental techniques can be overcome by using CFD techniques. Unlike experimental techniques flow data can be accessed at any point within the spatial domain. The ability to model the shear rate dependent viscosity of blood, as well as Newtonian models, allows the non-Newtonian nature of blood flow to be analysed and compared against Newtonian models.

The geometry used to represent the valve section is greatly simplified, with guiding struts and supports omitted to allow two dimensional or axisymetric grids to be defined. The simplified geometry means the effects of these omitted parts on the overall flow cannot be assessed and, as thrombus can develop particularly on these parts, this maybe a simplification that cannot be overlooked. The speed with which different valve geometry and flow conditions can be modelled is a major advantage of using CFD as part of a valve developement programme.

The simulation of time dependant flow through a valve is limited as not only does the flow need to be calculated but also the dynamics of the occluder i.e. the calculation of fluid dynamic forces to determine the position of the occluder within the flow.

Experimental methods are well established and follow the international standard ISO 5840. These methods provide important haemodynamic information relating to valve prosthesis performance and allow comparisons to be made between valves. The limitations of data acquisition to planes where the measuring beams and probes are not inhibited by the valve geometry and the use of blood analogue fluids, reduce both *in vivo* correlation and the ability to fully predict the haemolytic and thrombogenic effects of a particular valve.

The use of CFD can overcome both of the limitations mentioned above, providing data at any point within the spatial domain and using shear-rate-dependent rheological models allows the non-Newtonian behaviour of blood to be assessed. The speed with which models can be generated and run allows the valve designer to investigate the performance of a greater variety of valve geometryies under any flow condition. The improvements in CFD robustness and accuracy, and increasing processor speed allowing greater spatial density and increased range of time scales, can only help to improve the confidence of predicted results making CFD analysis a comparable method to experimental analysis.

3.3 Comparison Of Two Computational Fluid Dynamic Packages: PHOENICS and FLOTRAN

Over the past few years there has been an increasing number of computational fluid dynamics software packages capable of modelling fluid flow using either a Finite Volume (FV) or Finite Element (FE) technique to produce a mathematical model of the flow regime. These systems offer great flexibility in defining the fluid domain and the nature of the fluid, e.g. Newtonian, non-Newtonian, Gas, Steam, etc. Each system will have its own strengths but all solve for the Navier-Stokes and Continuity equations. It is not the purpose of the following sections to examine in depth the differences between FV and FE techniques but simply to outline the capabilities, using the analysis of steady Newtonian blood flow through a prosthetic conduit valve, of two commercially available software packages PHOENICS[43] (FV) and FLOTRAN[92] (FE) when used in a prosthesis analysis. The packages used for this analysis are the two main CFD systems used within the university and not necessarily the most advanced packages available.

3.3.1 FLOTRAN

FLOTRAN is a general purpose analysis tool for the treatment of two and three dimensional fluid flow and/or heat transfer. It can be fully integrated with ANSYS, I-DEAS and PATRAN which act as pre- and post-processors. The governing equations consist of the momentum equations, the continuity equation, the energy equation, and an equation of state. These governing equations are expressed in primitive variables i.e., velocity and pressure. A two-equation turbulence model, k-ε, is used requiring two additional equations to solve for turbulent kinetic energy and turbulent dissipation rate. The equations are solved using the Galerkin weighted integral method, streamline upwinding, and a sequential solution algorithm.

3.3.2 PHOENICS 1.6.6

PHOENICS is a computer code which uses the FV method to simulate fluid flow, heat transfer, chemical reaction and other related phenomena for both two and three dimensions. The package is self-contained having both pre- and post-processor capabilities. PHOENICS solves discretized versions of differential equations in the general form of equation (3).

$$\frac{\partial(r_i\rho_i\varphi_i)}{\partial t} + div(r_i\rho_i V_i\varphi_i - r_i\Gamma\varphi_i grad\varphi_i) = r_i S_i \qquad (3)$$

Where,

r=Volume fraction,
ρ=Density,
φ=Field variable,
Γ=Diffusion coefficient,
S=Source term,
V=Velocity,
t = Time,
i = Phase.

3.3.3 Computational Model

A 20 millimetre diameter conduit valve was chosen and analysed under a range of flow regimes with Reynolds numbers of 500, 1000, 2000, 4000, 8000, giving volume flowrates in litres per minute of 1.48, 2.97, 5.93, 11.86, 23.72, respectively. Blood is assumed to be a Newtonian fluid with a density of 1056.17 Kg/m^3 and a dynamic viscosity of 3.323×10^{-3} Pa s.

3.3.4 Model Geometry And Computational Fluid Model Assumptions

The geometry of the conduit valve can be seen in Figure 3.2. This spatial domain was discretised to produce a finite element mesh and finite volume grid. The FE mesh and FV grid shown in Figure 3.3. represent a Gentle conduit valve of 20 mm inlet diameter. The FE geometry was produced on a Unigraphics CAD station from where an IGES interface was used to produce a data file which could be read by the general purpose ANSYS FE package, used as a pre- and post- processor tool. The mesh produced was unstructured containing both quadrilateral and triangular bi-linear elements.

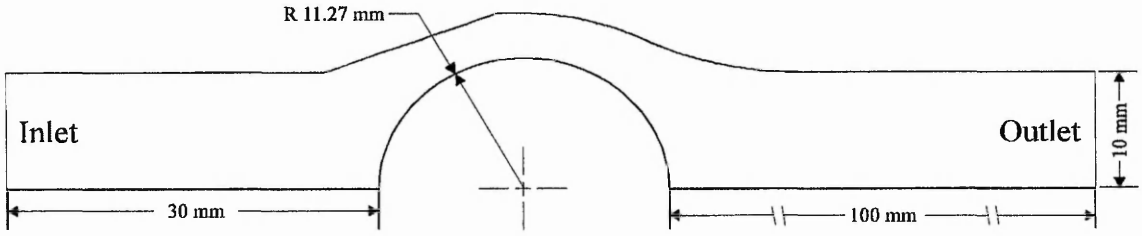

Figure 3.2: Valve geometry.

The FV grid was generated from a previous code[23]. The grid uses Body Fitted Co-ordinates which allow a more accurate representation of the valve than would be possible if an orthogonal grid was used. An axisymetric grid was assumed for both models and hence only half of the conduit cross-section needs to be considered.

The inlet velocity profile was set uniformly and a short inlet tract was chosen to allow a 'plug'

type velocity profile to develop before reaching the valve. At all wall boundaries the velocity components were set to zero. Logarithmic wall functions were used for both models. The pressure at the outlet plane for the models was set to a fixed value. For flowrates with Reynolds number up to 2000 laminar flow was assumed. At the higher flow rates turbulent flow was assumed and so the k-ε model was used. Convergence was assumed when residuals for both velocity components fell below 1×10^{-6}.

(a) (b)

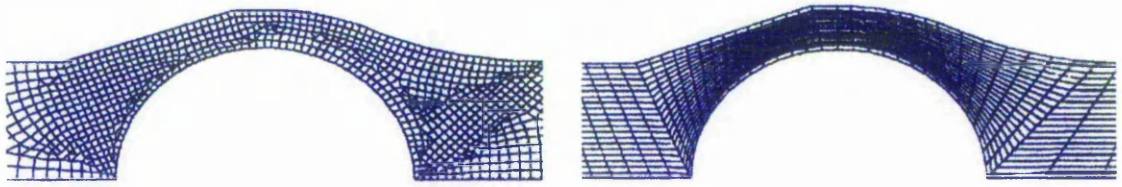

Figure 3.3: Geometric domain (a) FE, (b) FV.

3.3.5 Grid Density Comparisons

The first step in comparing the two packages was to study the effect of grid density on the accuracy of data produced. The grid size should be selected so that the flow may be modelled accurately without excessive use of computer time. For this purpose three grid sizes were chosen for each technique namely 1376, 5332, 8483 nodes for the FE grid and 1400, 5320, 7600 cells for the FV grid. For the FV package grid sizes were determined by specifying the total number of cells in the x, y, and z directions. This could not be done for the FE mesh as grid spacing values were chosen around 'keypoints' limiting the ability to produce models with the exact number of nodes when compared to the FV model. A Reynolds number of 8000 was chosen as a greater number of nodes is required to model turbulent flow, due to its high spatial density of occurrence, and so turbulence represents a more severe test for grid dependency.

For each model the centre line velocity and pressure, and time taken to reach convergence were recorded. The centre line is defined as a line tracing a path along the central axis for the inlet and outlet sections, but along the ball surface in the middle section. The centre line velocity can be seen in Figures 3.4 and 3.5 where the axial distance is measured from the left hand edge of the

grid, 41.46 mm upstream from the ball centre. The letters *F*, *M* and *C*, refer to the mesh/grid density, *F*ine, *M*edium, and *C*oarse respectively.

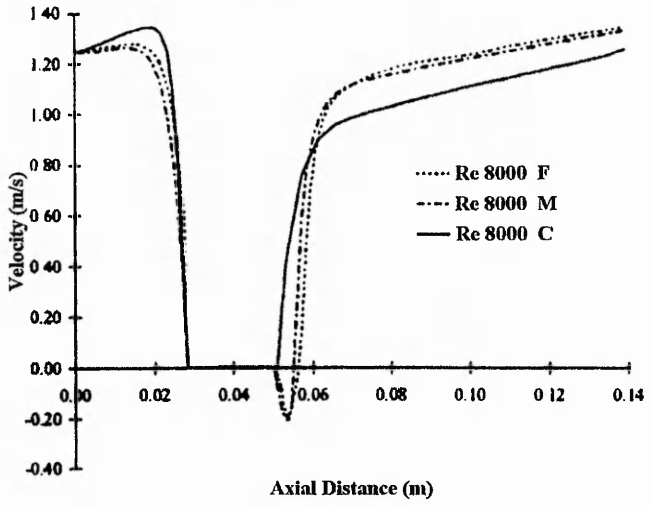

Figure 3.4: Velocity along centre line (PHOENICS).

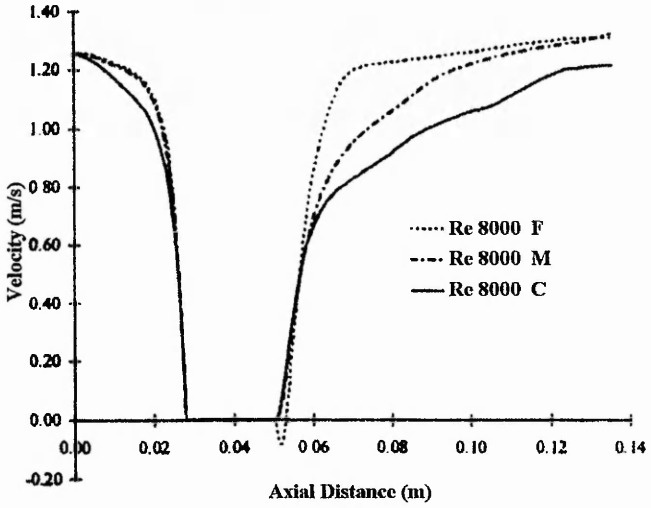

Figure 3.5: Velocity along centre line (FLOTRAN).

The CPU time taken to reach convergence on the medium grid for both models was approximately 2700 seconds, for the fine grid 5400 seconds, and 810 seconds for the coarse grid. The FV model for the fine grid would not converge fully and hence these results were treated with caution.

For the FV model, all grid sizes show an area of recirculation downstream of the conduit ball, the magnitude of which increases as the grid becomes finer. It can be seen that little difference exists between the fine and medium grids. The coarse mesh for the FE model shows a large deviation in flow velocity and does not predict any recirculation downstream of the ball. The coarse grid gave no recirculation but as grid density increased downstream of the ball a recirculation zone began to develop for both FLOTRAN and PHOENICS.

The pressure plots in Figure 3.6 and 3.7 show that for the FV model there is little difference between the values calculated with the medium and fine grids, but the coarse grid values only show close correlation in the outlet section of the valve. The fine and medium grids for the FE model produce very close correlation initially, as shown in Figure 3.7, but diverge from one another in the outlet section of the valve. The coarse mesh gives lower predicted values of pressure throughout the valve.

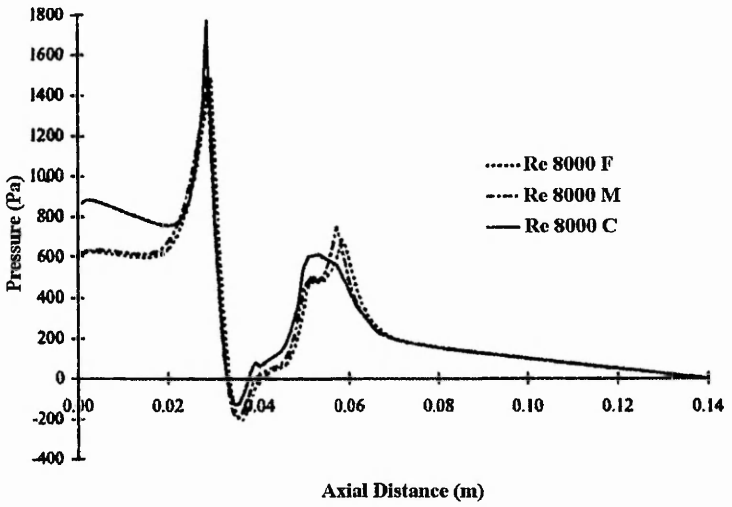

Figure 3.6: Pressure profile along centre line (PHOENICS).

It was decided that for the FV models the medium grid would be used for subsequent trials with the slight reduction in accuracy being offset by the saving in CPU time. The medium grid was also chosen for the FE models, even though the velocity values may be slightly under predicted,

because the pressure values were more closely related to those obtained from the FV model and again any reduction in accuracy would be offset by the saving in CPU time.

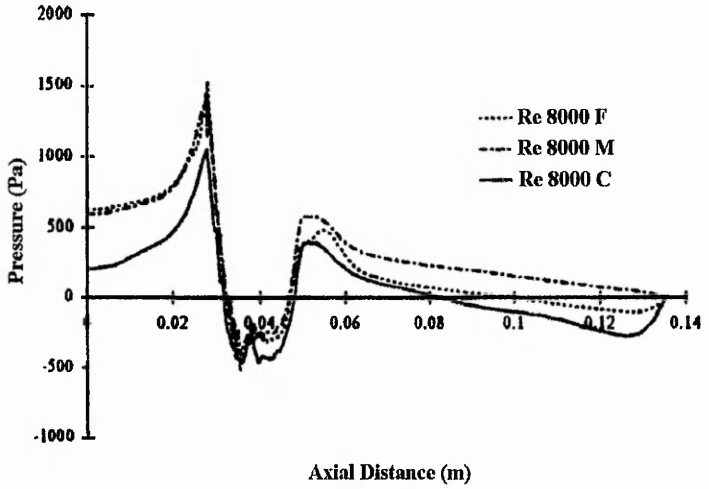

Figure 3.7: Pressure profile along centre line (FLOTRAN).

3.3.6 Results

The next step was to study the difference between the FE and FV models for the full range of Reynolds number, but with a constant, medium value of mesh or grid size. In total ten runs were conducted and the following parameters recorded:- velocity, pressure, shear stress (PHOENICS), and total run time.

The first three of these parameters are important in the evaluation of the haemodynamic efficiency, shear stress related haemolysis, and thrombus formation potential of the prosthesis. For the first three runs Reynolds numbers of 500, 1000 and 2000 were used and laminar flow was assumed. The final two runs had Reynolds numbers of 4000 and 8000 where the flow was ssumed to be turbulent. The initial comparison is based on the CPU time to perform all necessary calculations at a single grid point and is shown in Table 3.1.

Table 3.1: Time taken to perform calculations at single grid point.

Package	Laminar	Turbulent
PHOENICS	7.6992×10^{-4} s	7.9887×10^{-4} s
FLOTRAN	1.989×10^{-3} s	2.56039×10^{-3} s

This table shows the FV program was approximately three times faster when performing calculations at a single grid point. However, due to the need for considerable under-relaxation using a pseudo-time step to obtain convergence, any benefits in CPU time were lost as a result of the increased number of sweeps required to obtain a converged solution. Both packages took approximately the same overall CPU time, 2700 seconds, to produce a converged solution.

3.3.7 Flow Regime In The Upstream Half Of The Valve

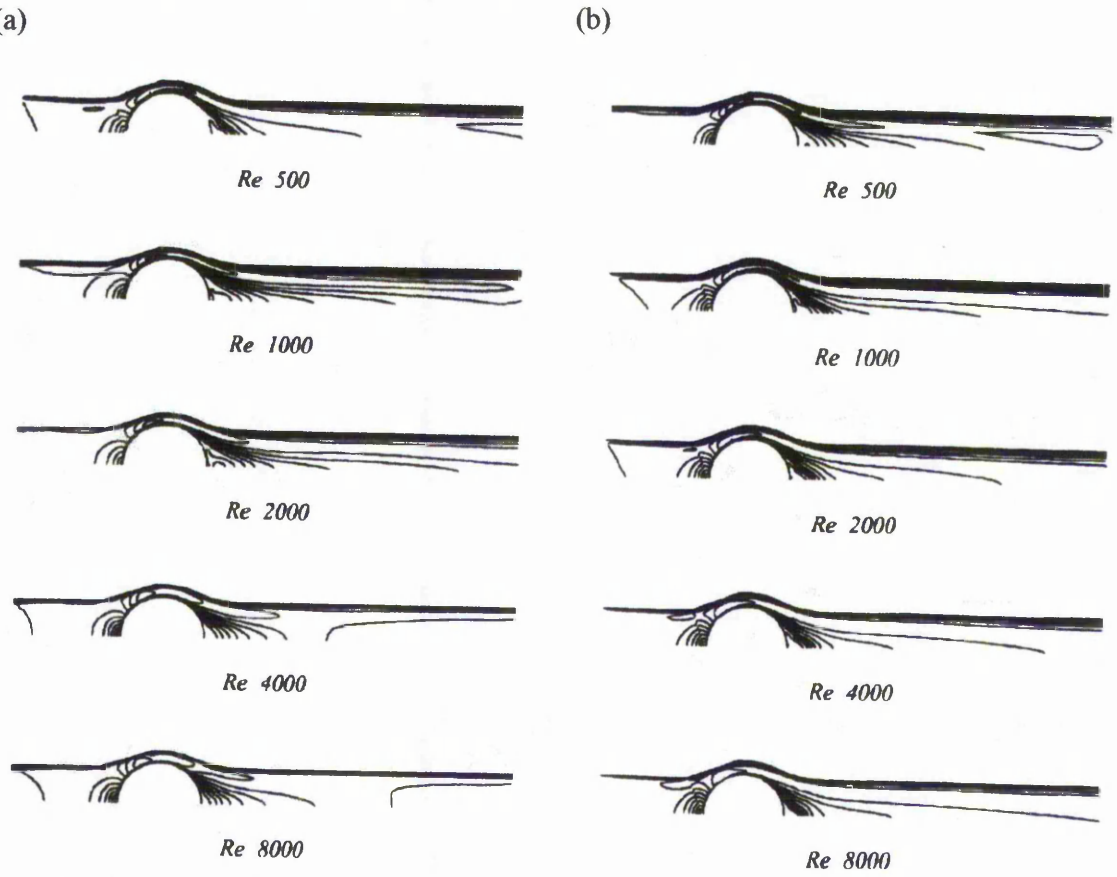

Figure 3.8: Velocity contours predicted by a) FLOTRAN and, b) PHOENICS.

Figure 3.8 shows the velocity contour plots produced by FLOTRAN and PHOENICS. As would be expected, there is an area of decelerating flow directly upstream of the ball. The flow is then accelerated through the convergent annulus section of the valve. The maximum velocities occur within this section of the valve and also the maximum shear stresses as the flow accelerates along the ball surface. The flow patterns are similar for both FE and FV models.

3.3.8 Flow Regime In The Downstream Half Of The Valve

In the divergent annulus section of the valve a free stream jet begins to form. The geometry of the valve guides the jet that develops so that no impingement occurs at the prosthetic surface, reducing the risk of wall shear stress induced haemolysis. Generally this jet then enters the outlet section and moves downstream, initially following the model boundary but with a gradual dissipation into the central flow region. This, however, does not occur for the models on FLOTRAN with Reynolds numbers of 4000 and 8000, where a jet is formed but is then broken down rapidly downstream of the valve. This is probably a quirk caused by the low grid density adopted and will be discussed later. Directly behind the ball exists an area of either recirculating flow or stasis. This recirculation is predicted for all laminar models but for the turbulent flows PHOENICS shows a distinct area of recirculation whereas FLOTRAN shows only an area of stasis. This again is probably due to a decrease in grid density for the FE model.

3.4 Discussion

The results produced by FLOTRAN and PHOENICS compare favourably with each other except at high Reynolds number where an area of stasis was predicted by FLOTRAN but an area of recirculation was predicted by PHOENICS. The discrepancy is due to the reduction in grid density downstream of the ball where low spatial grid density does not allow the correct prediction velocity for turbulent flow. The FE model with 5332 nodes was chosen, even though no recirculation was predicted, as at this present time no experimental data is available to verify the existence of a recirculation zone behind the ball. The analysis shows that damage to

erythrocytes and endothelium cells would not occur at any of the modelled flowrates. The possibility of thrombus formation is less clear, however, and this could take place behind the ball.

Both packages use a first order upwind solution scheme, but PHOENICS has the option to use a second order hybrid scheme which is more accurate. However, convergence difficulties arise if this scheme is used. The first order upwind solution scheme introduces an artificial diffusion term making the effective Reynolds number lower and thus reducing eddy lengths. This may lead to underestimation of shear rate and shear stress values. This can be avoided by using a higher order numerical scheme.

3.5 Conclusion

The use of CFD in the analysis of artificial heart valves has gradually increased over the past few years. Initial studies used the FV technique to predict the flow but, as understanding of the FE techniques in modelling flow has increased, the use and acceptance of FE analysis continues. There is no doubt that the ability to model a system using a computational approach has its advantages in both time and cost, and also allows a greater freedom for the designer's creativity.

The computational techniques have shown they can produce acceptable and meaningful results even though there is often a shortage of comparable *in vitro* results and so quantitative comparisons are not always possible. The models produced here were limited to steady Newtonian flow but could be extended to include a time dependent solution using a non-Newtonian blood viscosity model with dynamically varying model geometry and pulsatile flow.

The ability to access the FORTRAN coding and program user defined subroutines is a feature not present in FLOTRAN but is one of the main strengths of PHOENICS. This feature is a necessity rather than an option. Its was therefore decided that PHOENICS would be an ideal CFD tool to perform the analysis on a conduit valve in unsteady flow conditions with dynamically varying occluder positioning.

Chapter Four

Development Of Computational Model

4.1 Introduction

This chapter describes the development of the computational model used to analyse the dynamic performance of a conduit valve prosthesis. The model was designed to simulate the effects of a time varying flowrate on a conduit valve using an adaptive finite volume grid, defined around the occluder's displacement. The time period was discretised into a finite number of intervals and at each interval the dependent variables P1, V1, and W1 were solved. After convergence was satisfied for one time step the forces acting on the occluder were determined and the occluder displacement found. At the start of the next time step the finite volume domain was adjusted to take into account the occluders new position, the dependent variables were solved for and the cycle repeated. For each time step the following data were recorded:

i) Occluder displacement,
ii) Occluder velocity,
iii) Force acting on the occluder,
iv) Pressure drop across the valve,
v) Shear rate,
vi) Shear stress,

After every five time steps the dependent variables were recorded. The flow field images produced from this data were saved in Portable Pixel Map (PPM) form to produce an MPEG[93] file which was later played through an MPEG player[94] package allowing visual representation of the changing flow field during the flow cycle.

4.2 Model Requirements

The model was developed to determine the dynamic performance of the valve prosthesis and also to evaluate its haemolytic and thrombogenic potential during a cardiac cycle. The

occluder was allowed to move between its open and closed position depending upon the fluid forces acting on the occluder. In Figure 4.1 the two extremes of position are shown.

a)

b)

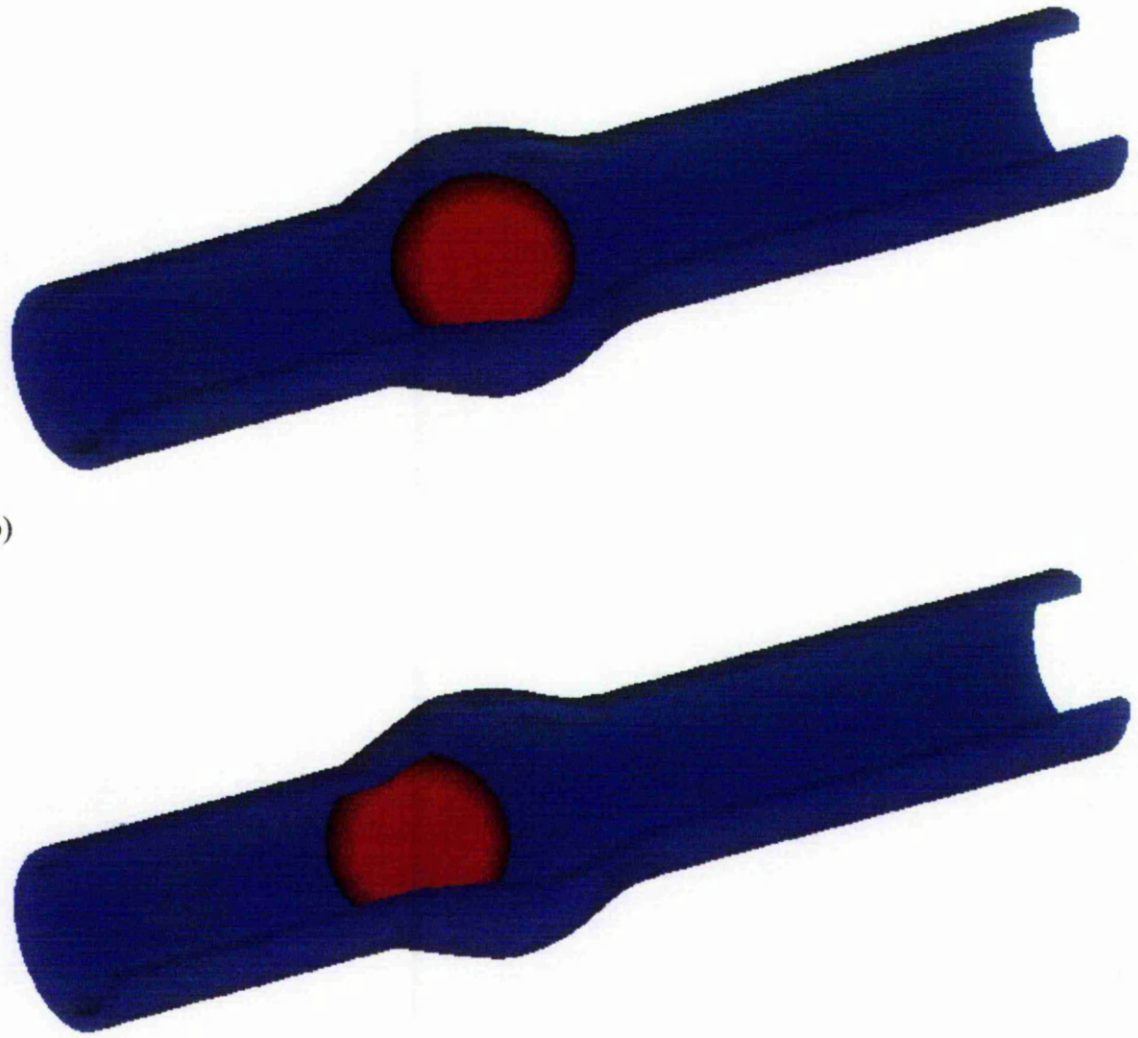

Figure 4.1: Occluder position a) Open, b) Closed.

To solve the time dependent form of the Navier-Stokes equation the CFD package PHOENICS was used, with the primitive variables being pressure (P1) and velocity (W1 and V1), on a body fitted co-ordinate grid.

4.3 Modelling Thrombus

One of the initial aims was to predict and model thrombus formation. This would be possible due to the time dependent nature of the analysis which would allow the growth of a thrombus to be modelled. Thrombus will occur in an area of low shear rate where damaged RBCs are located. It is therefore necessary to determine areas of low shear rate and whether these areas will contain damaged RBCs. Once the area has been located two modelling methods can be used to represent the presence of a thrombus, as follows:

i Two-Phase Model

A two-phase model involves modelling blood and any thrombus formation as two distinct fluids. A finite volume cell may contain only blood, only thrombus or a combination of the two. Each phase will have its own fluid properties, pressure, velocity components and cell volume fraction. It would also be necessary to develop an equation to determine the proportion of the cell occupied by the second phase (thrombus) as the cell would not instantaneously become occupied by thrombus. The implementation of such a model would require the storage of four additional variables: velocity (V2 and W2) and volume fraction (R1 and R2).

ii Porosity Model

A porosity model can be used to represent thrombus by 'blocking off' cells where a thrombus would form. This effectively reduces the fluid velocity within these cells to zero. The cells are 'blocked off' by setting their porosity to zero, i.e. no flow into or out of the cells. This can be achieved in GROUND by issuing the command SETPOR=T and then setting the porosity value for the desired cell to zero. It must be noted that if porosities are to be reset during a flow simulation no wall functions can be applied to the newly 'blocked off' cells. This method of 'blocking cells' can have the effect of producing irregularly shaped areas of thrombus formation causing convergence difficulties and distorted flow fields, as shown in Figure 4.2. The implementation of this type of model would require the

additional storage of three variables: cell porosity (VPOR), low cell face porosity (LPOR), and north cell face porosity (NPOR).

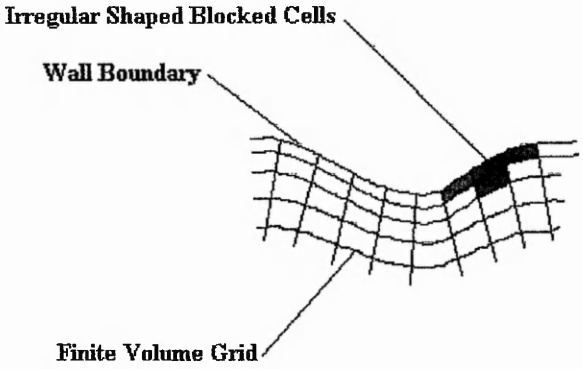

Figure 4.2: 'Blocked off' cells to represent thrombus.

4.3.1 Summary Of Modelling Thrombus

The methods described above show how thrombus formation could be modelled. The models could easily be incorporated into a CFD simulation of blood flow to represent thrombus formation. The main challenge, however, is to predict the onset of thrombus. The flow conditions where thrombus growth may occur are well documented, i.e. areas of recirculation or stasis with low shear rate, and in areas of high shear rate where cells aggregate in places like eddies. Determining these areas can be achieved by analysing the shear rate value of a particular cell and if this value lies within predetermined limits then a thrombus model can be invoked providing that the condition of erythrocytes entering the cell can be determined. This is the main limitation of the thrombus models mentioned above; they do not incorporate a method of determining the condition of erythrocytes within a cell. It would therefore be necessary to seed the inlet of the flow domain with particles, recording their displacement and the shear stress as they pass through the flow domain. If the particle passes through a computational cell with a shear rate value which is known to promote thrombus and the shear stress history of the particle indicates high values of shear stress, it could then be assumed that the fluid entering that particular cell would contain damaged

erythrocytes. This would increase the accuracy of the thrombus model, providing more realistic predictions. Due to the increased complexity and additional storage requirements (exceeding the incore memory available and thus requiring virtual memory storage which slowed the solution down to an unacceptable level) the modelling of thrombus formation was not performed.

4.4 Data Recorded

The advantage of using CFD is that it allows the user to determine field values of pressure, velocity, shear rate and shear stress at any point within the specified spatial domain.

To allow the haemolytic potential of the prosthesis to be determined the value of shear stress was recorded for each time step. Haemolysis is dependent upon both the size of the shear stress and the duration for which it is applied. Therefore the values of both shear stress and duration were recorded. It was not possible to evaluate shear stress and duration within the simulation at every time step due to the possible range of values that might occur requiring an extremely large storage array. It was therefore decided to determine the maximum shear stress value, found from steady state analysis, at peak flow velocity. This peak value was then split into ten intervals and the total volume of cells with shear stress values within each range was determined for every time step.

The thrombogenic potential was assessed by recording the percentage of flow with a shear rate value of less than 7 s^{-1} for each time step. This method also would indicate points within the cardiac cycle where thrombus development would most likely occur.

The dynamics of the occluder were analysed by recording the occluder displacement and velocity, and the fluid forces acting on it. Access to this data allowed the impact force on the support struts to be determined as the occluder reached its fully open position.

4.5 Fluid Properties

The modelling of blood can be conducted in two ways: firstly by assuming blood to be a Newtonian fluid, and hence having constant viscosity and secondly, using a shear rate dependent equation to determine the viscosity. For both cases the density and haematocrit values are assumed to remain constant. For the computational analysis both Newtonian and non-Newtonian (using Cassons[54] relationship, shown in equation (4)) flow was used.

$$\sqrt{\tau} = \sqrt{\tau_y} + S\sqrt{\dot{\gamma}} \qquad (4)$$

Where, $S = 72.42\times10^{-3}$ Pa $s^{1/2}$

$\tau_y = 2.89\times10^{-3}$ Pa

The viscosity for the Newtonian analysis was taken to be 3.323×10^{-3} Pa s. The density and haematocrit values used were 1056.17 kg/m^3 and 40%, respectively.

4.6 Input Velocity Profile

One of the decisions which needs to be taken at the start of modelling flow through a heart valve is whether to assume a fixed inlet pressure cycle for the blood entering the valve section, or a fixed velocity cycle. In the case of a conduit valve the valve section is somewhat remote from the ventricle itself, unlike a conventional valve which is mounted either in the atrioventricular wall or in the aortic root. Consequently it is reasonable to assume that the blood viscosity at the inlet to the conduit valve will be repeatable on a time cycle as well as in a spatial profile and, furthermore, that it will be largely indistinguishable from the aortic outflow of a healthy heart. Therefore the most straight forward approach in this case is to assume an inlet velocity cycle similar to that through a healthy aorta, as shown in Figure 4.3.

The cycle starts with contraction of the ventricle which causes the blood to accelerate up to a maximum flow rate at peak systole. The flow rate then falls away as the ventricle reaches full contraction, and falls to zero as the ventricle relaxes and enters diastole. As diastole gets under way there is a small amount of reverse flow as the cusps of the natural aortic valve, or the ball occluder in the conduit, close. Once this closure is complete, however, the flow returns to zero and stays at that value while the ventricle continues to fill throughout diastole.

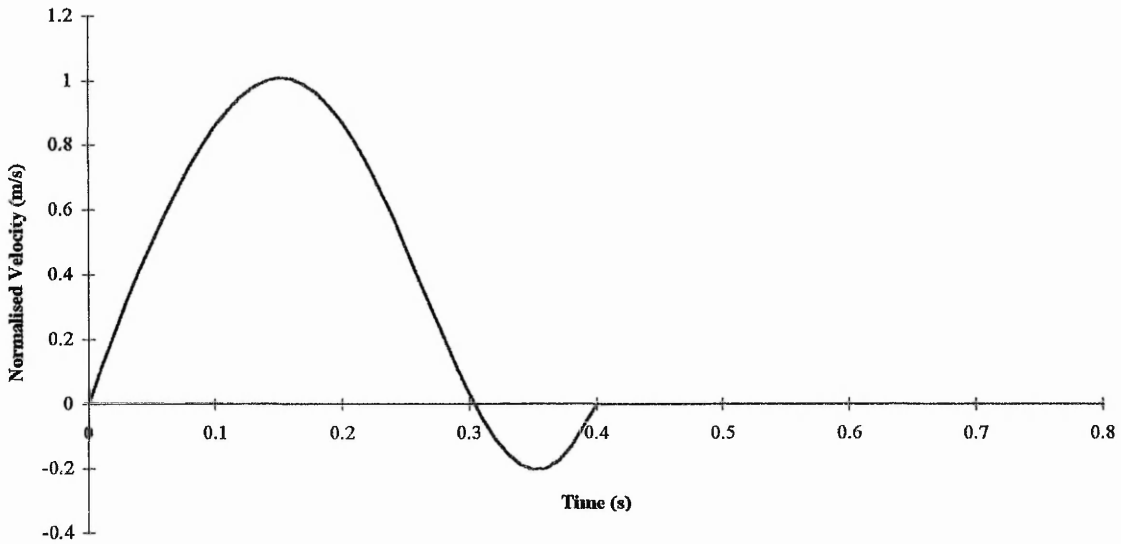

Figure 4.3: Blood velocity within the aorta.

To determine the instantaneous average flow velocity at the entrance to the valve section the volume flowrate was divided by the cross-sectional area of the aorta. An equation for the best fit curve was found using Microsoft EXCEL[95] to produce equation (5).

$$w = 7641.1t^6 + 8993.3t^5 - 3319.1t^4 + 430.01t^3 - 50.243t^2 + 11.809t \qquad 0 \le t \le 0.4$$

$$w = 0 \qquad t > 0.4 \qquad (5)$$

Where, t= Time, s

w= Velocity, m/s

The equation was normalised and only used to determine velocities up to a time period of 0.4 s after which the velocity was assumed to be zero. The complete cycle lasts for 0.8 s and corresponds to a heart rate of 75 beats per minute.

4.7 Grid Definition

Due to singularity occurring when the valve occluder is fully closed the starting point of the occluder was set at 0.5 mm downstream from the actual fully closed position. The initial grid was generated from a FORTRAN program which defines the corner points for the finite volume grid when the valve is in its open position.

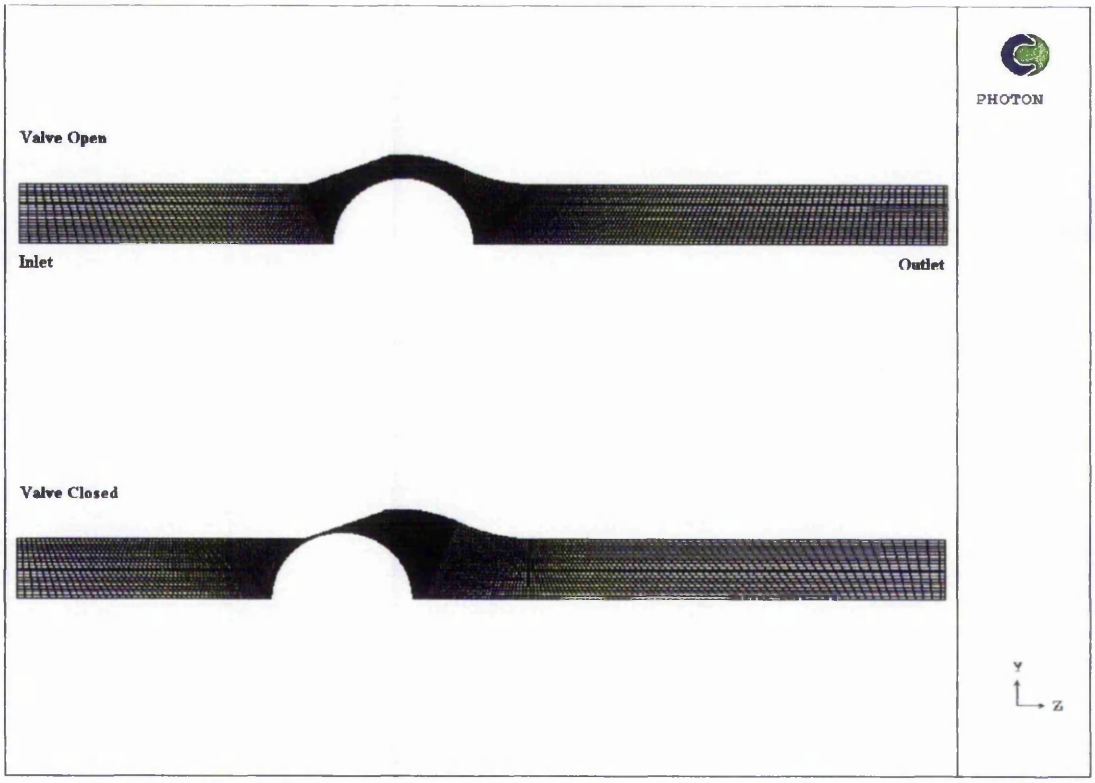

Figure 4.4: Finite volume grid specification.

The modified GROUND file reads the grid co-ordinates for cells of constant j=1 and j=NY for cells ranging from k=1 to k=NZ. It was found that, during the initial opening and late closing phase of the occluder, grid cells needed to be concentrated towards the area where the occluder was closest to the diverging inlet section of the valve housing. This was achieved by using a scaling factor linked to the occluder's displacement, producing the highest concentration of cells as the occluder displacement reached its lowest value and zero cell concentration when the valve was fully open. The two extremes of the grid can be seen in Figure 4.4.

4.8 Boundary Conditions

To allow solution of the partial differential equations (PDEs) describing the fluid flow, boundary conditions are required. The boundaries that required prescription can be seen in Figure 4.5. The four boundaries are the inlet, outlet, outer stationary wall, and occluder moving wall.

For the outer wall boundary no-slip conditions were assumed and the velocity components W1 and V1 were set to zero. At the outlet boundary the pressure value was allowed to float using the FIXP option in PHOENICS. The inlet boundary condition was required to change during the simulation to represent the change in fluid velocity during the cardiac cycle. Both pressure (P1) and velocity (W1) values were set within the PHOENICS user-definable GROUND coding at the beginning of each time step.

The wall boundary conditions on the occluder surface are dependent upon the occluder velocity. The velocity perpendicular to the surface of the occluder (V1) was set at zero and the velocity of the fluid parallel (W1) to the occluder surface was set to the occluder velocity. This was necessary as the velocities calculated within the flow domain are relative to a stationary point and the assumption that the fluid velocity at the occluder surface would be zero is incorrect in this frame of reference and only valid from a point on the occluder surface.

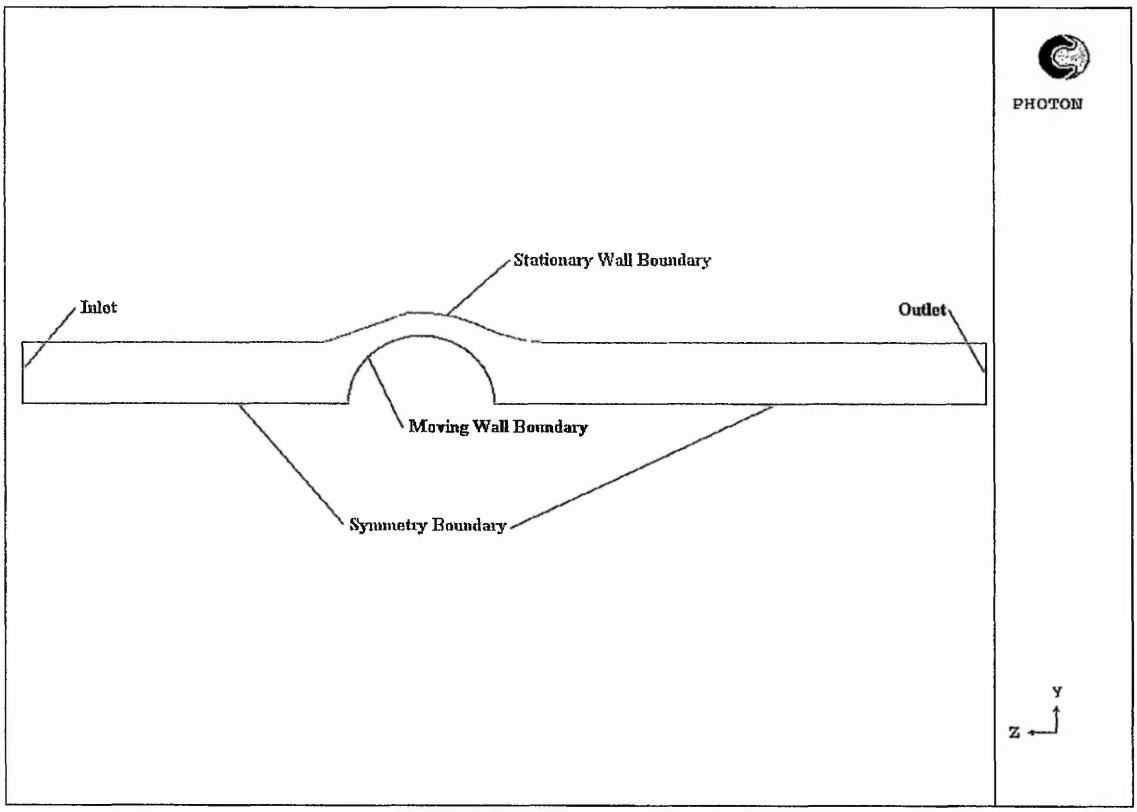

Figure 4.5: Boundary specification.

4.9 Calculation Of Ball Displacement

To calculate occluder displacement it was first necessary to determine the forces acting on the occluder during the current time step. Equations (6) and (7) show how the streamwise pressure and shear stress forces were calculated.

$$F_P = \sum P \partial A_P \tag{6}$$

$$F_\tau = \int_0^{2Rb} 2\pi \mu_{eff} r \frac{dw}{dy} \partial z \tag{7}$$

Where, F_P=Streamwise pressure force over the occluder surface,

P=Pressure,

A_P=Occluder surface area perpendicular to flow axis,

F_τ=Streamwise shear stress force,

μ_{eff}=Laminar viscosity, μ_l,

r=Elemental radius,

Rb=Ball radius.

Resolving a force balance equation acting on the occluder and then integrating produced equation (8) which was used to determine the distance travelled by the occluder at the current time step, *k*.

$$Z_o(t) = \frac{1}{2}\ddot{x}_o(k)(t - t_k)^2 + \dot{x}_o(t_k)(t - t_k) + x_o(t_k) \qquad (8)$$

Where, $t_k \le t \le t_k + \Delta t$,

$\ddot{x} = \frac{F_o}{m_o}$,

$F_o = F_p + F_\tau$, Total force acting on the occluder, N,

m_o = Mass of occluder, kg,

t = Time, s,

Z_o = Occluder displacement, m.

The occluder displacement was determined at the end of each time step and the new occluder position pertained over the following time step. This method is inherently explicit in nature and therefore requires a smaller time step division than an implicit technique. Section 4.11 examines the effect of varying the time step size

4.10 Solution Algorithm

The solution sequence at each time step can be seen in Figure 4.6. At the start of the time step the inlet velocity was calculated using equation (5), the boundary conditions for the inlet and occluder surface were then set.

If the occluder displacement differs from that of the previous time step then the finite volume grid is redefined using the new occluder position. The dependent variables were then solved for until the convergence criteria were satisfied. The forces acting on the occluder were then calculated and the occluder displacement found from equation (8). Information determined from the field data (see Section 4.3) was then recorded and the next time step started. Appendix A3.1 gives a full documented listing of the modified GROUND file. The entire solution period ends when the occluder returns to its closed position.

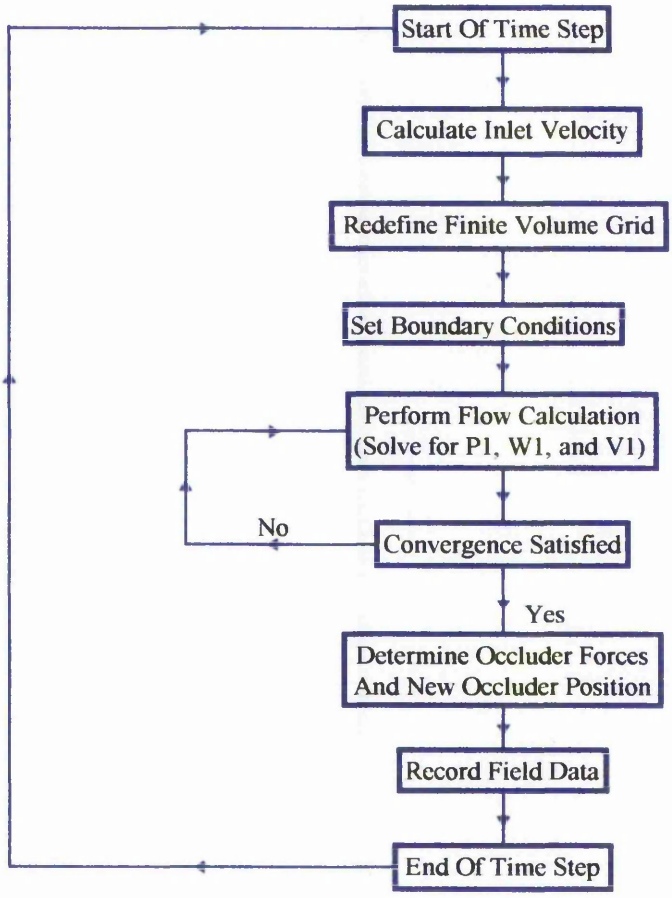

Figure 4.6: Solution sequence.

4.11 Grid Dependency

The accuracy of the results generated from a computational analysis is largely dependent upon the spatial density of the finite volume cells. In a steady state solution a grid independent solution can be found by performing the flow simulation on grids with increasing cell density. At some point it will be found that the variation of a dependent variable will no longer change or will only change by a small percentage of its previously predicted value from a less dense grid. It is at this point it can be assumed that the final grid would produce a grid independent result.

It is also necessary to ensure that the grid density it not so large as to require excessive computational effort, increasing the total time required to provide a solution. Therefore a compromise must be met between grid density and solution time.

When a grid is required for a time varying solution the size of the time step division would also affect the accuracy of the final results. To determine a satisfactory grid density for this type of problem would require simulation of the flow model using decreasing time step size and increasing grid density, but of course, the combinations of time step size and grid density are infinite. The grid density was therefore set to its maximum above which virtual memory would be required to act as a temporary store during the flow simulation. This ensured an acceptable level of computational performance with reasonable accuracy.

4.12 Time Step Size Validation

It was necessary to determine the minimum time step size required in order to predict the flow regime accurately but whilst still maintaining computation economy. The area of greatest interest was during occluder movement. It was important that the time step size should not be too great otherwise the occluder displacement would be over predicted. A peak Reynolds number of 4000 was chosen for this analysis as this would produce a rapid

acceleration of the occluder and hence provide a more accurate assessment of the minimum time step size required.

It was found that the occluder would be fully open after 0.05 s, therefore the simulation time was taken to be 0.05 s. This time period was discretised into 25, 50, 100, 150 and 200 steps producing time step sizes (Δt) of 2.0×10^{-3}, 1.0×10^{-3}, 5.0×10^{-4}, 3.3×10^{-4} and 2.4×10^{-4} seconds. The results of occluder displacement with respect to time can be seen in Figure 4.7. The figure shows that for large time step sizes the occluder displacement was over predicted but as the time step size becomes smaller the occluder displacement is more consistently predicted. It was therefore decided that the maximum time step size should be no greater than 5.0×10^{-4} s which corresponds to 100 time divisions per 0.05 s.

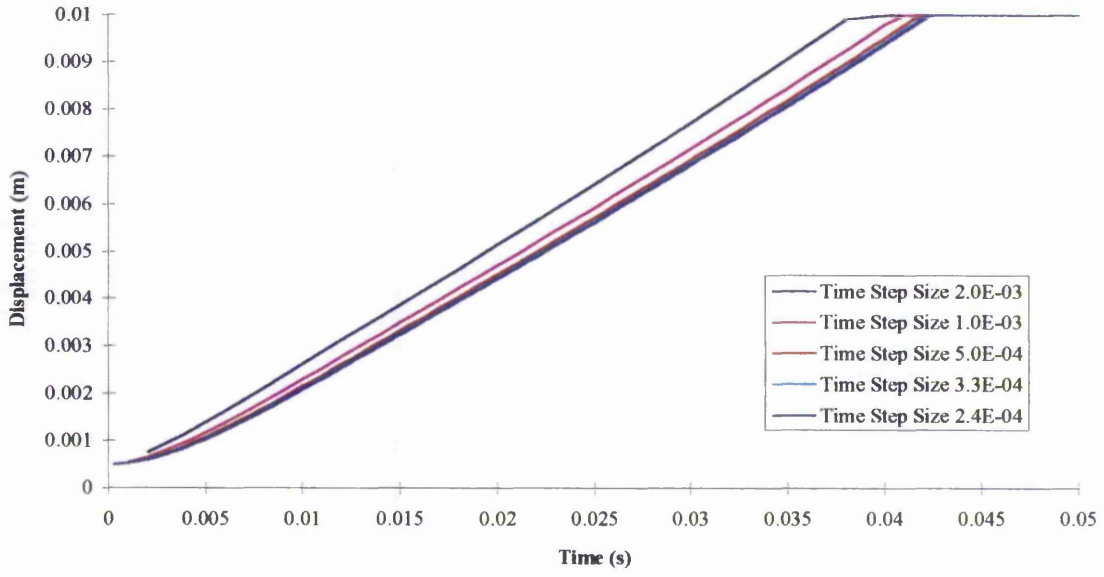

Figure 4.7: Occluder displacement for varying time step sizes.

Chapter Five

Validation Of Numerical Model From Experimental Analysis

5.1 Introduction

This chapter describes the experimental model used to determine occluder displacement when subjected to a varying flowrate. The experimental model was not used to determine the total flow characteristics of the prosthesis; the main aim was simply to determine occluder displacement during a pulse cycle. Full measurement of the flow field was not carried out due to its time varying nature and complexity, requiring Laser Doppler or Ultrasound Doppler data procurement methods. The results obtained from the experimental model were then compared to those obtained from CFD analysis using the same flow conditions, with the aim of providing some validation of the CFD predictions.

The results at the end of this chapter show poor predictions for the opening and closing times of the occluder. However the time predicted for the occluder to open and then close is very good with a maximum error of 6.244 %. The reason for the discrepancy in the results is explained in Chapter 7.

5.2 Experimental Model

The experimental model was designed to simulate a sinusoidal varying flowrate through the test valve using a reciprocating pump. It was not possible to accurately simulate the pulse produced by the contraction of a real ventricle but a reciprocating pump provides a close and readily achieved approximation. For each flowrate the position of the occluder was recorded at a predetermined time interval.

5.2.1 Aim Of Experimental Model

The experiment was designed to allow the occluder displacement, predicted by the computational model, to be compared against the experimental model.

5.3 Apparatus

With the aid of a reciprocating pump, the experimental rig was able to produce sinusoidal varying flow in a fluid circuit. With the addition of a heart valve prosthesis the reverse portion of the sinusoidal flow is largely suppressed and there is a net positive flow through the circuit

International standards exist for the testing of prosthetic heart halves (ISO 5840), therefore the experimental model incorporated the following features:

i) Produce pressure flow wave forms that approximate to those found in healthy adult humans,
ii) A variable stroke volume up to at least 100 ml,
iii) A variable cycle rate up to at least 150 cycles/minute,
iv) Simulate forward flow pressure of at least 120 mmHg ± 7.5 mmHg and reverse flow pressure of 80 mmHg ± 3.8 mmHg,
v) Allow the observer to view and photograph the test valve at all stages in the cycle,
vi) Permit measurement of time dependent pressure, flow, and occluder displacement.

The test rig was designed to comply with as many of the features listed above as possible. Figure 5.1 shows the basic layout of the test rig.

The pump consisted of a piston-cylinder assembly, attached to a motor via a connecting rod. The pump's maximum displacement was 160 ml which could be varied by adjusting the stroke of the piston. For each test the pump was set to its maximum travel thus ensuring a constant stroke volume of 160 ml for all tests.

The motor was a three phase Crompton-Parkinson motor (Serial Number TMF584TF1B640) which turned a flywheel via a Crofters 'Ritespeed' gearbox (Serial Number 3JJN2573/64).

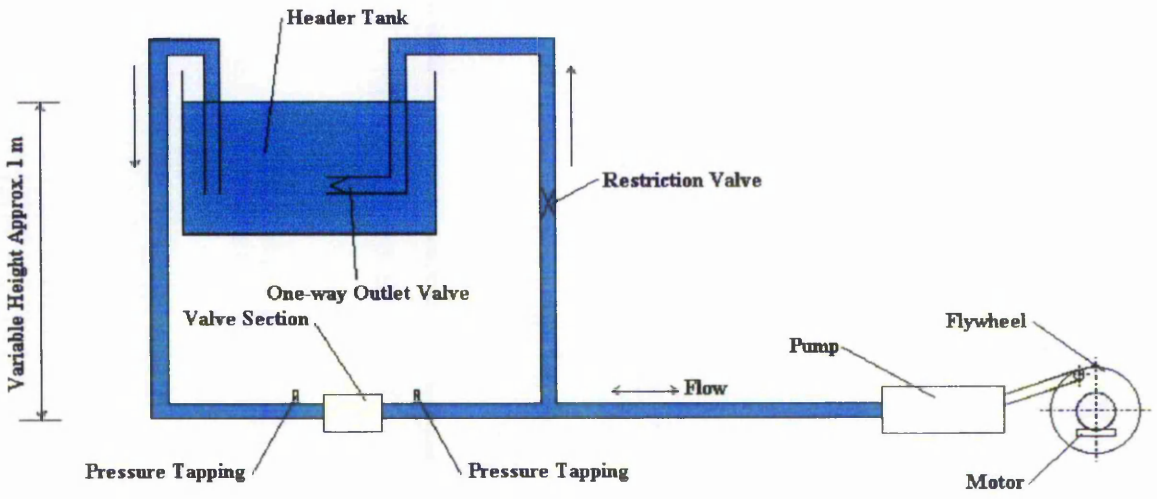

Figure 5.1: Schematic representation of test rig.

With the maximum speed of the motor at 230 rpm and a pump stroke volume of 160 ml compliance with ISO 5840 was achieved. The speed of the motor was controlled by an uncalibrated dial, therefore motor speed was determined from a tachometer.

Water was used as the working fluid and was pumped from a reservoir through the valve prosthesis. Therefore the forward pumping stroke of the piston, in the cylinder, was used to close the valve with the remaining fluid returning to the reservoir tank via a one-way valve.

5.3.1 Valve Housing

The valve section was secured between two pipes, as shown in Figure 5.2. The design of this section provided low light distortion properties, with smooth internal joints minimising flow disturbance. The section was robust to withstand the high pressures produced by the pump at high speeds.

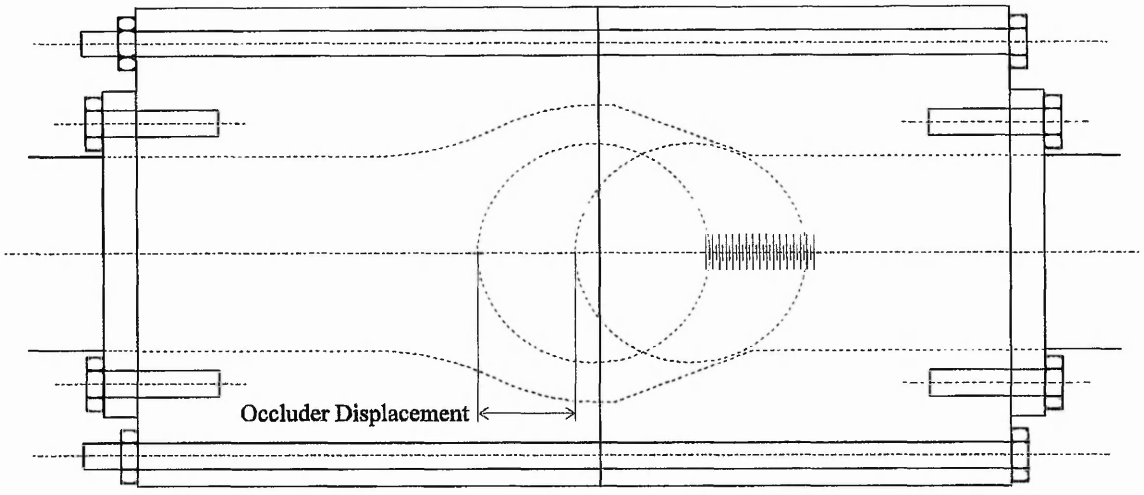

Figure 5.2: Valve section.

5.3.2 Pressure Reading Equipment

The data to be produced by these experiments were the positions of the ball occluder at set time intervals throughout the pumping cycle for a range of pump frequencies, and hence flow rates. the idea was to compare these position values with the ones predicted by the CFD analysis for the same frequency and overall flow rate. Hence there was no great need for accurate adjustment or recording of the pressure values; it was only necessary to ensure that the reverse pressure was high enough relative to the inlet pressure to close the valve properly. The actual pressure drop across the valve during forward flow was set by the flow resistance of the valve and therefore varied with flow rate.

For simplicity it was adequate to use simple manometer tubes to record inlet and outlet pressures. The manometer was connected to pressure tappings 200 mm either side of the valve section. Care also had to be taken that the manometer was set in the vertical position to minimise pressure head errors. Adjustment of reverse pressure drop was achieved by fitting restricter valves on the reservoir return pipe and the reservoir supply pipe and adjusting them to give a reading of approximately 1.1 m (~ 80 mm Hg).

5.3.3 Visualisation Technique To Determine Occluder Displacement

One possible method to record occluder movement was to use multiple exposures on a still camera to produce a series of ghost images on a film. This method would provide accurate recording of the occluders displacement, however this method would not be able to differentiate between images produces during the opening and closing phases of the occluder.

The second method, and the one used, involved videoing the occluder movement using a Matic video camera (Model Number GX-N7E) which could record at 50 frames per second providing a 0.02 s sampling frequency.

5.3.4 Measurement Method Used

To measure occluder displacement a 1 mm spaced grid was attached behind the valve section. Physically attaching the grid to the valve section eliminated any errors that may occur due to axial movement of the valve section. Measurements were taken from a datum point on the grid to the front edge of the occluder. The measurement positions can be seen in Figure 5.3.

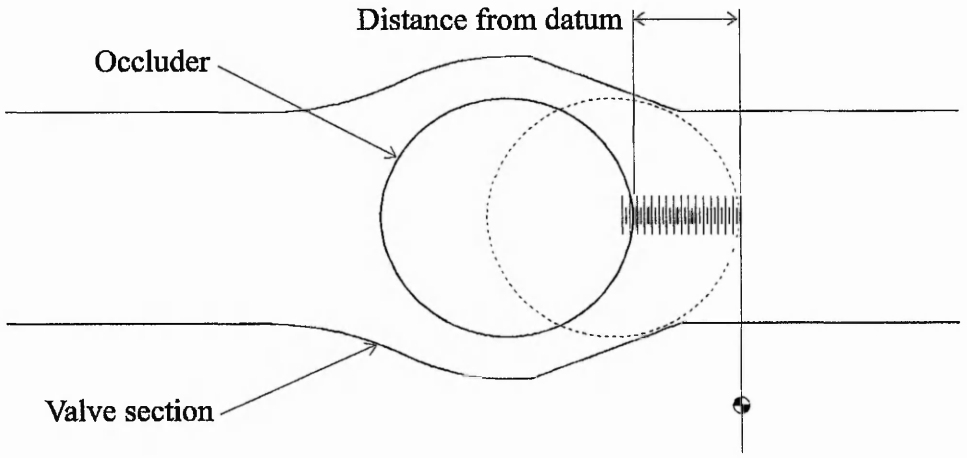

Figure 5.3: Occluder measurement from datum point.

5.4 Initial Set-up

Prior to any results being obtained the test rig was run to ensure no air pockets existed within the system. The manometer was purged of air and then adjusted to ensure the height of water in each tube was equal. The focus on the video camera was checked and the correct exposure level was set.

5.5 Experimental Procedure

Tests were carried out at 10 cycles per minute (cpm) intervals over a range of 60 cpm to 180 cpm, the speed being verified by a tachometer.

The pressure drop across the valve section was adjusted, using a restricter valve, to the value stated in section 5.3.2. Once the speed and pressure drop had been set the system was left to settle for three minutes. At the end of this settling time the occluder movement was recorded by the video camera. The speed of the motor was increased by 10 cpm and the procedure repeated until all tests speeds had been carried out. At the end of each test the tachometer reading was checked to ensure the motor speed had not changed.

The video film was then replayed and the occluder displacement, measured from the datum point, recorded for every 0.02 s frame.

5.6 Computational Model

The computational model examined the flow through the valve section. The inlet section length was 53 mm and the outlet section length 77 mm, the conduit diameter being 26 mm. The finite volume grid contained 20 cells in Y direction, 360 cells in Z direction and 1 cell in the X direction. The velocity profile of the fluid at the entrance to the inlet section was parabolic, matching the experimental flow profile, and varied in a sinusoidal manner with time.

The fluid properties were, density 1000 Kg/m^3 and viscosity 1.002×10^{-3} Pa s. Due to the length of time to run each model it was decided that only three of the experimental flowrates would be simulated. The models run had flowrates of 0.16, 0.32 and 0.48 l/s at 60, 120 and 180 cpm, respectively. The computational model was capable of recording more information than was recorded by the experiment, but only occluder displacement was compared.

5.7 Comparison Of Numerical And Experimental Results

The results obtained from the experimental and computational models for 60, 120 and 180 cpm are shown in Figures 5.4, 5.5 and 5.6 respectively. Comparing the first model (60 cpm) it can be seen that PHOENICS is over predicting the occluder displacement during the initial opening phase of the valve, also the computational model can be seen to predict the valve beginning to close, and closing, before the experimental model. The error in predicting the overall time it takes the valve to open and then close was only 6.244 %.

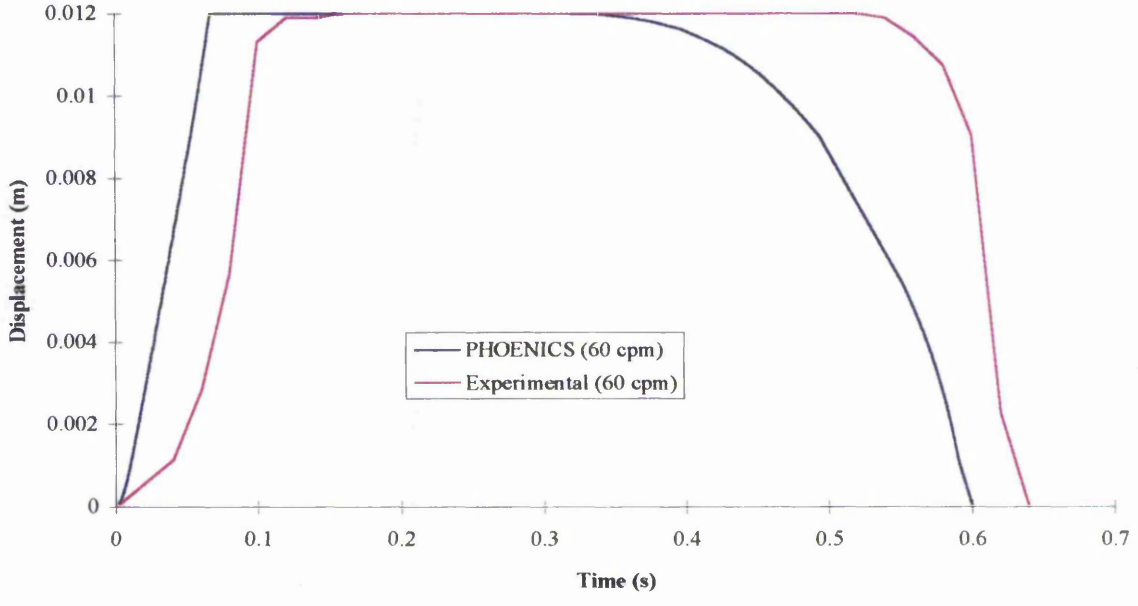

Figure 5.4: Results from 60 cpm experimental and computational model.

For the next model (120 cpm) the same happens except the computational model over predicts the total overall time for the occluder to open and then close by 3.589 %.

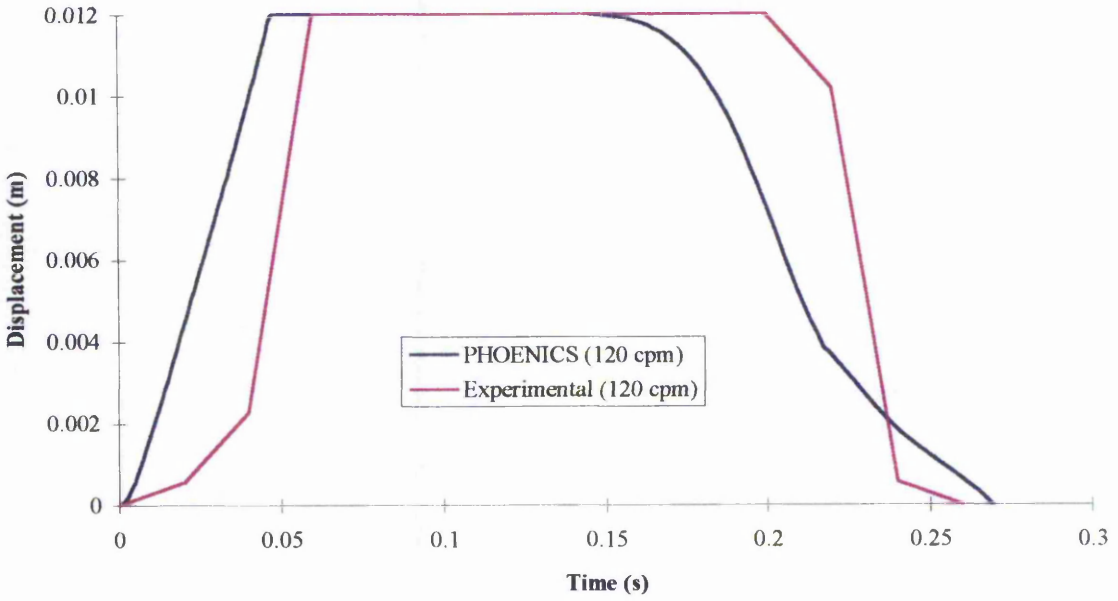

Figure 5.5: Results from 120 cpm experimental and computational model.

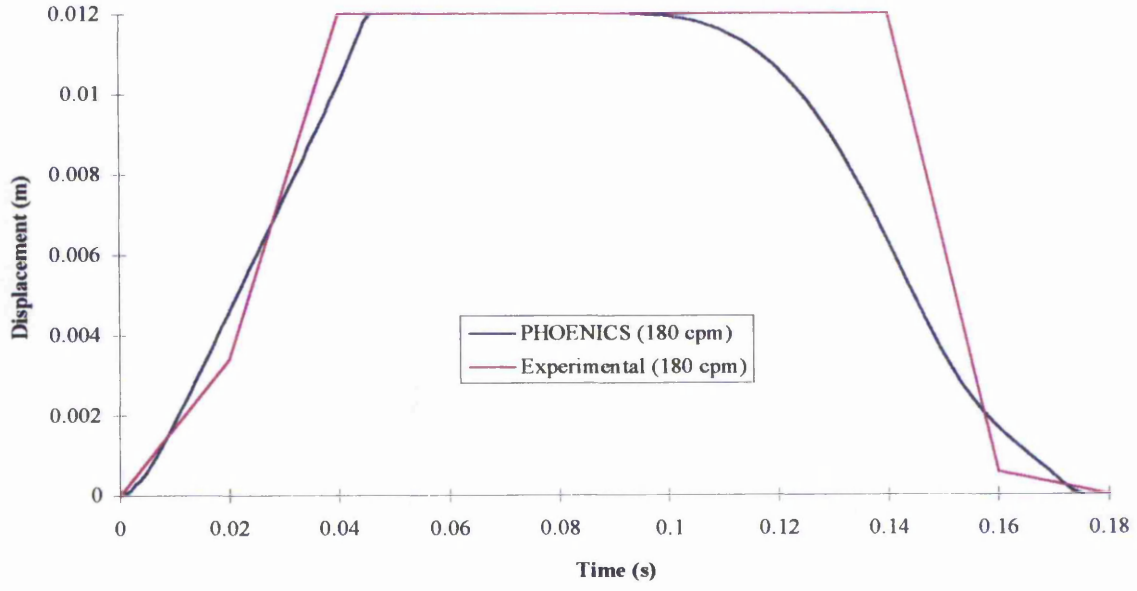

Figure 5.6: Results from 180 cpm experimental and computational model.

The final model (180 cpm) shows the occluder opening phase is being predicted very closely, with an error in predicting the initial opening time of 10.343 %. Again the PHOENICS model predicts the occluder closing sooner, but with an error, in the overall time, of just 2.611 %.

A summary of the errors comparing both models for; time to open, time at the beginning of the closing phase, and the overall time to return to the closed position, can be seen in Table 5.1. It can be seen that PHOENICS was not predicting the time when the occluder was starting to close correctly, with large errors occurring at this point. As the frequency increased the computational predictions of the occluder reaching its open position reduced. The smallest errors occurred in the prediction of the overall time, with a maximum error of 6.244% (60 cpm) and minimum error of 2.611 % (180 cpm).

Table 5.1: Error in PHOENICS predictions compared to experimental values.

Cycles Per Minute	**Time To Open (%)**	**Time At Begin Of Closing Phase (%)**	**Total Time To Return To Closed Position (%)**
60	57.643	43.888	6.244
120	20.667	34.848	3.589
180	10.343	42.916	2.611

Overall the performance of the computational model was quite good, but the detailed performance was poor, with large errors occurring at key points within the occluder displacement cycle. To be fair it must be noted that the displacement predicted by the experimental model has some considerable degree of error as readings could only be taken every 0.02 seconds. The reasons for PHOENICS poor performance will be show in the next chapter and a discussion of the possible causes of the models behaviour can be found in Chapter 7.

Chapter Six

Results From PHOENICS Flow Analysis

6.1 Introduction

The results from the PHOENICS flow analysis are presented within this chapter. The main areas considered are the field values of velocity, shear stress and shear rate, the dynamics of the occluder, and the clinical consequences.

The following sections present data in a manner that allows the overall performance of the conduit valve to be assessed in a situation representative of the *in vivo* application. The differences between the Newtonian and non-Newtonian models were minimal except in the prediction of peak shear stress where the Newtonian models exhibited higher values. The ability to access shear rates and shear stresses within the finite volume domain throughout the flow cycle allows a more detailed analysis of the clinical characteristics of the valve prosthesis than could be obtained from just *in vitro* testing.

Incorrect calculation of pressure by PHOENICS limits the confidence in the predicted occluder displacement and shows a limitation of this particular CFD package to the analysis of unsteady flow simulations.

6.2 Specification Of Computational Model

The conduit valve was analysed under a series of flow regimes. The peak Reynolds numbers for each flow model were 500, 1000 and 2000. Both Newtonian and non-Newtonian flow was considered. For all flow models laminar flow was assumed. In the non-Newtonian models, Casson's blood model was used to determine the viscosity of the fluid. In all cases the density remained constant at 1056.17 kg/m^3 and haemotacrit concentration at 40%. The Wormersley[96] number, defined in equation (9), was calculated at 5.042, assuming average fluid properties and cardiac frequency of 75 beats per minute.

$$\alpha = \frac{d}{2}\sqrt{\frac{\omega}{\nu}} \tag{9}$$

Where, α= Wormersley number,

d= Conduit diameter,

ω= Cardiac frequency,

ν= Kinematic viscosity.

The axisymetric finite volume grid was based around a 20 mm diameter conduit valve prosthesis with a conical inlet and curved outlet with a 30 mm blend radius. The dimensions of the geometric model can be seen in Figure 6.1.

The model consists of 20 cells in the Y (radial) direction, 360 cells in the Z (axial) direction, and 1 cell in the X (circumferential) direction. The initial Cartesian grid co-ordinates were produced using a FORTRAN program and read into PHOENICS through a GRID.DAT file.

The inlet velocity was uniform across the inlet section, producing a 'plug' type velocity profile at the entrance to the valve section. This velocity profile was chosen to represent the flow situation that would prevail with a conduit close to the ventricle.

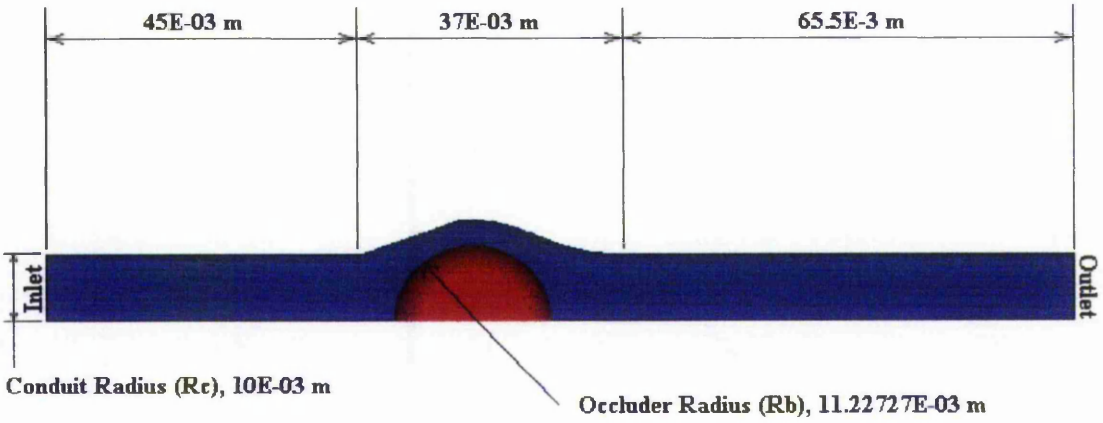

Figure 6.1: Grid geometry.

Each model was run for one cycle only. As the valve could not be modelled in its fully closed position, the cycle was considered complete when the occluder returned back to its start position which, as defined earlier,was with the ball 0.5 mm downstream from the actual fully closed position.

6.3 Time Steps, Convergence Criteria And Sweeps

Time Steps

To maximise computational efficiency with minimum effect to the accuracy of the dependent variables (P1, V1 and W1) the time step size (Δt) was varied depending upon the position of the occluder.

A smaller time step size was required whilst the occluder was opening and closing (see Section 4.9), therefore time step divisions were concentrated during these periods. When the occluder was in its fully open position the time step size was increased to increase computation economy. During the opening and closing phase of the valve the number of time steps varied from 100 to 150. The longer the occluder took to open, associated with lower flow rates, the more time steps were used to maintain the desired time step size. When the occluder was in its fully open position the number of time steps used was in the range of 150 to 250. Again the longer the occluder was in the open position, associated with the lower flow rates, the more time steps were required to maintain a consistent time step division between all the models.

Convergence Criteria

For each time step the convergence criteria, specified in the PHOENICS Q1.DAT input file, was to be satisfied before continuing to the next time step. The reference residual values, set in the Q1.DAT input file, for pressure and velocity components were 1×10^{-10} and 1×10^{-8}, respectively. When both pressure and velocity residuals fell below the predetermined value the solution for the current time step was assumed converged. The convergence characteristics of the velocity variables, for most of the time steps, followed the pattern of rapidly reducing residuals followed by a continuous period of values that fluctuated around the predetermined convergence cut-off point, see Figure 6.2.

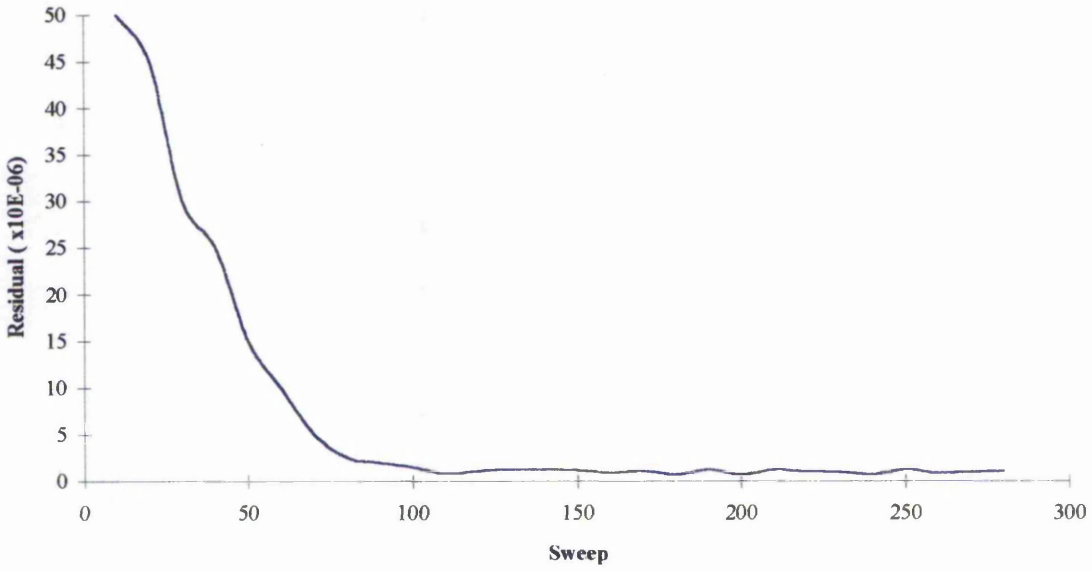

Figure 6.2: Plot of residuals versus number of sweeps.

The pressure residuals followed the same pattern but with residual values below the convergence cut-off point. To allow the solution of each time step to end it was decided that a maximum number of sweeps would be used, avoiding the situation where the solution would continue indefinitely. This also meant that if the convergence criteria for all the variables were satisfied the solution procedure would automatically end and the next time step commence. The maximum fluctuating residual value, for velocity, was found to be 1×10^{-7}, an acceptable value.

Sweeps

In time dependent flow models with stationary boundaries, with sufficiently small time step sizes, the number of sweeps per time step generally remains constant. This was found to be true while the occluder was in its fully open position but when the finite volume domain was modified during occluder movement the number of sweeps required for convergence increased during this period. The number of sweeps required per time step, to achieve convergence, ranged from 250 to 1000. The larger number of sweeps was required during the initial opening and closing phase of the occluder to allow sufficient reduction in the

residuals to satisfy convergence before the next time step was started. When the occluder was in its fully open position the minimum number of sweeps required to satisfy convergence was found to be 250. A relationship between occluder displacement and sweep number was produced to allow the number of sweeps to vary linearly between the two values of 1000 and 250.

The user defined GROUND coding was modified to allow the number of sweeps to be set at the beginning of each time step. The application of this method allowed the minimum number of sweeps to be used to produce a converged solution without incurring additional computational expense.

The computations were performed on a VAX4000/600 system with 128 megabyte of random access memory. The overall CPU time for each model was 143849 seconds, approximately 40 hours. The models were run in batch mode which meant the overall time for a model to run was between two and three weeks, depending on how much the system was being used by other users.

6.4 Field Values (MPEG Video)

The total size of the field variable files (PHI) and BFC geometry files (XYZ) for each model was about 80 megabytes. This information was saved at every five time steps; saving information for each time step would require more storage than was available. Representing this information in hardcopy form for each time step would take up too much space within this thesis, therefore the technique of converting the field value images into an MPEG movie stream file format was employed.

6.4.1 Velocity Distribution

To represent the flow field values of velocity for each model, an MPEG animated sequence was created. For each model, the field values were saved every five time steps. The

information was then saved as a series of screen pictures (in PPM format) and then compiled using an MPEG encoder to produce a file which could be played by an MPEG player. The disks in the back of this thesis contain the movie files of velocity (W1) for all the models. Flow visualisations studies, conducted in Australia, for a conduit valve, were converted to Windows AVI movie file format and can be found in the back of this thesis. The unit of velocity within the following figures being m/s.

All the models exhibited similar flow characteristics:

i) Initial Opening Of The Occluder

During the initial opening phase of the occluder an area of high fluid velocity develops in the region between the occluder and the diverging valve section wall, as shown in Figure 6.3.

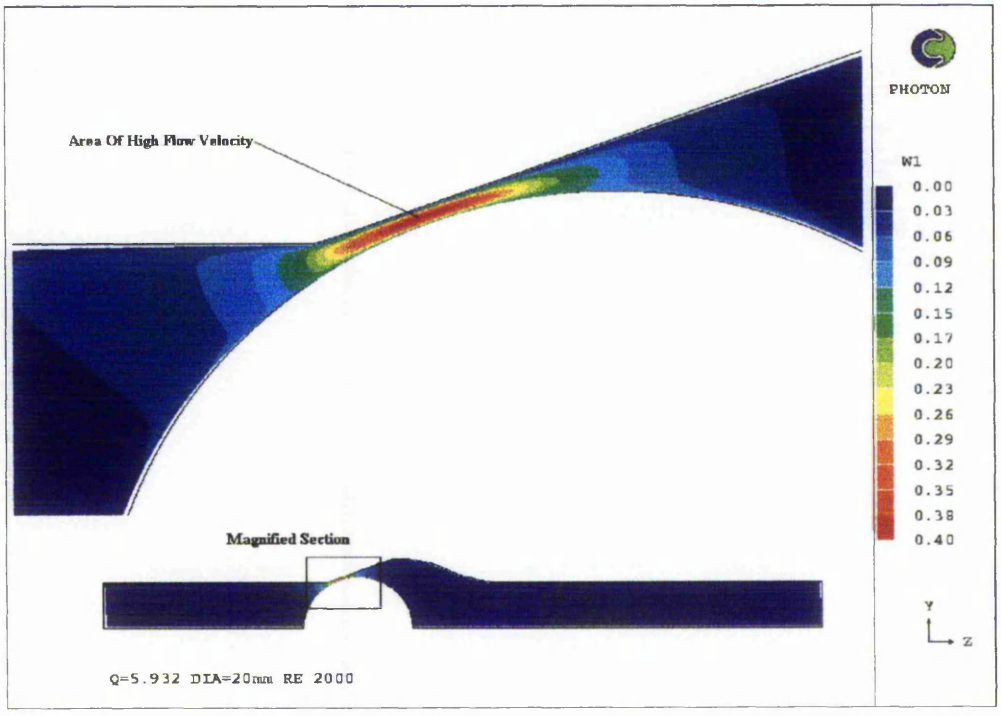

Figure 6.3: Contour plot showing area of high flow velocity during initial opening of the occluder.

The fluid velocity within this region is high, comparable to the maximum fluid velocity within the valve section at peak inlet velocity. As the occluder opens further the maximum velocity of the fluid reduces as the flow area, between the occluder and diverging section, increases.

ii) Flow Within The Valve Section Prior To The Valve Opening Fully

As the flow develops within the valve section an area of recirculation forms at the junction of the diverging and cylindrical sections of the valve, as shown in Figure 6.4.

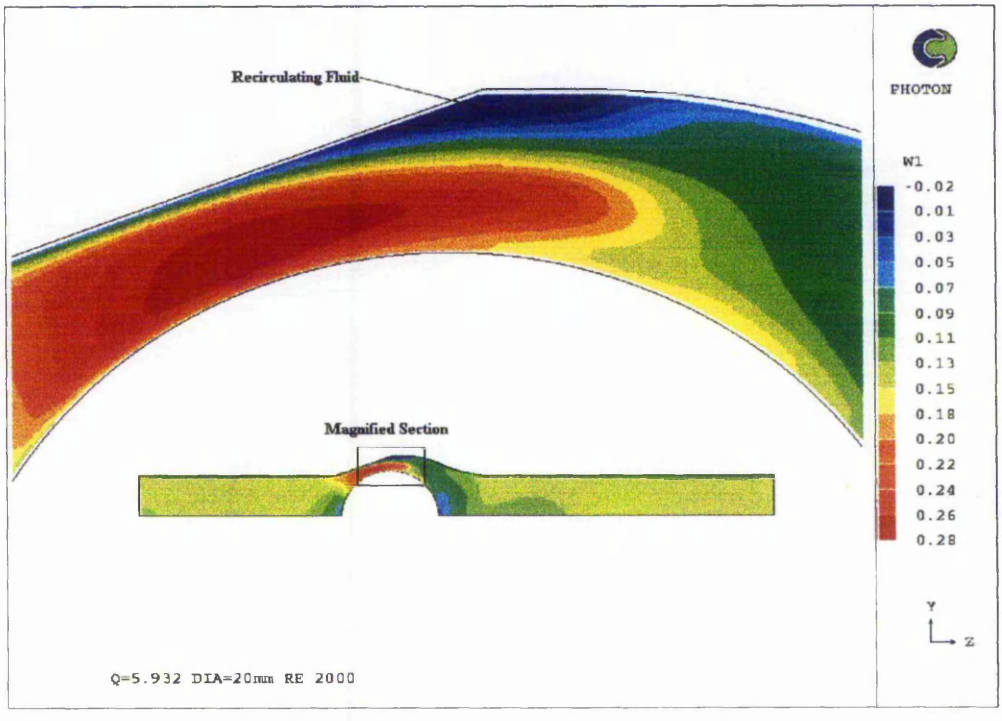

Figure 6.4: Velocity contour plot showing recirculation at the junction between the diverging inlet and flat section of the valve.

The area of increased flow velocity occupies most of the diverging section and extends into the cylindrical section of the valve. As the fluid next to the occluder surface has the same velocity as the occluder this increased flow velocity region is biased towards the moving

occluder. Upstream and downstream close to the occluder an area of stasis was formed around the conduit axis.

iii) Peak Inlet Velocity

When the inlet velocity reached its maximum value the data for that time step was recorded. The field values for velocity are shown in Figure 6.5. The area of increased flow velocity now extends into the converging outlet section of the valve. The area of recirculation at the junction of the diverging and cylindrical sections of the valve has disappeared and an area of recirculation has formed just behind the occluder. Comparing Figure 6.5 to those found in Section 2.5.1 it can be seen that the jet formed in the steady analysis extends much further, continuing right into the outlet section of the model and not just the converging section of the valve. This is due to the fact that steady analysis assumes the flow develops over an infinite time period whereas the time-dependent analysis assumes a finite time period.

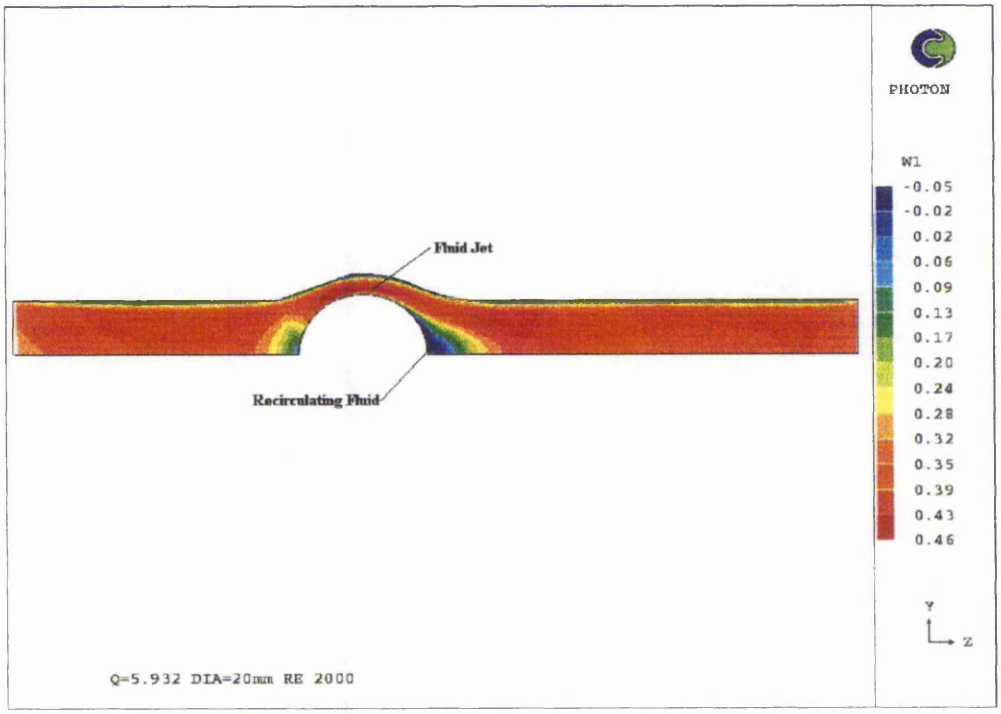

Figure 6.5: Velocity contour plot at peak inlet velocity.

iv) Late Closing Of The Occluder

After peak inlet flow had been reached and the inlet velocity began to decrease the fluid along the top boundary reversed direction. The area of reverse flow increased rapidly as the inlet velocity decreased further. The velocity contour plot, shown in Figure 6.6, displays the flow field just prior to the occluder reaching its fully closed position. The figure shows a fluid jet within the valve section and a large recirculation zone behind the occluder. An area of forward fluid flow can be seen in the inlet and outlet sections of the model.

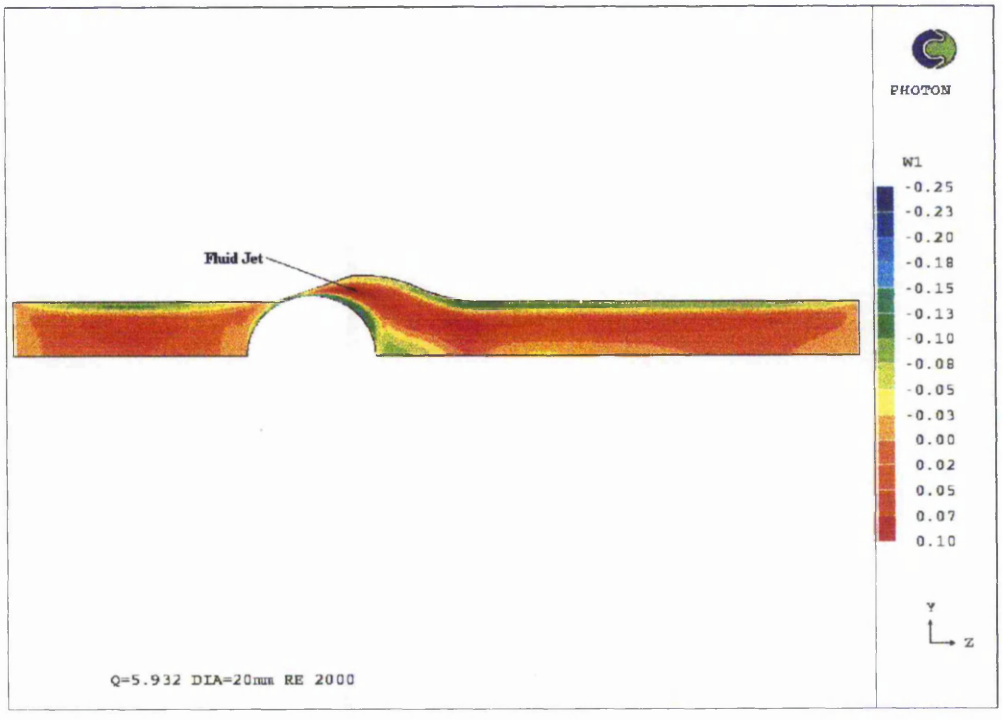

Figure 6.6: Velocity contour plot of flow jet during valve closure.

6.4.2 Shear Stress Distribution

The field values of shear stress for the non-Newtonian model with a peak Reynolds number of 2000 can be seen in the MPEG file Rn2000t.mpg. The unit of shear stress shown within the following figures being Pa. At the beginning of the flow cycle, during initial occluder

opening, the maximum shear stress for all the models occurs. The shear stress was concentrated within the diverging section of the valve housing, shown in Figure 6.7, with high values of shear stress occurring on the surface of the valve housing.

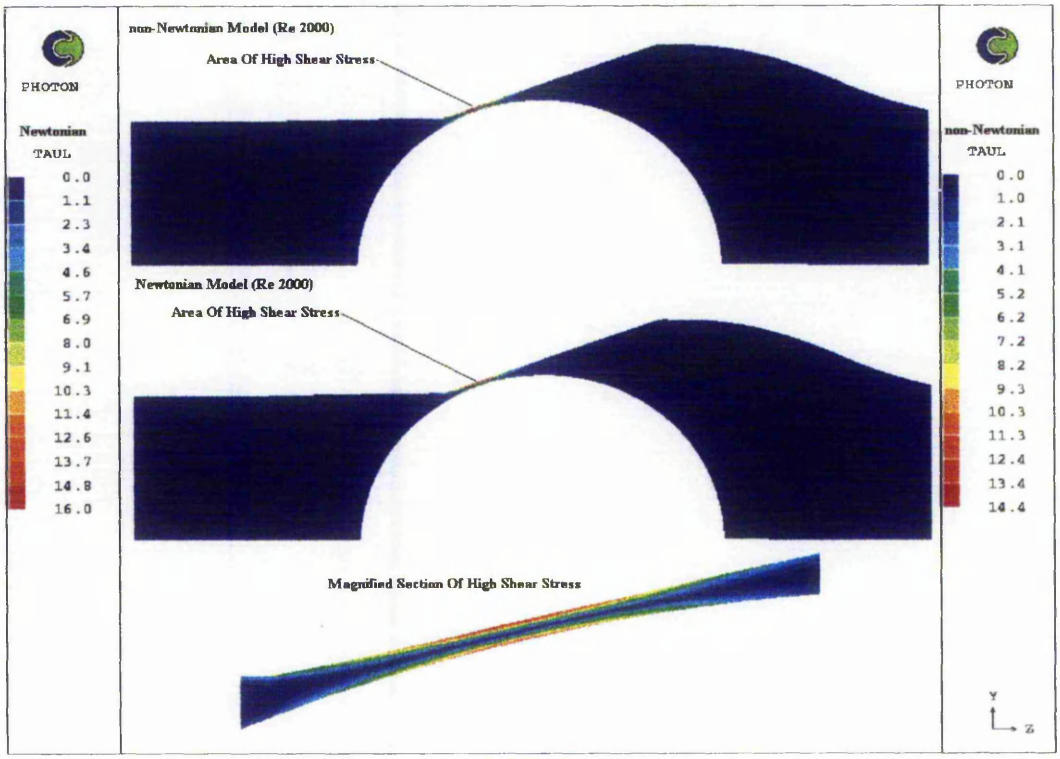

Figure 6.7: Shear stress contour plot during initial opening of the occluder (Re 2000).

As the occluder opened further the maximum value of shear stress fell quickly. By the time the inlet velocity had reached its maximum value, three distinct areas of elevated shear stress were observed: an area of high shear stress along the occluder surface (1), another on the diverging section surface (2), and a smaller region of rather lower shear stress along the surface of the converging section of the valve (3), shown in Figure 6.8.

The maximum shear stress occurred during the initial opening of the occluder. The maximum values of shear stress, seen in Table 6.1, were obtained from the first results file (saved at time step five) of each model and the peak flow shear stress was found at peak inlet flow velocity.

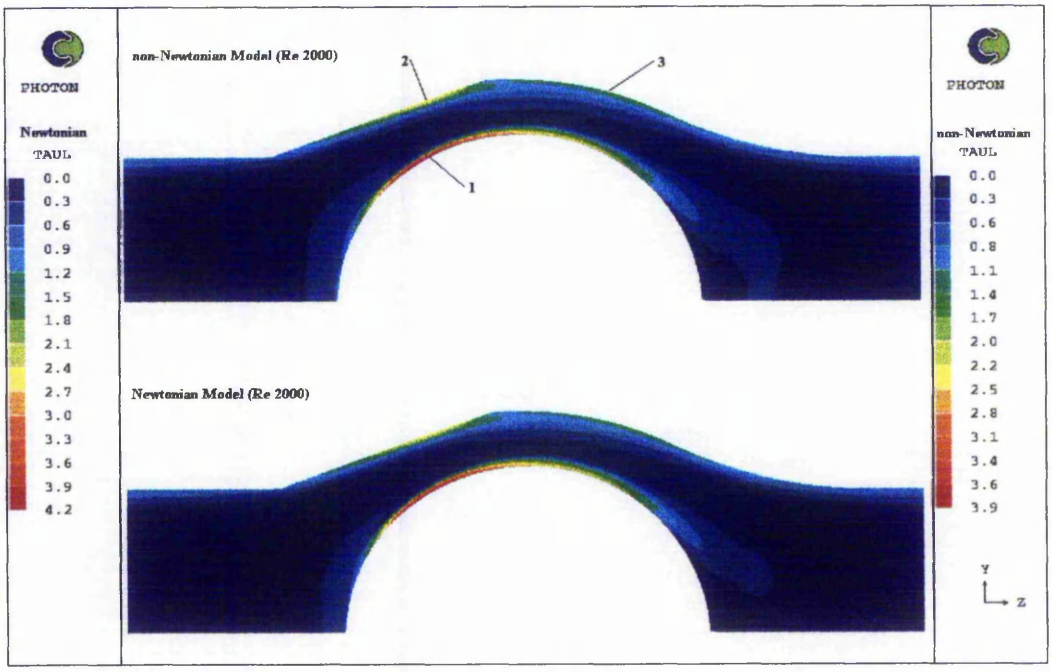

Figure 6.8: Shear stress contour plot at peak inlet flow velocity (Re 2000).

Table 6.1: Maximum and peak flow shear stress.

Model	**Maximum Shear Stress (Pa)**	**Peak Flow Shear Stress (Pa)**
Re 500 Newtonian	6.7	0.87
Re 500 non-Newtonian	6.1	0.81
Re 1000 Newtonian	9.9	1.78
Re 1000 non-Newtonian	8	1.73
Re 2000 Newtonian	16	4.2
Re 2000 non-Newtonian	14.4	3.9

The table shows that the maximum shear stress in considerably larger than that found at peak forward flow. The non-Newtonian models predicted lower shear stress values, in the region of 10-20 percent less than the Newtonian models. Steady, Newtonian, flow models with Reynolds number flows of 500, 1000 and 2000 gave maximum shear stress values of 1.24, 2.5 and 6.2 Pa, respectively. The differences may be due to the steady flow model assuming the flow to be developed over an infinite time period and not the finite time period for the unsteady models.

At the end of each time step the field shear stress values were grouped into ten sets. A peak value of shear stress was found from a steady analysis with the occluder in its fully open position, e.g. for a Reynolds number flow of 2000 the peak shear stress (τ) was found to be 4 Pa, the groups would then be $0 \leq \tau < 0.4$, $0.4 \leq \tau < 0.8 ... 3.2 \leq \tau < 3.6$ and $3.6 \leq \tau$. The final group also included shear stress values greater than 4 Pa. For each group the total volume of cells with shear stress values within the group range was calculated and then converted into a percentage of the total domain volume.

Figures 6.9 to 6.14 show this information as three dimensional surface contour plots. The x-axis represents shear stress, y-axis time, and z-axis percentage of the total volume. The figures show that the overall value of shear stress remains low during the model cycle time, less than 1% of the domain contains higher shear stress values. There is a reduction in the volume of the domain occupied by the lowest shear stress range between 0.075 and 0.275 s, which is when the occluder is in its fully open position.

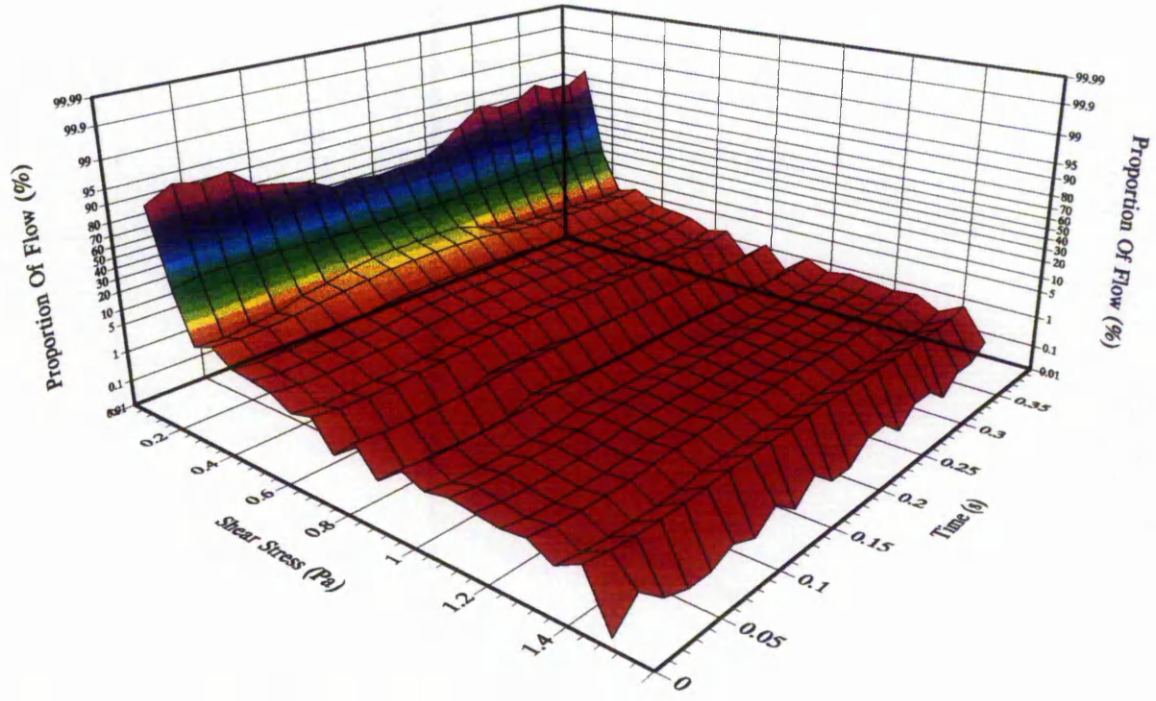

Figure 6.9: Proportion of flow domain occupied by a range of shear stress values, Re 500 Newtonian model.

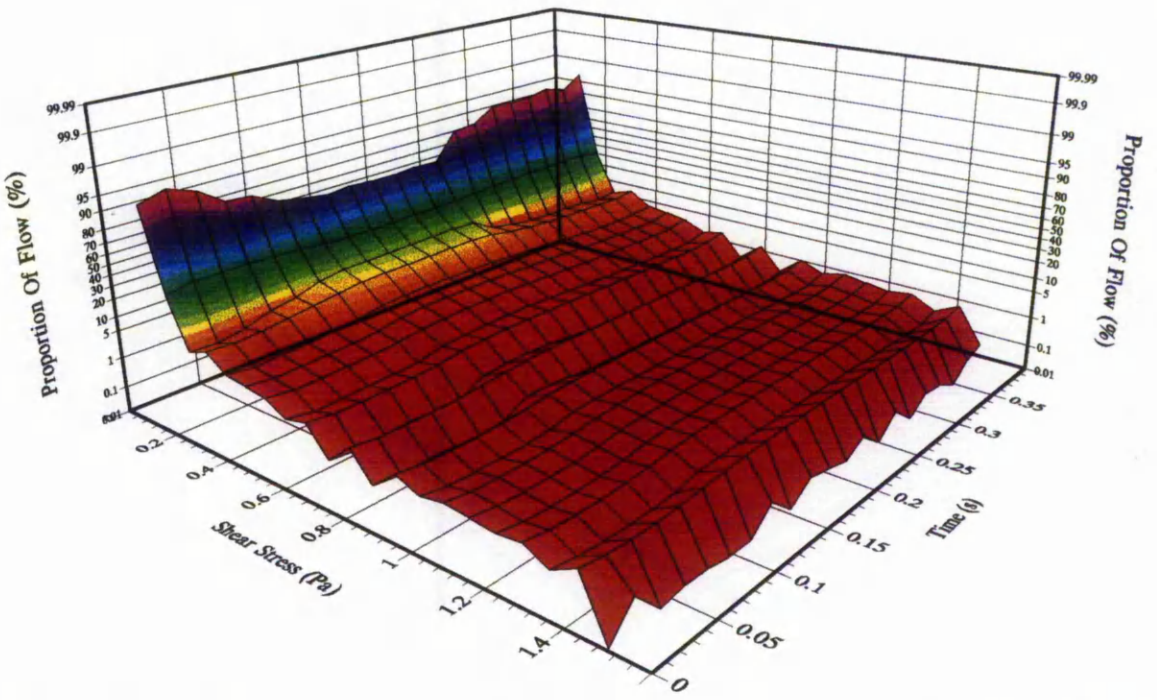

Figure 6.10: Proportion of flow domain occupied by a range of shear stress values, Re 500 non-Newtonian model.

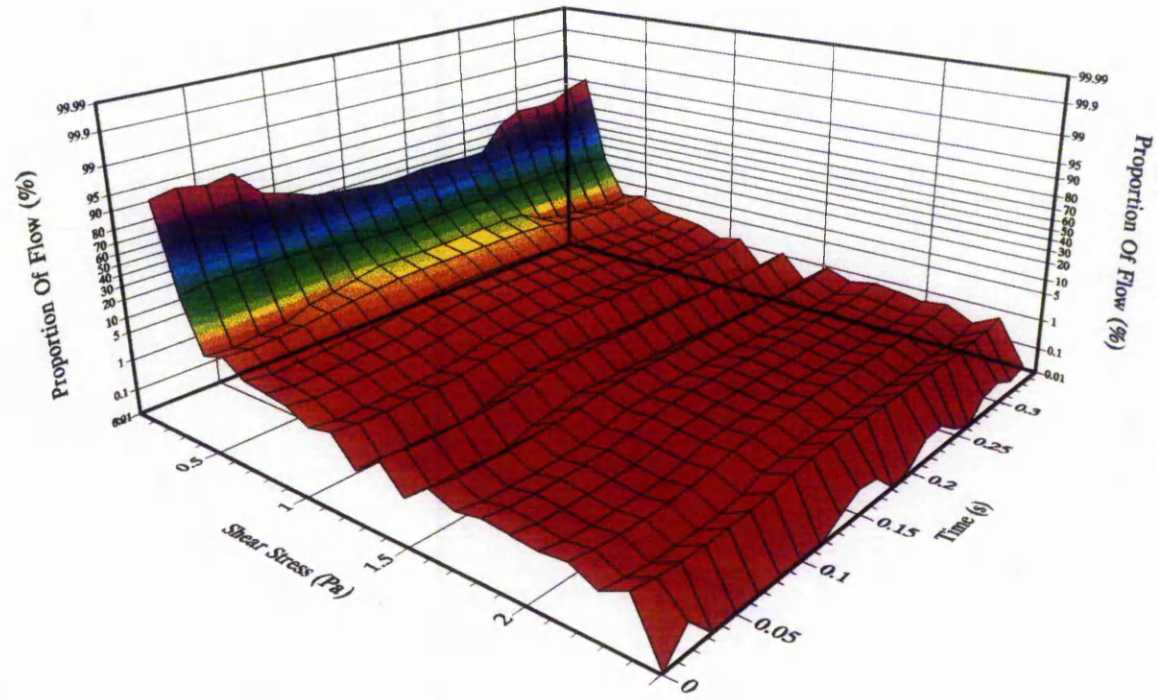

Figure 6.11: Proportion of flow domain occupied by a range of shear stress values, Re 1000 Newtonian model.

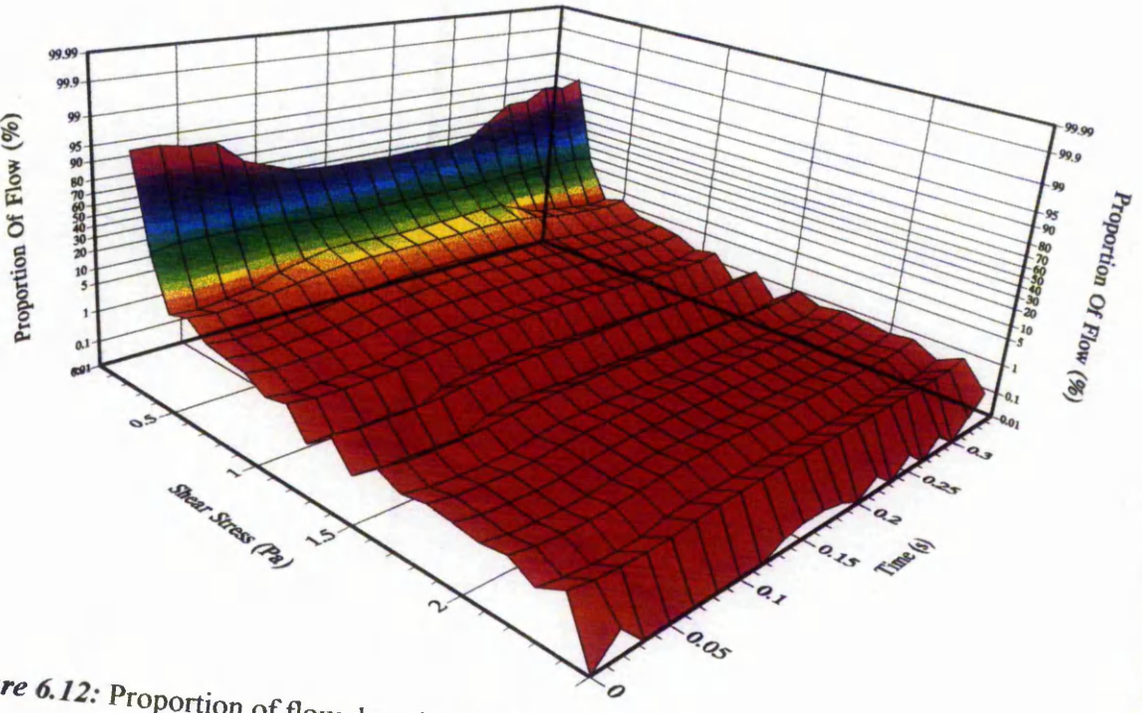

Figure 6.12: Proportion of flow domain occupied by a range of shear stress values, Re 1000 non-Newtonian model.

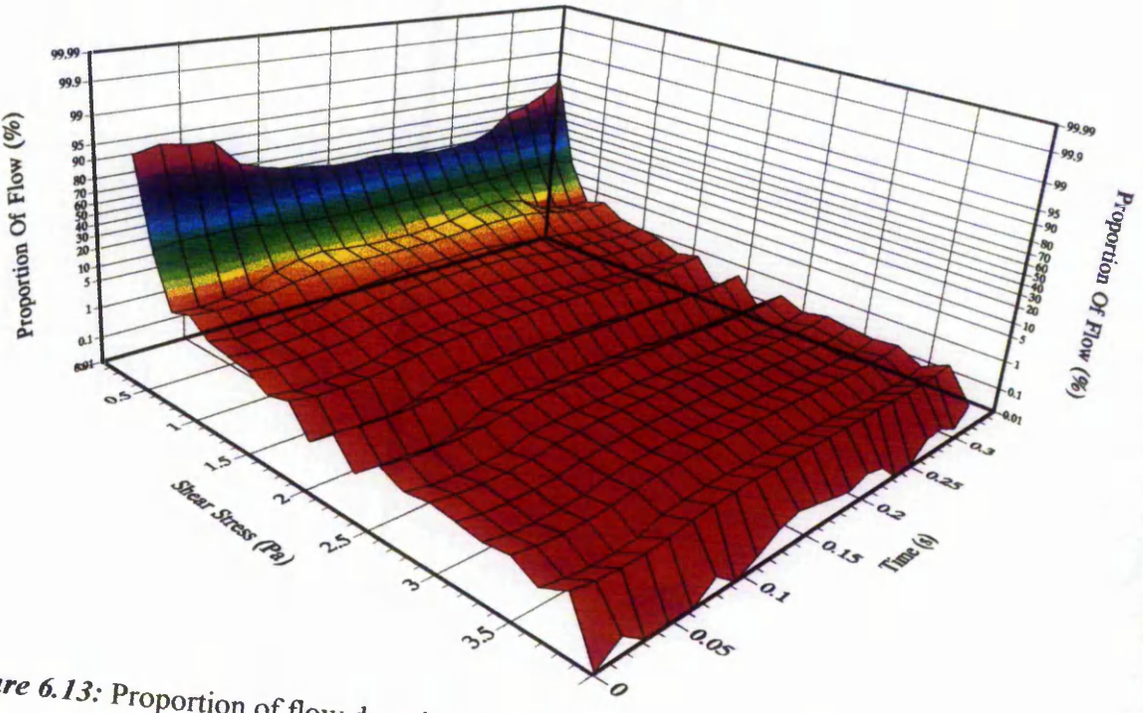

Figure 6.13: Proportion of flow domain occupied by a range of shear stress values, Re 2000 Newtonian model.

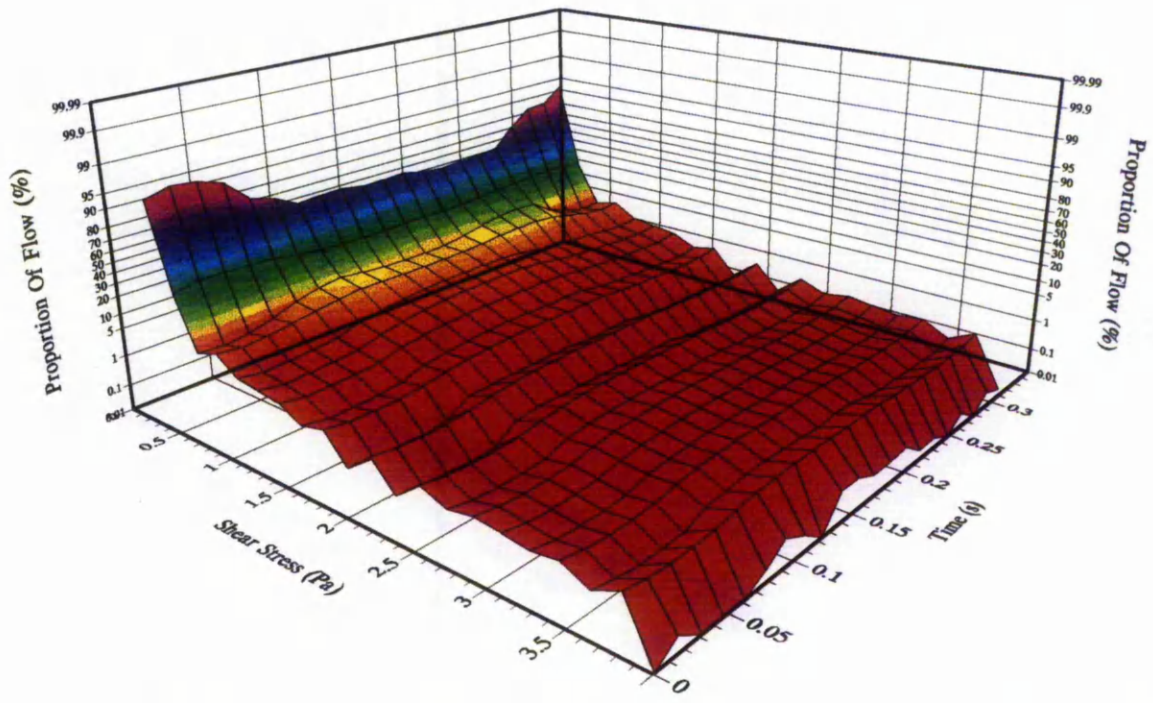

Figure 6.14: Proportion of flow domain occupied by a range of shear stress values, Re 2000 non-Newtonian model.

6.4.3 Shear Rate Distribution

The MPEG, Rn2000gm.mpg, shows the distribution of shear rate for the non-Newtonian model with peak Reynolds flow of 2000.

i) Average Shear Rate

At the end of each time step the average shear rate per unit volume was calculated. The graph in Figure 6.15 shows how the average shear rate varied over the model cycle time. At the point where the occluder reaches its fully open position there was an increase in the average value of shear rate, the peak value occurring when the inlet velocity was at a maximum. Comparing the Newtonian and non-Newtonian models it can be seen that during the opening of the occluder, the non-Newtonian models have a slightly higher average shear

rate value but after the occluder had reached its fully open position the Newtonian models displayed higher average shear rate values.

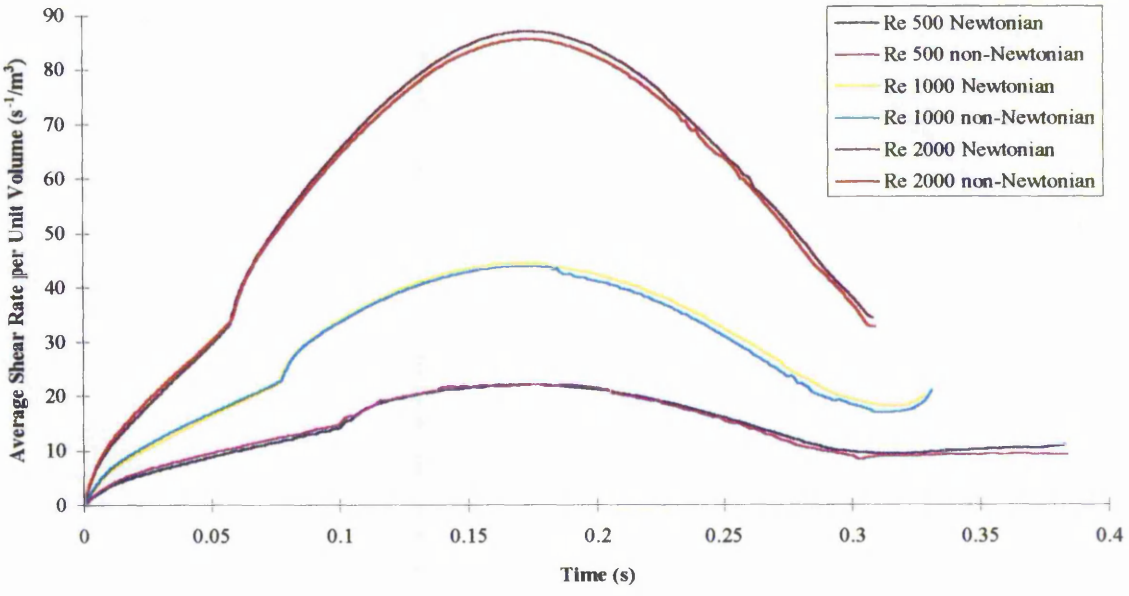

Figure 6.15: Average shear rate per unit volume.

ii) Proportion Of Flow With Shear Rate Value Less Than 100 s^{-1}

The graph in Figure 6.16 shows the percentage of the flow field with a shear rate value of less than 100 s^{-1}. The values predicted for the Newtonian and non-Newtonian models were very similar. It can be seen that during the opening of the occluder there was a rise in the proportion of the flow field with shear rate values less than 100 s^{-1}, until the occluder reached its fully open position when the value began to fall and continued to fall until peak inlet velocity was reached. After peak inlet velocity the proportion of the domain filled with low shear rate increased until the occluder was almost closed where the value began to fall.

In Chapter 2 section 2.3.2 reference was made to the application of non-Newtonian blood models where the average shear rate exceeds 100 s^{-1}. It is generally considered that for flows with high average shear rates, in excess of 100 s^{-1}, non-Newtonian blood models are unnecessary. However the results shown in Figure 6.16 show that the percentage of the

flow domain occupied by shear rates less than 100 s^{-1} can vary between 20 and 100 percent during the flow cycle.

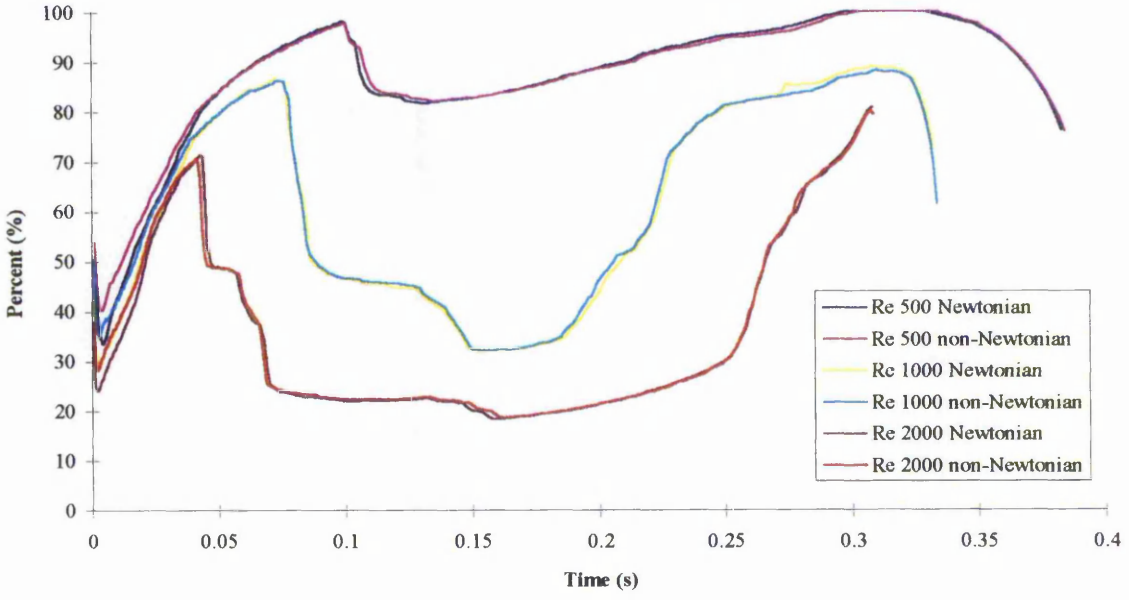

Figure 6.16: Proportion of flow with shear rate value less than 100 s^{-1}.

iii) Proportion Of Flow With Shear Rate Value Less Than 7 s^{-1}

Thrombus development can be accelerated by a factor of a thousand (Dintenfass[41]) when the shear rate is less than 7 s^{-1}. The graph in Figure 6.17 shows the percentage of the flow domain occupied by shear rate less than 7 s^{-1} during the flow cycle (results are only shown for peak Reynolds flow of 500 since this represents the worst case).

The graph shows, during the opening and closing of the occluder, large variations in the calculated values, but during the phase where the occluder was in its fully open position the curves are similar. A greater proportion of the flow domain was occupied by low shear rate values during the opening and closing phase of the occluder, with the lowest values found whilst the occluder was in its fully open position.

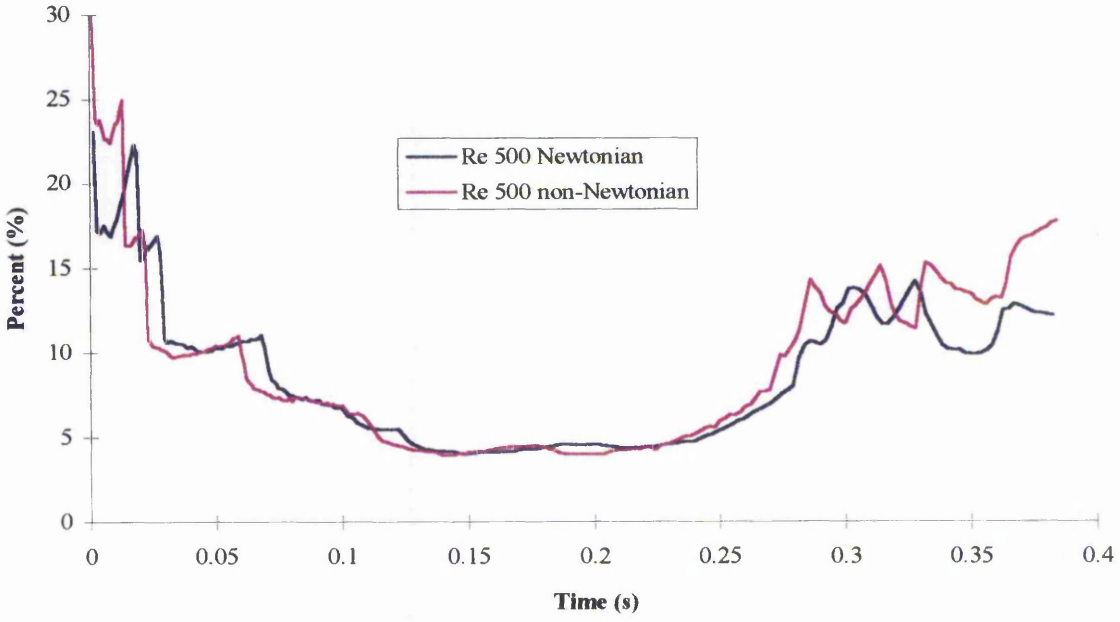

Figure 6.17: Proportion of flow with shear rate value less than 7 s^{-1}.

6.5 Occluder Displacement And Occluder Velocity

i) Occluder Displacement

The graph shown in Figure 6.18 represents the occluder displacement for all the models. The black line is a representation of the velocity of the incoming fluid at the inlet boundary. Comparing the Newtonian and non-Newtonian models it can be seen that the non-Newtonian models lag the Newtonian models during the opening and closing phases of the occluder. As would be expected the higher Reynolds number models open quicker and close sooner than the lower Reynolds number models. The graph also shows that all the models predict the occluder starting its closing phase at approximately the same time (0.176 s), a characteristic shown in section 5.7. In all the models the occluder was closing with forward flow entering the flow domain. A summary of the occluders performance can be seen in Table 6.2.

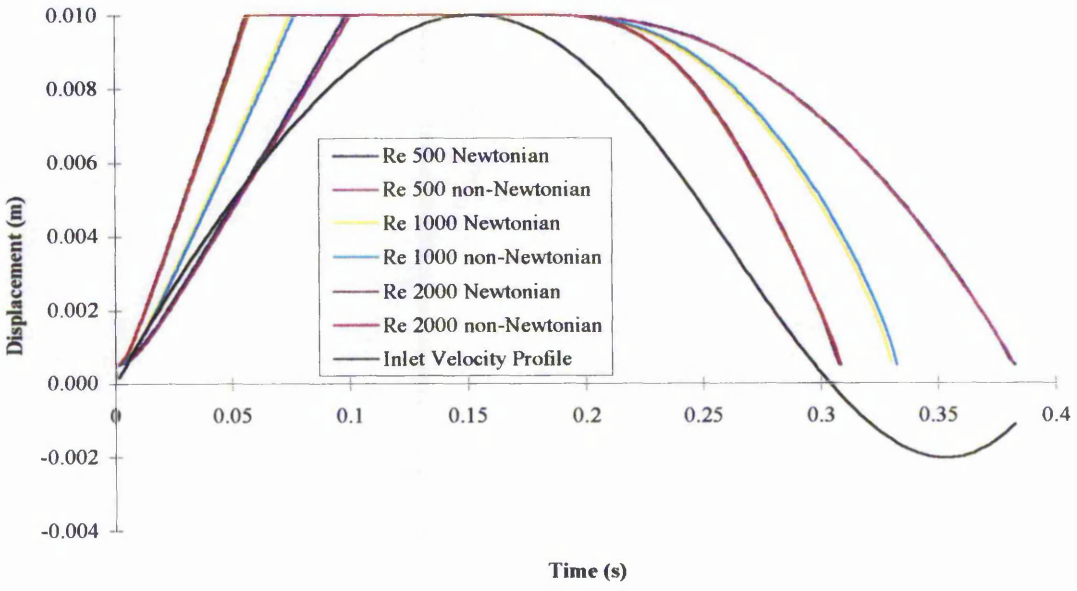

Figure 6.18: Occluder displacement.

Table 6.2: Occluder performance.

Model	**Time To Open (s)**	**Time Fully Open (s)**	**Overall Time To Return To Closed Position (s)**
Re 500 Newtonian	0.098667	0.077333	0.3826
Re 500 non-Newtonian	0.104	0.072	0.382
Re 1000 Newtonian	0.075333	0.100067	0.33
Re 1000 non-Newtonian	0.0762	0.0998	0.332
Re 2000 Newtonian	0.056	0.12	0.308
Re 2000 non-Newtonian	0.0567	0.1193	0.3085

Using the information supplied in Table 6.2, the graphs in Figure 6.19 show the relationship between valve performance times and the square of flow rate per unit area (m^2/s^2). Inserting a trend line for each performance criterion gives the equations down the right hand side of the graph with their regression values. This analysis allows the performance of the occluder to be assessed at flow rates not modelled in this analysis.

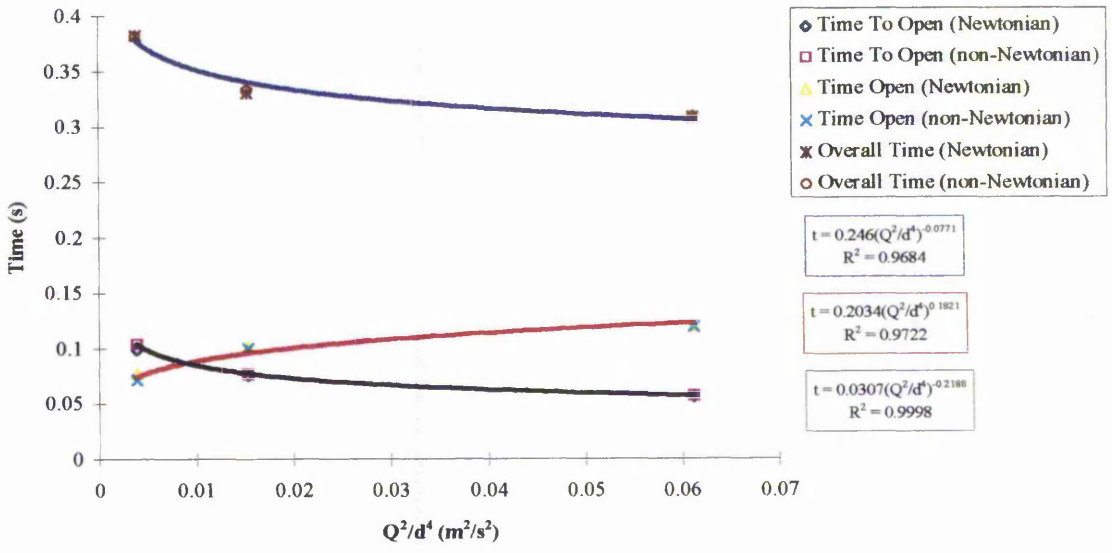

Figure 6.19: Regression analysis on occluder performance.

ii) Occluder Velocity

During the analysis the velocity of the occluder was recorded at the end of each time step. The results are shown in Figure 6.20. The results show little difference between the Newtonian and non-Newtonian models, except that during the opening phase of the occluder the Newtonian model velocities were slightly higher and during the closing phase the reverse happens. As the occluder opens it experiences high acceleration, shown by a steep rise in the velocity curve, after which the acceleration reduced almost to zero until the occluder was almost fully open, at which point the acceleration increased again slightly. During the closing phase the occluder experiences almost constant acceleration, but again there was a slight increase as the occluder approached its closed position.

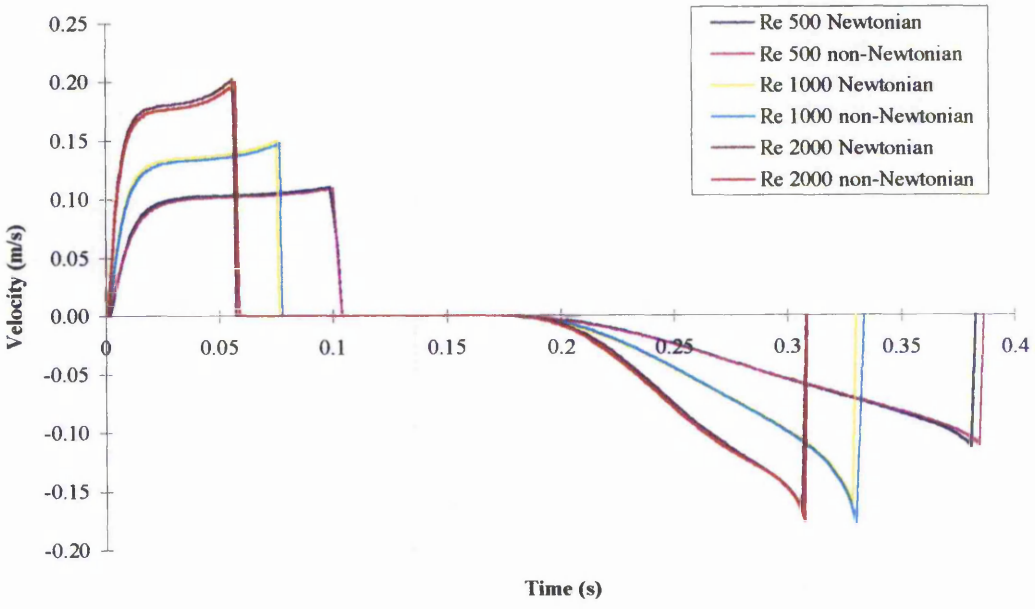

Figure 6.20: Occluder velocity.

6.7 Pressure Drop Predictions And Occluder Force Predictions

i) Pressure Drop Predictions

The area of most concern during the analysis was the values of pressure predicted by PHOENICS. The graph in Figure 6.21 shows the pressure drop across the occluder predicted by PHOENICS. The graph clearly does not show the expected pressure drop across the valve; the graph should show the pressure drop staring at a low value, at the start of the flow cycle, increasing to a maximum when the inlet velocity was at its peak and then falling as the inlet velocity decreased. It may be that PHOENICS was storing the pressure differential and not the actual pressure value in the storage array for P1. When the gradient of selected points on the curves was calculated the graphs took the form shown in Figure 6.22. These curves are more representative of the form that would be expected, i.e. they start at a low value and increase to give the maximum pressure drop at peak inlet velocity, followed by a reduction in pressure drop as the inlet velocity reduces.

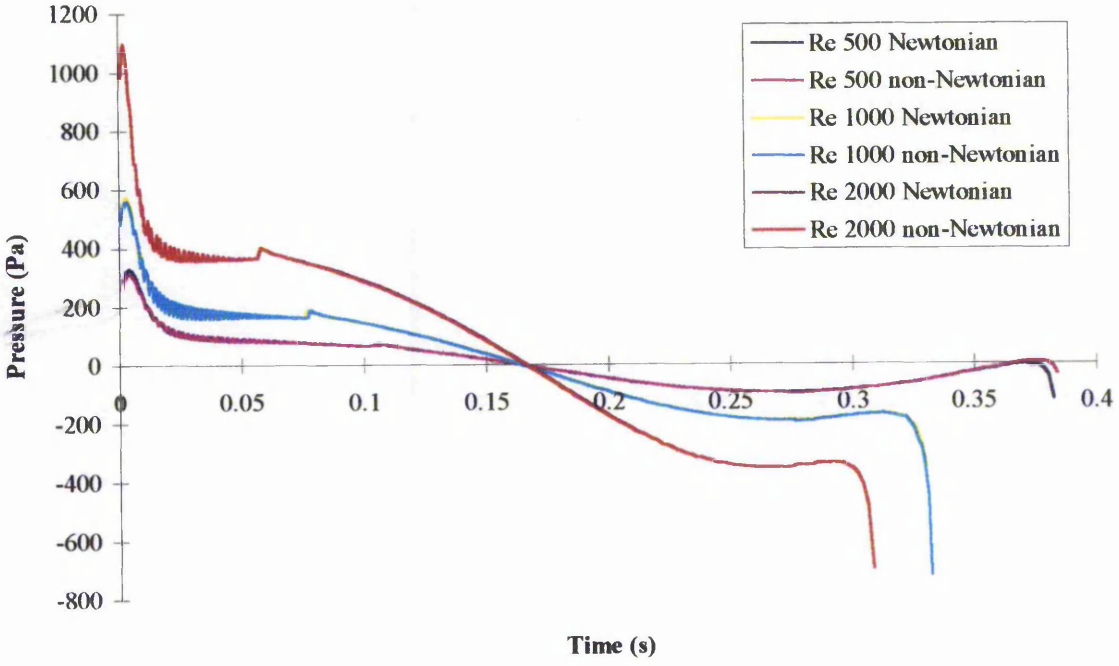

Figure 6.21: Pressure drop predicted by PHOENICS.

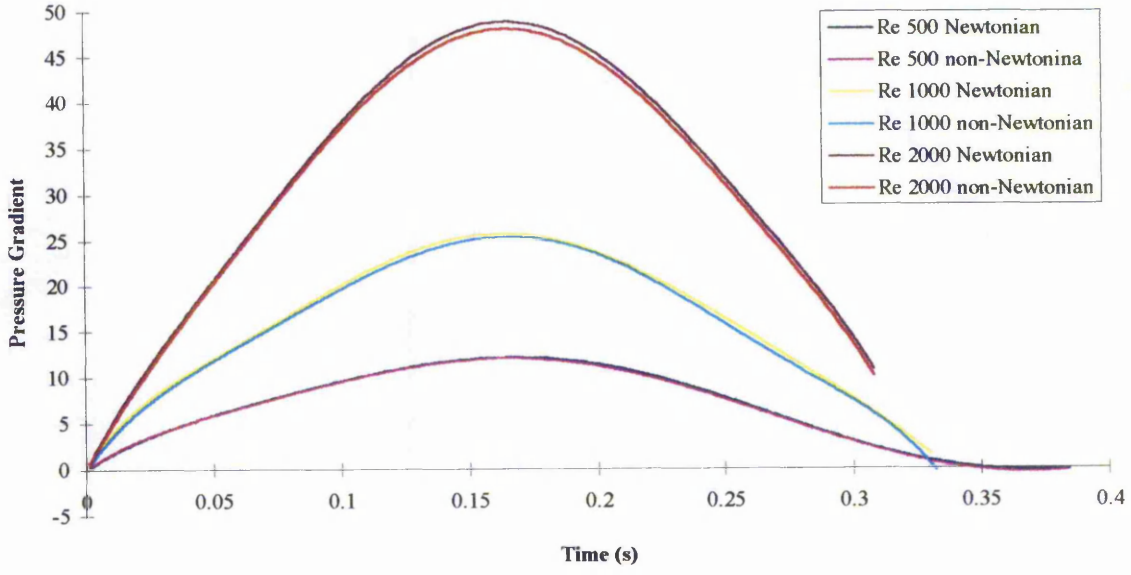

Figure 6.22: Gradient at selected points from PHOENICS predicted pressure drop.

ii) Occluder Force Predictions

The implications of the predicted pressure values by PHOENICS can be seen in Figure 6.23. This figure shows the force acting on the occluder during the flow cycle for each model, the force being calculated from the streamwise pressure and shear force acting over the occluder surface. The graph shows that the maximum force acting on the occluder occurs during the initial opening phase and soon after peak inlet velocity was reached the force then became zero and then for the remaining time negative values were calculated. It was not possible to convert the graph, by finding the gradient at selected points, as the lines are the sum of the pressure and shear force.

The possible cause for this behaviour is discussed in the next chapter.

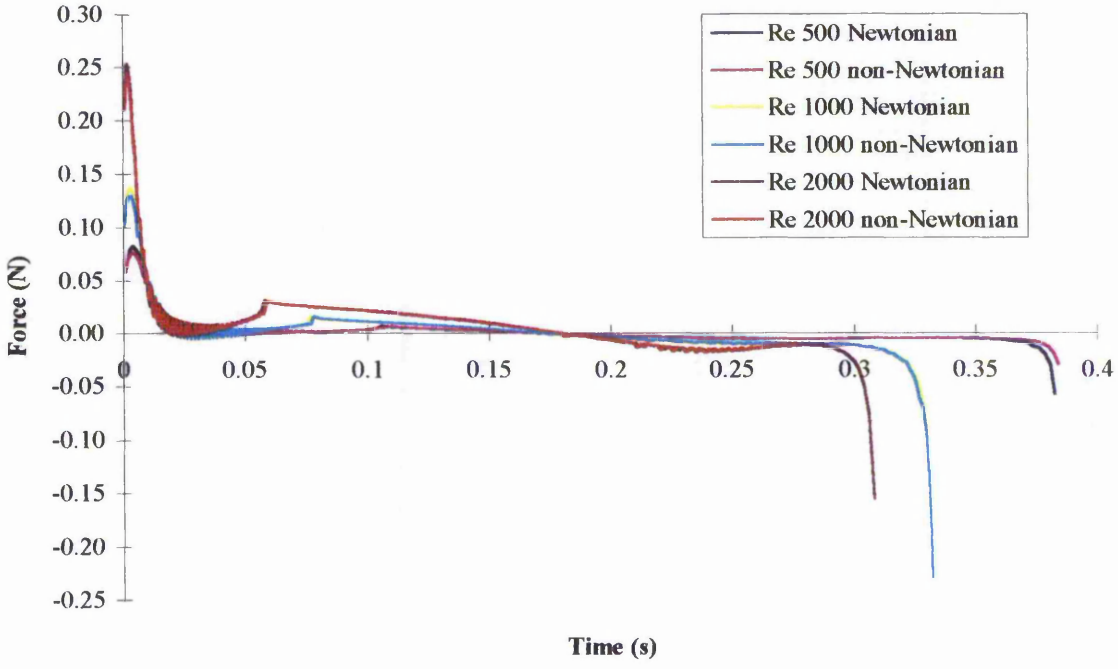

Figure 6.23: Force acting on the occluder predicted by PHOENICS.

6.8 Assessment Of Clinical Consequences

Due to the nature of the analysis, i.e over a complete flow cycle, it was possible to assess the clinical consequences at points in the cardiac cycle not available through steady flow analysis.

i) Bulk Shear Stress

The minimum value of in-bulk shear stress likely to cause haemolysis is 500 N/m^2 for a duration of 1×10^{-3} s, defined by Hellmus and Brown[29]. None of the models predicted in-bulk shear stress values above this threshold. The maximum values of shear stress occurred close to the prosthetic surface and were low when compared to this threshold. In all the models the highest shear stress was predicted during the initial opening phase of the occluder and reduced rapidly over a 0.01 s time period. Therefore due to the low value of shear stress found within the flow domain during the flow cycle it can be assumed that destruction of erythrocytes would not occur within the bulk flow.

ii) Shear Stress At The Prosthetic Surface

The value of shear stress to cause cell damage at the prosthetic surface is much lower than that in the above case. It has been reported that surface shear stress values below even 150 N/m^2 can cause haemolysis. The maximum shear stress predicted from the flow analysis was 16 N/m^2 (Re 2000, Newtonian) which is well below the value of 150 N/m^2. The low values of shear stress predicted in all the models shows that haemolysis of this type is unlikely to occur.

iii) Endothelium Damage Due To Jet Impingement

Fry[35] reports that damage begins to occur at shear stresses as low as 40 N/m^2 with cell erosion at a higher shear stress of 90 N/m^2. The MPEG files of velocity show that jet

impingement onto a prosthetic surface does not occur during the flow cycle and with a low maximum shear stress value it is not expected that endothelium damage will be a consequence of this prosthesis. Work by Dewey et. al.[36] and Nerem et. al.[37] shows that changes to the endothelium cell orientation and regeneration can occur at shear stress values of as little as 0.5 N/m^2. The elevated shear stress values on the surface of the diverging section of the valve, especially during the opening phase, may therefore affect the tissue coating which will line the inside of the prosthesis. This will only be shown from *in vivo* trials.

iv) Thrombus

Thrombus is known to form in areas of haemostasis or low shear. Dintenfass[41] brings to the attention a critical shear rate value of 7 s^{-1}, below which thrombus can be accelerated by a factor of a thousand. Thrombosis can also occur at higher shear rates as the aggregation of cells takes place in eddies, an environment where the contents are damaged erythrocytes.

Two areas of recirculating flow existed during the flow cycle. The first area developed behind the occluder and occupied this area for most of the duration of the flow cycle, but the possibility of thrombus formation within this region is unlikely as the occluder pulses backwards and forwards, rotating as it goes, during every cardiac cycle. The second area of recirculating flow was found at the junction of the diverging and cylindrical sections of the valve (see Figure 6.4). This region was transient, as it only appeared while the occluder was opening and by the time the occluder had reached its fully open position the area of recirculation no longer existed. This area of recirculation could provide a site for thrombus formation, particularly if cells were damaged as they passed through the area of high flow velocity and elevated shear stress (see Figures 6.3 and 6.7) formed during the initial opening of the occluder. If thrombus forms in this area it may become a thromboembolism due to the fluid jet (see Figure 6.5), formed between the occluder and valve inner surface, forcing the thrombus downstream. A possible solution would be to blend the diverging and cylindrical sections so that there was no discontinuity in the slope of the surface.

Chapter Seven

Discussion And Conclusion

7.1 Performance Of CFD Package PHOENICS

The CFD package PHOENICS is a commercially available program that can be used to analyse fluid flow and heat transfer. The main advantage of PHOENICS is the ability to alter the source coding, allowing the simulation of specialist flow regimes. The user, however, has no access to the main solver source coding and can only affect variables prior to and after the solver.

The flow regimes modelled were axisymmetric, laminar and unsteady. It may have been possible to write original coding to simulate this type of flow but this would have consumed a large amount of time with no guarantee of increased accuracy of the final results. It made sense to use a package well known within the Department and one that would allow the changes necessary to simulate the flow. The package was used as an analysis tool and not an experimental platform for new computational techniques. The final accuracy of any computational analysis is dependent upon both the user and the solution coding.

Using a CFD package meant that the flow model would produce far more information than would be gained from experimental studies (steady and unsteady) and from steady state computational analysis. Converting field value images to MPEG bit streams meant the flow field could be viewed over the entire cycle time allowing the user to visualise and interpret the information more effectively and efficiently.

Using a parametric grid generating FORTRAN program and incorporating a parametric philosophy within the modified GROUND coding allowed the valve geometry to be changed quickly.

The total CPU time for each model averaged 143849 seconds on a VAX4000/600 system. This could be seen as a disadvantage, because, the VAX system is relatively slow and a comparative test within the Department has shown a standard DEC Alpha workstation to be

five times quicker than the VAX. Therefore the overall CPU time could be reduced to a more acceptable level, if the model were run on a more efficient, up to date machine.

The main concern during the analysis was the pressure predicted by PHOENICS. This will be discussed in the next section.

7.1.1 Pressure And Force Predictions

The results from Chapter 6 show that PHOENICS was not predicting pressure correctly. A test model was therefore produced which simulated unsteady flow within a pipe, with an inlet velocity that varied sinusoidally with time. A total of five models were run with cycle times of 0.5, 1, 5, 25 and 50 seconds. The number of time step divisions was kept constant and hence only Δt increased in size. The results of the analysis, for half a cycle, can be seen in Figure 7.1. The graph shows increasingly realistic pressure drop across the pipe with increasing size of time step division, Δt. However as Δt increased convergence was slower and the solution became increasingly unstable. When a similar model was run with the cycle time held at 0.5 seconds with only the value of Δt changing, the curves produced were similar to that seen in Figure 7.1 for a cycle time of 0.5 seconds, with the exception that as Δt increased the maximum and minimum values of pressure drop reduced slightly.

This simple analysis shows that for small values of Δt the solution becomes unrealistic for pressure predictions, which is contrary to the accepted practice that small time step sizes increase accuracy. One possible reason for this behaviour may lie in the SIMPLEST[97] algorithm employed within PHOENICS, in that it is unsuitable for unsteady flow simulations. A paper by Manson *et.al.*[98] examines the limitations of traditional finite volume discretisations and concludes that a QUICKEST type differencing method, discussed within the paper, should be adopted for unsteady flows. Unfortunately it is not possible to use different discretisation techniques within PHOENICS when using body fitted co-ordinates, they can only be invoked on polar co-ordinate and orthogonal grids or to implement user coding.

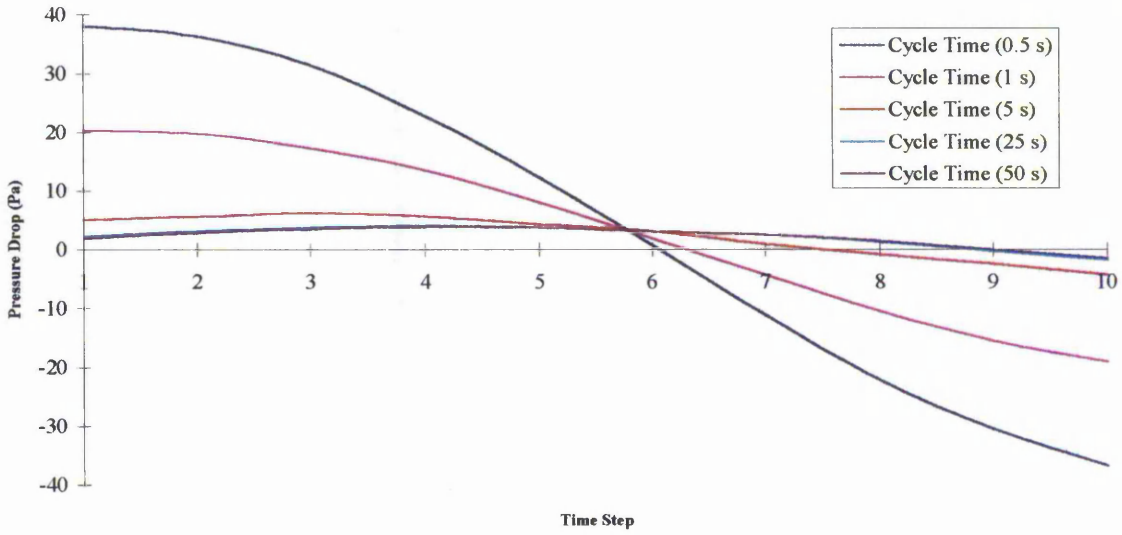

Figure 7.1: Pressure drop predictions for unsteady pipe flow.

The effect of the unrealistic pressure prediction on the models was to overestimate the force on the occluder, causing it to open quicker during the initial opening phase, and begin to close sooner than would be expected. Nevertheless the results from the experimental analysis do show that the total time taken for the occluder to open and return to its closed position was predicted with a high degree of accuracy.

7.1.2 Cassons Blood Model

The results obtained from the flow analysis show very little difference between the Newtonian and non-Newtonian models, even though the average value of shear rate per unit volume did not exceed 90 s^{-1}/m^3 for any of the models and the proportion of the flow domain which contained shear rate values of less than 100 s^{-1} ranged from 20 to 100 percent. This indicates that a large proportion of the flow domain experiences low shear rate over the flow time period.

The main differences between the two models can be seen from the maximum shear stress found within the flow regime. In all cases the Newtonian model predicted higher maximum

shear stress values. These had the effect of increasing the force on the occluder, causing it to open and close in a shorter length of time.

Another difference between the two models was observed when analysing the proportion of the flow domain with shear rate less than 7 s^{-1}. The results showed that the non-Newtonian model would predict, on average, a greater proportion of the domain occupied by low shear rate when the occluder was opening and closing. When the occluder was in its fully open position both graphs were very similar.

The effect of using a blood analogue model can lead to over prediction of shear stress and over estimate the shear rate when the flow rate is low, especially in the region where thrombus is likely to occur, i.e. shear rates less than 7 s^{-1}.

7.2 Assessment Of Clinical Consequences

The use of steady flow analysis to predict some of the clinical consequences of a valve prosthesis implant is common practice. The results from such analysis give an insight into the performance of the prosthesis when used in the *in vivo* environment. Steady flow analysis, however, can only reveal the prosthesis performance under one flow condition and therefore not allow a complete assessment to be made.

The analysis of a prosthesis through a complete flow cycle provides greater information on the valve's flow characteristics, providing a more in-depth assessment of its *in vivo* performance.

The results from the flow analysis show the valve's clinical performance to be good with low shear stress through the valve section during most of the flow cycle. One area of possible concern is the high shear stress encountered within the diverging section of the valve during the initial opening phase. Together with the presence of a recirculating flow region at the junction of the diverging and cylindrical section, this could promote the accumulation of

damaged erythrocytes. A second area of slight concern is that the inside wall of the valve is designed to be porous and hence it is expected to see a layer of tissue growth throughout the conduit. With the shear stresses within the problematic region being high there could be possible damage or erosion of the cells on the wall surface. The true consequences for this region can only be determined through animal and clinical trials.

7.3 Overall Design Performance Of The Valve Prosthesis

The overall dynamic performance of the prosthesis is difficult to assess from the computational analysis due to the poor performance of PHOENICS, except that it does allow the total time the valve is open to be predicted with good accuracy. The experimental model shows the valve opens and closes quickly, and remains open for a large proportion of the forward flow cycle all of which are excellent characteristics.

One parameter not included in the analysis was the ball's elasticity. The velocity of the occluder as it reaches its fully open position is high, approximately 0.2 m/s (Re 2000). A high velocity, as the occluder impacts on its locating struts, could cause the occluder to bounce back off the struts. Flow visualisation studies, conducted in Australia, have shown that occluder bounce does occur. However, it has been found that positioning the locating struts slightly further back in the valve section, increasing the distance travelled by the occluder, eliminates this characteristic without fundamentally changing the flow characteristics.

The flow model predicted an area of recirculation within the valve section during the initial opening phase of the occluder. The presence of such an area in reality is questionable, but flow visualisation studies, with the occluder not present, shows a detachment point within the diverging section with an area of recirculation forming downstream (a Windows AVI file can be found in the back of the thesis showing this). A large area of recirculation can be seen in Figure 7.2, which shows flow through the valve section. The presence of the occluder has the effect of directing the flow into the diverging section, minimising the

chance of a detachment point forming. It is plausible that an area of recirculating flow may develop in the diverging section due to an increase in flow area between the occluder and valve wall, shown in Figure 7.3. This recirculation zone could be eliminated by the inclusion of a blend radius at the point where the diverging and cylindrical sections join.

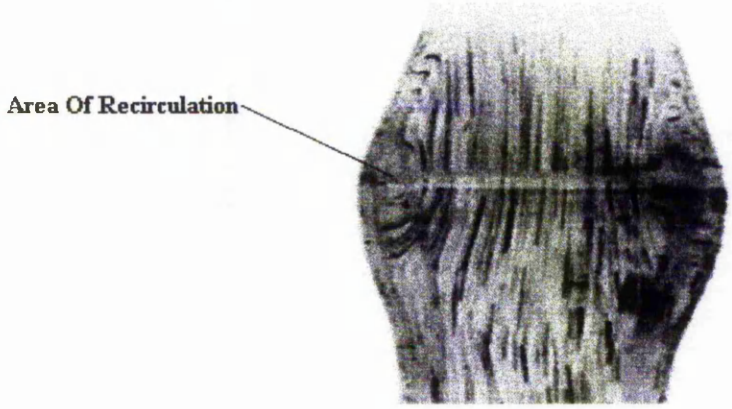

Figure 7.2: Area of recirculation with the valve section (no occluder).

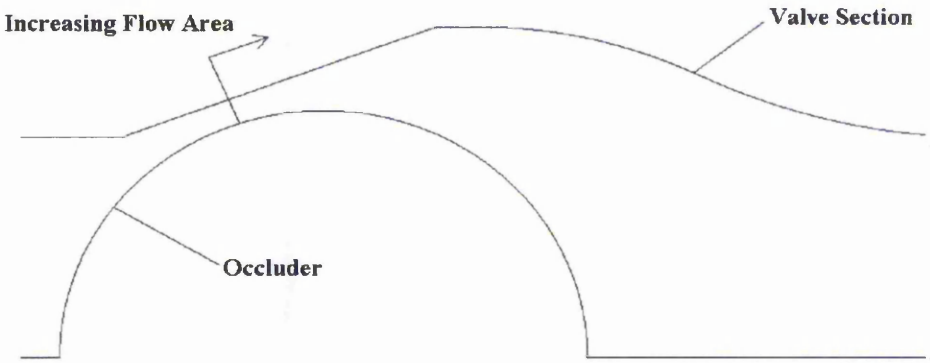

Figure 7.3: Outline of occluder and valve section showing increase in flow area.

7.4 Further Study Of *In Vivo* Application

The application of CFD to the unsteady analysis of a conduit valve has been shown to be possible. However, the performance of the flow package was poor and the analysis would be improved by the implementation of a more suitable solver. The amount of data available,

concerning the flow field and occluder dynamics, allows for a greater understanding of the valve's transient behaviour.

A progression of the computational model would be to integrate it into a more realistic geometry representing the *in vivo* situation. A typical model for representing the valve, when used in the replacement of a degenerating aorta, can be seen in Figure 7.4. Another application of the conduit valve, as an aortic shunt, can be seen in Figure 7.5

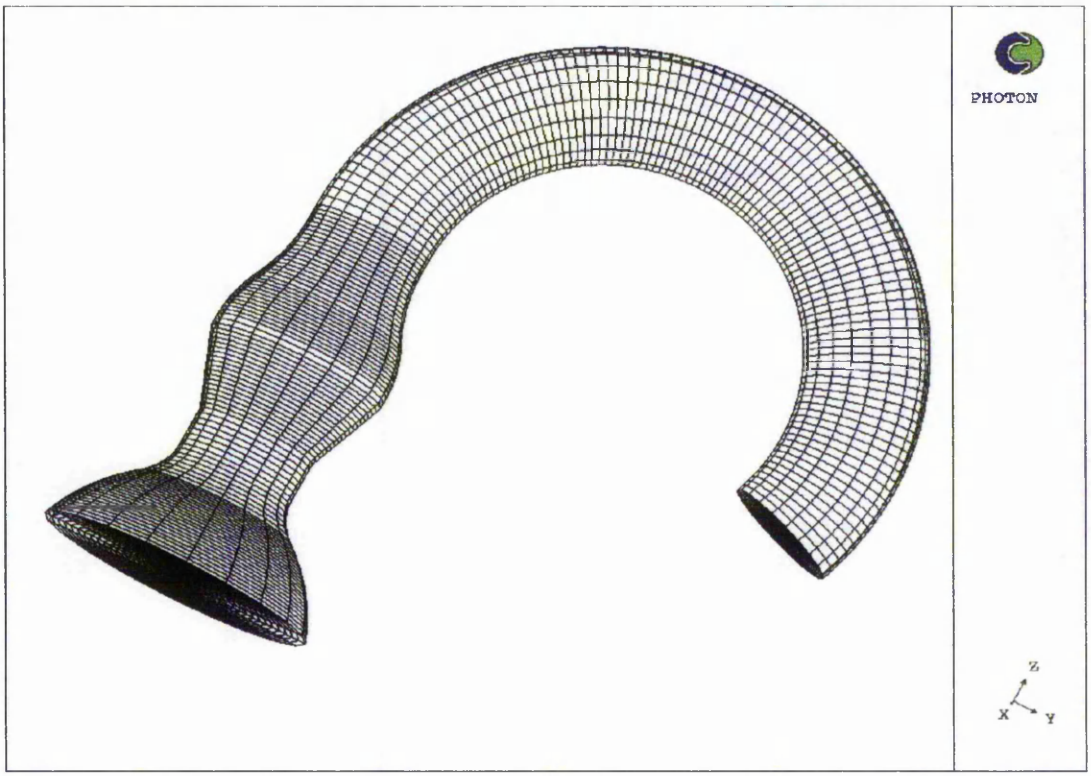

Figure 7.4: Finite volume grid representing a conduit valve used in the replacement of a degenerating aorta.

In both cases it would be possible to model the valve in a dynamic way, not just fully open, providing a more realistic representation of the *in vivo* environment. Progression to this type of analysis will provide information concerning the interaction between the conduit and the other portions of the circulatory systems.

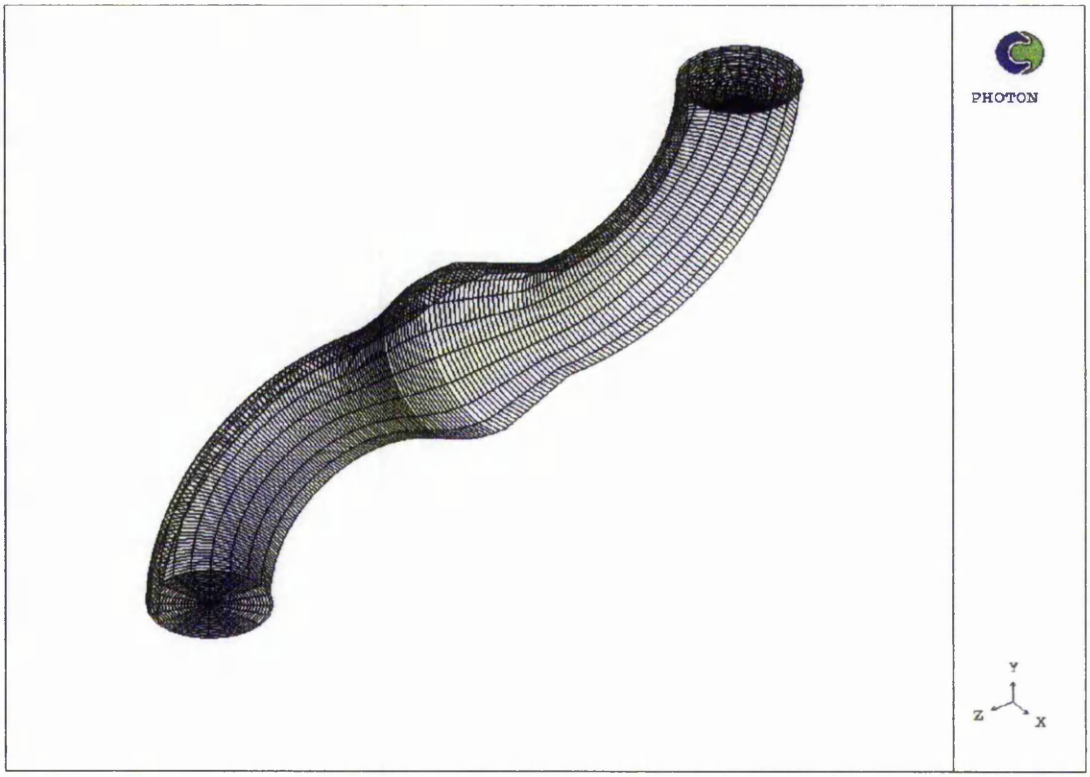

Figure 7.5: Finite volume grid representing a conduit valve used as an aortic shunt.

The progression to unsteady analysis brings us closer to the ability to model thrombus generation and growth. A discussion of possible methods to represent thrombus within a flow regime was conducted in Chapter 4. The main outcome was that if the shear rate, within a finite volume cell, was low and the cell contained damaged erythrocytes then thrombus could be modelled by either altering the cell porosity or by initiating a second phase. Determining the value of shear rate within a cell is straight forward, the main challenge is to ascertain if the cell is likely to contain damaged erythrocytes and hence thromboplastin. A possible method to accomplish this would be to 'seed' the flow domain with pseudo particles and monitor their position and the shear stresses acting on them as they flow through the domain. As a particle entered a cell with low shear rate, the particles shear stress history would be examined; if values of shear stress known to cause erythrocyte

damage were present then thrombus could be initiated within the cell. The development of such a model was not possible within this thesis due to the development time required and the limited variable storage available. It is an area that requires further consideration and development.

7.5 Conclusion

The aims of this thesis were:

To develop a computational model to predict occluder displacement using a time varying flow rate and an adaptive grid technique.

Evaluate the effects of modelling Newtonian and non-Newtonian blood flow.

Assess the clinical consequences for the valve prosthesis by examining the field shear stress and shear rate values.

Examine the possibility of developing a method to model thrombus.

Where possible validate the results predicted by the model against available experimental data.

To accomplish these aims a commercial CFD package, PHOENICS, was used. The package required extensive modification to allow the incorporation of a non-Newtonian blood model, grid generating algorithm and calculation routines to provide assessment of key variables.

The reason for using CFD as an analysis tool was its ability to allow the user access to field variables throughout the flow domain over a complete flow cycle, something not possible from experimental analysis. This advantage is diminished slightly as no CFD coding, to date,

can predict exactly the complex *in vivo* flow regimes, but observation of flow trends can be assessed with a high degree of confidence.

Representing complex geometry using finite volumes, accurately, can be achieved from the method of body fitted co-ordinates. Using BFCs allows structured finite volume grids to be produced which closely match the geometry of the bounded flow domain. It is an advantage when using BFCs to ensure the cells are close to being orthogonal, which reduces computational errors and reduces convergence time. To ensure a reasonable BFC grid was generated, for any occluder position, it was found that cells needed to be concentrated within and close to the valve section. This cell concentration was most important in the diverging section of the valve when the occluder was within 1 mm of its closed position. The narrow gap, between the diverging section and occluder, meant a high concentration of cells was needed to maintain a suitable cell aspect ratio. The effectiveness of the adaptive grid algorithm was seen from rapidly converging residuals and the small numbers of sweeps required, for a large proportion of the flow cycle, to obtain convergence. An increased number of sweeps was required when the occluder was within 1 mm of its closed position. Outside this region convergence was satisfied after 250 sweeps.

The accuracy of any unsteady flow simulation is largely dependent upon the size of time step division (Δt). A critical value for Δt was found from simulating occluder opening using different sizes of time step divisions. A minimum value of 5×10^{-5} seconds was found to produce consistent results, after which a reduction in the time size made no noticeable difference.

The flow was assumed to be laminar throughout. The implementation of turbulence models to unsteady flow is not common practice, due to their low level of performance and the presence of unknown quantities, i.e. most turbulence models require empirically derived constants found under steady flow conditions, making them unsuitable to model unsteady flow regimes.

Most experimental studies use an analogue fluid, usually a water/glycerol mix, to represent blood flow. The results from the Newtonian and non-Newtonian analysis show the valve's performance is virtually the same under both these conditions. Two areas where any noticeable differences occurred were in the values of shear stress and the proportion of the flow with shear rate less than 7 s^{-1}. In general the Newtonian model predicted higher values of shear stress and the non-Newtonian model showed a greater proportion of the domain contained low values of shear rate during the opening and closing phase of the occluder. The use of a blood analogue in experimentally determining the occluder's dynamic performance, would be quite acceptable. However the haemolytic and thrombogenic potentials of the prosthesis are dependent upon shear stress and shear rate, therefore the use of a blood analogue may not predict the true clinical consequences.

The results show the haemolytic and thrombogenic potential to be low. Only one area of concern has been shown. During the initial opening phase of the occluder high shear stress values occur in the diverging section of the valve between the occluder and valve surfaces. The main concern is that if erythrocyte damage occurs as the blood cells flow through this region, they may accumulate in an area of recirculation that forms at the junction of the diverging and cylindrical sections. Also the valve wall is to be made from a porous ceramic to encourage tissue growth along the inside surface. This growth may be damaged or eroded due to jet impingement, exposing the valve material with the possible result of increased cell damage at the prosthetic surface. Animal trials, starting in 1997 in Australia, will confirm or disprove this area of concern.

Methods for the simulation of thrombus formation have been discussed within this thesis. The conclusion of the investigation is that if a thrombus is to form within a finite volume cell, with low shear rate, the fluid that flows through the cell must contain damaged erythrocytes to initiate thrombosis. The thrombus model therefore requires the flow to be 'seeded' with pseudo particles, for which the position and 'experienced' shear stress must be calculated. Also an algorithm to simulate the growth of a thrombus must be determined.

The development of such a model is in itself a major piece of work and has not been attempted as it would have consumed too much time.

It is important when conducting a computational analysis to validate results obtained from experimental models. Experiments were conducted to allow the occluder's predicted displacement to be compared with reality. The results from the experiment showed some errors by the computational model in predicting the time taken for the occluder to fully open and the time when the occluder begins to close. When comparing the results for the total time the occluder was open, the PHOENICS model predicted values very close to the experimental model. The reason for the errors was shown to be a consequence of the pressure predicted by PHOENICS. The pressure drop across the valve was shown to be unrealistic, although taking the gradient at certain points along the graphs produced more acceptable results. As the force acting on the occluder is the sum of streamwise pressure and shear force, the unrealistic pressure field overestimated the occluder force and hence induced the errors. The reasons for PHOENICS predicting pressure incorrectly are still uncertain. Manson *et. al.*[98] discuss the limitations of the SIMPLEST[97] algorithm applied to unsteady flow simulations. Using a more applicable discretisation method should allow more realistic pressure predictions. Unfortunately the methods available in PHOENICS cannot be used on BFCs and an alternative package could not be used as one was not available within the department.

The poor performance of the CFD coding in this one respect should not discount the bulk of the data, let alone the application of CFD to modelling unsteady blood flow. The use of computational flow simulation as a design tool has many benefits, when compared to experimental models; allowing the user to determine critical values of shear stress and shear rate at any point within the flow domain. Employing a parametric philosophy means the user can easily modify flow conditions and valve geometry, while the changes in field values can be readily understood by the production of movie bit streams (MPEG) which provide greater insight and understanding of the valve's *in vivo* performance.

References

1. ***Hufnagel, C.A. and Harvey, W.P.*** (1953) The surgical correction of aortic insufficiency. Bull Georgetown U Med Cent 6:60.

2. ***McGoon, D.C.*** (1976) Left ventricle and biventricular extracardiac conduits. Journal of Thoracic and Cardiovascular Surgery, 72, 1, 7-14.

3. ***Wheat, M.W., Wilson, J.R., and Bartley, T.D.*** (1964) Successful replacement of the entire ascending aorta and aortic valve. Journal of American Medical Association, 188, 8, 717-719.

4. ***Kouchoukos, N.T., Karp, R.B. and Lell, W.A.*** (1977) Replacement of the ascending aorta and aortic valve with a composite graft: results in 25 patients. Annals of Thoracic Surgery, 24, 2, 140-148.

5. ***Kouchoukos, N.T., Karp, R.B., Blackstone, E.H., Kirklin, J.W., Pacifico, A.D., and Zorn, G.L.*** (1980) Replacement of the ascending aorta and aortic valve with a composite graft: results in 86 patients. Annals of Surgery, 192, 3, 403-413.

6. ***Mayer, J.E., Lindsay, W.G., Wang, Y., Jorgensen, C.R., and Nicoloff, D.M.*** (1978) Composite replacement of the aortic valve and ascending aorta. Journal of Thoracic and Cardiovascular Surgery, 76, 6, 816-823.

7. ***Piechler, J.M. and Pluth, J.R.*** (1982) Replacement of the ascending aorta and aortic valve with a composite graft in patients with non-displaced coronary ostia. Annals of Thoracic Surgery, 33, 4, 406-409.

8. ***Selle, J.G., Robicsek, F., Daughery, H.K., Cook, J.W. and Hess, P.J.*** (1981) Technical options in repairing the diseased ascending aorta with aortic valve involvement. Annals of Thoracic Surgery, 32, 6, 578-583.

9. ***Turinette, B., DiBartolomeo, R., Marinelli, G., Galli, R. and Pierangeli, A.*** (1983) Surgical replacement of the aortic valve and of the ascending aorta with a composite graft. Life Support Systems, 1, Supplement 1, 316-319.

10. ***Templeton, J.Y. III*** (1977) Cited by Dembitsky and Weldon: Ann Surg 184:317.

11. ***Al-Naaman, Y.D.*** (1963) Bypass procedure for aortic stenoses simplified. Medical Tribune, 4, 27.

12. ***Bernhard, W.F., Poirier, V. and LaFarge, C.G.*** (1975) Relief of congenital obstruction to left ventricular outflow with a ventricular-aortic prosthesis. Journal of Thoracic and Cardiovascular Surgery, 69, 2, 223-229.

13. ***Norman, J.C., Nihill, M.R. and Cooley, D.A.*** (1976) Creation of double outlet left ventricles for left ventricular outflow obstructions: initial clinical results in six patients. Trans Am Soc Artificial Internal Organs, 22, 332-339.

14. ***Cooley, D.A., Norman, J.C., Mullins, C.E., and Grace, R.R.*** (1975) Left ventricle to abdominal aorta conduit for relief of aortic stenosis. Bull Texas Heart Institute, 2, 3, 376-383.

15. ***Cooley, D.A., Norman, J.C., Reul, G.J. Kidd, J.N. and Nihill, M.R.*** (1976) Surgical treatment of left ventricular outflow tract obstruction with apicoaortic valved conduit. Surgery, 80, 6, 674-680.

16. ***Cooley, D.A.*** (1977) A double outlet to relieve left ventricular hypertension. Hospital Practice, June, 60-67.

17. ***Cooley, D.A., Norman, J.C.*** (1977) Severe intravascular hemolysis after aortic valve replacement. Journal of Thoracic and Cardiovascular Surgery, 7, 2, 322-324.

18. ***Dembitsky, W.P. and Weldon, C.S.*** (1976) Clinical experience with the use of a valve-bearing conduit to construct a second left-ventricular outflow tract in cases of unresectable intraventricular obstruction. Annals of Surgery, 184, 3, 317-323.

19. ***McGoon, D.C., Wallace, R.B. and Danielson, G.K.*** (1975) Transposition with ventricular septal defect and pulmonary stenosis: the Rastelli operation. Israeli Journal of Medical Science, 11, 2-3, 82-88.

20 ***Stewart, S.*** (1976) Reconstruction of right ventricular-pulmonary artery continuity with a valved external conduit: unusual technical considerations. Journal of Thoracic Cardiovascular Surgery, 72, 1, 39-47.

21. ***Norwood, W.I., Freed, M.D., Rocchini, A.P, Bernhard, W.F. and Castaneda, A.R.*** (1977) Experience with valved conduits for repair of congenital cardiac legions. Annals of Thoracic Surgery, 24, 3, 223-232.

22. ***Cartmill, T.B., Celermajer, J.M., Stuckey, D.S., Bowdler, J.D., Johnson, D.C. and Hawker, R.E.*** (1974) Use of Björk-Shiley tilting disc prosthesis in valved conduits for right ventricular outflow reconstruction. British Heart Journal, 36, 1106-1108.

23. ***Tansley, G.D.*** (1988) Computational investigation of turbulent non-Newtonian flow in heart valve conduits. PhD Thesis, The Nottingham Trent University.

24. ***Gentle, C.R.*** (1983) Minimisation of pressure drop across heart valve conduits: a preliminary study. Life Support Systems, 1, 263-270.

25. ***Haggag, Y.A.M.*** (1990) the central axis prosthetic cardiac valve: an *in vitro* study of pressure drop assessment under steady-state flow conditions. Journal of Biomedical Engineering, 12, 63-68.

26. ***Blackshear, P.L.*** (1972) Mechanical hemolysis in flowing blood. Biomechanics: its foundation and objectives. Prentice-Hall, New Jersey, USA, 501-528.

27. ***Williams, A.R., Huges, D.E. and Nyborg, W.L.*** (1970) Hemolysis near a transversely oscillating wire. Science, Washington, 169, 871-873.

28. ***Rooney, J.A.*** (1970) Hemolysis near an ultrasonically pulsating gas bubble. Science, Washington, 169, 869-871.

29. ***Hellmus, J.D. and Brown, C.H.*** (1975) Blood cell damage by mechanical forces. In "Cardiovascular Flow Dynamics and Measurements." Hwang, H.N.C. and Normann, N.A. (Eds), University Park Press, Baltimore, 799-823.

30. ***Bacher, R.P. and Williams, M.C.*** (1979) Hemolysis in capillary flow. Journal of Laboratory and Clinical Medicine, 76, 485-496.

31. ***Lampert, R.H. and Williams, M.C.*** (1978) Effect of surface materials on shear-induced hemolysis. Journal of Biomedical Materials Research, 6, 499-532.

32. ***Monroe, J.M., Lijana, R.C. and Williams, M.C.*** (1980) Hemolytic properties of special materials exposed to a shear flow, and plasma changes with shear. Biomaterials, Medical Devices, and Artificial Organs, 8, 2, 103-144.

33. ***Wielogorski, J.W., Davy, W.T.J. and Regan, R.J.*** (1976) The influence of surface rugosity on hemolysis occurring in tubing. Biomedical Engineering, 11, 91-94.

34. ***Blackshear, P.L.*** (1972) Mechanical haemolysis in flowing blood. In "Biomechanics: Its Foundation and Objectives." Fung, Y.C., Perrone, N. and Anliker, M. (Eds), Prentice Hall, New Jersey, 501-528.

35. ***Fry, D.L.*** (1968) Acute vascular endothelium changes associated with increased blood velocity gradients . Circ. Res., 12, 165-197.

36. ***Dewey, C.F., Bussolari, S.R., Gimbrone, M.A. and Davies, P.F.*** (1981) The dynamics response of vascular endothelial cells to fluid shear stress. ASME: Transactions of Journal of Biomedical Engineering, 103, 177-185.

37. ***Nerem, R.M., Levesque, M.J. and Sata, M.*** (1984) Vascular dynamics and the endothelium. Frontiers in Biomechanics, Symposium on Frontiers of Applied Mechanics and Biomechanics, San Diego, 324-341.

38. ***Nunez, L., Iglesias, A. and Sotillo, J.*** (1980) Entrapment of leaflets of St. Jude Medical cardiac valve prosthesis by minuscule thrombosis. Report of two cases. Annals of Thoracic Surgery, 29, 566-569.

39. ***Aston, S.J. and Mulder, D.G.*** (1971) Cardiac valve replacement: a seven year follow up. Journal of Thoracic and Cardiovascular Surgery, 61, 547-555.

40. ***Narducci, C., Russo, L., Battaglia, L., Angelica, G., Giovannini, E. and D'Alessandro, L.C.*** (1986) Dysfunction of double disc valvular prosthesis: report of 5 cases. In: Proceedings XIII Annual Meeting of the European Society for Artificial Organs Life Support Systems, 4, Supplement 2, 160-162.

41. ***Dintenfass, L.*** (1964) Rheological approach to thrombosis and atherosclerosis. Angiol., 333-343.

42. ***Whitmore, R.L.*** (1963) Hemorheology and hemodynamics. Biorheology, 1, 201-220.

43. ***PHOENICS.*** CHAM, Bakery House, 40 High Street, Wimbledon Village, London SW19 5AU.

44. ***Cho, V.I. and Kensey, K.R.*** (1991) Effects of the non-Newtonian viscosity of blood flow in a diseased arterial vessel. Biorheology, 28, 241-262.

45. ***Merrill, E.W., Gilliand, E.R., Cockelet, G., Shin, H., Britten, A. and Wells, R.E.*** (1963) Rheology of human blood near and at zero flow. Effects of temperature and haematocrit level. Journal Of Biophysical, 3, 199-213.

46. ***Schmid-Schönbien, H., Klose, H.J., Volger, E. and Weiss, J.*** (1973) Hypothermia and blood flow behaviour. research and Experimental Medicine, 161, 58-68.

47. ***Chimiel, H. and Walitza, E.*** (1980) On the rheology of blood and synovial fluids. Research Studies Press, John Wiley and Sons, Chichester.

48. ***Chien, S.*** (1971) Present state of blood rheology, Hemodilution. Theoretical Basis and Clinical Application. International Symposium, Rottach-Egern, Karger, Basel, 1-45.

49. ***Cokelet, G.R.*** (1987) The rheology of tube flow of blood. Handbook of Bioengineering, (Eds. Shalak, R. and Chien, S.), McGraw-Hill, chapter 14.

50. ***Gupta, B.B., Nigam, K.M. and Jaffrin, M.Y.*** (1982) A three-layer semi-empirical model for flow of blood and other particulate suspensions through narrow tubes. Transactions of the ASME Journal Of Biomedical Engineering, 104, 129-135.

51. ***Fàhaeus, R.*** (1929) The suspension Stability of the blood. Physiology Review, 9, 241-274.

52. ***Fàhaeus, R. and Lindqvist, T.*** (1931) The viscosity of blood in narrow capillary tubes. American Journal Of Physiology, 96, 562-568.

53. ***Hershey, D. and Cho, S.J.*** (1966) Blood flow in rigid tubes: Thickness and slip velocity of plasma film at the wall. Journal of Applied Physiology, 21, 27-32.

54. ***Casson, N.*** (1959) A flow equation for pigment-oil suspensions of the printing ink type. Rheology Of Disperse Systems (Ed. Mill, C.C.) Pergamon Press, London, 8-102.

55. ***Quemada, D.*** (1976) Hémorhéologie-Une nouvelle méthode de caractérisation de la viscosite sanguine. Compres Rendus Hebdomadaires des seances. Academie des Sciences, Paris série D, 282, 905-908.

56. ***Quemada, D.*** (1976) Hémorhéologie-Contraintes et vitesses de cisaillement associées à la destruction des agrégats de globules rouges sanguins: un abord viscosimétrique. Compres Rendus Hebdomadaires des seances. Academie des Sciences, Paris série D, 282, 119-122.

57. ***Cross, M.M.*** (1965) Rheology on non-Newtonian fluids: a new flow equation for psuedoplastic systems. Journal Of Colloid Science, 20, 417-437.

58. ***Cho, Y.I. and Kensey, R.*** (1991) Effects of the non-Newtonian viscosity of blood on flows in a diseased arterial vessel. Part 1: Steady flows. Biorheology, 28, 241-262.

59. ***Steffan, H., Brandstatter, W., Bachler, G. and Pucher, R.*** (1989) Comparison of Newtonian and non-Newtonian blood flow in stenotic vessels using numerical simulation. Proceedings 2nd International Symposium on Biofluid Mechanics & Biorheology, Munich, Germany, 695-701.

60. ***Bird, R.B., Armstrong, R.C. and Hassager, O.*** (1987) Dynamic of polymer materials. Fluid Mechanics (2nd Edition), John Wiley.

61. ***Eastthorp, P.L. and Brooks, D.E.*** (1980) A comparison of rheological constitutive functions for whole human blood. Biorheology, 17, 235-247.

62. ***Tansley, G.D.*** (1993) Aspects of non-Newtonian blood flow in prosthetic valve studies. Automedica, 15, 207-226.

63. ***Swales, P.D., Holden, M.P., Dowson, D. and Ionescu, M.I.*** (1973) Some experiments on tissue heart valve prostheses. Eng Med, 2, 2, 27-31.

64. ***Black, M.M.*** (1986) Artificial heart valves - past, present and future. Heart Valve Engineering, Seminar at the Institution of Mechanical Engineers, 4-5 December (Mechanical Engineering Publications Ltd, London), 65-74.

65. ***Tansley, G.D., Edwards, R.J. and Gentle, C.R.*** (1988) Role of computational fluid mechanics in the analysis of prosthetic heart valve flow. Medical and Biological Engineering and Computing, 26, 175-185.

66. ***ISO 5840*** *Cardiovascular implant-Cardiac valve prostheses.* International Standards Organisation, 1989-12-01. Also available as British Standards BS *Cardiovascular implants-Part 1, Methods of test for heart valve substitutes and requirements for their packaging and labelling.* British Standards Institution, 1990.

67. ***Yoganathan, A.P., Chaux, A., Gray, R.J., Woo, Y-R., DeRobertis, M., Williams, F.P. and Matloff, J.M.*** (1984) Bileaflet, tilting disc and porcine aortic valve substitutes: *In vitro* hydrodynamic characteristics. JACC, 3, 2, 313-320.

68. ***Yoganathan, A.P., Woo, Y-R. and Sung, H-W.*** (1986) Turbulent shear stress measurements in the vicinity of aortic heart valve prostheses. Journal Of Biomechnics, 19, 6, 433-442.

69. ***Yoganathan, A.P., Sung, H-W., Woo, Y-R. and Jones, M.*** (1988) *In vitro* velocity and turbulence measurements in the vicinity of three new mechanical aortic heart valve prostheses: Björk-Shiley Monostrut, Omni-Carbon, and Duromedics. The Journal Of Thoracic and Cardiovascular Surgery, 95, 929-939.

70. ***Chew, Y.T., Low, H.T., Lee, C.N. and Kwa, S.S.*** (1991) Performance evaluation of prosthetic heart valves using laser doppler anemometry. FLUCOME' 91: 3rd International Symposium, San Francisco, California, 705-713.

71. ***Chew, Y.T., Low, H.T., Lee, C.N. and Kwa, S.S.*** (1993) Laser anemometry measurements of steady flow past aortic valve prostheses. ASME: Journal Of Biomedical Engineering, 115, 290-298.

72. ***Figliola, R.S. and Mueller, T.J.*** (1981) On the haemolytic and thrombogenic potential of occluder prosthetic heart valves from *in vitro* measurements. Journal Of Biomedical Engineering, 103, 83-90.

73. ***Haggag, Y.A.M.*** (1990) The central axis prosthetic cardiac valve: an *in vitro* study of pressure drop assessment under steady-state flow conditions. Journal Of Biomedical Engineering, 12, 63-68.

74. ***Schoephoerster, R.T. and Chandran, K.B.*** (1989) Effect of systolic flow rate on the prediction of effective prosthetic valve orifice area. Journal Of Biomechanics, 22, 6/7, 705-715.

75. ***Hanle, D.D., Harrison, E.C., Yoganathan, A.P., Allens, D.T. and Corcoran, W.H.*** (1989) *In vitro* flow dynamics of four prosthetic aortic valves: A comparative analysis. Journal Of Biomechanics, 22, 6, 597-607.

76. ***Walker, P.G. and Yoganathan, A.P.*** (1992) *In vitro* pulsatile flow haemodynamics of five mechanical aortic heart valve prostheses. European Journal Of Cardiothoracic Surgery, 6, 113-123.

77. ***Woo, Y-R. and Yoganathan, A.P.*** (1985) *In vitro* pulsatile flow velocity and turbulent shear stress measurements in the vicinity of mechanical aortic heart valve prostheses. Life Support Systems, 3, 283-312.

78. ***Nygaard, H., Giersiepen, J.M., Hasenkam, D., Westphal, D., Paulsen, P.K. and Reul, H.*** (1990) Estimation of turbulent shear stresses in pulsatile flow immediately downstream of two artificial aortic valves *in vitro.* Journal Of Biomechanics, 23,12,1231-1238.

79. ***Schoephoerster, R.T. and Chandran, K.B.*** (1990) Velocity and turbulence measurements past mitral valve prostheses in a model left ventricle. Journal Of Biomechanics, 7, 549-562.

80. ***Walker, J.D., Tiederman, W.G. and Phillips, W.M.*** (1989) Effect of tilting disk, heart valve orientation on flow through a curved aortic model. Journal Of Biomedical Engineering, 111, 228-232.

81. ***Gentle, C.R. and Leefe, S.E.*** (1995) Pulsatile performance of two valve conduits used as cardiac valve replacements. Proc. Instn. Mech. Engrs. Part H; Journal Of Engineering in Medicine, 208, 177-183.

82. ***Thalassoudis, K., Mazumdar, J. and Noye, B.J.*** (1987) Numerical study of turbulent blood flow through a caged-ball prosthetic heart valve using boundary-fitted co-ordinate system. Medical and Biological Engineering and Computing, 25, 173-180.

83. ***Tansley, G.D., Mazumdar, J., Noye, B.J., Craig, I.H. and Thalassoudis, K.*** (1989) Assessment of haemolytic and thromboembolic potentials-from CFD studies of Starr-Edwards cardiac valve prostheses. Australasian Physical and Engineering Sciences in Medicine, 12,3,121-127

84. ***Jones, K.C., Tansley, G.D. and Mazumdar, J.*** (1992) Computational fluid mechanical evaluation of steady flow energy losses in cardiac valve prostheses. Australasian Physical and Engineering, 15, 4, 193-201.

85. ***King, M.J., David, T. and Fisher, J.*** (1994) An initial parametric study on fluid flow through bileaflet mechanical heart valves using computational fluid dynamics. IMechE: Journal Of Engineering in Medicine, 208, 63-72.

86. ***Underwood, F.N. and Mueller, T.J.*** (1977) Numerical study of the axisymmetric flow through a disk-type prosthetic heart valve in a constant diameter chamber. ASME Journal Of Biomechanical Engineering, 99, 91-97.

87. ***Underwood, F.N. and Mueller, T.J.*** (1979) Numerical study of the steady axisymmetric flow through a disk-type prosthetic heart valve in an

88. ***Merchant, G. and Mazumdar, J.*** (1986) A numerical model of non-Newtonian blood flow through a disk-type prosthetic heart valve. Automedica, 7, 159-177.

89. ***Stevenson, D.M. and Yoganathan, A.P.*** (1985) Numerical simulation of steady turbulent flow through trileaflet aortic heart valves-I. Computational scheme and methodology. Journal of Biomechanics, 18, 899-907.

90. ***Stevenson, D.M., Yoganathan, A.P. and Williams, F.P.*** (1985) Numerical simulation of steady turbulent flow through trileaflet aortic heart valves-II. Results of five models. Australasian Physical and Engineering Sciences in Medicine, 12, 3, 900-926.

91. ***Gentle, C.R. and Wilson, P.*** (1994) A computational flow design study of prototype heart valve conduits using 'FLOTRAN'. Biomechanika'94. Proceedings of the 12th School of Biomechanics. ISSN 0324-9646.

92. ***FLOTRAN.*** COMPUFLO®, 1575 State Farm Boulevard, Charlottesville, VA 22901.

93. ***MPEG2ENC.*** (1994) MPEG Software Simulation Group, video encoder version 1.1, Email MPEG-L@netcom.com.

94. ***Eckart, S.*** (1995) VMPEG V1.7 Lite video standard (ISO 11172-2). Windows 3.1 MPEG player, Email stefan@chromatic.com.

95. ***Microsoft Corporation.*** Microsoft Excel©.

96. ***Womersley, J.R.*** (1955) Method for the calculation of velocity, rate of flow and viscous drag in arteries when the pressure gradient is known. J. Phsysiology, 127, 553-563.

97. ***Patankar, S.V.*** (1980) Numerical Heat Transfer and Fluid Flow. Hemisphere, New York.

98. ***Manson, J.R, Pender, G and Wallis, S.G.*** (1996) Limitations of Traditional Finite Volume Discretizations for Unsteady Computational Fluid Dynamics. AIAA Journal, 34, 5, 1074-1076.

Appendices

A.1 Modified CVAL.FOR Program Listing To Generate Inital Valve Geometry

This CVAL.FOR program listing is a modified version of the one created by Tansley[23] with additional modification to allow the occluder position to be specified and the finite volume grid generated around this.

```
C     LRR SERIES GRID GENERATION CODING
C     This interactive Fortran program would read the required
C     geometry for each LRR series valve, calculate each of the
C     (NX+1)x(NY+1)x(NZ+1) points of the curvilinear grid. Output
C     from the program was in the format suitable for input to
C     PHOENICS via the 'readco' command. Geometry generation is based
C     on the 22mm diameter conduit, and size variation is achieved by
C     multiplication by a conversion factor.

      DIMENSION XC(10,40,400), YC(10,40,400), ZC(10,40,400)
      DIMENSION T(400),CSUBL(400), BSUBL(400), ZCSUBL(400)
      DIMENSION ZBSUBL(400)
      DIMENSION TZC(10,40,400),TYC(10,40,400)
      DOUBLE PRECISION Rb,Rc,A,Ro,C,D,pi,Dout,IRAD,Dwl,DCON
      DOUBLE PRECISION ZFRAC1,ZFRAC2,Ti,Tn,RES,Din,HT,TMPZC
      DOUBLE PRECISION ANG,YRAD,DRAD,ZRAD,YYCTR,ZYCTR,CONV
      DOUBLE PRECISION ZDIVO,ZDIVI,ZDISTO,ZDISTI,DISP,ZDIST
      DOUBLE PRECISION SRDISTN,SRDISTO,ANG1,ANG2,YDIST
      INTEGER NX,NY,NZ,NO,NC,NW,ITER,Nb,I,J,K,NE,NP,CC,CCD
      INTEGER NR, NT, IOF, OOF, NCON, NSUBL,CCY,NBI,NBO,FLAG
      CHARACTER ST, SO
      OPEN(UNIT=31,STATUS='UNKNOWN',FILE='GRID.DAT')
C
C     USER INPUT SECTION
C
C     NX is the number of CELLs in the X direction = 90 degrees/NX
C     NY is the number of CELLS in the Y direction (as per phoenics)
C     NZ is the number of CELLS in the Z direction (as per phoenics)
C     NO is the nuber of the cell at the ball centre line
C     Nb is the number of ball surface cells
C
      WRITE(6,15)
15    FORMAT(1X,'IS INLET PROFILE STRAIGHT? (Y/N)')
      READ(5,20) ST
20    FORMAT (A1)
      WRITE(6,16)
16    FORMAT(1X,'IS OUTLET PROFILE STRAIGHT? (Y/N)')
      READ (5,20) SO
```

```
      WRITE(6,30)
30    FORMAT(1X,'INPUT NX, NY, NZ')
      READ(5,*) NX,NY,NZ
      WRITE(6,40)
40    FORMAT(1X,'INPUT RADIUS (mm), ZFRAC1 (mm), ZFRAC2 (mm)')
      READ(5,*) IRAD, ZFRAC1,ZFRAC2
      ZFRAC1=ZFRAC1/1000
      ZFRAC2=ZFRAC2/1000
      WRITE(6,55)
55    FORMAT(1X,'BALL-CENTRE CELL, CELLS ON BALL INLET,
      OUTLET')
      READ(5,*) NBI, NBO
      WRITE(6,60)
60    FORMAT(1X,'INPUT X-DIRECTION ANGLE (degrees)')
      READ(5,*)ANG
      WRITE(6,10)
10    FORMAT(1X,'INPUT No. OF OFFSET NODES: INLET, OUTLET')
      READ(5,*) IOF,OOF
      WRITE(6,32)
32    FORMAT(1X,'INPUT FIRST THICKNESSES ON BALL (mE-4)')
      READ(5,*)BSUBL(1)
      WRITE(6,33)
33    FORMAT(1X,'INPUT FIRST THICKNESSES AT CONDUIT (mE-4)')
      READ(5,*)CSUBL(1)
      WRITE(6,34)
34    FORMAT(1X,'INPUT CONDUIT RADIUS (mm)')
      READ(5,*) Rc
      WRITE(6,35)
35    FORMAT(1X,'BALL DISPLACEMENT (mm): ')
      READ(5,*) DISP
      DISP=DISP/1000
      BSUBL(1)=BSUBL(1)/10000
      CSUBL(1)=CSUBL(1)/10000
      Rc=Rc/1000
C
C     CONSTANTS SECTION
C
C     A is the conduit area and Rb is the ball radius
      pi=3.1415926
      A=Rc**2*pi
      CONV=Rc/11.0E-3
      Rb=0.01235*CONV
      NX=NX+1
      NY=NY+1
      NZ=NZ+1
```

```
      NB=NBI+NBO
      HT=HT*CONV
      NSUBL=1
      DO 2 K= 1,NZ
      BSUBL(K)=BSUBL(1)
      CSUBL(K)=CSUBL(1)
2     CONTINUE
C
C     TO GENERATE Z-WISE NODES (Z INCREASING FROM 1 TO NZ)
C
C     For inlet at centreline
C
      NF=NO-NBI
      NE=NO+NBO
      DO 25 K=1,NF
      ZC(1,1,K)=ZFRAC1*(K-1)
25    CONTINUE
C
C     For the inlet face of the ball
C
      ZC(1,1,NO)=ZC(1,1,NF)+Rb
      DO 50 K=NF+1,NO-1
      ZC(1,1,K)=ZC(1,1,NO)-Rb*SIN(Pi*(NO-K)/(2*NBI))
50    CONTINUE
C
C     For the back face of the ball
C
      DO 75 K=NO,NE
      ZC(1,1,K)=ZC(1,1,NO)+Rb*SIN(Pi*(K-NO)/(2*NBO))
75    CONTINUE
C
C     For outlet at centreline
C
      DO 100 K=NE+1,NZ
      ZC(1,1,K)=ZC(1,1,NE)+ZFRAC2*(K-NE)
100   CONTINUE
C
C     For inlet conduit wall
C
      Dwl=ZC(1,1,NO)-(2.232069E-3*CONV)
      IF(ST.EQ.'Y') Din=ZC(1,1,NO)-(16.98356E-3*CONV)
      IF(ST.EQ.'N') Din=ZC(1,1,NO)-(15.51564E-3*CONV)
      NC=NF+IOF
      DO 125 K=1,NO
      IF(Dwl.GE.ZC(1,1,K).AND.Dwl.LE.ZC(1,1,K+1)) NW=K+1
```

```
125   CONTINUE
      DO 150 K=1,NC-1
      ZC(1,NY,K)=(Din/(NC-1))*(K-1)
150   CONTINUE
C
C     For divergent section
      IF(ST.EQ.'N') GOTO 165
      DO 160 K=NC,NW
      ZC(1,NY,K)=Din+((K-NC)*(Dwl-Din)/(NW-NC))
      YC(1,NY,K)=Rc+((K-NC)*(5.53853E-3*CONV)/(NW-NC))
160   CONTINUE
      DO 162 K=NW+1,NO
      ZC(1,NY,K)=Dwl+((K-NW)*(ZC(1,1,NO)-Dwl)/(NO-NW))
      YC(1,NY,K)=16.53852E-3*CONV
162   CONTINUE
      GOTO 212
165   DO 175 K=NC,NO
      Ti=(35.3352+((K-NC)*(90-35.3352)/(NO-NC)))*2*Pi/360
      Ro=(A/(Pi*DSIN(Ti))+Rb**2)**.5
      ZC(1,NY,K)=ZC(1,1,NO)-Ro*DCOS(Ti)
      YC(1,NY,K)=Ro*DSIN(Ti)
175   CONTINUE
C
C     For convergent outlet section
C
212   Dcon=ZC(1,1,NO)+4.6296E-3*CONV
      IF(SO.EQ.'Y') Dout=ZC(1,1,NO)+(30.06641E-3*CONV)
      IF(SO.EQ.'N') Dout=ZC(1,1,NO)+(15.51564E-3*conv)
      NP=NE-OOF
      ZC(1,NY,NP)=Dout
      DO 250 K=NO,NP
      ZC(1,NY,K)=ZC(1,1,NO)+(Dout-ZC(1,1,NO))*(K-NO)/(NP-NO)
      IF(Dcon.GE.ZC(1,1,K).AND.Dcon.LE.ZC(1,1,K+1)) NCON=K+1
250   CONTINUE
      IF(SO.EQ.'Y') ZC(1,NY,NCON)=Dcon
C
C     For conduit outlet
C
      DO 275 K=NP+1,NZ
      ZC(1,NY,K)=Dout+((K-NP)*(ZC(1,1,NZ)-Dout)/(NZ-NP))
275   CONTINUE
C
C     TO GENERATE Y-WISE NODES
C
C     Profile of the ball and centre line (inlet)
```

```
C
      DO 285 K=1,NF
      YC(1,1,K)=0.0
285   CONTINUE
      DO 300 K=NF+1,NO-1
      YC(1,1,K)=(Rb**2-(ZC(1,1,NO)-ZC(1,1,K))**2)**.5
300   CONTINUE
C
C     inlet Conduit wall
C
      DO 325 K=1,NC-1
      YC(1,NY,K)=Rc
325   CONTINUE
C
C     To generate the profile of the ball and centre line (outlet)
C
330   DO 400 K=NO,NE-1
      YC(1,1,K)=(Rb**2-(ZC(1,1,K)-ZC(1,1,NO))**2)**.5
400   CONTINUE
      DO 425 K=NE,NZ
      YC(1,1,K)=0.0
425   CONTINUE
C
C     To generate the outflow tract and conduit wall:
C     for straight outlet profile
C
      IF(SO.EQ.'Y') GOTO 675
C
C     via Newton_Raphson iteration for theta based on Z
C
      T(NO-1)=pi/2
      DO 650 K=NO,NP
      ITER=0
      Ti=T(K-1)
550   Ro=(A/(Pi*DSIN(Ti))+Rb**2)**.5
      C=Ro*DCOS(Ti)-(ZC(1,NY,K)-ZC(1,1,NO))
      D=(A/(2*pi*Ro*(DTAN(Ti))**2))+(Ro*DSIN(Ti))
      Tn=Ti+(C/D)
      RES=Tn-Ti
      IF((DABS(Tn-Ti)).LT.1E-16) GOTO 600
      Ti=Tn
      ITER=ITER+1
      GOTO 550
600   ITER=ITER+1
      T(K)=Tn
```

```
      YC(1,NY,K)=Ro*DSIN(Tn)
625   FORMAT(1x,'Z=',D14.7,' Y=',D14.7,' Theta=',D14.7,' Ro=',D14.7)
650   CONTINUE
      GOTO 710
675   DO 690 K=NO+1,NCON
      ZC(1,NY,K)=ZC(1,1,NO)+(Dcon-ZC(1,1,NO))*(K-NO)/(NCON-NO)
      YC(1,NY,K)=16.53852E-3*CONV
690   CONTINUE
      DO 700 K=NCON+1,NP
      ZC(1,NY,K)=Dcon+((K-NCON)*(Dout-Dcon)/(NP-Ncon))
      YC(1,NY,K)=(16.53852E-3*CONV)+((NCON-K)*
     1 (5.53852E-3*CONV)/(NP-NCON))
700   CONTINUE
C
C     Outlet Conduit wall
C
710   DO 725 K=NP+1,NZ
      YC(1,NY,K)=Rc
725   CONTINUE
C
C     To add blending radius at exit from convergent section
C
      IF(IRAD.EQ.0) GOTO 789
      IF(IRAD.EQ.5) GOTO 730
      IF(IRAD.EQ.10) GOTO 740
      IF(IRAD.EQ.15) GOTO 750
      IF(IRAD.EQ.20) GOTO 760
      IF(IRAD.EQ.25) GOTO 762
      IF(IRAD.EQ.30) GOTO 764
      IF(IRAD.EQ.35) GOTO 766
      IF(IRAD.EQ.40) GOTO 768
      IF(IRAD.EQ.45) GOTO 769
730   YRAD=16.0E-3*CONV
      ZRAD=ZC(1,1,NO)+(16.96194E-3*CONV)
      DRAD=ZRAD-(2.63495E-3*CONV)
      GOTO 770
740   YRAD=21.0E-3*CONV
      ZRAD=ZC(1,1,NO)+(18.36702E-3*CONV)
      DRAD=ZRAD-(5.13290E-3*CONV)
      GOTO 770
750   YRAD=26.0E-3*CONV
      ZRAD=ZC(1,1,NO)+(19.71856E-3*CONV)
      DRAD=ZRAD-(7.40829E-3*CONV)
      GOTO 770
760   YRAD=31.0E-3*CONV
```

```
      ZRAD=ZC(1,1,NO)+(21.00906E-3*CONV)
      DRAD=ZRAD-(10.26579E-3*CONV)
      GOTO 770
762   YRAD=36.0E-3*CONV
      ZRAD=ZC(1,1,NO)+(22.24108E-3*CONV)
      DRAD=ZRAD-(11.38148E-3*CONV)
      GOTO 770
764   YRAD=41.0E-3*CONV
      ZRAD=ZC(1,1,NO)+(23.41892E-3*CONV)
      DRAD=ZRAD-(13.13019E-3*CONV)
      GOTO 770
766   YRAD=46.0E-3*CONV
      ZRAD=ZC(1,1,NO)+(24.54724E-3*CONV)
      DRAD=ZRAD-(14.75082E-3*CONV)
      GOTO 770
768   YRAD=51.0E-3*CONV
      ZRAD=ZC(1,1,NO)+(25.63064E-3*CONV)
      DRAD=ZRAD-(16.26468E-3*CONV)
      GOTO 770
769   YRAD=56.0E-3*CONV
      ZRAD=ZC(1,1,NO)+(26.67348E-3*CONV)
      DRAD=ZRAD-(17.68767E-3*CONV)
770   DO 780 K=NO,NZ
      IF(DRAD.GE.ZC(1,NY,K).AND.DRAD.LE.ZC(1,NY,K+1)) NR=K
      IF(ZRAD.GE.ZC(1,NY,K).AND.ZRAD.LE.ZC(1,NY,K+1)) NT=K
780   CONTINUE
      ZC(1,NY,NR)=DRAD
      ZC(1,NY,NT)=ZRAD
      IRAD=IRAD*CONV/1000
      DO 790 K=NR,NT
      ZC(1,NY,K)=DRAD+((ZRAD-DRAD)*(K-NR)/(NT-NR))
      YC(1,NY,K)=YRAD-(IRAD**2-(ZRAD-ZC(1,NY,K))**2)**.5
790   CONTINUE
      ZC(1,NY,NT+1)=ZC(1,NY,NT)+0.5*ZFRAC2
789   CONTINUE
799   CONTINUE
      IF(DISP.EQ.30) GOTO 19191
      TMPZC=ZC(1,1,NO)
C
C     MODIFY GRID
C     DISPLACE J=NY+1 CELLS
C
      DO 9999 K=1,NZ
      ZC(1,NY,K)=ZC(1,NY,K)-DISP
9999  CONTINUE
```

```
      DO 814 K=1,NZ-1
      IF (TMPZC.GE.ZC(1,NY,K).AND.TMPZC.LE.ZC(1,NY,K+1)) CC=K-1
814   CONTINUE
      CCD=NO-CC
C
C     CALCULATE NEW INLET/OUTLET DISTANCES
C
      ZDISTI=ZC(1,NY,NC-CCD)
      ZDIVI=ZDISTI/(NC-1)
C
C     LOCATE OUTLET CELL
C
      DO 812 K=NO,NZ-1
      IF (RC.LE.YC(1,NY,K).AND.RC.GE.YC(1,NY,K+1)) THEN
      CCY=K
      GOTO 817
      END IF
812   CONTINUE
817   CONTINUE
      ZDISTO=ZC(1,1,NZ)-ZC(1,NY,CCY+1)
      ZDIVO=ZDISTO/(NZ-CCY-CCD)
C
C     VALVE
C
      DO 813 K=NC,CCY+CCD
      TZC(1,NY,K)=ZC(1,NY,K-CCD+1)
      TYC(1,NY,K)=YC(1,NY,K-CCD+1)
813   CONTINUE
C
C     RECALC INLET
C
      DO 811 K=1,NC-1
      TZC(1,NY,K)=ZDIVI*(K-1)
      TYC(1,NY,K)=RC
811   CONTINUE
C
C     OUTLET
C
      DO 815 K=CCY+CCD+1,NZ
      TZC(1,NY,K)=TZC(1,NY,K-1)+ZDIVO
      TYC(1,NY,K)=RC
815   CONTINUE
      ZC(1,1,NO)=TMPZC
      DO 816 K=1,NZ
      ZC(1,NY,K)=TZC(1,NY,K)
```

```
      YC(1,NY,K)=TYC(1,NY,K)
816   CONTINUE
800   CONTINUE
C
C     REDEFINE INLET CELLS
C
      DO 1500 K=1,NE
      IF(RC.GE.YC(1,NY,K).AND.RC.LE.YC(1,NY,K+1)) CCY=K-1
1500  CONTINUE
      ZDIVI=ZC(1,NY,CCY+1)/(CCY)
      DO 1505 K=1,CCY
      ZC(1,NY,K)=ZDIVI*(K-1)
1505  CONTINUE
C
C     MOVE GRID
C
      FLAG=0
      FLAT=16.53852E-03*CONV
      DO 1506 K=1,NZ-1
      IF(YC(1,NY,K).GT.RC.AND.FLAG.EQ.0) THEN
      CCY=K-1
      FLAG=1
      END IF
      IF(YC(1,NY,K).EQ.FLAT) THEN
      CCD=K-1
      GOTO 1507
      END IF
1506  CONTINUE
1507  CONTINUE
      FLAG=2
      DO 1510 K=CCY,CCD-1
C
C     TOP LINE
C
      ZDIST=ABS(ZC(1,NY,K)-ZC(1,NY,K+1))/FLAG
      YDIST=ABS(YC(1,NY,K)-YC(1,NY,K+1))/FLAG
      ZC(1,NY,K+1)=ZC(1,NY,K)+ZDIST
      YC(1,NY,K+1)=YC(1,NY,K)+YDIST
C
C     BALL
C
      ZDIST=(ZC(1,1,K+1)-ZC(1,1,K))/FLAG
      ZC(1,1,K+1)=ZC(1,1,K)+ZDIST
      YC(1,1,K+1)=(RB**2-(ZC(1,1,NF)+RB-ZC(1,1,K+1))**2)**0.5
      FLAG=FLAG*10
```

```
      IF (FLAG.GE.2000.AND.K.LE.NO+NF/2) THEN
      FLAG=2000
      ELSE
      FLAG=1.5
      END IF
1510  CONTINUE
19191 CONTINUE
C
C     TO GENERATE THE INTERMEDIATE Y VALUES (Y = 2 TO NY-1)
C
      DO 802 K=1,NZ
      BSUBL(K)=(YC(1,NY,K)-YC(1,1,K))/NY
      CSUBL(K)=BSUBL(K)
802   CONTINUE
      DO 801 K=1,NZ
      ZCSUBL(K)=(ZC(1,NY,K)-ZC(1,1,K))*CSUBL(K)/(YC(1,NY,K)
     1 -YC(1,1,K))
      ZBSUBL(K)=(ZC(1,NY,K)-ZC(1,1,K))*BSUBL(K)/(YC(1,NY,K)
     1 -YC(1,1,K))
801   CONTINUE
      DO 820 K=1,NZ
      ZYCTR=(ZC(1,NY,K)-ZC(1,1,K))-(ZCSUBL(K)+ZBSUBL(K))
      YYCTR=(YC(1,NY,K)-YC(1,1,K))-(CSUBL(K)+BSUBL(K))
      YC(1,2,K)=YC(1,1,K)+BSUBL(K)
      ZC(1,2,K)=ZC(1,1,K)+(ZBSUBL(K)/NSUBL)
      YC(1,NY-1,K)=YC(1,NY,K)-CSUBL(K)
      ZC(1,J,K)=ZC(1,NY,K)-ZCSUBL(K)
      DO 820 J=3,NY-2
      ZC(1,J,K)=ZC(1,1,K)+ZBSUBL(K)+(ZYCTR*(J-2)/(NY-3))
      YC(1,J,K)=YC(1,1,K)+BSUBL(K)+(YYCTR*(J-2)/(NY-3))
820   CONTINUE
C
C     TO INTRODUCE THREE-DIMENSIONALITY IN X-PLANE
C
      DX=(ANG/(NX-1))*2*Pi/360
      DO 900 K=1,NZ
      DO 900 J=1,NY
      DO 900 I=2,NX
      ZC(I,J,K)=ZC(1,J,K)
      YC(I,J,K)=YC(1,J,K)*COS(DX*(I-1))
      XC(I,J,K)=YC(1,J,K)*SIN(DX*(I-1))
900   CONTINUE
C
C     TO OUTPUT TO DISK THE GENERATED GRID FILE NAMED:
C     GRID.DAT
```

```
C
      WRITE(31,1200) NX, NY, NZ
      DO 1100 K=1,NZ
      WRITE(31,1225) ((XC(I,J,K),J=1,NY),I=1,NX)
      WRITE(31,1225) ((YC(I,J,K),J=1,NY),I=1,NX)
      WRITE(31,1225) ((ZC(I,J,K),J=1,NY),I=1,NX)
1100  CONTINUE
      WRITE(31,1125)
1125  FORMAT('FILENAME=GRID.DAT')
1200  FORMAT(3I5)
1225  FORMAT(5(1PE13.6))
      CLOSE(31)
      CLOSE(32)
      END
```

A.2 Q1.DAT Input File

This is the Q1.DAT input file read by the PHOENICS SATLIT program. It defines all boundaries, fluid properties, solution algorithm, variables stored, relaxation parameters, sweeps, and data communicated to the EAREXE.EXE file. Indented text indicates comment line.

```
TALK=F;RUN( 1, 1);VDU=t4107

   GROUP 1. Run title

TEXT(TRANSIENT MOVING MESH)
TEXT(Q=1.48 DIA=20mm RE 500 Casson Model)
REAL(REYNO,RAD,DIA,MU,YIELD,SLOPE,TKEIN,EPIN,GMIXL)
REAL(WIN,QIN,ANGLE,SUBL,BLEND,PI,DURATION)
REAL(TIMEINT,WINT,TMST,BINT,TAUMAX)
REAL(RC,RB,RHOBALL,INL,OUTL,FC)
INTEGER(NO,NF,NE,MAXSWP,RT)
INTEGER(PLT,TSTP,INTERVAL)

   GEOMETRY DATA

INL=10E-3
OUTL=140E-3
RC=10E-03
RB=11.22727E-03
RHOBALL=1056.17
NO=150
NF=60
NE=240
RAD=10.0E-3
BLEND=30
ANGLE=5
SUBL=0.4

   TIMESTEP DATA

BINT=0.5E-03
PI=22/7
DURATION=0.2
INTERVAL=100
MAXSWP=1000
FC=1E-03
RT=100
    TSTP=(36*INTERVAL)+1
```

TIMEINT=DURATION/TSTP

FLUID DATA

TAUMAX=1.5
MU=3.323E-3
RHO1=1056.17
WIN=0.07865
QIN=WIN*(PI*RAD**2)
SLOPE=0.053001
YIELD=0.004800
ENUL=GRND7
OLDSTO=T

GROUP 2. Transience; time-step specification
GROUP 3. X-direction grid specification

NX=1

GROUP 4. Y-direction grid specification

NY=20

GROUP 5. Z-direction grid specification

PARAB=F
NZ=360

GROUP 6. Body-fitted coordinates or grid distortion

STEADY=F
BFC=T;NONORT=T
NNORSL=T
READCO(GRID)
GRDPWR(T,INTERVAL,DURATION,1)
RSTGEO=F
SAVGEO=F

*PHI FILE
CSG1=D
* XYZ FILE
CSG2=F
IDISPA=5

GROUP 7. Variables stored, solved & named solve for pressure (whole-field) and velocity.

```
SOLVE(V1,W1)
SOLUTN(P1,Y,Y,Y,N,N,N)
VISL=17
NAME(17)=ENUL
NAME(19)=GAMA
NAME(20)=TAUL
STORE(WCRT,VCRT,GAMA,TAUL,LGEN,ENUL)
DIFCUT=0.0
```

GROUP 9. Properties of the medium (or media)
GROUP 10. Inter-phase-transfer processes and properties
GROUP 11. Initialization of variable or porosity fields
GROUP 12. Convection and diffusion adjustments
GROUP 13. Boundary conditions and special sources

```
WINT=0
FIINIT(P1)=0.1
FIINIT(V1)=WINT
FIINIT(W1)=WINT
FIINIT(ENUL)=MU/RHO1
FIINIT(GAMA)=100
INIADD=F

PATCH(INL,LOW,1,NX,1,NY,1,1,1,LSTEP)
COVAL(INL,P1,FIXFLU,GRND)
COVAL(INL,W1,ONLYMS,GRND)

PATCH(OUTLET,HIGH,1,NX,1,NY,NZ,NZ,1,LSTEP)
COVAL(OUTLET,P1,FIXP,0.0)

PATCH(BALL,SWALL,1,NX,1,1,60,239,1,LSTEP)
COVAL(BALL,V1,0.0,0.0)
COVAL(BALL,W1,1.0,GRND1)

PATCH(COND,NWALL,1,NX,NY,NY,1,NZ,1,LSTEP)
COVAL(COND,V1,0.0,0.0)
COVAL(COND,W1,1.0,0.0)
```

GROUP 14. Downstream pressure for PARAB=.TRUE.
GROUP 15. Termination of sweeps

SET ENUL=GRND5 FOR NEWTONIAN FLUID
SET ENUL=GRND7 FOR NON-NEWTONIAN FLUID

```
ENUL=GRND5
LSWEEP=MAXSWP
NCRT=1
```

GROUP 16. Termination of iterations
GROUP 17. Under-relaxation devices

```
RELAX(P1,LINRLX,0.3)
RELAX(V1,FALSDT,0.001)
RELAX(W1,FALSDT,0.001)
ENDIT(W1)=0
ENDIT(V1)=0
RESREF(P1)=1E-10
RESREF(W1)=1E-8
RESREF(V1)=1E-8
```

GROUP 18. Limit on variables or increments to them
GROUP 19. Data communicated by satellite to

```
PLT=0
RG(1)=RHO1
RG(2)=MU
RG(4)=SLOPE
RG(5)=YIELD
RG(6)=QIN
RG(7)=ANGLE
RG(8)=SUBL
RG(9)=BLEND
RG(10)=WIN
RG(11)=DURATION
RG(12)=RAD
RG(13)=RC
RG(14)=RB
RG(15)=RHOBALL
RG(16)=INL
RG(17)=OUTL
RG(18)=BINT
RG(19)=TAUMAX
RG(20)=FC
IG(1)=PLT
IG(2)=INTERVAL
IG(3)=MAXSWP
IG(4)=NO
```

IG(5)=NF
IG(6)=NE
IG(7)=TIMFR
IG(8)=RT
GENK=T

GROUP 20. Preliminary print-out
GROUP 21. Print-out of variables

OUTPUT(P1,Y,Y,Y,Y,Y,Y)
OUTPUT(V2,N,N,N,N,N,N)
OUTPUT(W2,N,N,N,N,N,N)
OUTPUT(VCRT,N,N,N,N,N,N)
OUTPUT(WCRT,N,N,N,N,N,N)
INIFLD=F

GROUP 22. Spot-value print-out

TSTSWP=25
NPRINT=LSWEEP
IPLTL=LSWEEP
IXMON=1;IYMON=1;IZMON=71

GROUP 23. Field print-out and plot control

NXPRIN=NX;NYPRIN=NY;NZPRIN=NZ
NPLT=1
NCOLCO=70
NUMCLS=7

GROUP 24. Dumps for restarts

SAVE=T
NOWIPE=T
RESTRT(ALL)
STOP

A.3 Modified GROUND.FOR Coding

This program listing shows the user modifications (*italics*) required to allow boundary conditions, inlet velocity, viscosity, occluder force, occluder displacement, creation of data files, and grid modification to be performed.

```
C     FILE NAME GROUND.FTN------------------------------011093
      SUBROUTINE GROUND
      INCLUDE 'phoinc:satear'
      INCLUDE 'phoinc:grdloc'
      INCLUDE 'phoinc:grdear'
      INCLUDE 'phoinc:grdbfc'
CXXXXXXXXXXXXXXXXXXXXXXXXXXXXXXXXXXXXXXXXX USER SECTION
CXXXXXXXXXXXXXXXXXXXXXXXXXXXXXXXXXXXXXXXXX STARTS:
C     TRANSIENT ANALYSIS OF CONDUIT VALVE V1.0
C
C 1   Set dimensions of data-for-GROUND arrays here. WARNING: the
C     corresponding arrays in the MAIN program of the satellite
C     and EARTH must have the same dimensions.
      PARAMETER (NLG=100, NIG=200, NRG=200, NCG=100)
      COMMON/LGRND/LG(NLG)/IGRND/IG(NIG)/RGRND/RG(NRG)/CGRND/CGN
      CG)
      LOGICAL LG
      CHARACTER*4 CG
C
C 2   User dimensions own arrays here, for example:
C     DIMENSION GUH(10,10),GUC(10,10),GUX(10,10),GUZ(10)
C
C 3   User places his data statements here, for example:
C     DATA NXDIM,NYDIM/10,10/
C
C 4   Insert own coding below as desired, guided by GREX examples.
C     Note that the satellite-to-GREX special data in the labelled
C     COMMONs /RSG/, /ISG/, /LSG/ and /CSG/ can be included and
C     used below but the user must check GREX for any conflicting
C     uses. The same comment applies to the EARTH-spare working
C     arrays EASP1, EASP2,....EASP20. In addition to the EASPs,
C     there are 10 GRound-earth SPare arrays, GRSP1,...,GRSP10,
C     supplied solely for the user, which are not used by GREX. If
C     the call to GREX has been deactivated then all of the arrays
C     may be used without reservation.
C
C     SET DUMMY PARAMETERS AND ASSIGN VARIABLES
C
```

```
C     SET VARIABLES FOR BALL DISPLACEMENT
      PARAMETER(MY=22,MX=3)
      PARAMETER(N=40,NINT=500)
      PARAMETER(HL=3,NZY=365)
      DIMENSION GZCO(HL,NZY),GYCO(HL,NZY),TZC(MX,MY,NZY)
      DIMENSION TYC(MX,MY,NZY),TNZC(MX,MY,NZY)
      DIMENSION GTMPYC(MY,MX),GTMPZC(MY,MX),GVOL(MY,MX)
      DIMENSION TXC(MX,MY,NZY),TNYC(MX,MY,NZY),GRNG(NINT,12)
      DIMENSION GTDISBALL(NINT),GDISPB(NINT),GFORCE(NINT)
      DIMENSION GBSUBL(NZY),GCSUBL(NZY),GZCSUBL(NZY),GTNG(NINT)
      DIMENSION GZBSUBL(NZY),GCORA(MY,MX)
      DIMENSION GCORB(MY,MX),GPR1(NINT)
      DIMENSION GBALLVEL(MY,MX),GBVEL(NINT)
      DIMENSION GPR2(NINT),GPDROP(NINT)
      DIMENSION GENUT(MY,MX),GAMMA(MY,MX)
      DIMENSION GENUL(MY,MX)
      DIMENSION GTAUL(MY,MX),GTAUT(MY,MX),GTTAU(MY,MX)
      DIMENSION GP1(MY,MX), GRDWDY(MY,MX), GSAREA(MY,MX)
      DIMENSION GA(3), GB(3), GC(3), GFT(NZY), GKE(MY,MX)
      DIMENSION GYPLUS(MY,MX), GYWC(MY,MX), GNYP(MY,MX)
      DIMENSION GVELZ(MY,MX),GKEIN(MY,MX)
      DIMENSION GEPIN(MY,MX),GW1(MY,MX)
      DIMENSION GPRES(MY,MX),GT(N),GTINT(NINT)
      DIMENSION GWCRT(MY,MX),GTIME(NINT)

      REAL GBALLDISP,GBMASS,GZDISTI,GZDISTO,GZDIVI,GZDIVO,GTEMPZC
      REAL GRB,GRHOBALL,GXC,GXC2,GYYC,GYC2,GZZC,GDX,GZDIV,GYDIV
      REAL GZYCTR,GYYCTR,GDIVN,GZDIST,GYDIST,GBD,GZDIVIB,GZDIVOB
      REAL GSCALE,YY,GCONTA,GCONTB,PIN
      REAL POUT,GINL,GOUTL,GTT,GTM,GMAX
      REAL GBVEL,GRC,GXX1,GXX2,GYY1,GYY2,GZZ1,GZZ2,GTMSTRT,GBINT
      REAL GT1,GT2,GVR,GTVL,GSRTOTAL,GSRLOW
      REAL GSRTIZ,GTVOLIZ,GSRTLWIZ
      REAL GR1,GR2,GR3,GR4,GR5,GR6,GR7,GR8,GR9,GR10,GTAUMAX
      REAL GXS,GXE,GLIM1,GCF,GXDIV,GSRTHR,GSRTHRIZ
      REAL GCCY,GSTRT,GEND,GKTMP
      REAL GRHO1,GMU,GSLOPE,GYIELD,GQIN,TOTP1,TOTP2,GDP,GFP,GENUL
      REAL GWIN,GTIME,GTOTDT,GPH,GMIXLL,GRAD,GTINTRL,TSTEP,GDIN
      REAL GFS, GTHETA, GANGLE, GFTSUM, GZG, GSUBL, GBLEND,GTEMP

      INTEGER GK,GJ,GNOO,GNFF,GNEE,GCC,GCCD
      INTEGER GMMESH,GCRO,GTF,GSAVE,GRT
      INTEGER OPN, GPLT, WRT,SWRT,GINTRL,GCOUNT,GFLG,GLP1,GMAXSWP

      EQUIVALENCE(GRHO1,RG(1))
```

```
      EQUIVALENCE(GMU,RG(2))
      EQUIVALENCE(GSLOPE,RG(4))
      EQUIVALENCE(GYIELD,RG(5))
      EQUIVALENCE(GQIN,RG(6))
      EQUIVALENCE(GANGLE,RG(7))
      EQUIVALENCE(GSUBL,RG(8))
      EQUIVALENCE(GBLEND,RG(9))
      EQUIVALENCE(GWIN,RG(10))
      EQUIVALENCE(GTIME,RG(11))
      EQUIVALENCE(GRAD,RG(12))
      EQUIVALENCE(GRC,RG(13))
      EQUIVALENCE(GRB,RG(14))
      EQUIVALENCE(GRHOBALL,RG(15))
      EQUIVALENCE(GINL,RG(16))
      EQUIVALENCE(GOUTL,RG(17))
      EQUIVALENCE(GBINT,RG(18))
      EQUIVALENCE(GTAUMAX,RG(19))
      EQUIVALENCE(GFC,RG(20))
      EQUIVALENCE(GPLT,IG(1))
      EQUIVALENCE(GINTRL,IG(2))
      EQUIVALENCE(GMAXSWP,IG(3))
      EQUIVALENCE(GNOO,IG(4))
      EQUIVALENCE(GNFF,IG(5))
      EQUIVALENCE(GNEE,IG(6))
      EQUIVALENCE(GTF,IG(7))
      EQUIVALENCE(GRT,IG(8))
      DATA OPN,WRT,TOTP1,TOTP2,SWRT/0,0,0.0,0.0,0/
      DATA GFP,GFS,GFTSUM,GBD/0.0,0.0,0.0,0.0/
C
C*********************************************************************
C
      IXL=IABS(IXL)
      IF(IGR.EQ.13) GO TO 13
      IF(IGR.EQ.19) GO TO 19
      GO TO (1,2,3,4,5,6,25,8,9,10,11,12,13,14,25,25,25,25,19,20,25,
     125,23,24),IGR
25    CONTINUE
      RETURN
C*********************************************************************
C
C---  GROUP 1. Run title and other preliminaries
C
1     GO TO (1001,1002),ISC
1001  CONTINUE
C
```

```
C     User may here change message transmitted to the VDU screen
      IF(IGR.EQ.1.AND.ISC.EQ.1.AND..NOT.NULLPR)
     1  CALL WRYT40('GROUND file is VALVE 2.0 of: 030595 ')
C
      CALL MAKE(LGEN1)
      CALL MAKE(GRSP1)
      CALL MAKE(ZGNZ)
      GR1=0
      GR2=GTAUMAX/10
      GR3=GR2+GTAUMAX/10
      GR4=GR3+GTAUMAX/10
      GR5=GR4+GTAUMAX/10
      GR6=GR5+GTAUMAX/10
      GR7=GR6+GTAUMAX/10
      GR8=GR7+GTAUMAX/10
      GR9=GR8+GTAUMAX/10
      GR10=GTAUMAX
C
C     TYPE*,'RANGE',GR1,GR2,GR3,GR4,GR5,GR6,GR7,GR8,GR9,GR10
C
C     OPEN FILE FOR TIME STEP TIME AND BALL DISPLACEMENT
C
      OPEN(UNIT=29,STATUS='UNKNOWN',FILE='INFO.DAT')
      READ(29,10010) GTMSTRT,GTDISBALL(ISTEP-
     1        2),GBALLDISP,GBVEL(ISTEP)
10010       FORMAT(1X,F10.6,2X,F10.6,2X,F10.6,2X,E12.5)
      TYPE*,'   ',GTMSTRT,GTDISBALL(ISTEP-2),GBALLDISP,GBVEL(ISTEP)
C
C     CALCULATE BALL MASS
C
      GBMASS=((4/3)*3.1415926*GRB**3)*GRHOBALL
      TYPE*,'BALL MASS=',GBMASS
      GDIN=0.0001
1002  CONTINUE
      RETURN
C*****************************************************************
C
C---  GROUP 2. Transience; time-step specification
C
2     CONTINUE
      RETURN
C*****************************************************************
C
C---  GROUP 3. X-direction grid specification
C
```

```
3     CONTINUE
      RETURN
C*********************************************************************
C
C---  GROUP 4. Y-direction grid specification
C
4     CONTINUE
      RETURN
C*********************************************************************
C
C---  GROUP 5. Z-direction grid specification
C
5     CONTINUE
      RETURN
C*********************************************************************
C
C---  GROUP 6. Body-fitted coordinates or grid distortion
C
6     CONTINUE
      RETURN
C*********************************************************************
C     * Make changes for this group only in group 19.
C---  GROUP 7. Variables stored, solved & named
C*********************************************************************
C
C---  GROUP 8. Terms (in differential equations) & devices
C
8     GO TO (81,82,83,84,85,86,87,88,89,810,811,812,813,814,815)
     1,ISC
81    CONTINUE
C  * ------------------ SECTION  1 -------------------------
C     For U1AD.LE.GRND--- phase 1 additional velocity. Index VELAD
      RETURN
82    CONTINUE
C  * ------------------ SECTION  2 -------------------------
C     For U2AD.LE.GRND--- phase 2 additional velocity. Index VELAD
      RETURN
83    CONTINUE
C  * ------------------ SECTION  3 -------------------------
C     For V1AD.LE.GRND--- phase 1 additional velocity. Index VELAD
      RETURN
84    CONTINUE
C  * ------------------ SECTION  4 -------------------------
C     For V2AD.LE.GRND--- phase 2 additional velocity. Index VELAD
      RETURN
```

```
85    CONTINUE
C  * ------------------- SECTION  5 -------------------------
C     For W1AD.LE.GRND--- phase 1 additional velocity. Index VELAD
      RETURN
86    CONTINUE
C  * ------------------- SECTION  6 -------------------------
C     For W2AD.LE.GRND--- phase 2 additional velocity. Index VELAD
      RETURN
87    CONTINUE
C  * ------------------- SECTION 7 ---- Volumetric source for gala
      RETURN
88    CONTINUE
C  * ------------------- SECTION 8 ---- Convection fluxes
      RETURN
89    CONTINUE
C  * ------------------- SECTION 9 ---- Diffusion coefficients
C---  Entered when UDIFF =.TRUE.; block-location indices are LAE
C     for east, LAW for west, LAN for north, LAS for
C     south, LD11 for high, and LD11 for low.
C     User should provide INDVAR and NDIREC IF's as above.
C     EARTH will apply the DIFCUT and GP12 modifications after the user
C     has made his settings.
C
      RETURN
810   CONTINUE
C  * ------------------- SECTION 10 --- Convection neighbours
      RETURN
811   CONTINUE
C  * ------------------- SECTION 11 --- Diffusion neighbours
      RETURN
812   CONTINUE
C  * ------------------- SECTION 12 --- Linearised sources
      RETURN
813   CONTINUE
C  * ------------------- SECTION 13 --- Correction coefficients
      RETURN
814   CONTINUE
C  * ------------------- SECTION 14 --- User's own solver
      RETURN
815   CONTINUE
C  * ------------------- SECTION 15 --- Change solution
      RETURN
C
C  * See the equivalent section in GREX for the indices to be
C     used in sections 7 - 15
```

```
C
C  * Make all other group-8 changes in GROUP 19.
C*****************************************************************
C
C---  GROUP 9. Properties of the medium (or media)
C
C     The sections in this group are arranged sequentially in their
C     order of calling from EARTH. Thus, as can be seen from below,
C     the temperature sections (10 and 11) precede the density
C     sections (1 and 3); so, density formulae can refer to
C     temperature stores already set.
9     GO TO (91,92,93,94,95,96,97,98,99,900,901,902,903,904,905),ISC
C*****************************************************************
900   CONTINUE
C  * ------------------ SECTION 10 --------------------------
C     For TMP1.LE.GRND--------- phase-1 temperature Index TEMP1
      RETURN
901   CONTINUE
C  * ------------------ SECTION 11 --------------------------
C     For TMP2.LE.GRND--------- phase-2 temperature Index TEMP2
      RETURN
902   CONTINUE
C  * ------------------ SECTION 12 --------------------------
C     For EL1.LE.GRND--------- phase-1 length scale Index LEN1
      RETURN
903   CONTINUE
C  * ------------------ SECTION 13 --------------------------
C     For EL2.LE.GRND--------- phase-2 length scale Index LEN2
      RETURN
904   CONTINUE
C  * ------------------ SECTION 14 --------------------------
C     For SOLVE(TEMP1)------------------------- phase-1 specic heat
      RETURN
905   CONTINUE
C  * ------------------ SECTION 15 --------------------------
C     For SOLVE(TEMP2)------------------------- phase-2 specic heat
      RETURN
91    CONTINUE
C  * ------------------ SECTION  1 --------------------------
C     For RHO1.LE.GRND--- density for phase 1       Index DEN1
      RETURN
92    CONTINUE
C  * ------------------ SECTION  2 --------------------------
C     For DRH1DP.LE.GRND--- D(LN(DEN))/DP for phase 1
C                                 Index D1DP
```

```
      RETURN
93    CONTINUE
C  * ------------------ SECTION  3 -------------------------
C     For RHO2.LE.GRND--- density for phase 2       Index DEN2
      RETURN
94    CONTINUE
C  * ------------------ SECTION  4 -------------------------
C     For DRH2DP.LE.GRND--- D(LN(DEN))/DP for phase 2
C                                  Index D2DP
      RETURN
95    CONTINUE
C  * ------------------ SECTION  5 -------------------------
C     For ENUT.LE.GRND--- reference turbulent kinematic viscosity
C                               Index VIST
      RETURN
96    CONTINUE
C  * ------------------ SECTION  6 -------------------------
C     For ENUL.LE.GRND--- reference laminar kinematic viscosity
C                               Index VISL
961   GOTO 19623
C     RETURN
97    CONTINUE
C  * ------------------ SECTION  7 -------------------------
C     For PRNDTL( ).LE.GRND--- laminar PRANDTL nos., or diffusivity
C                                  Index LAMPR
      RETURN
98    CONTINUE
C  * ------------------ SECTION  8 -------------------------
C     For PHINT( ).LE.GRND--- interface value of first phase
C                                  Index FII1
      RETURN
99    CONTINUE
C  * ------------------ SECTION  9 -------------------------
C     For PHINT( ).LE.GRND--- interface value of second phase
C                                  Index FII2
      RETURN
C*****************************************************************
C
C---  GROUP 10. Inter-phase-transfer processes and properties
C
10    GO TO (101,102,103,104),ISC
101   CONTINUE
C  * ------------------ SECTION  1 -------------------------
C     For CFIPS.LE.GRND--- inter-phase friction coeff.
C                               Index INTFRC
```

```
      RETURN
102   CONTINUE
C   * ------------------ SECTION  2 -------------------------
C     For CMDOT.EQ.GRND- inter-phase mass transfer  Index INTMDT
      RETURN
103   CONTINUE
C   * ------------------ SECTION  3 -------------------------
C     For CINT( ).EQ.GRND--- phase1-to-interface transfer coefficients
C                                Index COI1
      RETURN
104   CONTINUE
C   * ------------------ SECTION  4 -------------------------
C     For CINT( ).EQ.GRND--- phase2-to-interface transfer coefficients
C                                Index COI2
      RETURN
C*****************************************************************
C
C---  GROUP 11. Initialization of variable or porosity fields
C                   Index VAL
11    CONTINUE
      RETURN
C*****************************************************************
C
C---  GROUP 12. Convection and diffusion adjustments
C
12    CONTINUE
      RETURN
C*****************************************************************
C
C---  GROUP 13. Boundary conditions and special sources
C                   Index for Coefficient - CO
C                   Index for Value       - VAL
13    CONTINUE
      GO TO (130,131,132,133,134,135,136,137,138,139,1310,
     1 1311,1312,1313,1314,1315,1316,1317,1318,1319,1320,1321),ISC
130   CONTINUE
C------------------ SECTION  1 ------------ coefficient = GRND
      RETURN
131   CONTINUE
C------------------ SECTION  2 ------------ coefficient = GRND1
      RETURN
132   CONTINUE
C------------------ SECTION  3 ------------ coefficient = GRND2
      RETURN
133   CONTINUE
```

```
C------------------ SECTION  4 ------------ coefficient = GRND3
      RETURN
134   CONTINUE
C------------------ SECTION  5 ------------ coefficient = GRND4
      RETURN
135   CONTINUE
C------------------ SECTION  6 ------------ coefficient = GRND5
      RETURN
136   CONTINUE
C------------------ SECTION  7 ------------ coefficient = GRND6
      RETURN
137   CONTINUE
C------------------ SECTION  8 ------------ coefficient = GRND7
      RETURN
138   CONTINUE
C------------------ SECTION  9 ------------ coefficient = GRND8
      RETURN
139   CONTINUE
C------------------ SECTION 10 ------------ coefficient = GRND9
      RETURN
1310  CONTINUE
C------------------ SECTION 11 ------------ coefficient = GRND10
      RETURN
1311  CONTINUE
C------------------ SECTION 12 ------------------- value = GRND
C
C     THIS SECTION SETS THE INPUT VELOCITY FOR EACH TIME STEP
      DO 13111 IX=1,NX
      DO 13111 IY=1,NY
      GVELZ(IY,IX)=GTINT(ISTEP)*GWIN
      GPRES(IY,IX)=GRHO1*GVELZ(IY,IX)
13111       CONTINUE
      IF (NPATCH(1:3).EQ.'INL') THEN
        IF (INDVAR.EQ.P1) THEN
          CALL SETYX(VAL,GPRES,MY,MX)
        END IF
        IF (INDVAR.EQ.W1) THEN
          CALL SETYX(VAL,GVELZ,MY,MX)
        END IF
C       IF (INDVAR.EQ.KE) THEN
C         CALL SETYX(VAL,GKEIN,MY,MX)
C       END IF
C       IF (INDVAR.EQ.EP) THEN
C         CALL SETYX(VAL,GEPIN,MY,MX)
C       END IF
```

```
      END IF
C     RETURN
1312 CONTINUE
C------------------ SECTION 13 ------------------ value = GRND1
C
C     SET VELOCITY OF BALL PATCH CELLS
C
      IF (NPATCH(1:3).EQ.'BAL') THEN

      CALL GETYX(W1,GBALLVEL,MY,MX)
      CALL GETPT(1,1,IZSTEP,GXX1,GYY1,GZZ1)
      CALL GETPT(1,1,IZSTEP+1,GXX2,GYY2,GZZ2)
C
C     CALCULATE VELOCITY RESOLUTE
C
      GBALLVEL(1,1)=GBVEL(ISTEP-1)*COS(ATAN((GYY2-GYY1)/(GZZ2-GZZ1)))
C
C     SET VELOCITY ALONG BALL SURFACE
C
       IF (INDVAR.EQ.W1) THEN
         CALL SETYX(VAL,GBALLVEL,MY,MX)
       END IF
      END IF
      RETURN
1313 CONTINUE
C------------------ SECTION 14 ------------------ value = GRND2
      RETURN
1314 CONTINUE
C------------------ SECTION 15 ------------------ value = GRND3
      RETURN
1315 CONTINUE
C------------------ SECTION 16 ------------------ value = GRND4
      RETURN
1316 CONTINUE
C------------------ SECTION 17 ------------------ value = GRND5
      RETURN
1317 CONTINUE
C------------------ SECTION 18 ------------------ value = GRND6
      RETURN
1318 CONTINUE
C------------------ SECTION 19 ------------------ value = GRND7
      RETURN
1319 CONTINUE
C------------------ SECTION 20 ------------------ value = GRND8
      RETURN
```

```
1320 CONTINUE
C------------------ SECTION 21 ------------------- value = GRND9
      RETURN
1321 CONTINUE
C------------------ SECTION 22 ------------------- value = GRND10
      RETURN
C*****************************************************************
C
C---  GROUP 14. Downstream pressure for PARAB=.TRUE.
C
14    CONTINUE
      RETURN
C*****************************************************************
C*    Make changes to data for GROUPS 15, 16, 17, 18  GROUP 19.
C*****************************************************************
C
C---  GROUP 19. Special calls to GROUND from EARTH
C
19    GO TO (191,192,193,194,195,196,197,198,199,1910),ISC
191   CONTINUE
C   * ------------------ SECTION 1 ---- Start of time step.
C
C     REDUCE TIME STEPS AS VALVE OPENS, GMAXSWP TO 250
C
      IF (GBALLDISP.LE.1E-03) THEN
      LSWEEP=INT(GMAXSWP-750000*GBALLDISP)
      ELSE
      LSWEEP=250
      END IF
      TYPE*,'LSWEEP=',LSWEEP
C
C     DEFINE VELOCITY PROFILE
C
      GTM=TIM+GTMSTRT
      GTIME(ISTEP)=GTM
      GTINT(ISTEP)=(-7641.1*(GTM**6)+8993.3*(GTM**5)-3319.1*(GTM**4)
     1 +430.01*(GTM**3)-50.243*(GTM**2)+11.809*GTM)/1.007999481
      IF(GTM.GT.0.3969) GTINT(ISTEP)=0
C
C     FIND WHEN WIN MAX
C
      GT1=GTINT(ISTEP-1)
      GVR=GTM+(DT/GTF)
      GT2=(-7641.1*(GVR**6)+8993.3*(GVR**5)-3319.1*(GVR**4)
     1 +430.01*(GVR**3)-50.243*(GVR**2)+11.809*GVR)/1.007999481
```

```
      IF(GTM.LT.0.3969.AND.GTINT(ISTEP).GT.GT1.
     1  AND.GTINT(ISTEP).GT.GT2) THEN
      GSAVE=1
      TYPE*,'**MAX VELOCITY**'
      ELSE
      GSAVE=0
      ENDIF
C
C     DEFINE FULLY OPEN VALVE DIMENSIONS
C
      IF(ISTEP.EQ.1) THEN
      GMMESH=0
      DO 1911 GK=1,NZ+1
      CALL GETPT(1,NY+1,GK,GA(1),GA(2),GA(3))
      GZCO(2,GK)=GA(3)
      GYCO(2,GK)=GA(2)
      CALL GETPT(1,1,GK,GA(1),GA(2),GA(3))
      GZCO(1,GK)=GA(3)
      GYCO(1,GK)=GA(2)
C
C     SET INITIAL DISPLACEMENT
C
      GTDISBALL(ISTEP-1)=GBALLDISP
1911  CONTINUE
      END IF
C
C     WRITE INFORMATION FOR TIME STEP
C
      GBD=0
      TYPE*,'******************TIME STEP:',ISTEP
      TYPE*,'TIME (GTM)=',GTM
      TYPE*,'VELOCITY=',GTINT(ISTEP)*GWIN
      TYPE*,'TOTAL BALL DISPLACEMENT=',GTDISBALL(ISTEP-1)
      IF(ISTEP.EQ.1) GOTO 19190
      IF(GMMESH.EQ.0) GOTO 19199
19190       CONTINUE
      TYPE*,'*MODIFYING GEOMETRIC DOMAIN*'
C
C    CALCULATE NEW GRID FOR TIME STEP
C
C    DIPLACE GRID
C
      DO 19100 GK=1,NZ+1
      TZC(1,1,GK)=GZCO(1,GK)-(10E-03-GTDISBALL(ISTEP-1))
      TYC(1,1,GK)=GYCO(1,GK)
```

```
      TZC(1,NY+1,GK)=GZCO(2,GK)
      TYC(1,NY+1,GK)=GYCO(2,GK)
      TNYC(1,1,GK)=GYCO(1,GK)
      TNZC(1,1,GK)=GZCO(1,GK)-(10E-03-GTDISBALL(ISTEP-1))
19100      CONTINUE
      GTEMPZC=TZC(1,1,GNOO)
      DO 19101 GK=1,NZ
      IF(GTEMPZC.GE.TZC(1,NY+1,GK).AND.GTEMPZC.LE.
     1  TZC(1,NY+1,GK+1)) GCC=GK+1
19101      CONTINUE
      GCCD=GNOO-GCC
C
C    CALCULATE NEW INLET DISTANCES
C
      GZDISTI=TZC(1,NY+1,GNFF-GCCD)
      GZDIVI=GZDISTI/(GNFF-1)
      GZDIVIB=TZC(1,1,GNFF)/(GNFF-1)
C
C    LOCATE OUTLET CELL
C
      DO 19102 GK=GNOO,NZ
      IF(10E-03.LE.TYC(1,NY+1,GK).AND.10E-03.GE.
     1  TYC(1,NY+1,GK+1)) THEN
      GCCY=GK
      GCRO=GK
      GOTO 19103
      END IF
19102      CONTINUE
19103      CONTINUE
C
C     CALCULATE OUTLET DISTANCES
C
      GZDISTO=GZCO(2,NZ+1)-TZC(1,NY+1,GCCY)
      GZDIVO=GZDISTO/(NZ+1-GCCY-GCCD)
C
C     RECALCULATE INLET TRACT
C
      DO 19104 GK=1,GNFF-1
      TNZC(1,NY+1,GK)=GZDIVI*(GK-1)
      TNYC(1,NY+1,GK)=10E-03
      TNZC(1,1,GK)=GZDIVIB*(GK-1)
19104      CONTINUE
C
C     RECALCULATE VALVE
C
```

```
      DO 19105 GK=GNFF,GCCY+GCCD
      TNZC(1,NY+1,GK)=TZC(1,NY+1,GK-GCCD)
      TNYC(1,NY+1,GK)=TYC(1,NY+1,GK-GCCD)
19105      CONTINUE
C
C     RECALCULATE OUTLET
C
      DO 19106 GK=GCCY+GCCD+1,NZ+1
      TNZC(1,NY+1,GK)=TNZC(1,NY+1,GK-1)+GZDIVO
      TNYC(1,NY+1,GK)=10E-03
19106      CONTINUE
      GZDIVOB=(TNZC(1,NY+1,NZ+1)-TZC(1,1,GNEE))/(NZ+1-GNEE)
      DO 19107 GK=GNEE+1,NZ+1
      TNZC(1,1,GK)=TNZC(1,1,GK-1)+GZDIVOB
19107      CONTINUE
C
C     SET NEW CORNER POINTS INTO TZC,TYC ARRAY
C
      DO 19108 GK=1,NZ+1
      TZC(1,NY+1,GK)=TNZC(1,NY+1,GK)
      TYC(1,NY+1,GK)=TNYC(1,NY+1,GK)
      TZC(1,1,GK)=TNZC(1,1,GK)
      TYC(1,1,GK)=TNYC(1,1,GK)
19108      CONTINUE
C
C     REDEFINE INLET CELLS ON CONDUIT WALL
C
      DO 19109 GK=1,GNEE
      IF(10E-03.LT.TYC(1,NY+1,GK)) THEN
      GCCY=GK-1
      GOTO 19150
      END IF
19109      CONTINUE
19150      CONTINUE
      GZDIVI=TZC(1,NY+1,GCCY+1)/GCCY
      DO 19110 GK=1,GCCY
      TZC(1,NY+1,GK)=GZDIVI*(GK-1)
19110      CONTINUE
      GZDIVI=TZC(1,1,GNFF)/(GNFF-1)
      DO 19151 GK=1,GNFF
      TZC(1,1,GK)=GZDIVI*(GK-1)
19151      CONTINUE
C
C     CONCENTRATE GRID
C
```

```
C     LOCATE START AND END OF DIVERGING INLET SECTION
C
      GFLG=0
      DO 19111 GK=1,NZ
      IF(TYC(1,NY+1,GK).GT.10E-03.AND.GFLG.EQ.0) THEN
      GCCY=GK-1
      GFLG=1
      END IF
      IF(TYC(1,NY+1,GK)-TYC(1,NY+1,GK+1).
     1 EQ.0.AND.GFLG.EQ.1) THEN
      GCCD=GK
      GOTO 19112
      END IF
19111       CONTINUE
19112       CONTINUE
C
C     CONCENTRATE CELLS DIVERGENT INLET SECTION
C
      GSTRT=GCCY
      GEND=GCCD
      GSCALE=50*GTDISBALL(ISTEP-1)+0.5
      DO 19120 LP=1,INT((GEND-GSTRT)/2)
      DO 19113 GK=GSTRT,GEND-1
C
C     TOP LINE
C
      GYDIST=(TYC(1,NY+1,GK+1)-TYC(1,NY+1,GK))*GSCALE
      GZDIST=(TZC(1,NY+1,GK+1)-TZC(1,NY+1,GK))*GSCALE
      TNZC(1,NY+1,GK+1)=TZC(1,NY+1,GK)+GZDIST
      TNYC(1,NY+1,GK+1)=TYC(1,NY+1,GK)+GYDIST
C
C     BALL
C
      GZDIST=(TZC(1,1,GK+1)-TZC(1,1,GK))*GSCALE
      TNZC(1,1,GK+1)=TZC(1,1,GK)+GZDIST
      TNYC(1,1,GK+1)=(11.2272E-03**2-(TZC(1,1,GNFF)
     1          +11.2272E-03-TNZC(1,1,GK+1))**2)**0.5
19113       CONTINUE
      DO 19114 GK=GSTRT+1,GEND-1
      TZC(1,NY+1,GK)=TNZC(1,NY+1,GK)
      TYC(1,NY+1,GK)=TNYC(1,NY+1,GK)
      TZC(1,1,GK)=TNZC(1,1,GK)
      TYC(1,1,GK)=TNYC(1,1,GK)
19114       CONTINUE
      GSTRT=GSTRT+1
```

```
      GEND=GEND-1
19120      CONTINUE
C
C     CONCENTRATE CELLS TOWARDS BALL ON THE INLET SECTION
C
      GSCALE=50*GTDISBALL(ISTEP-1)+0.5
      GSTRT=GCCY
      GEND=GNFF+1
      DO 19130 LP=1,INT((GSTRT-GNFF)/2)
      DO 19121 GK=GEND+1,GSTRT
      GKTMP=GSTRT-GK+GEND+1
C
C    TOP LINE
C
      GYDIST=(TYC(1,NY+1,GKTMP)-TYC(1,NY+1,GKTMP-1))*GSCALE
      GZDIST=(TZC(1,NY+1,GKTMP)-TZC(1,NY+1,GKTMP-1))*GSCALE
      TNYC(1,NY+1,GKTMP-1)=TYC(1,NY+1,GKTMP)-GYDIST
      TNZC(1,NY+1,GKTMP-1)=TZC(1,NY+1,GKTMP)-GZDIST
C
C     BOTTOM LINE
C
      GZDIST=(TZC(1,1,GKTMP)-TZC(1,1,GKTMP-1))*GSCALE
      TNZC(1,1,GKTMP-1)=TZC(1,1,GKTMP)-GZDIST
      TNYC(1,1,GKTMP-1)=(11.22727E-03**2-(TZC(1,1,GNFF)
     1          +11.22727E-03-TNZC(1,1,GKTMP-1))**2)**0.5
19121      CONTINUE
      DO 19122 GK=GEND,GSTRT-1
      GKTMP=GSTRT-1-GK+GEND
      TZC(1,NY+1,GKTMP)=TNZC(1,NY+1,GKTMP)
      TYC(1,NY+1,GKTMP)=TNYC(1,NY+1,GKTMP)
      TZC(1,1,GKTMP)=TNZC(1,1,GKTMP)
      TYC(1,1,GKTMP)=TNYC(1,1,GKTMP)
19122      CONTINUE
      GSTRT=GSTRT-1
      GEND=GEND+1
19130      CONTINUE
      GSCALE=0.3
C
C    FIND OUTLET FLAT
C
      DO 19135 GK=GNOO,NZ
      IF (10E-03.GE.TYC(1,NY+1,GK)) THEN
      GCRO=GK
      GOTO 19136
      ENDIF
```

```
19135      CONTINUE
19136      CONTINUE
C
C     CONCENTRATE OUTLET TRACT
C
C     BOTTOM LINE
C
      GSTRT=GNEE
      GEND=NZ
      ZDIST=TZC(1,1,GEND)-TZC(1,1,GSTRT)
      GLIM1=GDIN
      GXS=GLIM1**0.5
      GXE=(GLIM1+ZDIST)**0.5
      GXDIV=(GXE-GXS)/(GEND-GSTRT)
      DO 19131 GK=GSTRT,GEND
      TZC(1,1,GK)=TZC(1,1,GSTRT)+((GXS+GXDIV*(GK-GSTRT))**2)-GLIM1
      TYC(1,1,GK)=0
19131      CONTINUE
C
C     TOP LINE
C
      GSTRT=GCRO-4
      GEND=NZ
      ZDIST=TZC(1,NY+1,GEND)-TZC(1,NY+1,GSTRT)
      GLIM1=GDIN*2
      GXS=GLIM1**0.5
      GXE=(GLIM1+ZDIST)**0.5
      GXDIV=(GXE-GXS)/(GEND-GSTRT)
      DO 19132 GK=GSTRT,GEND
      TZC(1,NY+1,GK)=TZC(1,NY+1,GSTRT)+((GXS+GXDIV*(GK-GSTRT))**2)-
     1      GLIM1
      TYC(1,NY+1,GK)=10E-03
19132      CONTINUE
C
C     CONCENTRATE INLET TRACT
C
C     BOTTOM LINE
C
      GSTRT=1
      GEND=GNFF
      ZDIST=TZC(1,1,GEND)-TZC(1,1,GSTRT)
      GLIM1=GDIN
      GXS=GLIM1**0.5
      GXE=(GLIM1+ZDIST)**0.5
      GXDIV=(GXE-GXS)/(GEND-GSTRT)
```

```
      DO 19161 GK=GSTRT,GEND
      GKTMP=GSTRT-GK+GEND
      TZC(1,1,GKTMP)=TZC(1,1,GEND)-((GXS+GXDIV*(GK-GSTRT))**2)+GLIM1
      TYC(1,1,GKTMP)=0
19161       CONTINUE
C
C     TOP LINE
C
      GSTRT=1
      GEND=GCCY+1
      ZDIST=TZC(1,NY+1,GEND)-TZC(1,NY+1,GSTRT)
      GLIM1=GDIN*0.5
      GXS=GLIM1**0.5
      GXE=(GLIM1+ZDIST)**0.5
      GXDIV=(GXE-GXS)/(GEND-GSTRT)
      DO 19171 GK=GSTRT,GEND
      GKTMP=GSTRT-GK+GEND
      TZC(1,NY+1,GKTMP)=TZC(1,NY+1,GEND)-
     1            ((GXS+GXDIV*(GK-GSTRT))**2)+GLIM1
      GKTMP=GSTRT-GK+GEND
      TYC(1,NY+1,GKTMP)=10E-03
19171       CONTINUE
C
C     DETERMINE INTERMEDIATE Z AND Y VALUE
C
      GDX=(GANGLE/NX)*2*3.1415926/360
      DO 19141 GK=1,NZ+1
      GBSUBL(GK)=(TYC(1,NY+1,GK)-TYC(1,1,GK))/(NY+1)
      GCSUBL(GK)=GBSUBL(GK)
19141       CONTINUE
      DO 19142 GK=1,NZ+1
      GZCSUBL(GK)=(TZC(1,NY+1,GK)-TZC(1,1,GK))*GCSUBL(GK)
     1          /(TYC(1,NY+1,GK)-TYC(1,1,GK))
      GZBSUBL(GK)=(TZC(1,NY+1,GK)-TZC(1,1,GK))*GBSUBL(GK)
     1          /(TYC(1,NY+1,GK)-TYC(1,1,GK))
19142       CONTINUE
      DO 19143 GK=1,NZ+1
      GZYCTR=(TZC(1,NY+1,GK)-TZC(1,1,GK))-(GZCSUBL(GK)+GZBSUBL(GK))
      GYYCTR=(TYC(1,NY+1,GK)-TYC(1,1,GK))-(GCSUBL(GK)+GBSUBL(GK))
      DO 19143 GJ=2,NY
      TZC(1,GJ,GK)=TZC(1,1,GK)+GZBSUBL(GK)+(GZYCTR*(GJ-2)/(NY-2))
      TYC(1,GJ,GK)=TYC(1,1,GK)+GBSUBL(GK)+(GYYCTR*(GJ-2)/(NY-2))
19143       CONTINUE
      DO 19145 GK=1,NZ+1
      DO 19145 GJ=1,NY+1
```

```
      DO 19145 GI=2,NX+1
      GXC=0
      TZC(GI,GJ,GK)=TZC(1,GJ,GK)
      TYC(GI,GJ,GK)=TYC(1,GJ,GK)*COS(GDX*(GI-1))
      TXC(GI,GJ,GK)=TYC(1,GJ,GK)*SIN(GDX*(GI-1))
      CALL SECORN(12,1,GJ,GK,GXC)
      CALL SECORN(14,1,GJ,GK,TYC(1,GJ,GK))
      CALL SECORN(16,1,GJ,GK,TZC(1,GJ,GK))
      CALL SECORN(12,2,GJ,GK,TXC(2,GJ,GK))
      CALL SECORN(14,2,GJ,GK,TYC(2,GJ,GK))
      CALL SECORN(16,2,GJ,GK,TZC(2,GJ,GK))
19145 CONTINUE
      CALL BGEOM(1)
      CALL BGEOM(2)
19199 CONTINUE
C
C     RESET SUM
C
      GTVL=0
      GSRTOTAL=0
      GSRLOW=0
      GSRTHR=0
      GSRTIZ=0
      GTVOLIZ=0
      GSRTLWIZ=0
      GFTSUM=0
      GSRTHRIZ=0
      RETURN
192   CONTINUE
C   * ------------------- SECTION 2 ---- Start of sweep.
      RETURN
193   CONTINUE
C   * ------------------- SECTION 3 ---- Start of iz slab.
      GETCAR=T
      RETURN
194   CONTINUE
C   * ------------------- SECTION 4 ---- Start of iterations over slab.
      CALL FNDWDY(GRSP1,LBNAME('WCRT'))
      RETURN
199   CONTINUE
C   * ------------------- SECTION 9 ---- Start of solution sequence for
C                                        a variable
      RETURN
1910  CONTINUE
C   * ------------------- SECTION 10---- Finish of solution sequence for
```

```
C                                        a variable
      RETURN
195   CONTINUE
C   * ------------------- SECTION 5 ---- Finish of iterations over slab.
      RETURN
196   CONTINUE
C   * ------------------- SECTION 6 ---- Finish of iz slab.
C
C     CALCULATE FORCE ACTING ON BALL ACLUDER
C     AND SHEAR STRESS
C
19623       CONTINUE

C     IF (ISWEEP.LE.2.AND.ISTEP.EQ.1) GOTO 1962
      CALL GETYX(VISL,GENUL,MY,MX)
      CALL GETYX(LGEN1,GAMMA,MY,MX)
      CALL GETYX(P1,GP1,MY,MX)
      CALL CORNER(3,IZ,GCORA,MY,MX)
      CALL CORNER(3,IZ+1,GCORB,MY,MX)
      CALL GTIZYX(4,IZ,GVOL,MY,MX)
C
C     CALCULATE VISCOSITY
C
      DO 1961 IX=1,NX
      DO 1961 IY=1,NY
      IF(GAMMA(IY,IX).EQ.0) GAMMA(IY,IX)=1
      GAMMA(IY,IX)=GAMMA(IY,IX)**0.5
C
C     CALC PRESSURE DROP ACROSS VALVE
C
      IF(10E-03.GE.GCORA(NY,1).AND.10E-03.LE.GCORB(NY,1))
     1 GPR1(ISTEP)=GP1(NY,1)
      IF(140E-03.GE.GCORA(NY,1).AND.140E-03.LE.GCORB(NY,1)) THEN
      GPR2(ISTEP)=GP1(NY,1)
      GPDROP(ISTEP)=GPR1(ISTEP)-GPR2(ISTEP)
      ENDIF
C
C     NEWTONIAN FLUID
C
      IF (ENUL.EQ.GRND5) THEN
C     GTAUT(IY,IX)=GAMMA(IY,IX)*GENUT(IY,IX)*GRHO1
      GTAUL(IY,IX)=GAMMA(IY,IX)*GENUL(IY,IX)*GRHO1
      GENUL(IY,IX)=GTAUL(IY,IX)/(GAMMA(IY,IX)*GRHO1)
      ENDIF
C
```

```
C     NON-NEWTONIAN FLUID
C
      IF (ENUL.EQ.GRND7) THEN
      GTAUL(IY,IX)=((GSLOPE*GAMMA(IY,IX)**.5)+GYIELD**.5)**2
      GENUL(IY,IX)=GTAUL(IY,IX)/(GAMMA(IY,IX)*GRHO1)
C     GTAUT(IY,IX)=GAMMA(IY,IX)*GENUT(IY,IX)*GRHO1
      ENDIF
C
C     CALCULATE AVERAGE SHEAR RATE
C
      IF(ISWEEP.EQ.LSWEEP.OR.ENUFSW.EQ.T) THEN
      GSRTOTAL=GSRTOTAL+GAMMA(IY,IX)*GVOL(IY,IX)
      IF(GAMMA(IY,IX).LE.100) THEN
      GSRLOW=GSRLOW+GAMMA(IY,IX)*GVOL(IY,IX)
      ENDIF
      IF(GAMMA(IY,IX).LE.7) THEN
      GSRTHR=GSRTHR+GAMMA(IY,IX)*GVOL(IY,IX)
      ENDIF
      GTVL=GTVL+GVOL(IY,IX)
C
C     CALCULATE RANGES OF SHEAR STRESS
C
      IF(GTAUL(IY,IX).GE.GR1.AND.GTAUL(IY,IX).LT.GR2) THEN
      GRNG(ISTEP,1)=GRNG(ISTEP,1)+GVOL(IY,IX)
      ENDIF
      IF(GTAUL(IY,IX).GE.GR2.AND.GTAUL(IY,IX).LT.GR3) THEN
      GRNG(ISTEP,2)=GRNG(ISTEP,2)+GVOL(IY,IX)
      ENDIF
      IF(GTAUL(IY,IX).GE.GR3.AND.GTAUL(IY,IX).LT.GR4) THEN
      GRNG(ISTEP,3)=GRNG(ISTEP,3)+GVOL(IY,IX)
      ENDIF
      IF(GTAUL(IY,IX).GE.GR4.AND.GTAUL(IY,IX).LT.GR5) THEN
      GRNG(ISTEP,4)=GRNG(ISTEP,4)+GVOL(IY,IX)
      ENDIF
      IF(GTAUL(IY,IX).GE.GR5.AND.GTAUL(IY,IX).LT.GR6) THEN
      GRNG(ISTEP,5)=GRNG(ISTEP,5)+GVOL(IY,IX)
      ENDIF
      IF(GTAUL(IY,IX).GE.GR6.AND.GTAUL(IY,IX).LT.GR7) THEN
      GRNG(ISTEP,6)=GRNG(ISTEP,6)+GVOL(IY,IX)
      ENDIF
      IF(GTAUL(IY,IX).GE.GR7.AND.GTAUL(IY,IX).LT.GR8) THEN
      GRNG(ISTEP,7)=GRNG(ISTEP,7)+GVOL(IY,IX)
      ENDIF
      IF(GTAUL(IY,IX).GE.GR8.AND.GTAUL(IY,IX).LT.GR9) THEN
      GRNG(ISTEP,8)=GRNG(ISTEP,8)+GVOL(IY,IX)
```

```
      ENDIF
      IF(GTAUL(IY,IX).GE.GR9.AND.GTAUL(IY,IX).LT.GR10) THEN
      GRNG(ISTEP,9)=GRNG(ISTEP,9)+GVOL(IY,IX)
      ENDIF
      IF(GTAUL(IY,IX).GE.GR10) THEN
      GRNG(ISTEP,10)=GRNG(ISTEP,10)+GVOL(IY,IX)
      ENDIF
      ENDIF
C
C     DETERMINE FORCE ON OCCLUDER
C
1961  CONTINUE
      IF (ISWEEP.EQ.LSWEEP.OR.ENUFSW.EQ.T) THEN
      CALL GETYX(GRSP1,GRDWDY,MY,MX)
      CALL GETPT(1,1,IZ,GA(1),GA(2),GA(3))
      CALL GETPT(1,1,IZ+1,GB(1),GB(2),GB(3))
      CALL SUB(GB,GA,GC)
      GZG=GC(3)/2+GA(3)
      IF (ABS(GC(2)).GT.0) GOTO 19624
      GOTO 19625
!9624CALL GTIZYX(8,IZ,GSAREA,MY,MX)
      GSAREA(1,1)=GSAREA(1,1)*360/GANGLE
      GTHETA=ATAN(GC(2)/GC(3))
      GFS=(GRDWDY(1,1)*GENUL(1,1)*GSAREA(1,1))*COS(GTHETA)
      GFP=(3.1415926*GP1(1,1)*(GB(2)**2-GA(2)**2))
      GFT(IZ)=GFP+GFS
19625       CONTINUE
      END IF
C
C     SET CALCULATED VALUES BACK INTO THE SOLVER
C
      CALL SETYX(VISL,GENUL,MY,MX)
      CALL SETYX(C4,GAMMA,MY,MX)
      CALL SETYX(C5,GTAUL,MY,MX)
C     CALL SETYX(C6,GTAUT,MY,MX)
C     CALL SETYX(C7,GTTAU,MY,MX)
C
C     FIND SHEAR RELATED TOTALS
C
      IF(ISWEEP.EQ.LSWEEP.OR.ENUFSW.EQ.T) THEN
      GSRTIZ=GSRTIZ+GSRTOTAL
      GSRTLWIZ=GSRTLWIZ+GSRLOW
      GTVOLIZ=GTVOLIZ+GTVL
      GSRTHRIZ=GSRTHRIZ+GSRTHR
      ENDIF
```

```
C
C     INITIAL SETTING OF VISCOSITY OF NON-NEWTONIAN ANALYSIS
C
C     GOTO 1964
C1962       CALL GETYX(VISL,GENUL,MY,MX)
C       DO 1963 IX=1,NX
C       DO 1963 IY=1,NY
C       GENUL(IY,IX)=3.323E-03/1056.17
C1963       CONTINUE
C     CALL SETYX(VISL,GENUL,MY,MX)
C1964       CONTINUE
      RETURN
197   CONTINUE
C   * ------------------- SECTION 7 ---- Finish of sweep.
      RETURN
198   CONTINUE
C   * ------------------- SECTION 8 ---- Finish of time step.
C
C     SUM BALL FORCES
C
      DO 1981 IZ=1,NZ
      GFTSUM=GFTSUM+GFT(IZ)
1981  CONTINUE
      DO 1982 LP=1,10
      GRNG(ISTEP,LP)=GRNG(ISTEP,LP)/GTVOLIZ
1982  CONTINUE
      TYPE*,'AVERAGE SHEAR RATE=',GSRTIZ/GTVOLIZ
      TYPE*,'PROPORTION OF SHEAR RATE <100=',GSRTLWIZ/GSRTIZ
      TYPE*,'PROPORTION OF FLOW <7=',GSRTHRIZ/GSRTIZ
      TYPE*,'PRESSURE DROP=',GPDROP(ISTEP)
C
C     SAVE PHI FILE
C
      IF(GSAVE.EQ.1) CALL FNDMPD(ISTEP)
C
C     FIND BALL DISPLACEMENT
C
      GFORCE(ISTEP)=GFTSUM
      GTT=DT
      IF (ISTEP.EQ.1.AND.GTDISBALL(ISTEP-1).EQ.0.5E-03) THEN
      GBVEL(ISTEP)=0
      ELSE
      GBVEL(ISTEP)=(GTDISBALL(ISTEP-1)-GTDISBALL(ISTEP-2))/GTT
      END IF
      GBD=((GFTSUM/(2*GBMASS))*GTT**2)+(GBVEL(ISTEP)*GTT)
```

```
      GBALLDISP=GTDISBALL(ISTEP-1)+GBD
C
C     GBALLDISP=GBD
C
C     INFORMATION RELATING TO BALL DISPLACEMENT CALCULATION
C
      TYPE*,'******** BALL OCCLUDER FORCE CALCULATION ********'
      TYPE*,'FORCE AT CURRENT TIME STEP=',GFTSUM
      TYPE*,'FORCE AT PREVIOUS TIME STEP=',GFORCE(ISTEP-1)
      TYPE*,'FORCE DIFFERENCE=',ABS(GFORCE(ISTEP)-GFORCE(ISTEP-1))
      TYPE*,'GBVEL=',GBVEL(ISTEP)

      IF(GBALLDISP.GE.10E-03) GBALLDISP=10E-03
      IF(GBALLDISP.LE.0.5E-03) GBALLDISP=0.5E-03
      TYPE*,'GBALLDISP',GBALLDISP
      GTDISBALL(ISTEP)=GBALLDISP
      IF(GTDISBALL(ISTEP).EQ.GTDISBALL(ISTEP-1)) THEN
      GMMESH=0
      ELSE
      GMMESH=1
      ENDIF
C
C     WRITE FORCE HISTORY TO 'FORCE.PA4' FILE
C     DISPLACEMENT TO 'DISP.PA4' FILE
C     PRESSURE DROP TO 'PDROP.PA4' FILE
C     INPUT VELOCITY TO 'VEL.PA4' FILE
C     BALL VELOCITY TO 'BVEL.PA4' FILE
C     TOTAL OF SHEAR STESS RANGE TO 'TAUR1.PA4' FILE
C     TOTAL OF SHEAR STESS RANGE TO 'TAUR2.PA4' FILE
C     SHEAR RATE PROPORTION TO 'SHRVL.PA4' FILE
C     TOTAL TIME FOR SHEAR STRESS RANGE TO 'RTIME.PA4' FILE
C
      IF(ISTEP.EQ.1) THEN
     OPEN(UNIT=30,STATUS='UNKNOWN',FILE='FORCE.PA4',ACCESS='APPEND')
     OPEN(UNIT=31,STATUS='UNKNOWN',FILE='DISP.PA4',ACCESS='APPEND')
     OPEN(UNIT=32,STATUS='UNKNOWN',FILE='PRESS.PA4',ACCESS='APPEND')
     OPEN(UNIT=33,STATUS='UNKNOWN',FILE='VEL.PA4',ACCESS='APPEND')
     OPEN(UNIT=34,STATUS='UNKNOWN',FILE='BVEL.PA4',ACCESS='APPEND')
     OPEN(UNIT=35,STATUS='UNKNOWN',FILE='TAUR1.PA4',ACCESS='APPEND')
     OPEN(UNIT=36,STATUS='UNKNOWN',FILE='SHRVL.PA4',ACCESS='APPEND')
     OPEN(UNIT=37,STATUS='UNKNOWN',FILE='TAUR2.PA4',ACCESS='APPEND')
      END IF
      WRITE(30,19626) GTIME(ISTEP),GFORCE(ISTEP)
      WRITE(31,19628) GTIME(ISTEP),GTDISBALL(ISTEP)
      WRITE(32,19627) GTIME(ISTEP),GPR1(ISTEP),GPR2(ISTEP),GPDROP(ISTEP)
```

```
      WRITE(33,19626) GTIME(ISTEP),GTINT(ISTEP)*GWIN
      WRITE(34,19626) GTIME(ISTEP),GBVEL(ISTEP)
      WRITE(35,19629) GTIME(ISTEP),(GRNG(ISTEP,LP),LP=1,5)
      WRITE(37,19629) GTIME(ISTEP),(GRNG(ISTEP,LP),LP=6,10)
      WRITE(36,19630) GTIME(ISTEP),GSRTIZ/GTVOLIZ,GSRTLWIZ/GSRTIZ,
     1 GSRTHRIZ/GSRTIZ
C
C     WRITE INFORMATION FILE
C
      IF(MOD(ISTEP,IDISPA).EQ.0) THEN
      OPEN(UNIT=29,STATUS='UNKNOWN',FILE='INFO.DAT')
      WRITE(29,10010) GTIME(ISTEP),GTDISBALL(ISTEP-2),
     1    GTDISBALL(ISTEP-1),GBVEL(ISTEP)
      CLOSE(29)
      ENDIF
19611      FORMAT(F8.4,' RAD BLEND*',/,'X,1,1',/,I3)
19622      FORMAT(1X,I3,2X,E12.5)
19626      FORMAT(1X,F10.6,2X,E12.5)
19627      FORMAT(1X,F10.6,2X,E12.5,2X,E12.5,2X,E12.5)
19628      FORMAT(1X,F10.6,1X,F10.6)
19629      FORMAT(1X,F10.6,1X,5E12.5)
19630      FORMAT(1X,F10.6,1X,E12.5,1X,E12.5,1X,E12.5)
      RETURN
C*********************************************************************
C
C---  GROUP 20. Preliminary print-out
C
20    CONTINUE
      RETURN
C*********************************************************************
C*    Make changes to data for GROUPS 21 and 22 only in GROUP 19.
C*********************************************************************
C
C---  GROUP 23. Field print-out and plot control
23    CONTINUE
      RETURN
C*********************************************************************
C
C---  GROUP 24. Dumps for restarts
C
24    CONTINUE
      END
C
C     SAVE PHI DATA
C
```

```
SUBROUTINE FNDMPD(ISTEP)
COMMON F(1)
COMMON/NMFILS/NMFIL(60)
CHARACTER STORNM*48 , NMFIL*48 , CH3*3
CH3='   '
WRITE(CH3,FMT='(I3.3)') ISTEP
STORNM=NMFIL(22)
NMFIL(22)='M'//CH3
CALL DUMP
NMFIL(22)=STORNM
CALL DMPXYZ
END
```

A.4 List Of Movie Files

MPEG Movie Files

Re500.mpg	Re 500 Newtonian, velocity.
Re500nn.mpg	Re 500 non-Newtonian, velocity.
Re1000.mpg	Re 1000 Newtonian, velocity.
Re1000nn.mpg	Re 1000 non-Newtonian, velocity.
Re2000.mpg	Re 2000 Newtonian, velocity.
Re2000nn.mpg	Re 2000 non-Newtonian, velocity.
Rn2000t.mpg	Re 2000 non-Newtonian, shear stress.
Rn2000gm.mpg	Re 2000 non-Newtonian, shear rate.

AVI Movie Files

Conduit.avi	Flow visualisation of conduit valve.
Nooccl.avi	Flow visualisation of conduit valve with no occluder.

A.5 Papers Published And Submitted

Gentle, C.R. and Wilson, P. (1994) A Computational Flow Design Study Of Prototype Heart Valve Conduit Using 'FLOTRAN'. Biomechanika '94. Proceedings of the 12th School of Biomechanics. ISSN 0324-9646.

Gentle, C.R. and Wilson, P. (1994) Comparison Of Finite Element And Finite Volume Methods In The Analysis Of Steady State Newtonian Blood Flow Through A Prosthetic Heart Valve. Submitted to Journal Of Medical And Biological Engineering And Computing.

Gentle, C.R. and Wilson, P. (1994) The Effect Of Haematocrit Volume On Blood Flow In A Heart Valve Prosthesis. Submitted to Journal Of Medical And Biological Engineering And Computing.

Comparison Of Finite Element And Finite Volume Methods In The Analysis Of Steady State Newtonian Blood Flow Through A Prosthetic Heart Valve

C.R.Gentle And P.Wilson

Department Of Mechanical Engineering, The Nottingham Trent University, Burton Street, Nottingham NG1 4BU, UK

Abstract

The use of computational techniques to obtain data on prosthetic heart valve flow has steadily increased. This increase is partly due to the improved availability of data relating to flow velocity, shear stress, and shear rate and (with increased correlation between computational techniques and clinical flow regimes) more realistic blood models. This paper compares the techniques of Finite Volume (FV) and Finite Element (FE) through the analysis of blood flow within a prosthetic heart valve under steady conditions assuming Newtonian flow. The predicted flow velocities, shear stresses and shear rates were used to determine the haemodynamic performance, thrombus formation, and shear stress related haemolysis of the prosthesis. The results obtained show that simple Newtonian blood models can accurately predict pressure drop across prosthetic heart valve conduits and can indicate areas of main stream jet formation and jet impingement on conduit surfaces. The limitations of the FE package meant no shear stress/rate data could be obtained and hence no comparison of this was made. For the simple Newtonian models it was shown that they can be used to represent certain in-vitro simulations using blood analogue solutions. The main conclusion drawn is that a simple model, either FE or FV, can yield accurate predictions of pressure drop and flow patterns at peak systole, minimising the need for a large amount of *in vitro* testing and thus allowing a greater freedom in the design of prosthetic heart valves.

Keywords

Conduit, Finite Element, Finite Volume, Blood Flow.

---

1 Introduction

Over the past few years there has been an increasing number of computational fluid dynamics (CFD) software packages capable of modelling fluid flow using either a Finite Volume (FV) or Finite Element (FE) technique to produce a mathematical model of the flow regime. These systems offer great flexibility in defining the fluid domain and the nature of the fluid, i.e. Newtonian, non-Newtonian, Gas, Steam, etc. Each system will have its own strengths but all solve for the Navier-Stokes and Continuity equations. It is not the purpose of this paper to examine in depth the differences between FV and FE techniques but simply to outline the capabilities, using the analysis of steady Newtonian blood flow through a prosthetic conduit valve, of two commercially available software packages PHOENICS[1] (FV) and FLOTRAN[2] (FE) when used in a prosthesis analysis.

Conduit valves are most commonly used in children with congenital malformations of the heart where it is often impossible to implant a conventional valve prosthesis. In the Gentle[3] conduit valve considered here a ball occluder is used to provide the valve action and flow is directed around the ball with a near constant flow area to maintain blood velocities within an acceptable range. This will minimise pressure drops, shear stress, and areas of recirculation or stasis. A 20 millimetre diameter conduit valve was chosen and analysed under a range of flow regimes with Reynolds numbers of 500, 1000, 2000, 4000, 8000, giving volume flowrates in litres per minute of 1.48,

2.97, 5.93, 11.86, 23.72, respectively. Blood is assumed to be a Newtonian fluid with a density of 1056.17 Kg/m^3 and a dynamic viscosity of 3.323×10^{-3} Pa s.

2 Computational Software Packages

FLOTRAN

FLOTRAN is a general purpose analysis tool for the treatment of two and three dimensional fluid flow and/or heat transfer. It can be fully integrated with ANSYS, I-DEAS and PATRAN which act as pre and post processors. The governing equations consist of the momentum equations, the continuity equation, the energy equation, and an equation of state. These governing equations are expressed in primitive variables i.e., velocity and pressure. A two-equation turbulence model, k-ε, is used requiring two additional equations to solve for turbulent kinetic energy and turbulent dissipation rate. The equations are solved using the Galerkin weighted integral method, streamline upwinding, and a sequential solution algorithm.

PHOENICS 1.6.6

PHOENICS is a computer code, which uses the FV method to simulate fluid flow, heat transfer, chemical reaction and other related phenomena for both two and three dimensions. The package is self-contained having both pre and post processor capabilities. PHOENICS solves discretized versions of differential equations in the general form of:

$$\frac{\partial (r_i \rho_i \varphi_i)}{\partial t} + div(r_i \rho_i V_i \varphi_i - r_i \Gamma \varphi_i grad \varphi_i) = r_i S_i$$

where,

r=Volume fraction,
ρ=Density,
φ=Field variable,
Γ=Diffusion coefficient,
S=Source term,
V=Velocity,
t = Time,
i = Phase.

PHOENICS has two turbulence models namely k-ε and Prandtl mixing length. Both upwinding and hybrid solution algorithms are available. Both packages allow either linear relaxation or pseudo time step relaxation to be used.

3 Model Geometry And Computational Fluid Model Assumptions

The FE mesh and FV grid shown in Figure 1 represent a Gentle conduit valve of 20 mm inlet diameter. The FE geometry was produced on a Unigraphics CAD station from where an IGES interface was used to produce a data file which could be read by the general purpose ANSYS FE package, used as a pre- and post-processor tool. The mesh produced contained both quadrilateral and triangular bi-linear elements.

The FV grid was generated from a previous code[4]. The grid uses Body Fitted Co-ordinates (BFC) which allow a more accurate representation of the valve than would be possible if an orthogonal grid was used. An axisymetric grid was assumed for both models and hence only half of the conduit cross-section needs to be considered.

(a)

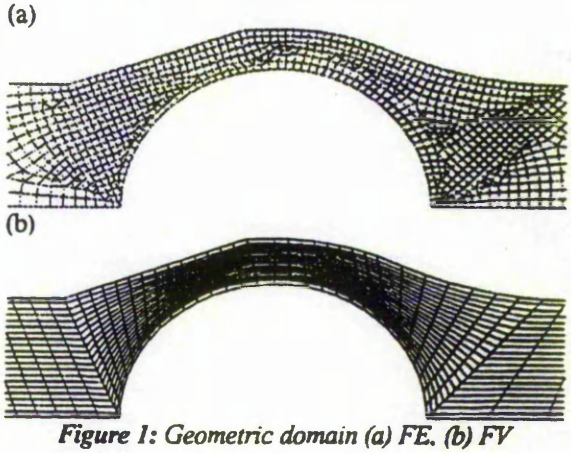

(b)

Figure 1: Geometric domain (a) FE. (b) FV

The inlet velocity profile was set uniformly and a short inlet tract was chosen to allow a 'plug' type velocity profile to develop before reaching the valve. At all wall boundaries the velocity components were set to zero. Logarithmic wall functions were used for both models. The pressure at the outlet plane for the models was set to a fixed value. For flowrates with Reynolds number up to 2000 laminar flow was assumed; for the higher flow rates turbulent flow was assumed and so the k-ε model was used. Convergence was assumed when residuals for both velocity components fell below 1×10^{-5}.

4 Grid Size Comparisons

The first step in the comparing the two packages was to study the effect of grid size on the accuracy of data produced. The grid size should be selected so that the flow may be modelled accurately without excessive use of computer time. For this purpose three grid sizes were chosen for each technique namely 1376, 5332, 8483 nodes for the FE grid and 1400, 5320, 7600 cells for the FV grid. For the FV package grid sizes were determined by specifying the total number of cells in the x, y, and z directions. This could not be done for the FE mesh as grid spacing values were chosen around 'keypoints' limiting the ability to produce models with the exact number of nodes when compared to the FV model. A Reynolds number of 8000 was chosen as a greater number of nodes is required to model turbulent flow, due to its high

spatial density of occurrence, and so turbulence represents a more severe test for grid dependency. For each model the centre line velocity and pressure, and time taken to reach convergence were recorded. The centre line is defined as a line tracing a path along the central axis for the inlet and outlet sections, but along the ball surface in the middle section. The centre line velocity can be seen in Figures 2 and 3 where the axial distance is measured from the left hand edge of the grid, 41.46 mm upstream from the ball centre. The letters F, M, and, C, refer to the mesh/grid density, fine, medium, and coarse respectively.

The CPU time taken to reach convergence on the medium grid for both models was approximately 2700 seconds, for the fine grid 5400 seconds, and 810 seconds for the coarse grid. The FV model for the fine grid would not converge fully and hence these results were treated with caution.

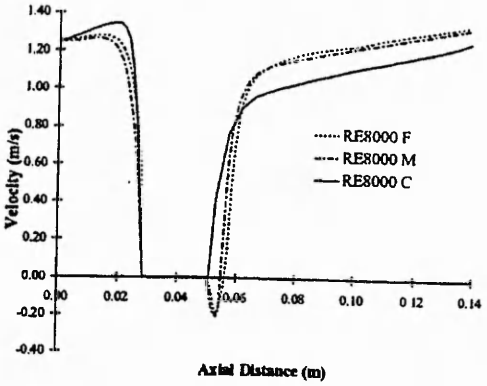

Figure 2: *Velocity along centre line (PHOENICS)*

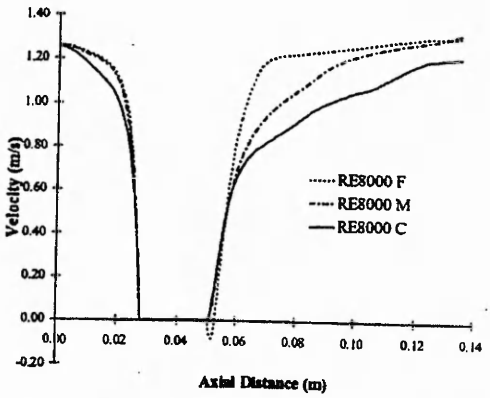

Figure 3: *Velocity along centre line (FLOTRAN)*

For the FV model, all grid sizes show an area of recirculation downstream of the conduit ball, the magnitude of which increases as the grid becomes finer. It can be seen that little difference exists between the fine and medium grids. The coarse mesh for the FE model shows a large deviation in flow velocity and does not predict any recirculation downstream of the ball. The coarse grid gave no recirculation but as grid density increased downstream of the ball a recirculation zone began to develop for both FLOTRAN and PHOENICS.

The pressure plots in Figure 4 show that for the FV model there is little difference between the values calculated with the medium and fine grids, but the

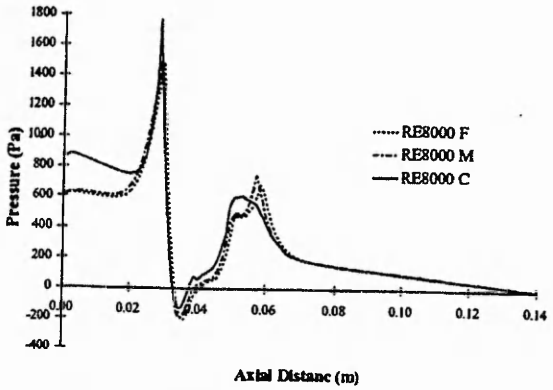

Figure 4: *Pressure profile along centre line (PHOENICS)*

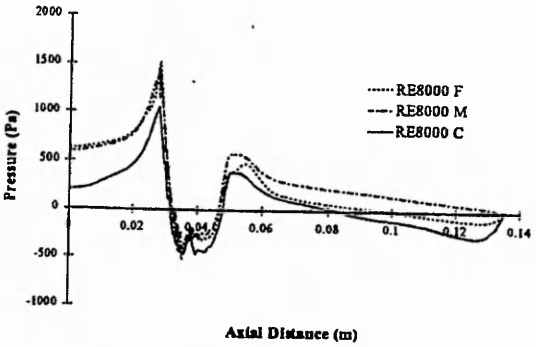

Figure 5: *Pressure profile along centre line (FLOTRAN)*

coarse grid values only show close correlation in the outlet section of the valve. The fine and medium grids for the FE model produce very close correlation initially, as shown in Figure 5, but diverge from one another in the outlet section of the valve. The coarse mesh gives lower predicted values throughout the valve.

It was decided that for the FV models the medium grid would be used for subsequent trials with the slight reduction in accuracy being offset by the saving in CPU time. The medium grid was also chosen for the FE models, even though the velocity values may be slightly under- predicted, because the pressure values were more closely related to those obtained from the FV model and again any reduction in accuracy would be offset by the saving in CPU time.

5 Results Of Flow Analysis

The next step was to study the difference between the FE and FV models for the full range of Reynolds

number, but with a constant, medium value of mesh or grid size. In total ten runs were conducted and the following parameters recorded, velocity, pressure, shear stress (PHOENICS), and total run time. These parameters allow the evaluation of the haemodynamic efficiency, shear stress related haemolysis, and thrombus formation potential of the prosthesis. For the first three runs Reynolds numbers of 500, 1000, 2000 were used and laminar flow assumed. The final two runs had Reynolds numbers of 4000 and 8000 where the flow was assumed to be turbulent. The initial comparison is based on the CPU time to perform all necessary calculations at a single grid point and is shown in Table 1.

Table 1: *Time taken to perform calculations at single grid point*

Package	Laminar	Turbulent
FV	7.6992×10^{-4} s	7.9887×10^{-4} s
FE	1.989×10^{-3} s	2.56039×10^{-3} s

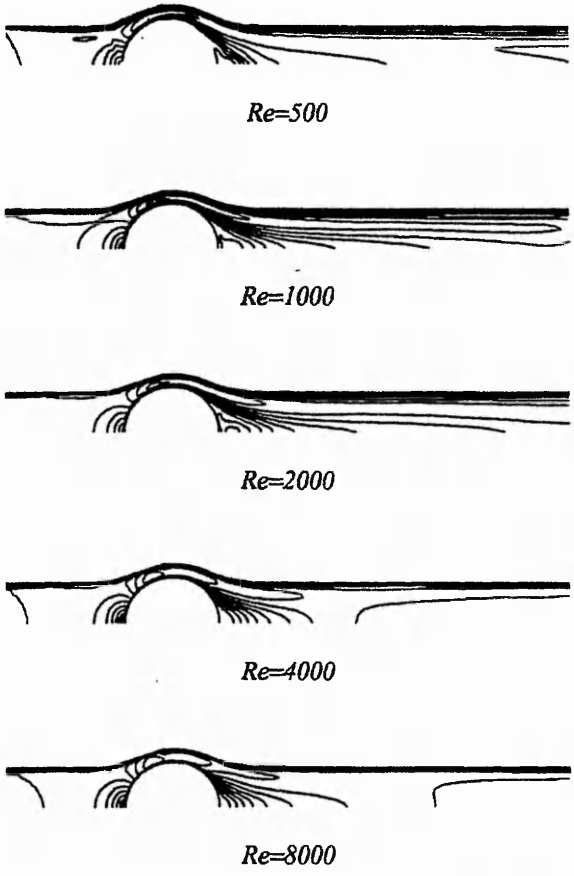

Figure 6: *Velocity contours predicted by FLOTRAN*

This table shows the FV program was approximately three times faster when performing calculations at a single grid point. However due to the need for considerable under-relaxation using a pseudo-time step to obtain convergence, any benefits in CPU time were lost as a result of the increased number of sweeps required to obtain a converged solution. Both packages took approximately the same overall CPU time, 2700 seconds, to produce a converged solution.

5.1 *Flow Regime In The Upstream Half Of The Valve*

Figures 6 and 7 show the velocity contour plots produced by FLOTRAN and PHOENICS, respectively. As would be expected there is an area of decelerating flow directly upstream of the ball. The flow is then accelerated through the convergent annulus section of the valve. The maximum velocities occur within this section of the valve and also the maximum shear stresses as the flow accelerates along the ball surface. The flow patterns are similar for both FE and FV models.

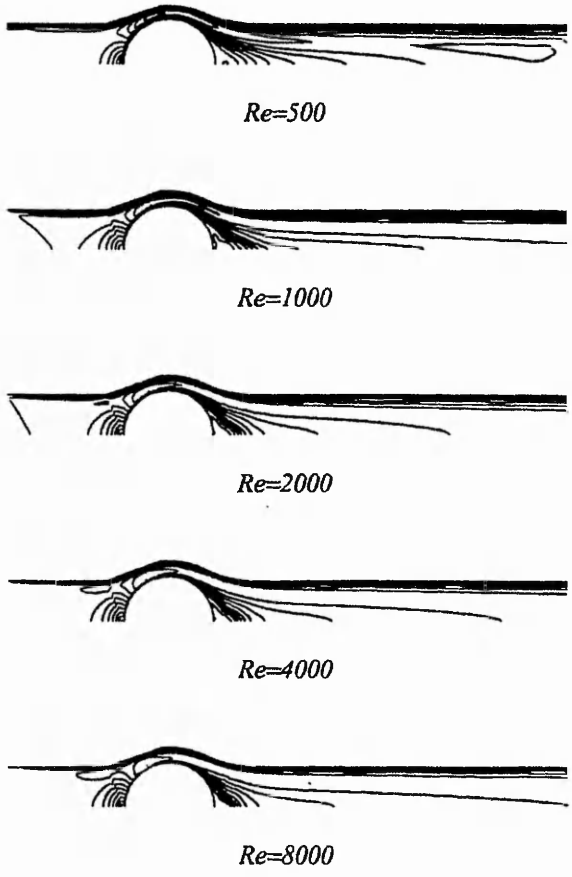

Figure 7: *Velocity contours predicted by PHOENICS*

5.2 *Flow Regime In The Downstream Half Of The Valve*

In the divergent annulus section of the valve a free stream jet begins to form. The geometry of the valve guides the jet that develops so that no impingement occurs at the prosthetic surface, reducing the risk of wall shear stress induced haemolysis. Generally this jet then enters the outlet section and moves downstream, initially following the model boundary but with a gradual dissipation into the central flow region. This, however, does not occur for the models on FLOTRAN with Reynolds numbers of 4000 and 8000, where a jet is formed but is then broken down rapidly downstream of the valve. This is probably due to the low grid density adopted and will be discussed later. Directly behind the ball exists an area of either recirculating flow or stasis. This recirculation is predicted for all laminar models but for the turbulent flows PHOENICS shows a distinct area of recirculation whereas FLOTRAN shows only an area of stasis. This again is probably due to a decrease in grid density for the FE model.

5.3 *Shear Stress Distribution*

Table 2 shows the maximum value of shear stress found at the front face of the ball. The shear stress value is calculated in PHOENICS for each flow, using the relationship:

$$\tau = \mu \dot{\gamma}$$

where μ = Effective viscosity equal to $\mu_L + \mu_T$.
μ_L = Laminar viscosity,
μ_T = Turbulent viscosity,
$\dot{\gamma}$ = Shear rate,
τ = Shear stress.

Table 2: *Maximum shear stress*

Reynolds Number	500	1000	2000	4000	8000
Shear Stress (N/m^2)	1.24	2.5	6.2	13.2	47

Figures 8 and 9 show shear stress contours produced by PHOENICS for Reynolds numbers of 500 and 8000. The shear stress is not accessible to the FLOTRAN user.

Figure 8: *Shear stress contours for Re=500*

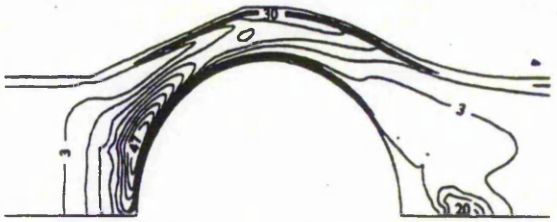

Figure 9: *Shear stress contours for Re=8000*

The haemodynamic significance of the shear stress contours may be assessed as follows:

(a) *Bulk shear stress:* Hellmus and Brown[5] use a threshold, for haemolysis, of 500 N/m^2 applied for a duration of 1×10^{-3} s. With all the fluid models considered here the value of bulk shear stress is very low compared to this threshold, even for the highest values occurring close to the prosthesis surface. It can therefore be assumed that destruction of erythrocytes does not occur within the bulk flow.

(b) *Shear stress at the prosthetic wall*: The value of shear stress to cause cell damage at the prosthesis surface is much lower than in the above case. Shear stress values below 150 N/m^2 can cause haemolysis. Blackshear[6] argues that additional stresses are encountered as erythrocytes adhere to and are then torn from the prosthetic surface and also that high shear stresses near a prosthetic surface increase the cell contact and hence the risk of haemolysis. The maximum surface shear stress predicted in any of the cases here was 26 N/m^2, occurring on the ball surface at the highest flowrate. Haemolysis is therefore unlikely to be a problem with this valve.

(c) *Endothelium damage due to jet impingement:* This type of damage, reported by Fry[7] , begin to occur at shear stresses as low as 40 N/m^2, with steady erosion of the cells occurring at a higher shear stress of 90 N/m^2. As can be seen from the velocity contours in Figures 6 and 7 the jet formed in the divergent section does not impinge on any surface. This is confirmed by the fact that areas of elevated wall shear stress do not occur within the divergent section of the valve. Therefore the jet formation in the downstream portion of the valve would not cause any problems for an endothelium. Consequently there is unlikely to be any jet impingement damage to the tissue lining which is expected to form on the inner wall of the conduit[8].

(d) *Thrombus:* Thrombus can form in areas of haemostasis or low shear. Dintenfass[9] brings to the attention a critical lower shear rate, 7 s^{-1}, below which clotting can be accelerated by a thousand fold. The prediction of recirculation or stasis and associated low shear rate values implies that thrombus formation is possible behind the ball. This situation would be

more significant at higher flowrates when the area of high shear at the upstream side of the ball could damage any cells passing through the into recirculation/stasis region and encourage a thrombus to form. It must be remembered, however that the ball actually pulses backwards and forwards, rotating as it goes, so thrombus growth is unlikely.

5.4 *Haemodynamic performance*

Earlier work by Gentle and Wilson[10] showed that FLOTRAN could accurately predict pressure drop, within 3%, across a caged ball valve between two chambers. The predicted values were slightly less than the experimental values of Lewis and Macleod[11] and it was speculated that this was due to surface roughness not being taken into account for the FE

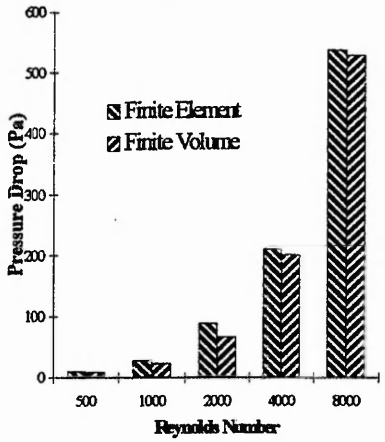

Figure 10: *Pressure drop across the prosthesis*

model. The conclusion drawn was that FLOTRAN would be able to predict pressure drop across a conduit valve within a high degree of acceptability. Figure 10 shows the predicted pressure drop across the conduit valve for PHOENICS and FLOTRAN. It can be seen that predicted pressure drop varies little between the two techniques and that the value predicted by FLOTRAN is always larger than the PHOENICS value.

6 Discussion

The results produced by FLOTRAN and PHOENICS compare favourably with each other except at high Reynolds number where an area of stasis was predicted by FLOTRAN but an area of recirculation was predicted by PHOENICS. The discrepancy is due to the reduction in grid density downstream of the ball where low spatial grid density does not allow the correct prediction of turbulent flow. The FE model with 5332 nodes was chosen, even though no recirculation was predicted, as at this present time no experimental data is available to verify the existence of a recirculation zone behind the ball. The analysis shows that damage to erythrocytes and endothelium cells would not occur at any of the modelled flowrates. The possibility of thrombus formation is less clear, however, and could take place behind the ball.

Both packages use a first order upwind solution scheme, but PHOENICS has the option to use a second order hybrid scheme which is more accurate. However, this means it is more difficult to converge. The first order upwind solution scheme introduces an artificial diffusion term making the effective Reynolds number lower and thus reducing eddy lengths. This may lead to underestimation of shear rate and shear stress values. This can be avoided by using a higher order numerical scheme.

7 Conclusion

The use of CFD in the analysis of artificial heart valves has gradually increased over the past few years. Initial studies used the FV technique to predict the flow but, as understanding of the FE techniques in modelling flow has increased ,the use and acceptance of FE analysis continues. There is no doubt that the ability to model a system using a computational approach has its advantages in both time and cost, and also allows a greater freedom for the designer's creativity.

The computational techniques have shown they can produce acceptable and meaningful results even though there is often a shortage of comparable *in vitro* results and so quantitative comparisons are not always possible. The models produced here were limited to steady Newtonian flow but could be extended to include a time dependent solution using a non-Newtonian blood viscosity model with dynamically varying model geometry and pulsatile flow.

References

1. ***PHOENICS.*** CHAM, Bakery House, 40 High Street, Wimbledon Village, London SW19 5AU.

2. ***FLOTRAN.*** COMPUFLO®, 1575 State Farm Boulevard, Charlottesville, VA 22901.

3. ***Gentle, C.R.*** (1983) Minimisation of pressure drop across heart valve conduits: a preliminary study. Life Support Systems, 1, 263-270.

4. ***Tansley, G.D.*** (1988) Computational investigation of turbulent non-Newtonian flow in heart valve conduits. PhD Thesis, The Nottingham Trent University.

5. ***Hellmus, J.D. and Brown, C.H.*** (1975) Blood cell damage by mechanical forces. In "Cardiovascular Flow Dynamics and Measurements." Hwang, H.N.C.

and Normann, N.A. (Eds), University Park Press, Baltimore, 799-823.

6. ***Blackshear, P.L.*** (1972) Mechanical haemolysis in flowing blood. In "Biomechanics: Its Foundation and Objectives." Fung, Y.C., Perrone, N. and Anliker, M. (Eds), Prentice Hall, New Jersey, 501-528.

7. ***Fry, D.L.*** (1968) Acute vascular endothelium changes associated with increased blood velocity gradients. Circ. Res., 12, 165-197.

8. ***Juden, H. Gentle,C.R. and Dowson, D.*** (1983) Scanning electron microscopy examination of a porous alumina prosthetic heart valve. Biomaterials, 4, 139-141.

9. ***Dintenfass, L.*** (1964) Rheological approach to thrombosis and atherosclerosis. Angiol., 333-343.

10. ***Gentle, C.R. and Wilson, P.*** (1994) A computational flow design study of prototype heart valve conduits using 'FLOTRAN'. Biomechanika'94. Proceedings of the 12th School of Biomechanics. ISSN 0324-9646, 115-121.

11. ***Lewis, J.M.O. and Macleod, N.*** (1978) Development of the Edinburgh prosthetic heart valve: review of *in vivo* and *in vitro* evaluation studies. In "Heart Valve Research In The UK." Eds Gentle, C.R. and Swales, P.D. Leeds University Press.

Prace Naukowe Instytutu Konstrukcji i Eksploatacji Maszyn
Nr 75 Politechniki Wrocławskiej Nr 75
Konferencje Nr 21 1994

BIOMECHANIKA '94
BIOMECHANICS

A COMPUTATIONAL FLOW DESIGN STUDY OF PROTOTYPE HEART VALVE CONDUITS USING "FLOTRAN"

R. Gentle, P. Wilson
The Nottingham Trent University

Abstract

A Computational Fluid Dynamics (CFD) study of conduit heart valves is presented. **Flotran**, a finite element CFD package based on **Ansys**, was used to investigate steady flow pressure drop, shear rates and recirculation within several variants of a basic design consisting of a ball occluder inside a rigid, shaped valve body. The methodology was validated against experimental results obtained with a conventional ball-and-cage valve prosthesis and, although there are still many shortcomings, has proved to offer useful time savings to the process of conduit valve design.

Keywords

Conduit, valve, prosthesis, heart, flow, computer.

Introduction

Heart valve prostheses are a well known example of the application of engineering techniques to medical situations and must be considered a great success by any measure (Black et al, 1983). Occasionally, however, there is a need for a valve to be mounted in a short length of conduit tubing rather than directly into the heart at the normal anatomical site. This need arises particularly in children where there is also some reconstructive surgery to be carried out on the great vessels to correct a congenital abnormality (McGoon, 1976). At present this need is largely met commercially by fixing a conventional mechanical valve, without its sewing ring, into a fabric tube of the type used in arterial grafts (Lefrak and Starr, 1979). This has the advantages that all the component parts are readily available and have been proved in many thousands of implants. This does not imply, however, that this approach to conduit valves is ideal or even satisfactory.

The main problem with existing valved conduits is that the valves in them were designed for insertion between two chambers of the heart (generally the left atrium and the ventricle, or the ventricle and the aortic sinus chamber) and were never intended for placing in the confined flow conditions to be found in a cylindrical tube. Most valve prostheses rely on the formation of vortices or

recirculating flow patterns behind the occluder or leaflets to assist their closure (Duff and Fox, 1972) and it is difficult to achieve this fully in a straight tube, which is not shaped to reproduce ventricular or sinus flow. Hence there is evidence that some existing conduit valves do not function properly at certain operating conditions (Leefe, 1993).

The prosthesis shown in Fig 1 was initially developed to overcome this drawback to the existing limited range of conduit valves, and the design philosophy adopted was to use a rigid conduit body so that the blood flow could be guided around a ball occluder, maintaining a near constant flow area and hence minimising pressure drops, shear rates and areas of stasis or recirculation. The ball occluder, much employed in this discipline over the years, e.g. in the Starr-Edwards series of valves, lends itself to this approach because of its inherently streamlined shape. Unfortunately the concept of constant flow area is impossible to achieve completely and so there have been several models constructed, as indicated in Fig 2, to study the best way of achieving satisfactory flow conditions in practice. In the examples shown here the included angle of the inlet cone was varied to find a compromise between low pressure drop and the overall length of the prosthesis. The outcome has been a conduit valve with a reliable valve action and demonstrably good pressure drop (Gentle, 1983), but one which which does not necessarily meet the full set of criteria for good flow properties:

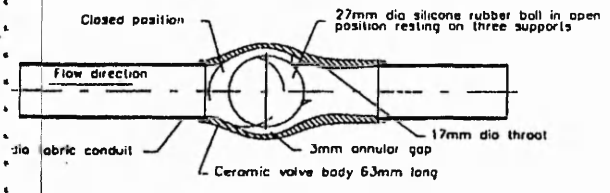

1. Schematic of the ball conduit valve

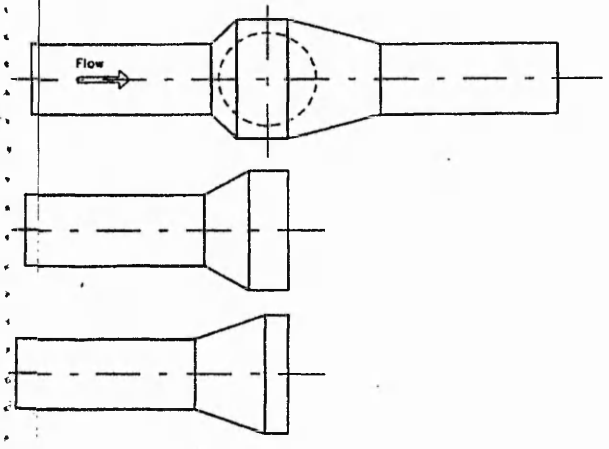

2. Some Model Stages in the Conduit Valve Design

* low pressure drop to minimise the load on the heart

* low shear rates to reduce the damage to blood cells

* no areas of stasis or recirculation in order to minimise formation of thrombus or emboli.

In order to investigate these criteria further there are two avenues which could be followed:

i. a full experimental study of a blood analogue fluid through many carefully constructed prototypes, each modelling a slightly different geometry

OR

ii. a CFD study which gives rapid, direct indications of pressure drop, shear and recirculation for easily varied geometries.

Clearly the second method of study offers the fastest and cheapest approach at the

design and development stage although it must be recognised that the techniques of the first method would be required to satisfy the international standard on heart valve prostheses, ISO 5840. This paper therefore outlines how a commercial finite element package, Flotran, was used to investigate several variations on the original geometry of the conduit valve. The many shortcomings of this type of approach are discussed, but it is concluded that the method can be a great help at the concept design stage.

Validation

One of the most important steps in any CFD study is the validation of the general approach by comparing at least part of the work against independent experimental data on a similar flow situation. The situation chosen here to be the subject of the validation exercise was the Starr-Edwards ball and cage aortic valve, for the following reasons:

* the ball occluder is identical to that proposed for the valved conduit

* independent data is readily available

* the flow pattern around a ball occluder does not vary much from the free stream case even when there is a flow boundary close by, such as the aortic root or the conduit body.

The data chosen for the validation (Lewis and Macleod, 1978) relates to the pressure drop resulting from steady flow of a 40% glycerol/water mixture from one large chamber to another through a Starr-Edwards 14A aortic valve. The first step in the validation was therefore to reproduce this geometry in the computer and fit a finite element grid to it. It should be noted that the axisymmetric nature of the situation means that only one half of the flow channel is drawn. Furthermore, although the output can be used to give a three-dimensional picture of the flow, the model is really only a rotated two-dimensional one and cannot be used to represent the struts of the Starr-Edwards valve cage. Even so, ninety keypoints were used in defining the boundaries of this geometry.

The finite elements are arranged automatically by the Ansys pre-processing software, using an element size in this case of 0.75×10^{-3} mm. Since these elements can be triangles as well quadrilaterals, the result is an element grid which follows the contours of the boundary very closely, even for a complicated shape. The number of elements generated by the system was between 5000 and 6000, depending on the precise length of the inlet and outlet sections specified.

The overflow error was set so that the analysis converged within 50 iterations. This was acceptable in terms of time as it was found that iterations took approximately 1 minute each on the VAX mainframe computer that was available for the work. Some tests were carried out with a smaller overflow error limit, leading to a total of 500 iterations, but this produced hardly any discernible change in the output.

The length and diameter of the inlet and outlet sections could be varied but little difference could be detected. The important attribute was the velocity profile selected for the inlet flow within Flotran. The one finally adopted was the familiar parabolic profile associated with streamlined flow since the maximum Reynolds Number was approximately 2500. The fluid parameters specified were:

* density = 1103 kg/m^3

* viscosity = 3.5x10^{-3} Pa s

Typical outputs are displayed in Fig 3 and Fig 4, showing velocity vectors and pressure respectively.

The purpose of the velocity vector plot was simply to check if the flow pattern qualitatively resembled the type of flow pattern observed experimentally in the steady flow tests. Fig 3 clearly shows a strong jet sweeping round the front of the ball and part of the way round the back, but with an area of stasis immediately behind the ball, exactly as observed experimentally.

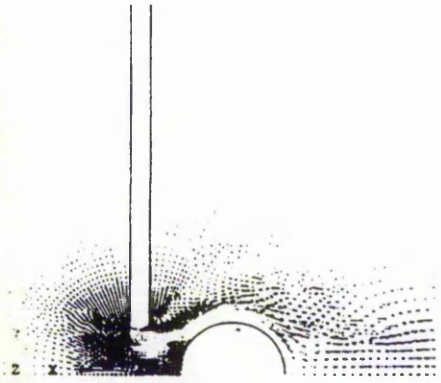

3. Typical Flotran Velocity Vector Plot for Starr-Edwards Valve

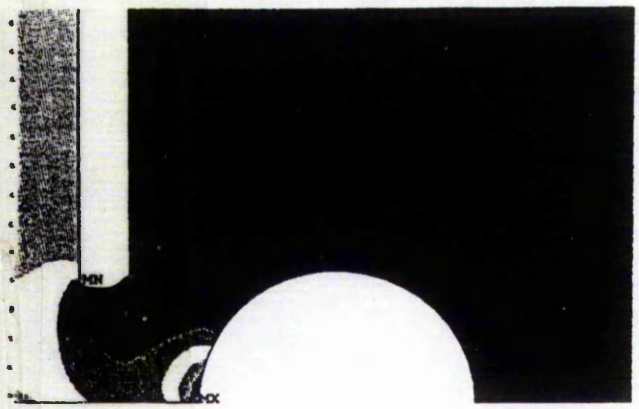

4. Typical Flotran Pressure Plot for Starr-Edwards Valve

The quantitative check on the Flotran output was provided by comparing the overall pressure drop, derived from plots such as Fig 4, against the experimental pressure drops. One adjustment was required before this comparison could proceed; the effect of Flotran not being able to model the cage struts needed to be taken into account. The presence of the struts on the real valve will lead to the measured pressure drop being larger than the equivalent figure for the computer-modelled valve. Therefore the pressure drop from the Flotran study was increased by 12%, a figure which was based on a measurement of the proportion of the real valve orifice circumference obstructed by the struts and the assumption that the pressure drop is inversely proportional to the square of the unobstructed flow area.

The outcome of this comparison is shown in Fig 5, which plots transvalvular pressure drop against the volume flow rate. The agreement is close, but with the pressure drop for the Flotran case consistently slightly lower than the real case. This is only to be expected since the computer model does not include the effects of surface roughness which will lead to the real pressure drops being higher. The conclusion from this validation exercise is that the Flotran software package can be used to model axisymmetric heart valves satisfactorily by employing a rotated two-dimensional geometry. This allows the element number to be limited to such an extent that each flow situation can be analysed within approximately one hour of computing time. On the basis of this conclusion the study proceeded to consider the various versions of the conduit valves.

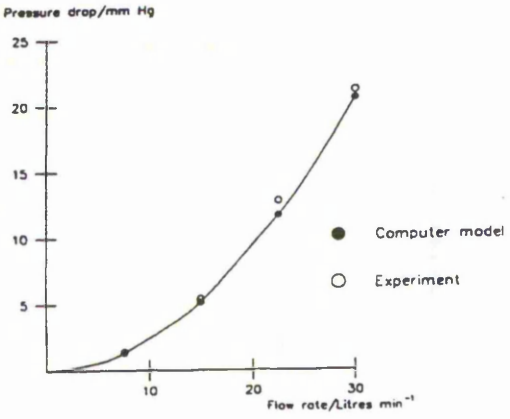

5. Pressure drop across a Starr-Edwards 14A Valve

CFD Applied to the Conduit Valves

The method outlined above for the Starr-Edwards valve was now applied to three different versions of the basic design for the ball valve conduit. The overflow error was maintained at the same value, giving convergence in approximately 50 iterations. The three versions were designated as follows:

CICO (Curved Inlet Curved Outlet) - this was an attempt to maintain as constant a flow area around the ball as possible.

SICO (Straight Inlet Curved Outlet) - with this version the inlet flow direction is more gradually changed.

SISO (Straight Inlet Straight Outlet) - the original concept.

The three parameters recorded in this study were the pressure within the fluid, the magnitude of the velocity and the turbulent kinetic level. The velocity vector plots were not found to be particularly useful since the fluid was largely constrained to follow a narrow path between the bal and the conduit body.

Results For CICO

Fig 6 and Fig 7 show the pressure and velocity magnitude respectively. They show that there is a pressure build up in front of the ball where the fluid impacts bluntly, and that there are high velocity regions at the abrupt corners.

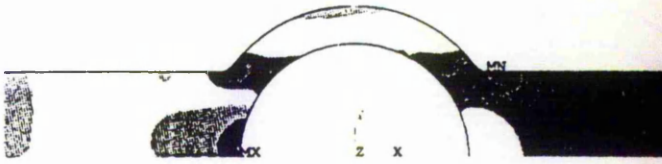

6. Pressure Plot for CICO Conduit Valve

7. Velocity Magnitude Plot for CICO Conduit Valve

Results For SICO

To reduce the pressure build up found in CICO, the inlet shape was made more gradual by reverting to the earlier concept of a conical inlet. Fig 8 shows that the resulting pressure build up in front of the ball is much less pronounced, while Fig 9 shows that the high velocity region associated with the join between the cylindrical conduit and the inlet curve of CICO is now removed. However the high velocities are simply pushed further downstream, as will be seen from Fig 9. This, combined with the strong inwards radial velocity component caused by the curved profile of the outlet portion, leads to a region of high turbulent kinetic energy immediately behind the ball, as shown in Fig 10.

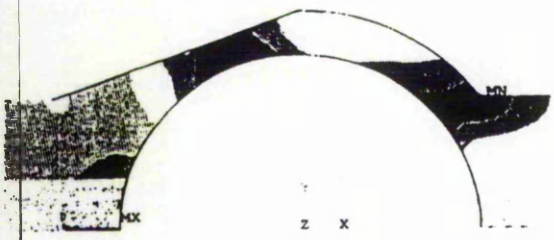

8. Pressure Plot for SICO Conduit Valve

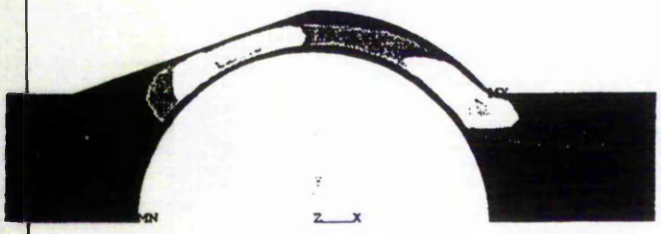

9. Velocity Magnitude Plot for SICO Conduit Valve

10. Turbulent Kinetic Energy Plot for SICO Conduit Valve

11. Pressure Plot for SISO Conduit Valve

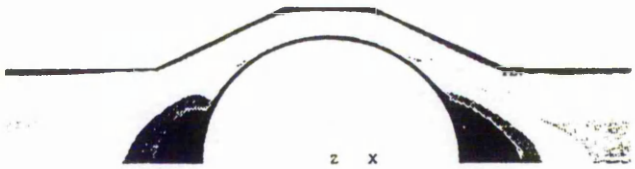

12. Velocity Magnitude Plot for SISO Conduit Valve

13. Turbulent Kinetic Energy Plot for SISO Conduit Valve

Results For SISO

To ameliorate the situation encountered in the SICO model, a third and final model was examined in which the original concept of conical inlets and outlets was reintroduced. As will be seen from Fig 11 the change in overall pressure drop produced by this modification is small but the velocity levels shown in Fig 12 are markedly different. The only remaining regions of high velocity are at the joins between the various sections. This improvement is confirmed by the turbulent kinetic energy plot of Fig 13 where it is apparent that the region of high turbulence behind the ball has largely been removed.

Conclusion

The introduction of CFD techniques to the design process for a conduit heart valve has been extremely useful in terms of allowing several different models to be studied and eliminated without the need to construct any of them. Any doubts about the validity of the methodology were largely removed by the successful application of the computer software to the reproduction of some existing experimental data on a very similar situation. This allowed a degree of confidence to be placed on the results produced by the technique when applied to the conduit situation, although there would still be a need to carry

experimental trials on a physical model of the version chosen finally.

Nevertheless the technique showed clearly that the original concept of a shaped conduit and a ball occluder is very promising, with the conical inlet and outlet sections offering the best combination of the key flow parameters. The need for further work was indicated by the continued existence of high velocity zones near to the joins between the various sections, but this is expected to be largely a matter of rounding off the sharp changes.

One problem, which was not addressed by validating the model against a series of experimental tests using a glycerol/water mixture, is the fact that the conduit is intended for use ultimately with blood. Since blood is a highly non-Newtonian liquid there may be unforeseen differences when compared with the Newtonian blood model used here. The eventual aim of this research is to move to some non-Newtonian representation of the blood within the CFD model.

A second problem is that the CFD analysis has been limited for the time being to a steady flow situation. Although the bulk of the blood flow occurs at a fairly steady rate during peak systole it is important not to neglect the opening and closing phases of the valve in order to assess the action of the ball occluder. Research is under way at the moment to split the cycle up into a series of quasi-steady flow situations involving different positions of the ball along the axis of the valve

References

Black, M.M.,Drury, P.J. and Smith, G.H. (1983)
Longterm clinical assessment of heart valve substitutes
Life Support Systems,1,Supplement 1,301-304

Duff, W.R. and Fox,R.W. (1972)
Prosthetic cardiac valves - an in vitro study
Jnl of Thoracic and Cardiovascular Surgery,63,1,131-142

Gentle, C.R. (1983)
Minimisation of pressure drop across heart valve conduits: a preliminary study
Life Support Systems,1,263-270

Leefe, S.E. (1993)
Pulsatile flow testing and development of prosthetic heart valves in conduits
PhD Thesis, The Nottingham Trent University

Lefrak, E.A. and Starr, A. (1979)
Cardiac Valve Prostheses
Appleton-Century-Crofts, New york

Lewis, J.M.O. and Macleod, N. (1978)
Development of the Edinburgh prosthetic heart valve: review of in vivo and in vitro evaluation studies
In "Heart Valve Research in the UK", Eds. C.R.Gentle and P.D.Swales, Leeds university Press.

McGoon, D.C. (1976)
Left ventricular and biventricular extracardiac conduits
Jnl of Thoracic and Cardiovascular Surgery,72,1,7-14

The Effect Of Haematocrit Volume On Blood Flow In A Heart Valve Prosthesis

C.R. Gentle and P. Wilson

Department Of Mechanical Engineering, The Nottingham Trent University, Burton Street, Nottingham, NG1 4BU, UK.

Abstract

This paper assesses the effect of haematocrit volume on blood flow through a heart valve prosthesis using the Computational Fluid Dynamics (CFD) package PHOENICS. The haematocrit volume values ranged from 21%, representing anaemia, through the normal 40%, to 75%, representing polycythaemia. A representative range of laminar and turbulent flows were modelled. For each flowrate the pressure drop, flow velocities, shear stresses and occluder force were calculated to determine the haemolytic and haemodynamic performance of the valve. The results indicate that haematocrit volume has a marked effect on the valve's flow performance and that haemolytic damage increases with haematocrit value.

Keywords

Conduit valve, Computational Fluid Dynamics, Haematocrit, Steady flow.

1 Introduction

Blood is a suspension of cells in a clear fluid, the plasma. If whole blood is centrifuged then the solid cells separate from the plasma and the relative volumes of the two components can readily be measured. The proportion of solids, expressed as a percentage of the total by volume, is known as the haematocrit and typically has a value of 40% for healthy humans[1]. In practice a range of between 21% and 75% is not uncommon in some parts of the world, leading to substantial variations in blood viscosity, quite apart from a variety of medical symptoms. This variation of viscosity does not appear to have been considered in previous experimental or CFD analyses of blood flow through heart valve prostheses, even though there must be a significant effect on shear stresses, shear rates, etc.. This paper therefore tries to remedy that situation by using CFD to analyse the effect that haematocrit volume has on the performance of a representative heart valve prosthesis for the two extreme cases of anaemia (21%) and polycythaemia (75%).

Anaemia is characterised by a reduction in the number of red blood cells and an increased fragility of the cell membrane which in turn raises the risk of cell rupture during periods of high shear stress. Ruptured cells release haemoglobin into the blood stream, thus reducing the level of oxygen passed to organs and tissue. There are several different kinds of anaemia, i.e. iron deficiency, haemolytic, pernicious, and aplastic anaemia. The condition often induces an enlargement of the spleen, a feeling of tiredness, lassitude, breathlessness, and a yellow tint to the skin. Of particular interest to this field of study is haemolytic anaemia, anaemia resulting from the destruction of red blood cells, since such a reduction can be caused by the mechanical crushing or high shear stresses found in many valvular prostheses.

Polycythaemia is an increase in the number of red blood cells as a result of increased red cell production by the bone marrow. It causes flushed skin, headaches, high blood pressure and blurred vision but more importantly strokes are a common complication. Treatment is by bloodletting (venesection), sometimes supplemented by the use of anticancer drugs or radioactive phosphorus. Although generally regarded as an abnormality, it can occur naturally in people living at high altitudes. For this reason it is important to consider its effect on blood flow through heart valve prostheses since there are many examples of high altitude cities, such as Johannesburg or Mexico City, where valve implants are routinely carried out.

Almost any heart valve prosthesis could have been used as the vehicle for this study since they all produce the high shear stresses which are the most significant factor. In fact a conduit valve prosthesis was chosen since it was already the subject of a research and development programme being carried out at Nottingham Trent University. Conduit valves are generally conventional heart valve prostheses

mounted in short lengths of graft tube. Although they may be used in adults for replacement of a degenerating ascending aorta or as aortic shunts to produce a second ventricular outlet, they are particularly useful in paediatrics to overcome congenital deformities,[2]. The Gentle[3] conduit valve considered here therefore has been especially designed to minimise pressure drops, shear stresses, and areas of recirculation or stasis so that its flow properties will remain adequate into adulthood. Hence if any problem is identified by this study then it is likely to be a general problem for all valves.

2 Model Specification

2.1 Blood Model Specification

Blood is considered to be an incompressible, Newtonian fluid with a dynamic viscosity μ_l which is dependent upon the haematocrit H, expressed as a proportion of the total volume, according to the following relationship:

$$\mu_l = \frac{1.4175 + 5.878H - 15.98H^2 + 31.964H^3}{1000} \quad (1)$$

Where, μ_l =Laminar viscosity, Pa s
H=Haematocrit volume.

The density for blood was found by the following relationship:

$$\rho = 7.925H + 1053 \quad (2)$$

Where, ρ= Blood density, Kg/m^3
H=Haematocrit volume.

The values considered for H were 0.21, 0.3, 0.4, 0.55 and 0.75.

2.2 CFD Model

The essential design philosophy of the conduit valve considered here is to provide a constant flow area path, as nearly as can be achieved, around a ball occluder. Earlier work[4] has shown how this basis has been developed into a final design which is indicated in Fig. 1. Compared with tilting disc or twin flap valves it is therefore a relatively simple matter to model the Gentle valve geometrically using a FORTRAN program since there is axial symmetry. The same program was further used to define all the cell corner points necessary to produce the finite volume domain or grid, also represented in Fig. 1, which is employed by the commercial CFD package, PHOENICS[5].

Figure 1: Finite volume domain.

The grid contained 5320 cells, comprising 140 cells in the Z direction, 38 cells in the Y direction and 1 cell in the X direction. Previous work[6] has shown that this grid density is sufficient to provide a grid-independent solution. A uniform inlet velocity was set to allow a 'plug' type velocity profile to develop at the entrance to the valve conduit and a free stream condition was specified at the outlet. This combination was chosen to represent the flow situation that would prevail with a conduit very close to the ventricle and experiencing pulsatile flow. Hence although only steady flow was considered, the correct choice of undeveloped inlet conditions goes some way to giving the model broader credibility.

Flowrates of 2.97, 5.93, 11.86 and 23.73 l/min were used giving inflow velocities, based on a 20 mm diameter conduit valve, of 0.1573, 0.3146, 0.6292 and 1.2584 m/s respectively. Laminar flow was assumed for the three lowest flowrates while turbulent flow was specified for the highest flowrate.

The CFD code PHOENICS was used to solve the governing equations. Convergence was deemed to have been satisfied when the residuals for pressure, velocity and turbulence properties fell below 1×10^{-8}, 1×10^{-8} and 1×10^{-6} respectively. The average CPU time to reach convergence was approximately 40 minutes.

3 Results Of Flow Analysis

For each model the flow field velocities, the shear stress distribution, the pressure drop and the force acting on the ball occluder were recorded. There were fundamental differences between the laminar flow situations and the turbulent flow case so the outcomes will be reported separately.

3.1 Laminar Flow Models

A typical contour plot of flow field velocities can be seen in Fig. 2. All models exhibited the same characteristics, i.e. deceleration of velocity upstream of the ball occluder, accelerating flow through the valve section, recirculating flow behind the ball occluder, and a main stream jet forming in the outlet section.

As the value of haematocrit increased for each of the laminar flowrates certain common features were observed:

- the magnitude of the maximum reverse flow velocity in zone C remained constant
- the peak forward flow velocity, in zone B, increased by an average of 12.36% between haematocrit volumes of 0.21 and 0.75 indicating that increased viscosity leads to a wider range of velocities for the same mean value, i.e. the shear rates are significantly higher
- the most noticeable effect was seen in the outlet section, zone D, where the fluid decelerated more rapidly with increasing haematocrit volume due to the higher viscosity.

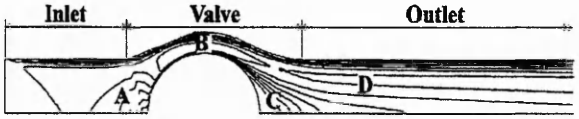

Figure 2: General flow field velocity pattern.

A) Decelerating flow,
B) accelerating flow,
C) recirculation zone,
D) main stream jet formation.

The shear stress at any point was determined from the shear rate by using the relationship:

$$\tau = \mu_{eff}\,\dot{\gamma} \qquad (3)$$

Where, τ=Shear stress, N/m^2,
$\mu_{eff}=\mu_l$, Laminar viscosity, Pa s,
$\dot{\gamma}$=Shear rate, s^{-1}.

A typical shear stress distribution can be seen in Fig. 3, with selected contour values indicated in Pascals.

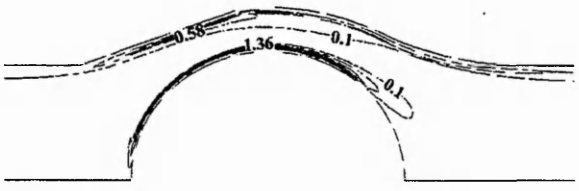

Figure 3: Shear stress distribution (Q=2.97l/m,H=21%).

This pattern of shear stress distribution was similar in all models, i.e. with the highest values concentrated around the ball and the diverging inlet section of the valve. The variation in peak shear stress values with haematocrit was considerable and is shown in Fig. 4.

As would be expected, the peak shear stress value increases with increasing haematocrit, but what is more surprising is that the relationship is highly non-linear. It must be remembered, however, that the increase in gradient of the curves towards the right of the graph is due to an increase not only in viscosity but also shear rate, as indicated above, with increasing haematocrit. This double dependence on haematocrit leads to a sixfold increase in peak shear rates at the highest flow rate between haematocrit values of 21% and 75%.

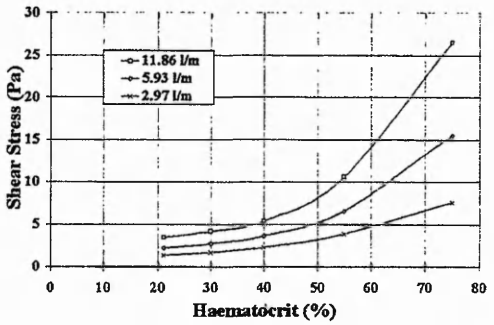

Figure 4: Variation in peak shear stress values

In conduit valves, since the inlet and outlet diameters are equal, the pressure drop across the prostheses is caused by viscous dissipation within the valve section, as explained more fully by Leefe and Gentle[7].

Hence it is to be expected that the valve's flow performance would be adversely affected by an increase in haematocrit, as shown in Fig. 5. Pressure was recorded at points located 18 mm and 55 mm before and after the valve section respectively, in line with experimental testing which has been carried out on similar prosthesis by Gentle and Leefe[8]. At all flow rates the pressure drop doubles approximately over the range of haematocrits considered here, which implies a much greater load on the heart.

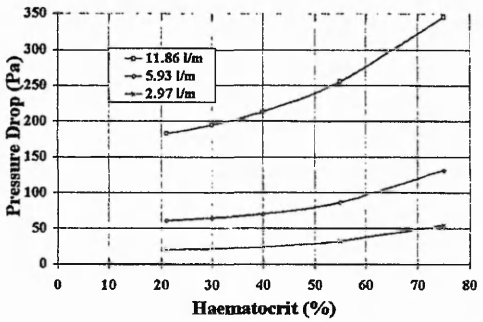

Figure 5: Pressure drop across valve prosthesis

One parameter which is generally not considered in CFD studies of valve prostheses is the axial force on the occluder even though this is fundamental to the

proper functioning of the valve and in the estimation of the useful life. The force on a ball occluder can quite easily be predicted because of the axial symmetry and was calculated here from the streamwise shear stress and pressure forces acting over the ball surface, as follows.

$$F_P = \sum P \partial A_P \tag{4}$$

$$F_V = \int_0^{2Rb} 2\pi \mu_{eff} r \frac{dw}{dy} \partial z \tag{5}$$

Where, F_P=Streamwise pressure force,
P=Pressure,
A_P=Occluder surface area perpendicular to flow axis,
F_V=Streamwise shear stress force,
μ_{eff}=Laminar viscosity, μ_l,
r=Elemental radius,
Rb=Ball radius.

Equations (4) and (5) were calculated after convergence was satisfied for each model with the velocity gradient term found using the Cartesian velocity resolute. The results obtained are shown in Fig. 6. It can be seen that as the flowrate increases the effect of increasing haematocrit is more marked due to an increase in shear rate found in these flows. Forces are doubled between the normal haematocrit value and the maximum value, indicating that the effect on wear rate or fatigue could be significant.

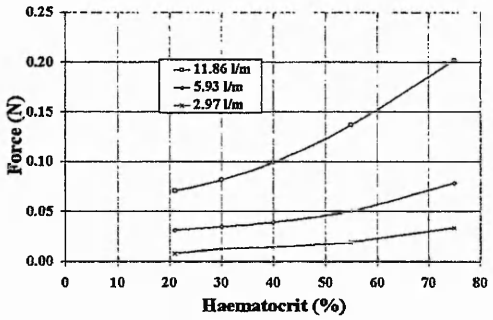

Figure 6: Force on ball occluder

3.2 Turbulent Flow Model

The overall velocity results obtained for turbulent flow were similar to those for the laminar flow models in that the peak velocities increased with haematocrit. The increase between the two extreme values of haematocrit was somewhat smaller at 11.1%, presumably because the turbulence itself acts towards reducing any large velocity gradients. Deceleration of the fluid in the outlet section varied little between each haematocrit value due to the increased momentum produced by the higher flowrate used in the turbulent case.

The most significant difference between the turbulent and laminar results occurs for the shear stress values, which were calculated as in Equation (3) but with the addition of a turbulent viscosity term, μ_t, making $\mu_{eff}=\mu_l+\mu_t$. A typical shear stress distribution can be seen in Fig. 7 and, by comparison with Fig. 3, it is apparent that many more contours are now present upstream of the ball. This increase arises purely from the effects of turbulence since a random transverse motion is now superimposed on the overall axial blood flow, leading to high stress values close to the ball surface. The peak values of shear stress for each value of haematocrit are shown in Fig. 8, which indicates both the total shear stress ($\tau_t+\tau_l$) and the laminar shear stress (τ_l). The three fold increase in the total shear stress between the extreme values of haematocrit may seem small compared to the six fold increase for the laminar cases observed in Fig. 4, but the shear stress values themselves are many times higher for the turbulent case.

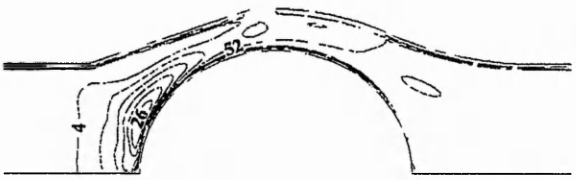

Figure 7: Shear stress distribution (Q=11.86l/m,H=21%)

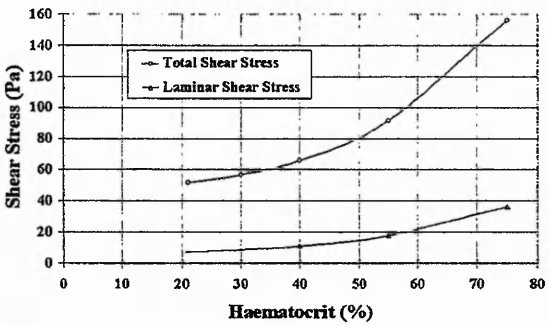

Figure 8: Variation in peak shear stress values

The turbulent results for pressure drop across the valve and force on the ball occluder show very similar trends to those for the laminar cases.

4 Clinical Consequences

4.1 Haemolysis

Hellmus and Brown[9] use a threshold value of bulk shear stress, for haemolysis, of 500 Pa applied for a

duration of at least 1×10^{-3} s. Even for the turbulent case with the highest haematocrit and at the highest flowrate, the greatest value of bulk shear stress found here was only 156 Pa and so it must be assumed that destruction of erythrocytes would not occur within the bulk flow.

However, the value of shear stress required to cause cell damage at a prosthesis surface is known to be much lower than the bulk value mentioned above. Blackshear[10] states that surface shear stress values below 150 Pa can cause haemolysis, arguing that additional stresses are encountered as erythrocytes adhere to and are then torn from the prosthetic surface. For most of the cases considered here this again does not apply, but for the turbulent flow model with the highest haematocrit volume, erythrocyte cell damage would start to occur at the ball surface. It might be argued that this haemolysis is advantageous since it would act to alleviate the polycythaemia which caused it, but this ignores the fact that haemolysis is implicated in the initiation of thromboembolisms. Consequently it may be concluded that a high haematocrit volume may lead to an increased risk of thromboembolism with a typical valve prosthesis.

4.2 Thrombus

Thrombus can form in areas of haemostasis or low shear and Dintenfass[11] shows that there is a critical shear rate, 7 s^{-1}, below which clotting can be accelerated a thousand fold. The prediction of recirculation behind the ball therefore implies that thrombus formation may occur there, especially for the case of high flowrates and haematocrit volumes outlined above where the recirculating cells may already be damaged. However, since occluders in reality pulse to and fro, shedding the recirculation zone, it is impossible to draw conclusions from steady flow studies about thrombus growth.

4.3 Haemodynamic Performance

The pressure drop across the prosthesis gives an indication of the load on the heart. The variation in pressure drop with haematocrit is considerable, generally doubling in value between haematocrit volumes of 21% and 75%. This is not a consequence of this particular valve prosthesis but of how the viscous resistance of the flow increases as haematocrit volume rises.

5 Discussion

There are two main drawbacks to this work: first, the studies are only in steady flow and second, there is no way of validating the data by comparison with clinical or experimental results.

The first criticism is being addressed in an extension of the CFD analysis to pulsatile flows but it may also be countered by pointing out that valves are fully open for most of the forward flow period and experience little variation of flow rate during that period. Hence consideration of only steady flow is unlikely to be grossly misleading.

The second criticism cannot be answered so readily, except to reiterate that there do not appear to have been any relevant studies against which to compare. Indeed, the real usefulness of this work would become apparent if it led to experimental studies of the effect of varying blood viscosity on heart valve performance and clinical studies of the effect of abnormal haematocrit volume on valve implant recipients.

Nevertheless, the results show that variations in haematocrit have a marked effect on the haemodynamic function of a typical cardiac valve prosthesis, producing large variations in pressure drops, occluder forces and shear stresses. Only at the highest value of haematocrit and flow rate is any damage to the erythrocytes indicated on normal criteria. However, it must be remembered that these haemolysis criteria are based on threshold values for healthy cells; the increase in fragility of cells associated with anaemia would cause a reduction in these values that might lead to haemolysis at the lowest haematocrit volumes. On the other hand the lower shear stress values produced by lowering the haematocrit would counteract this tendency and minimise any haemolytic damage.

The increase in force on the occluder as haematocrit volume rises could increase the chance of RBCs being crushed between the occluder and its supports and reduce the fatigue life of the valve. The reduction in fatigue life may be more relevant to valves that use support or guide struts.

6 Conclusion

This work analyses the effect of varying haematocrit volume on the haemodynamic performance of a conduit valve prosthesis over a representative range of laminar and turbulent flows. Using solely CFD techniques for the investigation considerably reduces its credibility but in mitigation it must be pointed out that the total computing time to run all the models was only 14 hours, far less than any comparable *in vitro* technique. It is therefore arguable that this kind of study is justifiable if it alerts the research community to a potential problem which is worthy of

more detailed investigation and where there is no existing work.

The results showed that the change in blood viscosity resulting from the variation in haematocrit volume caused a wide variation in haemolytic and haemodynamic conditions within the valve prosthesis. The most evident functional change would be a large increase in the pressure drop across the valve at high haematocrits but there would also be longer term implications to the rate of haemolysis, thromboembolism and fatigue life.

References

1. ***Folkow, B. and Neil, E.*** (1971) Circulation. Oxford University Press.

2. ***Gentle, C.R. and Leefe, S.E.*** (1996) Conduit mounted cardiac valves: a review of their uses, design and *in vivo* performance. Medical Engineering and Physics. In the press.

3. ***Gentle, C.R.*** (1983) Minimisation of pressure drop across heart valve conduits: a preliminary study. Life Support Systems, 1, 263-270.

4. ***Gentle, C.R. and Tansley, G.D.*** (1995) Development of a ceramic conduit valve prosthesis for corrective cardiovascular surgery. Biomaterials, 16, 3, 245-249

5. ***PHOENICS.*** CHAM, Bakery House, 40 High Street, Wimbledon Village, London SW19 5AU.

6. ***Tansley, G.D.*** (1988) Computational investigation of turbulent non-Newtonian flow in heart valve conduits. PhD Thesis, The Nottingham Trent University.

7. ***Leefe, S.E. and Gentle, C.R.*** (1987) Theoretical evaluation of energy loss methods in the analysis of prosthetic heart valves. Journal of Biomedical Engineering, 9, 121-127

8. ***Gentle, C.R. and Leefe, S.E.*** (1994) Pulsatile performance of two valved conduits used as cardiac valve replacements. Proceedings of the Institution of Mechanical Engineers, Part H, Journal of Engineering in Medicine, 208, 177-183

9. ***Hellmus, J.D. and Brown, C.H.*** (1975) Blood cell damage by mechanical forces. In "Cardiovascular Flow Dynamics and Measurements." Hwang, H.N.C. and Normann, N.A. (Eds), University Park Press, Baltimore, 799-823.

10. ***Blackshear, P.L.*** (1972) Mechanical haemolysis in flowing blood. In "Biomechanics: Its Foundation and Objectives." Fung, Y.C., Perrone, N. and Anliker, M. (Eds), Prentice Hall, New Jersey, 501-528.

11. ***Dintenfass, L.*** (1964) Rheological approach to thrombosis and atherosclerosis. Angiology, 333-343.